

INFRARED PHOTODISSOCIATION SPECTROSCOPY OF CLUSTER ANIONS IN THE GAS PHASE


by

Holger Schneider

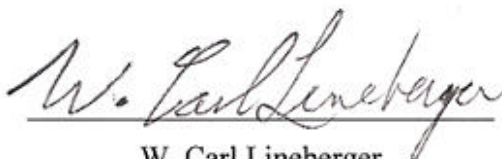
Diploma (Chemistry), Universität Karlsruhe (TH), 2004

A thesis submitted to the
Faculty of the Graduate School of the
University of Colorado in partial fulfillment
of the requirements for the degree of
Doctor of Philosophy
Department of Chemistry and Biochemistry
2008

This thesis entitled:
Infrared Photodissociation Spectroscopy of Cluster Anions in the Gas Phase
Written by Holger Schneider
has been approved for the
Department of Chemistry and Biochemistry



J. Mathias Weber



W. Carl Lineberger

Date: December 17, 2008

The final copy of this thesis has been examined by both signatories, and we find that both the content and the form meet acceptable presentation standards of scholarly work in the above mentioned discipline

Schneider, Holger (Ph.D. Physical Chemistry)

Infrared Photodissociation Spectroscopy of Cluster Anions in the Gas Phase

Thesis directed by Professor J. Mathias Weber

Infrared photodissociation spectroscopy has been applied to mass-selected anion-molecule complexes in the gas phase. In combination with quantum chemical calculations, this technique has proven to be very successful for gaining insight into the structures and interaction behavior of such species. We have used the “Ar nanomatrix” approach (which means tagging of the target clusters with a small number of Ar atoms) in order to produce cold complexes close to their ground state equilibrium structures and to facilitate dissociation upon absorption of one infrared photon.

The first part of this work deals with the investigation of the hydration of anions. While the hydration behavior of atomic anions such as halides is well understood, not much is known about the interaction between metal anions and water. Infrared spectra of $M \cdot H_2O$ ($M = Au, Ag, Cu$) have been measured in this study and it has been shown that they introduce a new motif for the solvation of small atomic anions, intermediate between the clear-cut hydration motifs known so far due to the shallowness of their potential energy curves. A second focus of the work on anion hydration has been on complexes of water molecules and anions with extended negative charge distribution such as the $C_6F_nH_{6-n}^-(H_2O)_m$ ($n = 4 - 6, m = 1, 2$) and $SF_6^-(H_2O)_m$ ($m = 1 - 3$) clusters. While the binding motifs of water ligands to the fluorobenzenes have been found to correspond mostly to the structures displayed by other anions where the charge is not localized in a small part of the molecule (such as anions with triatomic domains), the $SF_6^-(H_2O)_m$ ($m = 1 - 3$) complexes show another binding motif, reminiscent of the heavier halide-water complexes. Moreover, the hydration shell of the sulfur hexafluoride anion was found to exhibit delayed onset of water-water network

formation, leading to water-water interaction only upon binding of a third water ligand.

An intramolecular, infrared triggered reaction is described in the example of the $\text{SF}_6^- \cdot \text{HCOOH}$ complex. It was found that the reaction could be influenced by the degree of Ar solvation, effectively shutting down upon attachment of two or more Ar atoms with the Ar acting as a coolant. The structure of the complex and three different reaction channels identified could be determined. Aided by high-level quantum calculations, a possible reaction pathway is proposed.

Lastly, a study on $\text{A}^- \cdot \text{C}_6\text{F}_n\text{H}_{6-n}$ ($n = 0 - 5$, $\text{A} = \text{Cl}, \text{I}, \text{SF}_6$) is presented. This system is of considerable interest in the context of anion recognition via interactions with electron-deficient aromatic systems. Varying the number of fluorine atoms around the carbon ring one at a time offers the possibility of tuning the electronic properties of the aromatic molecule. Arenes with a high degree of fluorination offer two competing binding motifs to an anion, namely binding to the top of the ring (displaying a positive electrostatic potential) and binding to the periphery of the ring via hydrogen bonding to one of the CH groups, which become increasingly acidic upon increasing the number of fluorine atoms. It has been shown that the latter prevails up to pentafluorobenzene, so that full fluorination of the ring is needed in the case of fluorinated benzenes to make the binding motif switch to the top of the ring.

To my parents and my sisters

Acknowledgements

There are many people I do owe a lot and without the help of whom I would have never managed to accomplish this work. First of all, I would like to thank my advisor Mathias Weber. He has been both a great friend and advisor, who has always been able to pass on his own passion for physical chemistry. Not only did he never get tired of teaching me the secrets of working in a laboratory, but he was always ready to help out whenever problems occurred, and I could always count on his support in personal issues and the planning of my future. Without his willingness to take me along the next step in his own career after finishing in Karlsruhe and starting in his new position in Colorado, I would have never been offered the opportunity to spend most of my time as a graduate student abroad, which has been a great experience. I want to use the opportunity to express that I am truly grateful at this point!

I would also like to thank Manfred Kappes, who accepted me to work with his group in Karlsruhe in Germany already as an undergraduate. Getting introduced to the fascinating research in his group certainly helped me to make the decision about my major in favor of physical chemistry. I did my diploma thesis and started as a graduate student in his group as well, but even after leaving for Colorado, he was always willing to support me whenever it turned out to be necessary.

A special place in this list is taken by my family. My parents supported me immensely through all my life and studies, and without their neverending willingness to discuss and help me with all issues in my life, it is impossible I would have ever made it through. I would also like to thank my sisters Irmhild and Dagmar at this point, on whose unlimited support I could always count as well!

I was very lucky to have great friends and coworkers both in Karlsruhe and in Boulder. My two labmates in JILA, Jesse Marcum and Chris Adams, deserve a special thank you at this point. They were immensely helpful in building up the laboratory and getting experiments to run and work, and I certainly learnt a lot in the numerous discussions we had about science in general and physical chemistry specifically. But more than that, they have both been great friends, without whom

working in the laboratory would have been only half as much fun and who offered me much insight into life in the US. I hope I will still know both of them many years from now! I also want to thank the people in the “ion-molecule” groups of Carl Lineberger, Veronica Bierbaum and Barney Ellison, with whom I had many fruitful interactions and who were always willing stop their own work in order to help out.

I would also like to say thank you to the people from the machine and electronics shop and the IT support for their help with the setup of the laboratory and the experiments, and their patience in dealing with all the obstacles which occurred along the way.

Lastly, without writing down any further names, I would like to thank all friends and coworkers I had along the way of my studies, who all contributed to the fact that I can say at this point that I greatly enjoyed the last years and I learnt a lot not only with respect to science but also personally.

Thanks a lot!

Contents

1. Motivation	1
1.1. References for Chapter I.....	3
2. Experiment	5
2.1. Overview.....	5
2.2. Ion source.....	6
2.3. Reflectron Time-of-Flight Mass Spectrometer	10
2.4. Laser system.....	12
2.5. Infrared predissociation spectroscopy and effects of Ar solvation.....	15
2.6. References for Chapter II.....	19
3. Anion Hydration	21
3.1. General background	21
3.1.1. Condensed phase experiments	21
3.1.2. Infrared spectroscopy and binding motifs of $X^-(H_2O)_n$ clusters	22
3.2. Binary complexes of coinage metal anions with water	31
3.2.1. Introduction.....	31
3.2.2. Calculations.....	32
3.2.3. Results and discussion	32
3.2.4. Summary and conclusions	43

3.3.	Anionic hydrated fluorobenzenes	44
3.3.1.	Background	44
3.3.2.	Theoretical and mass spectrometric results	46
3.3.3.	Results and discussion	56
3.3.4.	Summary and conclusions	73
3.4.	Infrared Spectra of $\text{SF}_6^- \cdot (\text{H}_2\text{O})_n$ ($n = 1 - 3$): Incipient reaction and delayed onset of water network formation	75
3.4.1.	Introduction	75
3.4.2.	Calculations	76
3.4.3.	Results and discussion	79
3.5.	References for Chapter III	98
4.	Infrared-Triggered Reactions	105
4.1.	Some general remarks on ion-molecule reactions	105
4.2.	Infrared Spectra of $\text{SF}_6^- \cdot \text{HCOOH} \cdot \text{Ar}_n$ ($n = 0 - 2$): Infrared-Triggered Reaction and Ar-Induced Inhibition	108
4.2.1.	Introduction	108
4.2.2.	Calculations	109
4.2.3.	Results and discussion	111
4.2.4.	Summary and conclusions	123
4.3.	References for Chapter IV	124

5. Probing anion-π interactions: $\text{Cl}^- \cdot \text{C}_6\text{F}_{6-n}\text{H}_n$ complexes.....	127
5.1. Ion coordination and recognition	127
5.2. Aromatic molecules in anion recognition	129
5.3. $\text{Cl}^- \cdot \text{C}_6\text{F}_n\text{H}_{6-n}$ complexes as prototypes for the investigation of the binding behavior between anions and aromatic molecules.....	136
5.3.1. Introduction.....	136
5.3.2. Calculations.....	137
5.3.3. The $\text{Cl}^- \cdot \text{C}_6\text{H}_6$ complex dimer	138
5.3.4. Spectra and structures of the $\text{Cl}^- \cdot \text{C}_6\text{F}_n\text{H}_{6-n}$ complexes	143
5.3.5. Vibrational spectrum and binding motif for the $\text{Cl}^- \cdot \text{C}_6\text{F}_5\text{H}$ complex	146
5.3.6. Role of the anion.....	152
5.3.7. Summary and conclusions	154
5.4. References for Chapter V.....	156

List of Tables and Figures

Table 3.1	Theoretical results for some of the energetic and geometric properties of the $M \cdot H_2O$ complexes ($M = Au, Ag, Cu$).....	36
Table 3.2	Experimental and calculated IR band positions of the $M \cdot H_2O$ complexes ($M = Au, Ag, Cu$).....	38
Table 3.3	Relevant geometric values for the $C_6F_6^-$ anion as calculated by DFT/B3-LYP/TZVPP (for labeling of atoms compare Figure 3.9).....	47
Table 3.4	Relevant geometric values for the $C_6F_5H^-$ anion as calculated by DFT/B3-LYP/TZVPP (for labeling of atoms compare Figure 3.9).....	51
Table 3.5	Relevant geometric values for the $1,2,3,4-C_6F_4H_2^-$ anion as calculated by DFT/B3-LYP/TZVPP (for labeling of atoms compare Figure 3.9).....	53
Table 3.6	Experimental and calculated (DFT, B3-LYP, TZVPP, scaled for anharmonicity) positions of the symmetric (ν_s) and antisymmetric (ν_{as}) OH stretching bands of the water molecule in the $C_6F_6^- \cdot H_2O$ complex for the six lowest lying isomers; $\Delta\nu_s / \Delta\nu_{as}$ – corresponding band widths; $\delta\nu$ - splitting between these two bands; the numbers in the first row refer to the respective isomer as labeled in Figure 3.15	60
Table 3.7	Experimental band positions (ν_s for the symmetric, ν_{as} for the antisymmetric OH stretching band), widths ($\Delta\nu_s$ and $\Delta\nu_{as}$ respectively) and splittings ($\delta\nu$) for the $C_6F_6^- \cdot H_2O \cdot Ar_3$, $C_6F_5H^- \cdot H_2O \cdot Ar_2$ and $1,2,3,4-C_6F_4H_2^- \cdot H_2O \cdot Ar_3$ clusters.....	62
Table 3.8	Experimental and calculated (DFT, B3-LYP, TZVP, scaled for anharmonicity) positions of the symmetric (ν_s) and antisymmetric (ν_{as}) OH stretching bands of the water molecule in the $C_6F_5H^- \cdot H_2O$ complex for the six lowest lying isomers; $\Delta\nu_s / \Delta\nu_{as}$ – corresponding band widths; $\delta\nu$ - splitting between these two bands; the numbers in the first row refer to the respective isomer as labeled in Figure 3.17	65

Table 3.9	Calculated geometric properties, electronic energies and harmonic vibrational frequencies (in cm^{-1}) of SF_6^- from this work and Ref. ⁸¹ . Note that experimental values for the high frequency t_{1u} mode are 619 cm^{-1} [from Ar matrix isolation studies ⁸²] and $683(5) \text{ cm}^{-1}$ [from Ar predissociation spectroscopy ⁸³]	78
Table 3.10	Experimental and calculated (MP2, TZVP and aug-cc-pVTZ basis set, respectively, scaled for anharmonicity) positions of the symmetric (ν_s) and antisymmetric (ν_{as}) OH stretching bands of the water molecule in the $\text{SF}_6^- \cdot \text{H}_2\text{O}$ complex for the two lowest lying isomers (SIHB ground state and DIHB transition state); the numbering of the isomers in the first row refers to the respective geometry as labeled in Figure 3.21	82
Table 4.1	Fundamental and overtone frequencies and intensities calculated by the one-dimensional model (see section 4.2.2) for the two isomers of $\text{SF}_6^- \cdot \text{HCOOH}$	113
Table 4.2	Fundamental and overtone frequencies and intensities calculated by the three-dimensional model for isomer 1	114
Table 4.3	Fundamental and overtone frequencies and intensities calculated by the one-dimensional model for $\text{SF}_6^- \cdot \text{DCOOH}$ and $\text{SF}_6^- \cdot \text{HCOOD}$	115
Table 5.1	Candidates for Fermi interaction responsible for the group of bands around 2540 cm^{-1} in the spectrum of the $\text{Cl}^- \cdot \text{C}_6\text{F}_5\text{H}$ complex	148

Figure 2.1	Schematic overview of the setup for the infrared photodissociation spectroscopy experiment (top view).....	5
Figure 2.2	Schematic overview of the entrainment ion source ³	7
Figure 2.3	Schematic overview of the entrainment source modified for the generation of metal-ion molecule complexes ⁶	9
Figure 2.4	Schematic overview of the IR-OPO/OPA	13
Figure 2.5	Schematic representation of the photodissociation process after vibrational excitation of the chromophore (represented here by the evaporation of the Ar atoms from the $C_6F_6^-\cdot H_2O\cdot Ar_3$ parent).....	16
Figure 3.1	Typical binding motifs found for anions in a complex with a water molecule; A – SIHB motif (single ionic hydrogen bond); B – DIHB motif (double ionic hydrogen bond)	23
Figure 3.2	Ar predissociation spectra as taken from Ref. ⁹ ; (a) $F^-\cdot H_2O\cdot Ar_2$, (b) $Cl^-\cdot H_2O\cdot Ar_{11}$, (c) $Br^-\cdot H_2O\cdot Ar_3$ and $I^-\cdot H_2O\cdot Ar_3$; Free – OH not involved in a hydrogen bond, IHB – ionic H bond, B – overtone of the water intramolecular bending mode, IM – combination band involving the ion-water intermolecular stretching vibration.....	24
Figure 3.3	Spectra of $X^-\cdot(H_2O)_2$ clusters as taken from Ref. ⁹ ; (a) $F^-\cdot(H_2O)_2\cdot Ar_3$ (structure shown in inset) (b) $Cl^-\cdot(H_2O)_2\cdot Ar_3$ (c) $Br^-\cdot(H_2O)_2\cdot Ar_3$ (d) $I^-\cdot(H_2O)_2\cdot Ar_3$ (structure of species (b) – (d) depicted in inset); arrow: position of H bonded OH stretch in the neutral water dimer, F – position of free OH stretch; IHB _{AD} – Ionic H bond of a water molecule acting as a hydrogen bond donor to the ion and acceptor to the neighboring water; IHB _{DD} – Ionic H bond of a water molecule acting as a hydrogen bond donor to both the ion and the neighboring water; IW – Signature of the OH stretch involved in the hydrogen bond between the two water molecules	27
Figure 3.4	Infrared spectra of the $M^-\cdot(H_2O)$ complexes (M = Cu, Ag, Au; see inset of respective spectra); ν_B – bending overtone, ν_s – symmetric OH	

- stretching mode; ν_{as} – antisymmetric OH stretching mode; (IHB – IHB band; F – (quasi) free OH stretch, see Figure 3.2)..... 33
- Figure 3.5 IHB band positions for the known anion-water complexes as a function of the proton affinities of the ions (from Refs.^{11,43}); open squares – known SIHB complexes; open triangles – known DIHB complexes; full squares – coinage metal-water complexes; in the case of (suspected) DIHB configurations the lower energy (i.e. symmetric stretch) IHB band is listed 35
- Figure 3.6 Calculated potential energy curves (CCSD(T) without zero-point corrections) from Ref.⁴² for the $M \cdot H_2O$ complexes ($M = Au, Ag, Cu$, see inset) along the M-H-O angle 37
- Figure 3.7 IR spectra of the $M \cdot H_2O \cdot Ar_n$ complexes ($M = Au, Ag, Cu$; $n = 1,2$).... 40
- Figure 3.8 Calculated OH Born-Oppenheimer surface and OH stretching fundamentals along the water-rocking motion, measured as angle $\Phi(M-O-H)$ between water and metal (see sketch on top of graph). The symmetric OH stretching mode undergoes a considerable red shift as it develops into the H-bonded IHB band at high and low angles. All values are determined via equation (3.1), with $n_1 = n_2 = 0$ for the lower trace and $n_{1/2} = 1$ for the upper trace. The two dashed lines mark the minimum energy positions of the ground-state BO surface. 42
- Figure 3.9 Calculated structures (B3-LYP/TZVPP) of (A) $C_6F_6^-$ (B) $C_6F_5H^-$ (C) 1,2,3,4- $C_6F_4H_2^-$ 47
- Figure 3.10 Schematic representation of the Jahn-Teller effect and orbital stabilization upon geometric distortion (taken from Ref.⁵⁹) 48
- Figure 3.11 Mass spectrum showing the $C_6F_6^- \cdot Ar_n$ anion progression (n is shown in intervals of five, as indicated in the Figure).....49
- Figure 3.12 Mass spectra of the Ar progressions of $C_6F_6^- \cdot H_2O \cdot Ar_n$ and $C_6F_6^- \cdot Ar_n$, produced by entrainment of small amounts of C_6F_6 and H_2O vapor into an expansion of neat Ar 54

- Figure 3.13 Mass Spectrum of $C_6F_5H \cdot H_2O \cdot Ar_n$ and $C_6F_5H \cdot Ar_n$ progressions, produced by entrainment of small amounts of C_6F_5H and H_2O vapor into an expansion of neat Ar 55
- Figure 3.14 Infrared spectrum of $C_6F_6^- \cdot H_2O \cdot Ar_3$ (recorded via registering loss of all three Ar atoms); ν_s – symmetric OH stretching mode of the water ligand; ν_{as} – antisymmetric OH stretching mode of the water ligand 57
- Figure 3.15 Calculated structures (DFT/B3-LYP/TZVPP) of the six isomers within 100 meV above the global energy minimum (isomer 1) 59
- Figure 3.16 Infrared spectra of $C_6F_6^- \cdot H_2O \cdot Ar_3$ (top), $C_6F_5H \cdot H_2O \cdot Ar_2$ (center) and 1,2,3,4- $C_6F_4H_2^- \cdot H_2O \cdot Ar_3$ (bottom) measured via the loss of all Ar atoms both over the entire covered spectral range (left column) and zoomed in around the symmetric (ν_s) and antisymmetric (ν_{as}) OH stretching vibration (right column) 61
- Figure 3.17 Calculated structures (DFT/B3-LYP/TZVPP) of the six isomers within 100 meV above the global energy minimum (isomer 1) 64
- Figure 3.18 Electron autodetachment (AD) and vibrational predissociation (VP) spectra of the $C_6F_5H \cdot Ar_n$ ($n = 0 - 3$) anions. (The VP spectra are recorded via loss of the attached argon atoms). The lowest spectrum is a simulation using the scaled calculated harmonic value for the CH stretching vibration of the bare pentafluorobenzene anion using a Gaussian fit with 6 cm^{-1} half width 67
- Figure 3.19 Infrared Spectra of $C_6F_6^- \cdot (H_2O)_2 \cdot Ar_2$ (top trace) and $C_6F_5H \cdot (H_2O)_2 \cdot Ar_2$ (bottom trace) measured by monitoring loss of the two Ar atoms upon irradiation 71
- Figure 3.20 Infrared spectra of $SF_6^- \cdot H_2O \cdot Ar_n$ ($n = 1,2$) monitored by Ar loss; ν_s – symmetric OH stretching mode of the water ligand; ν_{as} – antisymmetric OH stretching mode of the water ligand, 2B – bending overtone of the water ligand; dotted lines mark combinations bands of the bending overtone and the IHB band (ν_s) with the water rocking mode 79

- Figure 3.21 Structures of the three isomers lowest in energy of the $\text{SF}_6^-\cdot\text{H}_2\text{O}$ complex. Dotted lines indicate hydrogen bonds. Relative energies are based on MP2 calculations (zero-point corrected) with a TZVPP basis set for all atoms. 81
- Figure 3.22 Experimental spectrum of the $\text{SF}_6^-\cdot\text{H}_2\text{O}$ (monitored by the loss of one Ar atom, see top trace) as compared to the simulated spectra (MP2/TZVPP, scaled for anharmonicity, see text) of isomer (a) and isomer (b), Figure 3.21. Simulations assume a Gaussian peak shape and a FWHM of 6 cm^{-1}) 83
- Figure 3.23 Infrared spectra of $\text{SF}_6^-\cdot(\text{H}_2\text{O})_n\cdot\text{Ar}$ ($n = 1,2$) monitored by Ar loss; ν_s – symmetric OH stretching mode of the water ligand; ν_{as} – antisymmetric OH stretching mode of the water ligand, 2B – bending overtone of the water ligand; dotted lines mark combinations bands of the bending overtone and the IHB band (ν_s) with the water rocking mode..... 85
- Figure 3.24 Structures of the isomers lowest in energy of the $\text{SF}_6^-\cdot(\text{H}_2\text{O})_2$ complex. Dotted lines indicate hydrogen bonds. Relative energies are based on MP2 calculations with a TZVPP basis set for all atoms. Geometries (d) and (e) are saddle points along several coordinates. 87
- Figure 3.25 Experimental spectrum of the $\text{SF}_6^-\cdot(\text{H}_2\text{O})_2$ complex (monitored by the loss of one Ar atom, see top trace) as compared to the simulated spectra (MP2/TZVPP, scaled for anharmonicity, see text) of isomer (a), (b) and (c), Figure 3.24. (Simulations assume a Gaussian peak shape and a FWHM of 6 cm^{-1}) 88
- Figure 3.26 Infrared spectra of $\text{SF}_6^-\cdot(\text{H}_2\text{O})_n\cdot\text{Ar}$ ($n = 1 - 3$) monitored by Ar loss; ν_s – symmetric OH stretching mode of the water ligand; ν_{as} – antisymmetric OH stretching mode of the water ligand, 2B – bending overtone of the water ligand; dotted lines mark combinations bands of the bending overtone and the IHB band (ν_s) with the water rocking mode 90
- Figure 3.27 Structures of the isomers lowest in energy of the $\text{SF}_6^-\cdot(\text{H}_2\text{O})_3$ complex. Dotted lines indicate hydrogen bonds. Relative energies are based on MP2 calculations with a TZVPP basis set for all atoms. 91

- Figure 3.28 Experimental spectrum of the $\text{SF}_6^-\cdot(\text{H}_2\text{O})_3$ (monitored by the loss of one Ar atom, see top trace) as compared to the simulated spectra (MP2/TZVPP, scaled for anharmonicity, see text) of isomer (a) and (b), Figure 3.27. The simulation for isomer (b) fits the experimental spectrum better, although it is higher in energy than isomer (a) (Simulations assume a Gaussian peak shape and a FWHM of 6 cm^{-1}). 93
- Figure 3.29 Highest occupied molecular orbital (HOMO) of the $\text{SF}_6^-\cdot(\text{H}_2\text{O})$ complex. The localization of negative charge by the presence of the water ligand is clearly visible. 94
- Figure 4.1 One-dimensional potential energy profile for a nucleophilic substitution ($\text{S}_{\text{N}}2$) both in the gas phase and in solution (from Ref.⁸)..... 107
- Figure 4.2 Structures of the two lowest lying isomers of $\text{SF}_6^-\cdot\text{HCOOH}$, isomer 1 is the global minimum 110
- Figure 4.3 Vibrational Ar predissociation spectra of $\text{SF}_6^-\cdot\text{HCOOH}\cdot\text{Ar}_2$, $\text{SF}_6^-\cdot\text{DCOOH}\cdot\text{Ar}_2$ and $\text{SF}_6^-\cdot\text{HCOOD}\cdot\text{Ar}_2$ 111
- Figure 4.4 Spectrum of $\text{SF}_6^-\cdot\text{HCOOH}$ complex recorded via registering the product ions of all possible fragmentation channels: SF_4^- , “ $\text{CO}_2^-\cdot 2\text{HF}$ ” and “ $\text{CO}_2^-\cdot\text{HF}$ ” 118
- Figure 4.5 Spectra of the $\text{SF}_6^-\cdot\text{HCOOH}$ and the $\text{SF}_6^-\cdot\text{HCOOH}\cdot\text{Ar}$ complexes recorded via registering the product ions of the fragmentation channel leading to the SF_4^- product ion and of the $\text{SF}_6^-\cdot\text{HCOOH}\cdot\text{Ar}_2$ complex via registering the loss of two Ar atoms 119
- Figure 4.6 Adiabatic potential energy curve along the intrinsic reaction coordinate (calculated at the DFT level of theory)..... 121
- Figure 4.7 Evolution of relevant bond lengths along the reaction coordinate, see Figure 4.6 for the labeling of the atoms 121

- Figure 5.1 Illustration of the electrostatic potential around C_6H_6 (left) and C_6F_6 (right) (calculated with Gaussian03W, HF/3-21G* level¹⁷). The color coding from blue to red represents positive to negative electrostatic potentials..... 130
- Figure 5.2 Schematic representations of the quadrupole moments of benzene (left) and hexafluorobenzene (right) and their suggested interaction motifs with an anionic moiety..... 130
- Figure 5.3 Illustration of possible binding motifs for the interaction of anions with electron-deficient arenes on the example of MP2/aug-cc-pVDZ optimized geometries for Cl^- complexes with tetracyanobenzene (from Ref.²⁸)..... 133
- Figure 5.4 Ar predissociation spectra for $Cl^- \cdot C_6H_6 \cdot Ar$ (top trace) and $Cl^- \cdot C_6H_6 \cdot Ar_3$ (bottom trace)..... 139
- Figure 5.5 Benzene CH stretching tetrad (according to Ref.^{54,56})..... 140
- Figure 5.6 Calculated minimum energy structures for the chloride-benzene complex 141
- Figure 5.7 Ar predissociation spectra for all isomers at all fluorination levels (each row corresponds to a certain number of fluorine atoms (marked as green in the sketches of the ligand structures) in the ligand, starting with benzene on top) of $Cl^- \cdot C_6F_nH_{6-n} \cdot Ar_m$ clusters. Horizontal axis: photon energy in cm^{-1} ; Vertical axis: photofragment yield in arbitrary units. The arrows indicate the calculated scaled harmonic frequencies of the most intense CH stretching bands..... 144
- Figure 5.8 Ar predissociation spectra for all isomers at all fluorination levels (complexes with equal number of fluorine atoms in the ligand are marked by the same color) of $Cl^- \cdot C_6F_nH_{6-n} \cdot Ar_m$ clusters (monitored by the loss of the Ar messenger atoms) 144
- Figure 5.9 Ar predissociation spectra for $Cl^- \cdot C_6H_6 \cdot Ar$ (top trace) and $Cl^- \cdot C_6F_5H \cdot Ar$ (bottom trace)..... 147

- Figure 5.10 Calculated structure for the $\text{Cl}^- \cdot \text{C}_6\text{F}_5\text{H}$ complex (DFT/B3-LYP/TZVP) via ring bonding 149
- Figure 5.11 Calculated potential energy surface along the CH stretching coordinate in $[\text{C}_6\text{F}_5 \cdots \text{H} \cdots \text{Cl}]^-$ (MP2/TZVP). The squares are single-point energies at various C-H distances, with fixed C-Cl distance, whereas the rest of the coordinates were relaxed but constrained to C_{2v} symmetry..... 151
- Figure 5.12 Centroid frequency as a function of the number of fluorine atoms. Open squares denote complexes with bifurcated hydrogen bonds, while data corresponding to hydrogen bonds involving isolated CH groups are shown as full squares. 152
- Figure 5.13 Infrared predissociation spectra of $\text{X} \cdot \text{C}_6\text{F}_5\text{H} \cdot \text{Ar}_3$ with $\text{X} = \text{SF}_6$ (top trace) and I (bottom trace)..... 153

1. Motivation

The mutual interaction between ions and their chemical environment plays a crucial role in chemistry. A detailed understanding of these interactions at a molecular level is therefore important in many areas, ranging from processes in biological systems and organisms to chemical reaction mechanisms, in which anions frequently occur as important reactive intermediates. However, investigations of the intrinsic properties governing the interactions between ions and their surroundings are difficult to perform in liquid phase, due to many-body forces, fluctuations in their solvent shell and solvent molecules further away from the ion. A convenient approach to circumvent these problems inherent to experiments in solution is to perform experiments on the systems of interest in the gas phase, where ionic species can be easily mass selected, making sure that only one particular system is probed each time. Moreover, ion-molecule complexes can be studied without the influence of other chemical environments, allowing access to their intrinsic interaction features. At the same time, the number of ligand molecules around the respective ion can be varied one at a time, making investigations of the structure of solvation shells and the influence of the solvent shell size on the interaction properties experimentally amenable. For very large clusters, one might eventually be able to extrapolate to the bulk limit, with the cluster sizes necessary for a good approximation depending on the property under consideration.¹ A variety of different techniques has been developed or modified to study ion-molecule complexes and clusters in the gas phase, such as mass spectrometry and reactivity studies,¹⁻⁴ ion mobility experiments,⁵ photoelectron spectroscopy⁶ and photodissociation experiments,^{3,4,7,8} to name just a few. Infrared predissociation spectroscopy^{3,7,9} has turned out to be very fruitful for the investigation of the structural properties of ion-molecule complexes, especially if accompanied by quantum chemical calculations to aid the interpretation of the vibrational spectra obtained. The successful application of this method is based on the changes in the bonding properties and the symmetries of the respective free ions and molecules upon introducing interactions between them, as any deformations and perturbations will be

encoded in the vibrational spectrum of the complexes. Infrared spectroscopy therefore provides a very sensitive tool for registering the geometries of the complexes under consideration as compared to their uncomplexed constituents. The vibrational signatures of the fundamental transitions of some important functional groups (such as CH or OH groups) fall within the mid-infrared range of the spectrum, making a wide range of complexes and clusters accessible to this experimental technique. As will be explained in detail in chapter two, it is not possible to use conventional infrared absorption spectroscopy in order to realize these experiments while working with a molecular beam of mass selected ions in the gas phase. However, photodissociation action spectroscopy turns out to be a convenient experimental approach. Several studies that have been performed using this technique are presented in this work. An investigation of the hydration behavior of atomic metal anions is presented using the example of the coinage metal anions and put into context with earlier studies on the hydration of small and medium sized anions. The dependence of hydration structure motifs on the size and polarizability of the charge distribution within the respective anionic charge carrier is investigated in complexes of $C_6F_nH_{6-n}^-$ ($n = 4 - 6$) and SF_6^- anions with water ligands. Having demonstrated the power of the technique on studying the interaction of these anions with their chemical surroundings and solvation shells, a study on the sulfur hexafluoride-formic acid complex is discussed, showing that in some cases it is possible to trigger an intracluster reaction upon excitation of the ion-molecule complex with an infrared photon. Finally a study of chloride-fluorobenzene complexes is presented, shedding light on the interactions of anions with electron-deficient aromatic molecules.

1.1. References for Chapter I

- ¹ V. E. Bondybey and M. K. Beyer, *International Reviews in Physical Chemistry* **21** (2), 277 (2002).
- ² *Gas Phase Ion Chemistry*, edited by M. T. Bowers (Academic Press, New York, 1979); M. P. Irion, *International Journal of Mass Spectrometry and Ion Processes* **121** (1-2), 1 (1992); A. G. Marshall and L. Schweikhard, *International Journal of Mass Spectrometry and Ion Processes* **118**, 37 (1992); P. B. Armentrout and T. Baer, *J. Phys. Chem.* **100** (31), 12866 (1996); M. T. Bowers, A. G. Marshall, and F. W. McLafferty, *J. Phys. Chem.* **100** (31), 12897 (1996); D. C. Parent and S. L. Anderson, *Chemical Reviews* **92** (7), 1541 (1992); P. B. Armentrout, *International Journal of Mass Spectrometry* **200** (1-3), 219 (2000); J. E. Braun, T. Mehnert, and H. J. Neusser, *International Journal of Mass Spectrometry* **203** (1-3), 1 (2000); B. S. Freiser, *Journal of Mass Spectrometry* **31** (7), 703 (1996); A. A. Viggiano, S. T. Arnold, and R. A. Morris, *International Reviews in Physical Chemistry* **17** (2), 147 (1998); P. B. Armentrout, *Annual Review of Physical Chemistry* **52**, 423 (2001); G. Niedner-Schatteburg and V. E. Bondybey, *Chemical Reviews* **100** (11), 4059 (2000); M. T. Rodgers and P. B. Armentrout, *Mass Spectrometry Reviews* **19** (4), 215 (2000); M. K. Beyer, *Mass Spectrometry Reviews* **26** (4), 517 (2007); P. B. Armentrout, *International Journal of Mass Spectrometry* **227** (3), 289 (2003); D. K. Böhme and H. Schwarz, *Angewandte Chemie-International Edition* **44** (16), 2336 (2005); D. Schröder and H. Schwarz, in *Modern Mass Spectrometry* (2003), Vol. 225, pp. 133; H. Schwarz, *Angewandte Chemie-International Edition* **42** (37), 4442 (2003); H. Schwarz, *International Journal of Mass Spectrometry* **237** (1), 75 (2004).
- ³ B. Brutschy, *Chemical Reviews* **92** (7), 1567 (1992).
- ⁴ J. M. Farrar, *International Reviews in Physical Chemistry* **22** (4), 593 (2003).
- ⁵ D. E. Clemmer and M. F. Jarrold, *Journal of Mass Spectrometry* **32** (6), 577 (1997); A. A. Shvartsburg, R. R. Hudgins, P. Dugourd, and M. F. Jarrold, *Chemical Society Reviews* **30** (1), 26 (2001); T. Wyttenbach and M. T. Bowers, in *Modern Mass Spectrometry* (2003), Vol. 225, pp. 207; P. Weis, S. Gilb, P. Gerhardt, and M. M. Kappes, *International Journal of Mass Spectrometry* **216** (1), 59 (2002).
- ⁶ U. Boesl and W. J. Knott, *Mass Spectrometry Reviews* **17** (4), 275 (1998); A. W. Castleman and K. H. Bowen, *Journal of Physical Chemistry* **100** (31), 12911 (1996); O. Cheshnovsky, S. H. Yang, C. L. Pettiette, M. J. Craycraft, and R. E. Smalley, *Review of Scientific Instruments* **58** (11), 2131 (1987); C. E. H. Dessent, J. Kim, and M. A. Johnson, *Accounts of Chemical Research* **31**

(9), 527 (1998); G. Gantefor, G. S. IckingKonert, H. Handschuh, and W. Eberhardt, *International Journal of Mass Spectrometry and Ion Processes* **159**, 81 (1996); K. Müller-Dethlefs, O. Dopfer, and T. G. Wright, *Chemical Reviews* **94** (7), 1845 (1994); R. E. Continetti, *International Reviews in Physical Chemistry* **17** (2), 227 (1998); C. E. H. Dessent, M. A. Johnson, I. Becker, and O. Cheshnovsky, in *Electron Transfer-from Isolated Molecules to Biomolecules, Pt 1* (1999), Vol. 106, pp. 265; K. Müller-Dethlefs and E. W. Schlag, *Angewandte Chemie-International Edition* **37** (10), 1346 (1998); D. M. Neumark, *Annual Review of Physical Chemistry* **52**, 255 (2001); J. H. Hendricks, H. L. de Clercq, C. B. Freidhoff, S. T. Arnold, J. G. Eaton, C. Fancher, S. A. Lyapustina, J. T. Snodgrass, and K. H. Bowen, *Journal of Chemical Physics* **116** (18), 7926 (2002); D. M. Neumark, *Physical Chemistry Chemical Physics* **7** (3), 433 (2005); A. Sanov and W. C. Lineberger, *Physical Chemistry Chemical Physics* **6** (9), 2018 (2004); A. Stolow, A. E. Bragg, and D. M. Neumark, *Chemical Reviews* **104** (4), 1719 (2004); X. B. Wang, X. Yang, and L. S. Wang, *International Reviews in Physical Chemistry* **21** (3), 473 (2002).

- ⁷ E. J. Bieske and O. Dopfer, *Chemical Reviews* **100** (11), 3963 (2000); E. J. Bieske and J. P. Maier, *Chemical Reviews* **93** (8), 2603 (1993); O. Dopfer, *International Reviews in Physical Chemistry* **22** (3), 437 (2003); M. A. Duncan, *International Reviews in Physical Chemistry* **22** (2), 407 (2003); J. M. Lisy, *International Reviews in Physical Chemistry* **16** (3), 267 (1997).
- ⁸ O. Dopfer, *Zeitschrift Fur Physikalische Chemie-International Journal of Research in Physical Chemistry & Chemical Physics* **219** (2), 125 (2005); M. A. Duncan, *Annual Review of Physical Chemistry* **48**, 69 (1997); T. Ebata, A. Fujii, and N. Mikami, *International Reviews in Physical Chemistry* **17** (3), 331 (1998); A. Fujii, T. Sawamura, S. Tanabe, T. Ebata, and N. Mikami, *Chemical Physics Letters* **225** (1-3), 104 (1994).
- ⁹ S. Djafari, G. Lembach, H. D. Barth, and B. Brutschy, *Zeitschrift Fur Physikalische Chemie-International Journal of Research in Physical Chemistry & Chemical Physics* **195**, 253 (1996); R. C. Dunbar, *International Journal of Mass Spectrometry* **200** (1-3), 571 (2000); M. B. Knickelbein, *Philosophical Magazine B-Physics of Condensed Matter Statistical Mechanics Electronic Optical and Magnetic Properties* **79** (9), 1379 (1999); C. Riehn, K. Buchhold, B. Reimann, S. Djafari, H. D. Barth, B. Brutschy, P. Tarakeshwar, and K. S. Kim, *Journal of Chemical Physics* **112** (3), 1170 (2000); W. H. Robertson and M. A. Johnson, *Annual Review of Physical Chemistry* **54**, 173 (2003); E. J. Bieske, *Chemical Society Reviews* **32** (4), 231 (2003).

2. Experiment

2.1. Overview

A schematic overview of the photodissociation spectrometer used for the investigation of the systems presented in this work is shown in Figure 2.1. It consists of a supersonic entrainment ion source for the production of the anionic complexes of interest, a reflectron-time-of-flight mass spectrometer (TOF-MS) and an infrared optical parametric converter as a light source. These components are described in detail in the following sections, together with the specific parameters employed for running the experiments presented here.

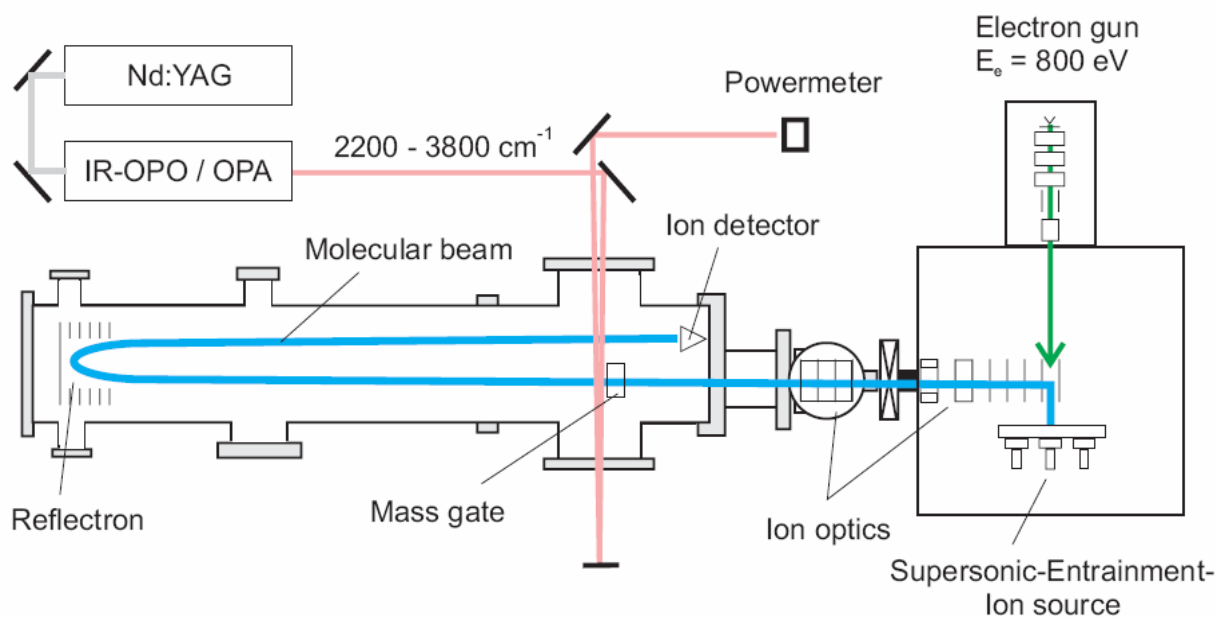


Figure 2.1 Schematic overview of the setup for the infrared photodissociation spectroscopy experiment (top view)

2.2. Ion source

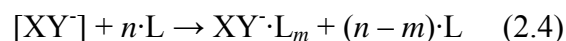
The anionic species of interest are generated employing an electron impact plasma ion source in combination with a pulsed supersonic expansion (see Ref.¹ and references therein). A neutral plasma is generated by impact of electrons with energies at 800 eV (emitted from a heated thoriated tungsten wire, 0.005", 1% ThO, in the electron gun) into the high density region of a supersonic expansion. There, anions can be formed via attachment of slow secondary electrons (which mostly stem from ionization of argon atoms by the highly energetic electrons generated via the electron gun) to molecular precursor molecules XY. This results in the formation of temporary negative ions according to reactions of the type:



The transient negative ions formed this way can then either autodeattach the electron or be stabilized in collisions or by dissociation, forming stable anions in one of the following ways:



The ion-molecule cluster ions which are to be investigated can be created in association reactions with the respective ligand:



It can be very difficult, however, to find the optimal conditions for the generation of the desired species, if a premix of suitable gases is co-expanded. In addition, although some cooling is provided by the expansion of the mixture from moderate backing pressures (between ~ 3 - 14 bar, depending on the system) into high vacuum (typical operating pressures of the source chamber range between the low 10⁻⁶ to mid

10^{-5} mbar region), the anionic clusters produced via reaction (2.4) often still contain a considerable amount of internal energy, as they are formed in an evaporative ensemble.² For the investigation of the interactions governing the structures of these species and in order to facilitate comparison of the results obtained in the infrared spectroscopic experiments to quantum chemical calculations, generation of the target complexes with a minimum amount of internal energy is desired, to ensure they are close to their equilibrium geometry. In order to meet these conditions, the local concentrations of the reactant gases must remain low, so that collisions with the inert carrier gas always dominate, thereby leading to an effective cooling of the clusters. This requires very low concentrations of precursors and ligands in the expansion. Although these conditions can be met using premixed gases from a gas cylinder, it is a difficult task to optimize the composition beforehand, especially in the limit of low seed gas concentrations, as surface adsorption of the reactant gases in the gas inlet system and remaining impurities in the carrier gas can considerably complicate the final gas mixture. In order to circumvent at least some of these problems, Robertson *et al.*³ developed the concept of the supersonic entrainment source, a schematic overview of which is shown in Figure 2.2.

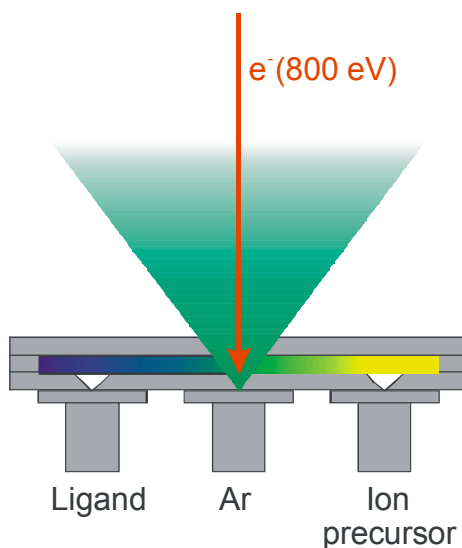


Figure 2.2 Schematic overview of the entrainment ion source³

The working principle of this source is based on a hydrodynamic process first described by Campargue.⁴ The entrainment of molecules into the flow of an expansion is most efficient for molecules in the vicinity of the nozzle orifice, where they penetrate through the border of the expansion cone and mix with the expanding carrier gas. Moreover, the plasma region of the molecular beam can be found in the same volume, and negative ions are formed at this point by attachment of slow secondary electrons. One of the great advantages of this source in comparison to the co-expansion of premixed gases is that it allows for *in situ* optimization of the composition of the gas mixture, so that among all of the ions formed in the expansion the anionic complex of interest can be optimized for maximum intensity. This is achieved by controlling the valves independently (both with respect to start time and gas pulse duration), providing great flexibility in the relative timing and composition of the expanding gas cloud and therefore eventually of the species generated. Pulsed valves of the General Valve Series 9 (1 mm orifice) are used for the introduction of the ligand molecules into the reactor. An expansion of neat Ar (99.9999% purity) is generated by an Even-Lavie-Valve, allowing for very short opening times (typically 25 μ s) and high backing pressures (up to 100 bar, typically operated at 14 bar in this experiment), which in turn allows operating the source chamber at relatively low background pressures. In addition, cold, Ar solvated complexes $X \cdot L_n \cdot Ar_m$ can be generated via sequential ligand exchange reactions:



The source chamber is pumped by a 2000 L/s diffusion pump (BOC Edwards Diffstak) and a 1000 L/s turbomolecular pump (Turbovac 1000C, Leybold). The experiment is operated at 20 Hz repetition rate, which results in pressures in the source chamber between several 10^{-6} to several 10^{-5} mbar during operation. Within the source chamber, the molecular beam expands freely between the repeller and extractor plate of a home-built Wiley-McLaren⁵ TOF-MS, where the anions are accelerated to kinetic energies of approximately 3.5 keV into a differential pumping stage pumped by a 520 L/s turbomolecular pump (Pfeiffer TMU 521 YP) to operating

pressures of several 10^{-8} mbar. The ion source described so far has been designed for the generation and optimization of ionic molecular clusters, relying on substances with sufficiently high vapor pressures. For the production of clusters containing metal anions a modification has been developed in our group to allow for the production of such species as well.⁶ In order to achieve this, one of the entraining valves is replaced by a rotating steel plate, on which a wire consisting of the target metal is mounted. By focusing an intense laser beam (generated by a Nd:YAG laser, Innolas Spitlight 300, typically operated at 50 mJ per pulse / 1064 nm) onto the rim of the rotating wire, the metal is vaporized and subsequently entrained into the main Ar expansion. The rest of the settings and parameters remains similar as has been described for the metal-free targets. A schematic representation of the entrainment ion source modified for the generation of metal ion-molecule complexes is shown in Figure 2.3.

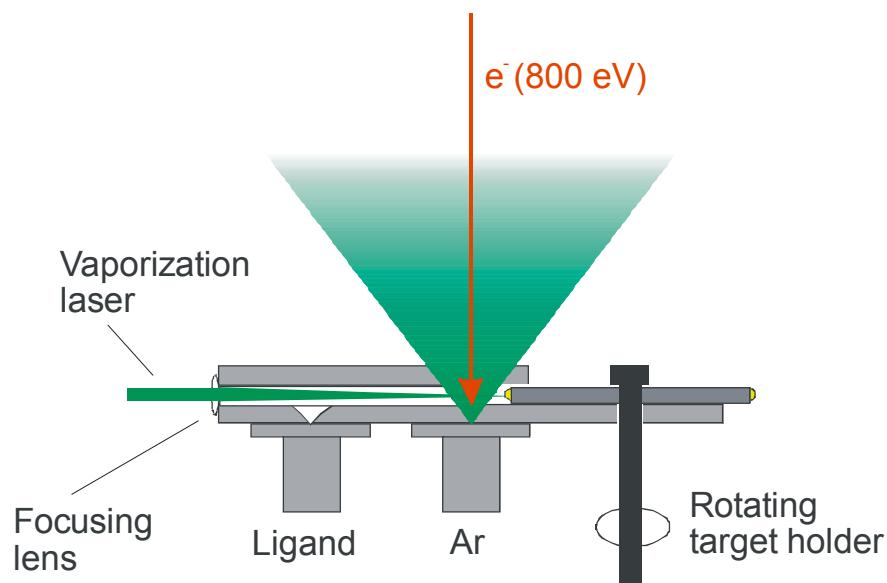


Figure 2.3 Schematic overview of the entrainment source modified for the generation of metal-ion molecule complexes⁶

2.3. Reflectron Time-of-Flight Mass Spectrometer

The ion source described above generates a multitude of anionic species based on the introduced precursor molecules. These ions are accelerated into the flight tube of the mass spectrometer (pumped by another 520 L/s turbomolecular pump (Pfeiffer TMU 521 YP), maintaining operational pressures of several 10^{-8} mbar), a two stage Wiley-McLaren setup.⁵ In the mass spectrometer, the ions are separated according to their mass-to-charge (m/q) ratio, as for the overall flight time of an ion with mass m and charge q the following relationship applies:

$$t \propto \sqrt{\frac{m}{q}} \quad (2.6)$$

Moreover, the Wiley-McLaren design allows for freely choosing the position of a first space focus in the mass spectrometer, where all ions of the same mass-to-charge ratio arrive at the same time. In order to only transmit a specific range of ions with certain m/q values, a pulsed mass gate is installed in this first space focus, consisting of a stack of plate electrodes, to which a potential can be applied (alternately positive and negative, typically around ± 150 V).⁷ If the electric field is switched on, arriving ions are deflected from their original trajectory and are therefore removed from the molecular beam. Directly after the mass gate (~ 10 mm downstream), the ions are irradiated with the output of an infrared optical parametric converter (OPO, Laser Vision), which is described in more detail in section 2.4. The ions are reflected in a two-stage electrostatic mirror (reflectron, R.M. Jordan Company) and registered in the second space focus of the mass spectrometer (provided by the reflectron) on a micro channel plate (MCP) ion detector. In addition, the reflectron also allows for the separation of the fragment ions resulting from dissociation after absorption of an infrared photon in the irradiation region from their parent ions: undissociated parent ions penetrate deeper into the field of the reflectron and arrive therefore later at the detector than the lighter fragment ions (enabling their independent registration).⁸

Employing a reflectron also helps to extend the flight path of the ions considerably and therefore to increase the resolution of the mass spectrometer, which is defined as

$$R = \frac{m}{\Delta m} = \frac{t}{2\Delta t} \quad (2.7)$$

and in the present mode of operation typically reaches values around $R \sim 800$. In principle, there are two different strategies for measuring the desired photodissociation spectra. One possibility is to measure the depletion of the parent ion signal upon irradiation with the infrared light. Analogously to Lambert-Beer's law, the parent ion intensity is measured with (N_P) and without ($N_{P,0}$) the laser beam, with the ratio of these two values being related to the cross section in the following way $\sigma(\nu)$:⁹

$$\frac{N_P(\nu)}{N_{P,0}} = 1 - \alpha + \alpha \cdot \exp\{-\sigma(\nu) \cdot F(\nu)\} \quad (2.8)$$

where $F(\nu)$ is the number of photons per area integrated over the laser pulse, and α the imperfect overlap of the ion packets and the laser beam ($0 < \alpha < 1$), which can be determined by measuring the depletion of the ion beam as a function of the laser intensity. However, measuring the depletion of the parent ion signal in the described way works well only if an appreciable part of the ion beam (at least $\sim 10\%$) is depleted upon irradiation with light.¹⁰ However, typical infrared photodissociation experiments result in a depletion of the parent ion signal on the order of 0.1 – 1%, preventing this approach from being a convenient route for obtaining the desired results. These problems can be circumvented by measurement of the photofragment action. In this case, not the depletion of the parent ions, but the intensity of fragment ions produced (N_F) following irradiation is monitored as a function of the infrared frequency ν . In the limit of small depletion (which for infrared predissociation experiments can be assumed to hold), the following relation between cross section, fragment ion yield and laser intensity applies:

$$N_F(\nu) \propto \sigma(\nu) \cdot I(\nu) / \nu \quad (2.9)$$

The main drawback of this approach is that absolute cross sections are usually not obtainable. However, most of the structural information is encoded in the relative cross sections. In most of the experiments presented in this work, Ar solvated complexes have been investigated, which decay on a time scale short compared to the flight time of the parent ion through the mass spectrometer and therefore with near-unit efficiency.

2.4. Laser system

The infrared light used to irradiate the complexes in the mass spectrometer is provided by an optical parametric oscillator (OPO) and optical parametric amplifier (OPA), shown in Figure 2.4. The setup is pumped with the output of a Nd:YAG laser (Innolas Spitlight 600, typical pump energies are 450 mJ/per pulse, pulse length: ~ 7 ns). The pump radiation of frequency ω_p (fundamental of the Nd:YAG laser, $\lambda_p = 1064$ nm) is split in two parts with the relative ratio 1:2. The weaker beam is used to pump the OPO (consisting of two potassium titanyl phosphate (KTP) crystals) after being frequency-doubled in a KTP crystal. This results in the generation of a signal wave in the range between 710 - 885 nm and an idler wave in the range between 1330 - 2120 nm. After a double pass through the OPO crystals, both the signal wave and the remaining pump radiation are filtered out of the OPO resonator by a Si filter. The OPO cavity is resonant for the idler wave.

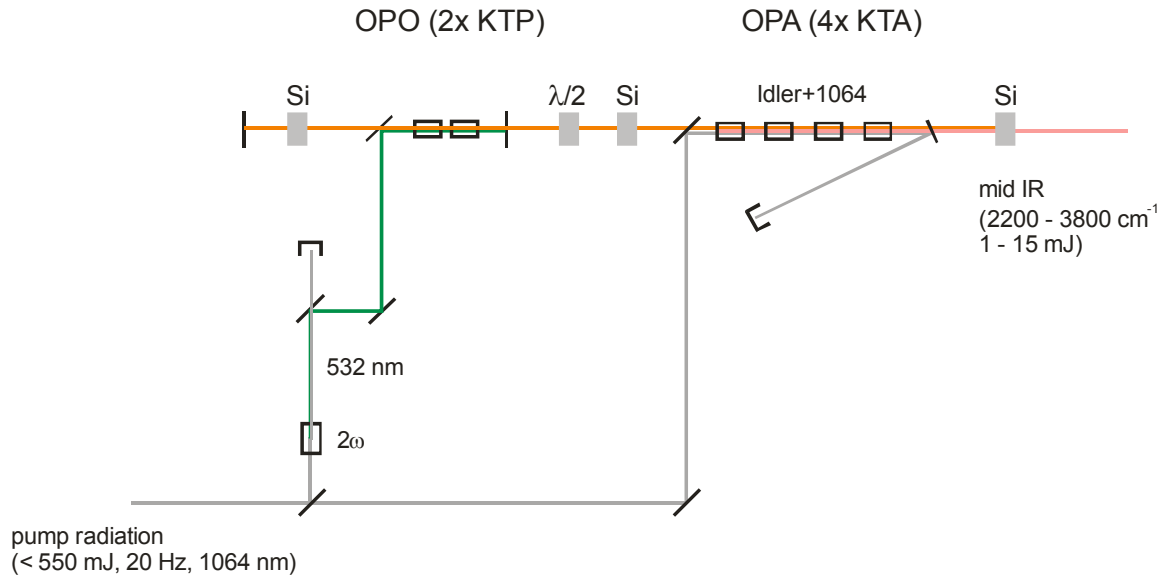


Figure 2.4 Schematic overview of the IR-OPO/OPA

The idler wave is then superimposed with the second part of the original pump beam in a chain of four potassium titanyl arsenate (KTA) crystals forming the OPA. This leads to difference frequency mixing between pump and idler radiation in the OPA stage, providing light in the mid-infrared range between $2200 - 3800 \text{ cm}^{-1}$:

$$\omega_{IR} = \omega_p - \omega_i \quad (2.10)$$

Additionally, energy conservation requires

$$\omega_p = \frac{1}{2}(\omega_s - \omega_i) \quad (2.11)$$

so that the frequency of light generated via difference frequency mixing will be given by:

$$\omega_{IR} = \omega_P - (2\omega_P - \omega_S) = \omega_S - \omega_P = 2 \cdot \pi \cdot c \cdot \left\{ \frac{1}{\lambda_S} - \frac{1}{\lambda_P} \right\} = 2 \cdot \pi \cdot c \cdot \left\{ \frac{1}{\lambda_S} - \frac{1}{1064nm} \right\} \quad (2.12)$$

- ω_{IR} : angular frequency of the mid-infrared radiation generated by difference frequency mixing in the OPA, $\lambda_{IR} \in [2600nm, 4550nm]$
- ω_I : angular frequency of the idler wave $\lambda_I \in [1.3\mu m, 2.2\mu m]$
- ω_S : angular frequency of the signal wave $\lambda_S \in [710nm, 885nm]$
- ω_P : angular frequency of the pump radiation provided by the Nd:YAG laser, $\lambda_P = 1064nm$

Light in this frequency range can be used for the investigation of the structures of a wide range of complexes, as important fundamental vibrational transitions of many molecules fall within that region of the spectrum, such as OH and CH stretching modes. The OPO is tunable in that range without gaps and provides pulses of ~ 7 ns duration and energies of 1 - 15 mJ, depending on the pump laser intensity and the infrared frequency. After the OPA stage, a dichroic mirror is installed to remove the residual pump radiation from the light beam. A Brewster “stack of plates” polarizer is used to isolate either the horizontally polarized mid-infrared or the vertically polarized idler wave from the output. The band width of the OPO is $\sim 2 \text{ cm}^{-1}$. The infrared beam is routed to the mass spectrometer via gold mirrors and passed twice through the interaction region in order to double the signal-to-noise ratio before eventually being measured by a pyroelectric detector (Molelectron J-4). A Si and an anti-reflection coated Ge filter are placed in the beam in order to filter the remaining 1064 nm radiation from the pump laser and amplified idler radiation out of the light beam. The IR-OPO/OPA and the infrared beam path can be purged by dry nitrogen in order to avoid absorption of the infrared light by ambient atmospheric trace gases such as water or carbon dioxide prior to reaching the mass spectrometer. Frequency calibration of the setup is achieved by analyzing the signal wave of the OPO (transmitted through the OPO output coupler) with a fiber optic spectrometer (Ocean

Optics), which in turn is calibrated against the well-known emission spectrum of an Ar discharge. On the basis of the resolution of the spectrometer in the spectral region in question ($\sim 2 \text{ cm}^{-1}$) and the intrinsic bandwidth of the optical parametric converter ($\sim 2 \text{ cm}^{-1}$), we conservatively assume our frequency scale to be accurate within 3 cm^{-1} . The photofragment signal is eventually measured as described in the previous paragraph as a function of the OPO frequency and during each scan, 16 laser shots are acquired and averaged per data point (employing digital oscilloscopes, Tektronix TDS 2022). The fragment ion intensity is normalized to the infrared intensity (thereby correcting for fluctuations in the infrared pulse energy). Several spectra are recorded on different days to ensure reproducibility and averaged to increase the signal-to-noise ratio.

2.5. Infrared predissociation spectroscopy and effects of Ar solvation

The investigation of molecular complexes in the gas phase prevents the application of classical absorption spectroscopy due to the low particle densities in the molecular beam. Usually, minimum analyte particle densities on the order of $> 10^{11} \text{ particles/cm}^3$ for bulk samples or $> 10^{14} \text{ particles/cm}^3$ for surface samples are required. These conditions allow for measuring the attenuation of the light beam passing through a sample and eventually the determination of the absorption cross section according to Lambert-Beer's law:

$$\frac{I_v}{I_0} = \exp\{-n \cdot \sigma_v \cdot l\} \quad (2.13)$$

However, typical particle densities in a molecular beam are on the order of $< 10^5 \text{ particles/cm}^3$ (and typically even considerably lower), thereby precluding this approach. Alternatively, instead of measuring the absorbance of the light beam before and after interacting with the particles under investigation, one can monitor the effect it exerts on the sample particles by registering their dissociation after photon

absorption. As described in section 2.3, this can be achieved by employing the action spectroscopy technique, based on monitoring the fragment ions resulting from the irradiation process as a function of the frequency of the infrared light. A sketch of the process leading to fragmentation is shown in Figure 2.5.

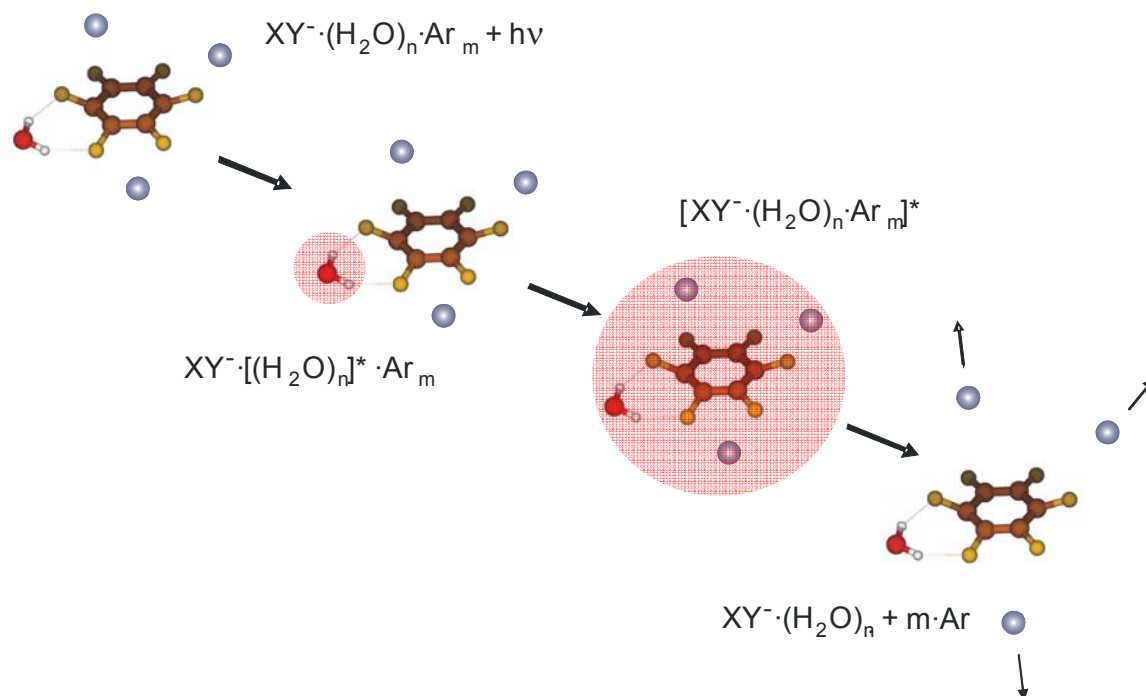
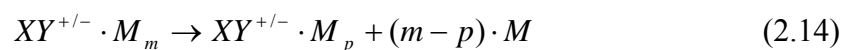


Figure 2.5 Schematic representation of the photodissociation process after vibrational excitation of the chromophore (represented here by the evaporation of the Ar atoms from the $C_6F_6^{\cdot-} \cdot H_2O \cdot Ar_3$ parent)

However, an intrinsic problem of the photodissociation approach is that it is only feasible if the absorption of one photon will lead to dissociation of the parent ion on the timescale of the experiment with (near) unit efficiency, which is often the case for molecular cluster targets and photon energies in the visible and ultraviolet region. However, even the non-covalent ion-molecule interactions considered in this work will often exceed the infrared photon energies used for excitation of fundamental vibrational transitions, which means that only cluster ions already containing a certain

amount of internal energy would be accessible for dissociation. One solution is to apply sequential absorption of several photons in order to reach the dissociation limit of the target ion.¹¹ However, this approach requires high intensity infrared light sources such as free electron lasers¹² which are not easily available. In addition, most information on the relative intensities of the observed spectral features is lost due to the nonlinearity of multi-photon processes. In order to circumvent these problems, the so-called messenger technique can be used, in which weakly bound “messenger” or “spy” atoms are attached to the complex of interest.^{9,13} This technique has been widely used in photodissociation experiments and relies on the evaporation of some or all messenger atoms upon irradiation of the chromophore (represented by the infrared active mode of the untagged ion-molecule complex which absorbs the photon):



This technique offers two advantages. First, the complexes under investigation are cold, since they necessarily have a low internal energy content due to the low binding energy of the messenger atom. As a result, one can hope that the Ar-tagged complexes are close to their equilibrium structures, which is important for meaningful comparison to the results of quantum chemical calculations. Moreover, table top laser systems can be used, as the complex fragments upon absorption of one photon. The non-covalent interaction with the weakly bound messenger atom will be broken as soon as the excitation energy is redistributed into a normal mode leading to dissociation. This intracuster or intermolecular redistribution of vibrational energy follows the mechanism of internal vibrational redistribution (IVR).¹⁴ Of course, it can be argued that the introduction of additional atoms into the cluster of interest might introduce new problems by perturbing its structure away from the equilibrium geometry of the bare species. This might pose experimental difficulties for studying cationic species,¹⁵ where the interaction between ion and messenger atom is not purely based on dispersion forces but is often also characterized by some amount of covalent contributions. This is usually only a minor effect in the investigation of

anionic complexes, due to the low interaction energies (typically on the order of a few hundred wavenumbers), and the influence of the messenger atom on the overall complex geometry is generally negligible. Suitable candidates for serving as messenger atoms, which have been frequently employed before, include nitrogen and rare gas atoms. Among the latter, Ar constitutes the most convenient species in many cases, as it is sufficiently weakly bound to the ion-molecule complex to leave the geometry essentially unperturbed but strong enough to achieve a sufficient abundance of Ar-tagged ions in the molecular beam to obtain good signal-to-noise ratios within reasonable data acquisition times. Moreover, it is chemically inert and has no rotational or vibrational degrees of freedom. Finally, it is monoisotopic, thereby simplifying the mass spectrometric analysis. Typical shifts in the vibrational spectra caused by Ar solvation lie within the range of 0 - 10 cm⁻¹/Ar atom. With an increasing number of Ar atoms attached to the ion-molecule complex under investigation, these shifts approach those seen in the infrared spectra of species trapped in cold Ar matrices, which can amount to several 10 cm⁻¹. They represent essentially the bulk analogue to the messenger technique or “Ar nanomatrix” approach in the gas phase.

2.6. References for Chapter II

- ¹ M. A. Johnson and W. C. Lineberger, in *Techniques for the Study of Gas-Phase Ion Molecule Reactions*, edited by J. M. Farrar and W. Saunders (Wiley, New York, 1988), pp. 591.
- ² C. E. Klots, *Journal of Chemical Physics* **83** (11), 5854 (1985).
- ³ W. H. Robertson, J. A. Kelley, and M. A. Johnson, *Review of Scientific Instruments* **71** (12), 4431 (2000).
- ⁴ R. Campargue, *Journal of Chemical Physics* **52** (4), 1795 (1970).
- ⁵ W. C. Wiley and I. H. McLaren, *Review of Scientific Instruments* **26** (12), 1150 (1955).
- ⁶ J. M. Weber, *Rev. Sci. Instrum.* **76**, 043301 (2005).
- ⁷ C. W. Stoermer, S. Gilb, J. Friedrich, D. Schooss, and M. M. Kappes, *Review of Scientific Instruments* **69** (4), 1661 (1998); R. Weinkauff, K. Walter, C. Weickhardt, U. Boesl, and E. W. Schlag, *Zeitschrift Fur Naturforschung Section a-a Journal of Physical Sciences* **44** (12), 1219 (1989).
- ⁸ U. Boesl, R. Weinkauff, and E. W. Schlag, *International Journal of Mass Spectrometry and Ion Processes* **112** (2-3), 121 (1992).
- ⁹ D. Schooss, S. Gilb, J. Kaller, M. M. Kappes, F. Furche, A. Köhn, K. May, and R. Ahlrichs, *Journal of Chemical Physics* **113** (13), 5361 (2000).
- ¹⁰ D. Schooss, Dissertation, Universität Karlsruhe (TH) (1999).
- ¹¹ R. C. Dunbar, *International Journal of Mass Spectrometry* **200** (1-3), 571 (2000); M. A. Duncan, *International Reviews in Physical Chemistry* **22** (2), 407 (2003); R. B. Metz, *International Reviews in Physical Chemistry* **23** (1), 79 (2004); J. Oomens, D. T. Moore, G. Meijer, and G. von Helden, *Physical Chemistry Chemical Physics* **6** (4), 710 (2004); B. Simard, S. Denomme, D. M. Rayner, D. van Heijnsbergen, G. Meijer, and G. von Helden, *Chemical Physics Letters* **357** (3-4), 195 (2002); J. Oomens, B. G. Sartakov, G. Meijer, and G. Von Helden, *International Journal of Mass Spectrometry* **254** (1-2), 1 (2006).
- ¹² D. Oepts, A. F. G. Vandermeer, and P. W. Vanamersfoort, *Infrared Physics & Technology* **36** (1), 297 (1995).

- ¹³ P. Ayotte, G. H. Weddle, J. Kim, and M. A. Johnson, *Chemical Physics* **239** (1-3), 485 (1998); B. A. Collings, K. Athanassenas, D. Lacombe, D. M. Rayner, and P. A. Hackett, *Journal of Chemical Physics* **101** (5), 3506 (1994); F. Federmann, K. Hoffmann, N. Quaas, and J. P. Toennies, *European Physical Journal D* **9** (1-4), 11 (1999); A. Terasaki, S. Minemoto, M. Iseda, and T. Kondow, *European Physical Journal D* **9** (1-4), 163 (1999); T. Diederich, J. Tiggesbäumker, and K. H. Meiwes-Broer, *Journal of Chemical Physics* **116** (8), 3263 (2002); S. Grebenev, E. Lugovoi, B. G. Sartakov, J. P. Toennies, and A. F. Vilesov, *Faraday Discussions* **118**, 19 (2001); J. M. Lisy, *Journal of Chemical Physics* **125** (13) (2006).
- ¹⁴ F. F. Crim, *Annual Review of Physical Chemistry* **44**, 397 (1993); D. J. Nesbitt and R. W. Field, *Journal of Physical Chemistry* **100** (31), 12735 (1996); C. G. Elles and F. F. Crim, *Annual Review of Physical Chemistry* **57**, 273 (2006).
- ¹⁵ N. Solca and O. Dopfer, *Chemical Physics Letters* **325** (4), 354 (2000); R. V. Olkhov, S. A. Nizkorodov, and O. Dopfer, *Journal of Chemical Physics* **108** (24), 10046 (1998).

3. Anion Hydration

3.1. *General background*

3.1.1. Condensed phase experiments

The structure of the hydration shell of ions has long been of interest, as its understanding on a molecular level is of crucial importance in chemistry. Early work on the hydration of ions in the condensed phase already yielded important results. Neutron diffraction studies showed that water binds to cations via the oxygen atom while simple anions like the chloride anion are bound in an asymmetric motif, with one hydrogen atom being involved in a strong hydrogen bond to the anion (therefore called ionic H-bonded (IHB) OH group) while the other one points away.¹ As a consequence, water molecules in the solvation shell around a cation tend to avoid each other, while the water ligands grouped around an anion are able to form a delicate binding network, as the free hydrogen atom can be tethered to neighboring water ligands in hydrogen bonds. In addition to these fundamental insights into the basic solvation behavior of ions in the liquid phase, it was possible to unveil some of the infrared signatures of this asymmetric binding motif (displayed e.g. by the halide ions) by investigating the infrared spectra of dilute frozen electrolytes.² It could be shown that a unique band characteristic for the H-bonded OH stretch vibration exists, red shifted more than 100 cm^{-1} as compared to the pure solvent spectrum. Unfortunately, it was neither possible to infer any additional features from the spectrum nor could the method be used to elucidate the structure of a hydration shell around an ion, thereby demonstrating some of the major limitations of condensed phase experiments, where fluctuations in the solvation shell and the bulk water molecules not coordinated to ions tend to mask the spectroscopic signature of the interaction between the solvated ions and their surrounding ligands. Experimentally, this leads to broad, unresolved spectra which cannot be used to obtain any information about subtle details like hydration shells, at least for linear spectroscopy

methods. This is demonstrated by the broad infrared signatures of the OH stretch vibrations in bulk liquid water.³ These problems can be circumvented by the cluster approach in gas phase experiments, which allows mass selection of specific cluster sizes and permits building up a hydration shell around an ion one solvent molecule at a time while obtaining detailed spectroscopic information on the respective structures.

3.1.2. Infrared spectroscopy and binding motifs of $X^-(H_2O)_n$ clusters

As described above, infrared spectroscopy of clusters constitutes an ideal tool to gain the desired structural information, since the OH stretching vibrations are highly sensitive to the interactions both between the solvated ion and the surrounding water molecules and between the water ligands themselves. The focus of the investigations presented in this work is on the hydration of anions, which is multifaceted and whose details are still not completely understood due to the interplay of water bonding motifs to the anion and the other water ligands.

3.1.2.1. The binary complex $X^-\cdot H_2O$

The interaction and binding motifs of atomic and small molecular anions and single water molecules has been thoroughly investigated and is now fairly well understood. Complexes of an atomic anion (such as the halides) and a water ligand adopt a binding motif which has C_s symmetry and is referred to as the “single ionic H bond” (SIHB) motif shown in Figure 3.1 (A).⁴⁻⁹ In this structure, one strong hydrogen bond is formed between one of the OH groups of the water molecule and the anion, while the second OH group points away from the anion and is essentially a free OH group.

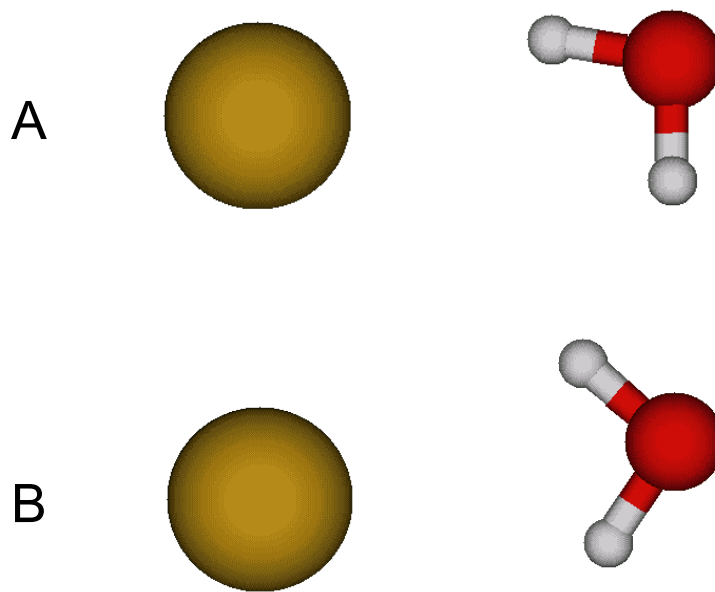


Figure 3.1 Typical binding motifs found for anions in a complex with a water molecule; A – SIHB motif (single ionic hydrogen bond); B – DIHB motif (double ionic hydrogen bond)

As a result of this symmetry lowering compared to the free water molecule (C_{2v}), the two OH oscillators are decoupled. The symmetric stretching mode of the free water molecule develops into an intense band in the IR spectrum, characterized predominantly by the motion of the OH group involved in the hydrogen bond to the anion and giving rise to a red shift of up to several hundred wavenumbers in comparison to the centroid of the symmetric and antisymmetric stretch vibrations of bare water (3707 cm^{-1}). It is therefore generally referred to as the IHB band (“ionic H bond”). The antisymmetric stretching mode evolves into a weak band dominated by the motion of the free OH group, which shows up in the IR spectrum around the position of the average of the symmetric and antisymmetric stretching vibrations of bare water (3707 cm^{-1}). It is named for this reason F band (“free”). The spectra and vibrational signatures of the binary halide-water clusters have been extensively studied, both experimentally^{7,8} and theoretically,^{4,10} and it is instructive to take a closer look at some of these results. Figure 3.2 shows the IR spectra of the $X\cdot\text{H}_2\text{O}\cdot\text{Ar}_n$ ($X = \text{F}, \text{Cl}, \text{Br}, \text{I}$) clusters as taken from Ref.⁹

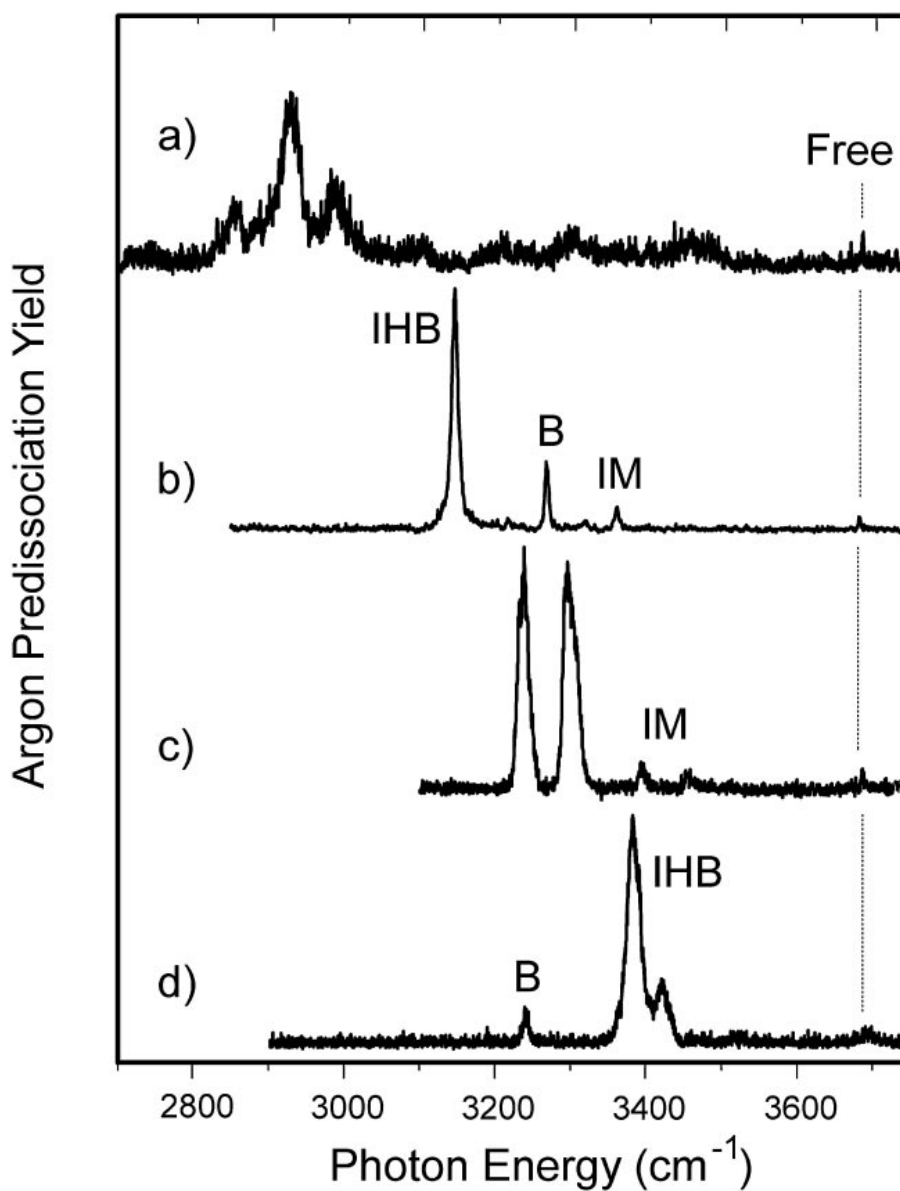


Figure 3.2 Ar predissociation spectra as taken from Ref.⁹; (a) $F^- \cdot H_2O \cdot Ar_2$, (b) $Cl^- \cdot H_2O \cdot Ar_{11}$, (c) $Br^- \cdot H_2O \cdot Ar_3$ and (d) $I^- \cdot H_2O \cdot Ar_3$; Free – OH not involved in a hydrogen bond, IHB – ionic H bond, B – overtone of the water intramolecular bending mode, IM – combination band involving the ion-water intermolecular stretching vibration

In the case of the $I^- \cdot H_2O$ and the $Cl^- \cdot H_2O$ the features discussed above can be clearly recognized: There is a weak band around 3700 cm^{-1} , which is the signature of the F band and an intense, strongly red-shifted IHB band. The red shift of this band

increases with the proton affinity of the anion,¹¹ leading to an increasingly elongated OH_{IHB} bond and to a more pronounced anharmonicity of the OH stretching potential. Moreover, both spectra display an additional band denoted as “B”, which is attributed to the overtone of the water intramolecular bending mode, gaining intensity through a Fermi resonance with the strong IHB band. Interestingly, in the spectrum of the $\text{Br}^- \cdot \text{H}_2\text{O}$ complex a strong doublet appears instead of the IHB band. This can be attributed to the same Fermi resonance (matrix element for the interaction is about 30 cm^{-1} in this case⁷), as the frequency of the IHB band is tuned to lower wavenumbers going from Cl^- to I^- and coincides with the position of the unperturbed bend overtone for Br^- . Finally, there is an additional weak band denoted as “IM”, which stems from a combination band of the IHB band with the ion-molecule stretch vibration. The spectrum of the $\text{F}^- \cdot \text{H}_2\text{O}$ complex falls out of this scheme, as the red shift of the IHB band is so strong that only the $2 \leftarrow 0$ overtone can be recorded in the energy range shown in Figure 3.2. This can be rationalized based on the high proton affinity of the F^- anion, which leads to a low-lying proton transfer channel showing up as a distinct shelf in the potential energy surface along the hydrogen displacement coordinate.^{9,12} While this shelf is much less pronounced for the heavier halides and lies comparatively high in energy, in the case of $\text{F}^- \cdot \text{H}_2\text{O}$ it can be explored already by the first overtone of the OH stretching vibration, leading effectively to the complex sampling the proton transfer region of the potential energy surface following the $1 \leftarrow 0$ excitation. This is even more pronounced to the point of delocalizing the proton between “donor” and “acceptor” if the proton affinity of the two corresponding bases is exactly the same such as in the $\text{OH}^- \cdot \text{H}_2\text{O}$ system.¹³ It has been shown that it is crucial to include charge-transfer from the anion to the OH stretch antibonding orbital in order to arrive at models which describe the observed red shifts accurately,¹⁴ and in line with the experimental findings outlined above it was found that the importance of charge transfer decreases on moving down the group of halogens ($\text{F} > \text{Cl} > \text{Br} > \text{I}$).¹⁴ Qualitative trends, however, can be understood on the basis of the electrostatic effects involved.¹⁵ In anions where the negative charge is delocalized over several centers, a water molecule can form two hydrogen bonds to the ion, a binding motif which is therefore referred to as DIHB motif (“double ionic H

bond”, see Figure 3.1 (B)). A class of molecules in which this motif frequently occurs are anions where the negative charge is distributed over triatomic domains, such as in CH_3NO_2^- , or if the anion itself is triatomic, as is the case for SO_2^- (Ref.¹⁶) or OCS^- (Ref.¹¹), therefore offering a template for docking a water ligand via two hydrogen bonds. This binding motif is only avoided if the DIHB geometry puts too much strain on the water molecule. For this reason, NO_2^- shows a SIHB motif:¹¹ due to the shorter distance between the oxygen atoms the bending angle of the water ligand would have to be lowered significantly, which makes the DIHB motif energetically unfavorable. Since the symmetry of the water molecule (C_{2v}) is at least approximately conserved in the DIHB motif, the IR spectra of the respective complexes are expected to show the same vibrational signatures as the bare water molecule itself, namely a symmetric (ν_s) and an antisymmetric (ν_{as}) OH stretching mode. The former is usually more intense and the splitting between the two is often somewhat smaller than in free water ($\sim 99 \text{ cm}^{-1}$). Both of them are red shifted as compared to their positions in free water due to the hydrogen bonding interaction, but to a considerably lesser extent than the IHB band in the case of the complexes displaying an SIHB binding motif. However, the red shift of the bands involved in the hydrogen bonding increases in both cases with the proton affinity of the anion. The signatures discussed above are observed experimentally e.g. for the $\text{SO}_2^- \cdot \text{H}_2\text{O}$ complex.¹⁶

3.1.2.2. Higher solvation levels: $\text{X}^-(\text{H}_2\text{O})_n$ clusters

An increase of the number of water molecules solvating the core anion raises new complications, as not only the binding motifs between the anion and its water ligands have to be considered, but also the interactions of the water molecules with each other will be of crucial importance for determining the overall structural motif. An interesting question, which arises with increasing cluster size in that context is whether the anions are eventually bound to the surface of a water cluster via hydrogen bonds (“surface solvated”), or if they reside inside such a cluster (“internal solvation”).¹⁷ This depends very much on the chemical nature of the respective anion. Considering the halide anions again as prototypes for the hydration of small atomic

anions, increasing the degree of solvation to two water molecules surrounding the respective anion leads to the observation of the binding motifs^{18,19} and vibrational spectra displayed in Figure 3.3 (taken from Ref.⁹).

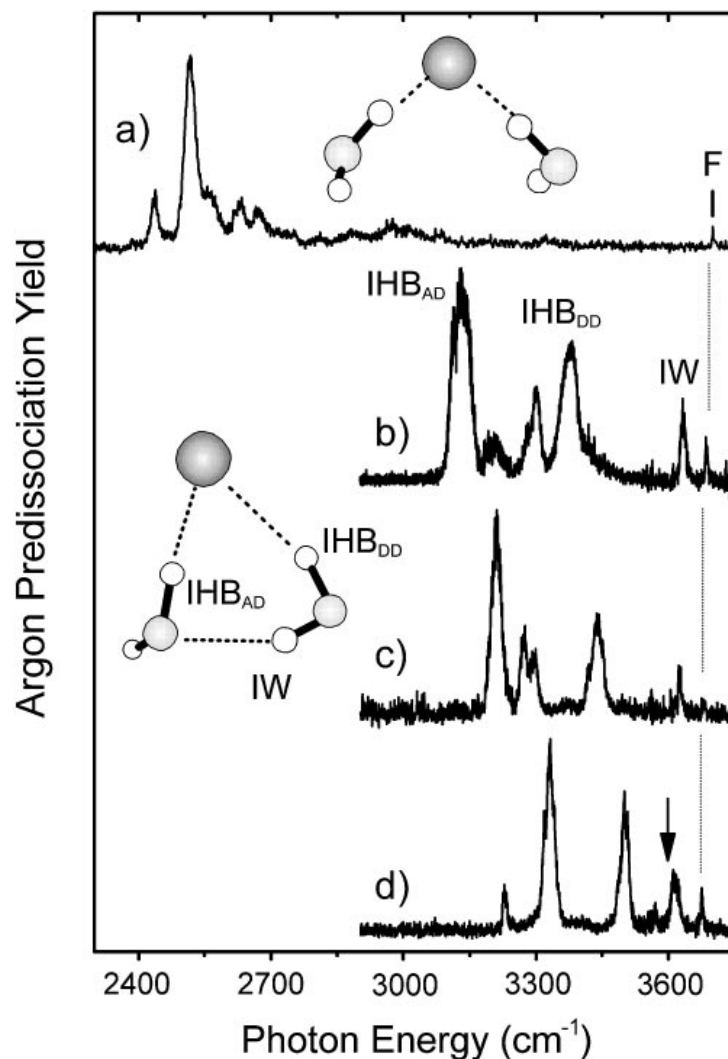


Figure 3.3 Spectra of $X^{\cdot-}(\text{H}_2\text{O})_2$ clusters as taken from Ref.⁹; (a) $\text{F}^{\cdot-}(\text{H}_2\text{O})_2\cdot\text{Ar}_3$ (structure shown in inset) (b) $\text{Cl}^{\cdot-}(\text{H}_2\text{O})_2\cdot\text{Ar}_3$ (c) $\text{Br}^{\cdot-}(\text{H}_2\text{O})_2\cdot\text{Ar}_3$ (d) $\text{I}^{\cdot-}(\text{H}_2\text{O})_2\cdot\text{Ar}_3$ (structure of species (b) – (d) depicted in inset); arrow: position of H bonded OH stretch in the neutral water dimer, F – position of free OH stretch; IHB_{AD} – ionic H bond of a water molecule acting as a hydrogen bond donor to the ion and acceptor to the neighboring water; IHB_{DD} – ionic H bond of a water molecule acting as a hydrogen bond donor to both the ion and the neighboring water; IW – signature of the OH stretch involved in the hydrogen bond between the two water molecules

The $X^-(H_2O)_2$ ($X = Cl, Br, I$) clusters adopt an asymmetric geometry, where the anion is bound to a water dimer via one hydrogen bond to each water molecule. The remaining OH group of one of the water ligands (referred to as “DD” for “double-donor”) is involved in the hydrogen bonding interaction with the second water molecule. The hydrogen bond of this ligand to the ion is therefore weaker than for a single water molecule in the ion-water complex. The second OH group of the other water ligand is essentially free. It is referred to as “AD” (“acceptor-donor”). The oxygen atom of this water molecule serves as a docking point for the hydrogen atom of the interwater hydrogen bond and a small part of its electron density is shifted into the antibonding orbital of the corresponding OH bond. This leads in turn to a strengthening of the hydrogen bond of the AD water molecule to the anion. Overall, this geometry can be viewed as a “surface solvated” anion. The binding motif gives rise to a four-band spectral pattern which can be interpreted based on the spectra of the monohydrates, taking the cooperative effects in the hydrogen bonding interactions just described into account. The most red shifted IHB band and the F band (compare Figure 3.3) can be attributed to the water molecule which serves as an acceptor for the hydrogen from the neighboring water (IHB_{AD}), while a second less red shifted IHB band is the signature of the OH stretching mode involved in the hydrogen bond of the second water molecule in the ion. The band marked as “IW” (for “interwater”) in Figure 3.3 is assigned to the stretching mode of the OH group involved in the interwater hydrogen bond, as its position is close to the hydrogen bonded OH stretching mode in the neutral water dimer.²⁰ Finally, the F band marks the signature of the dangling OH group of the AD water ligand. Obviously, for these ion-water complexes, the formation of an interwater hydrogen bond energetically outweighs the loss in linearity in the hydrogen bonding to the anion, which is a consequence of the formation of the water dimer. However, if the interaction strength between anion and water ligands is increased, it is expected that the formation of the most favorable (i.e. linear) hydrogen bond between anion and ligands prevails over the formation of interwater networks, leading to a cluster geometry which can be described as “internally solvated”. Interestingly, the spectral position of the IW band is slightly blue shifted with increasing proton affinity of the anion, showing that the

intermolecular water-water interaction is reduced as the binding interaction to the anion becomes stronger. The vibrational spectrum of the fluoride dihydrate (Figure 3.3) differs completely from the spectra of the other halide water clusters described so far, which means that the local environment of the two water molecules must be different in that case. This can be rationalized in view of the higher proton affinity of the fluorine anion, leading to a strong enough hydrogen bonding interaction to its water ligands to break the interwater hydrogen bond. The spectrum shows a strong, red shifted IHB band (which falls into the energy range displayed in Figure 3.3 in contrast to the IHB signature in the fluoride monohydrate, since the red shift of the bands decreases with an increasing number of ligands). The F band is present as well, while there is no signature in the spectral region where the IW band would be expected. Thus, the fluoride anion is the only halide anion which can be viewed as “internally solvated”, but the same is true for other anions exhibiting a strong hydrogen bond to their water ligands, such as the $\text{OH}^{\cdot}(\text{H}_2\text{O})_2$ system.²¹ However, the formation of hydrogen bonding interactions between the water ligands upon addition of a second water molecule has been found to take place in the hydration of most anions and even for extended charge distributions, such as the naphthalene anion.²² It is worth noting that the most important features described for the $\text{X}^{\cdot}(\text{H}_2\text{O})_2$ systems are also observed upon increasing the degree of hydration further to the trihydrates.²³ While the fluoride anion in the $\text{F}^{\cdot}(\text{H}_2\text{O})_3$ cluster (as well as the hydroxide anion in $\text{OH}^{\cdot}(\text{H}_2\text{O})_3$) still binds every water ligand via a single hydrogen bond (internal solvation),^{21,24} all heavier halides display geometries where the water molecules form hydrogen bonds among each other (surface solvation) (see Ref.⁹ and references therein). In the IR spectrum, this motif can again be recognized by the signature of the OH stretches involved in the intermolecular water bonds. They form “ring modes” similar to $(\text{H}_2\text{O})_3$ ²⁰ for the $\text{X}^{\cdot}(\text{H}_2\text{O})_3$ clusters ($\text{X} = \text{Cl}, \text{Br}, \text{I}$) and result from the highly symmetric motif these systems adopt. Each water molecule is involved in one H bond to its neighbor and another one to the anion. The formation of intermolecular hydrogen bonds for the trihydrates has been found also for anions, which exhibit a DIHB motif for the monohydrate such as $\text{Cl}_2^{\cdot}(\text{H}_2\text{O})_n$.²⁵ For the internally solvated

anions, it takes up to four ($\text{OH}^{\cdot}(\text{H}_2\text{O})_n$) and five ($\text{F}^{\cdot}(\text{H}_2\text{O})_n$) water ligands,²¹ respectively, before the onset of water network formation is observed.

Despite these well-established results on the hydration of atomic and small molecular anions, not much is known about the binding behavior between water molecules and larger anions, where the negative charge is not necessarily localized in a well defined place but can be smeared out over the whole molecule. One exception is a pioneering paper on the hydration of naphthalene.²² Also, there is not much information about complexes of negatively charged metal atoms with water, although there is some experimental and theoretical work on $\text{Cu}^{\cdot}\text{H}_2\text{O}$ ²⁶⁻²⁹ and $\text{Au}^{\cdot}\text{H}_2\text{O}$.²⁶ In the present work, we studied the hydration of the coinage metal anions with one water ligand. Moreover, we investigated the $\text{C}_6\text{F}_{6-n}\text{H}_n^{\cdot}(\text{H}_2\text{O})_m$ ($n = 0 - 2$, $m = 1,2$) and $\text{SF}_6^{\cdot}(\text{H}_2\text{O})_m$ ($m = 1 - 3$) complexes as prototypes for the hydration of more extended charge distributions.

3.2. Binary complexes of coinage metal anions with water

3.2.1. Introduction

There has been great interest in studying the intrinsic interaction of metal ions with their environment, due to the crucial role they play in catalytic processes in chemistry. While most infrared investigations in the gas phase have been performed on metal cations with various ligands,³⁰ negatively charged supported metallic clusters have been proven to be catalytically active as well.^{31,32} Especially gold has received a lot of attention^{33,34} and it was shown that small gold clusters are catalytically active if deposited on defect sites on metallic surfaces.^{32,34,35} In this context, it is interesting to gain some deeper insight into the interaction behavior of metal anions with their chemical environment. Therefore, we performed an infrared spectroscopy study of the coinage metal anions in a complex with one water ligand. In light of the above discussion, $M \cdot H_2O$ complexes ($M = Au, Ag, Cu$) are expected to show a similar hydration behavior as the halide anions, as they also constitute closed-shell, atomic anions. The elucidation of their properties has triggered a growing number of computational and experimental studies, the latter mainly employing photoelectron spectroscopy (including imaging techniques and time-resolved experiments).^{26,28,29,36,37} The similarity of their structural motifs to the halide-water complexes has been supported by calculations carried out employing second-order Møller-Plesset perturbation theory (MP2) and density functional theory²⁶ (DFT, with a B3-LYP functional). However, recent investigations of the $Cu \cdot H_2O$ complex^{28,37} have shown that the situation might be more complicated: although the minimum energy structure displays the expected SIHB motif (C_s symmetry), the barrier corresponding to the C_{2v} transition state between the two equivalent C_s structures along the potential energy surface lies rather low in energy (0.02 eV²⁸), challenging the idea of the robust SIHB motif found for the halide-water clusters. Moreover, earlier theoretical investigations have suggested a C_{2v} minimum energy structure for the $Cu \cdot H_2O$ complex.²⁷ Infrared spectra in combination with high level quantum

chemical calculations are ideally suited to resolve the issue of the hydration motif in the $M^{\cdot-}\cdot H_2O$ complexes.

3.2.2. Calculations

Two routes have been applied to elucidate the structural motifs and the vibrational signatures of the species under consideration. First, structure optimizations have been performed using density-functional theory³⁸ (DFT) on the B3-LYP level³⁹ with TZVPP basis sets for all atoms,⁴⁰ as implemented in the TURBOMOLE program suite.⁴¹ On top of that, higher-level calculations have been carried out by Boese *et al.*⁴² on both a DFT/B97-1 and a CCSD(T) level of theory. The anharmonicity of the potential energy curves has been accounted for in these calculations in order to get an improved description of the vibrational patterns found experimentally and to include effects anharmonic in nature, such as Fermi resonances. The computational details can be found in Ref.⁴² (and references therein). The findings of the calculations are summarized in Table 3.1 (energetic and geometric properties of the respective structures of the complexes) and Table 3.2 (vibrational frequencies) and discussed in comparison to the experimental results in the following section.

3.2.3. Results and discussion

The mid-infrared spectra of the $M^{\cdot-}\cdot H_2O\cdot Ar_2$ clusters, recorded via the loss of two Ar atoms are presented in Figure 3.4.⁴² The $Au^{\cdot-}\cdot H_2O$ complex displays a spectrum which is reminiscent of the SIHB motif of the heavier halide-water systems described in the preceding section. An intense, strongly red-shifted band (IHB band, evolved from the symmetric stretching mode of the free water molecule, ν_s) around 3145 cm^{-1} is the signature of the OH group involved in the hydrogen bond between metal anion and water ligand. It is accompanied at higher energies by a band which can be assigned to the bending mode overtone gaining intensity through a Fermi resonance with the IHB band. Both of them form combination bands $\sim 150\text{ cm}^{-1}$ higher in energy involving

the ion-water intermolecular stretch vibration, which even resemble the line shapes of the “parent” bands (IHB and B respectively, see Figure 3.4) they build on.

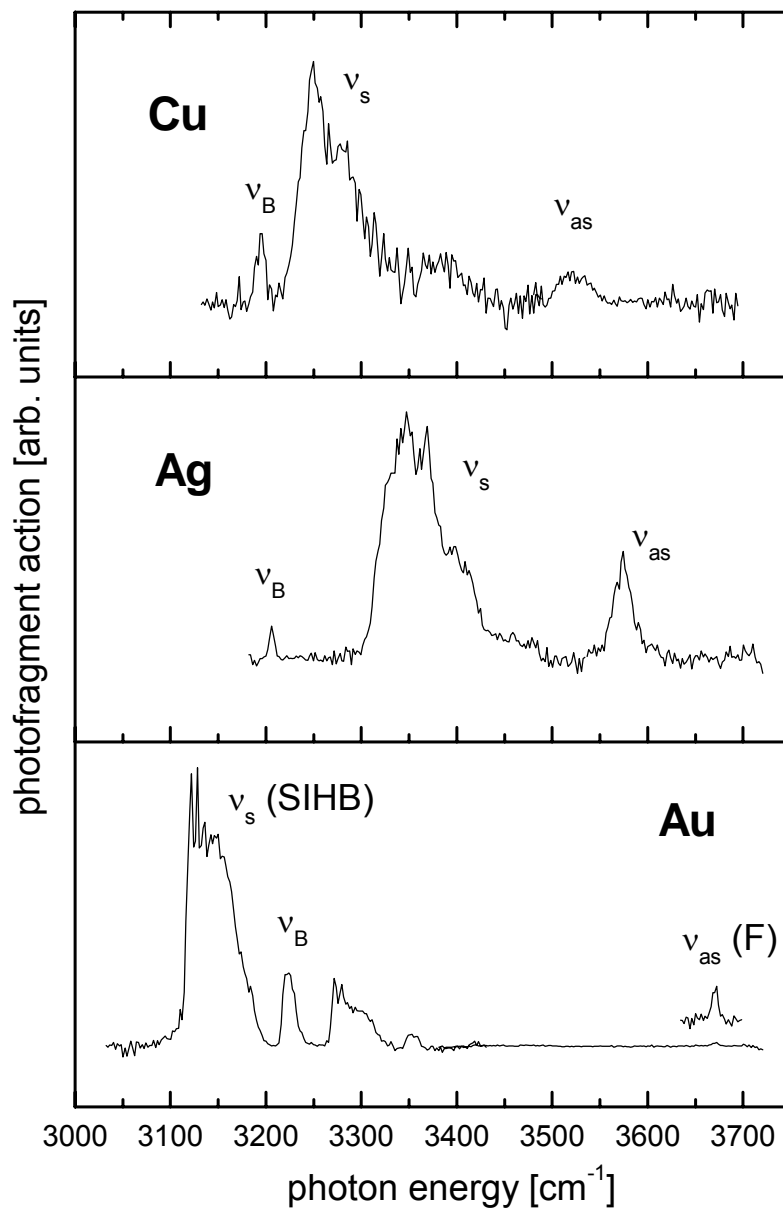


Figure 3.4 Infrared spectra of the $M \cdot (H_2O)$ complexes ($M = Cu, Ag, Au$; see inset of respective spectra); ν_B – bending overtone, ν_s – symmetric OH stretching mode; ν_{as} – antisymmetric OH stretching mode; (IHB – IHB band; F – (quasi) free OH stretch, see Figure 3.2)

The final proof that the structural motif is indeed of C_s symmetry is delivered by the weak band at 3671 cm^{-1} , which is the signature of the free OH oscillator (F band, evolved from the antisymmetric stretching mode of the free water molecule, ν_{as}). However, the situation is less clear in the case of the $\text{Ag}^-\cdot\text{H}_2\text{O}$ and the $\text{Cu}^-\cdot\text{H}_2\text{O}$ complexes, although both of them do display an intense symmetric stretching band and an antisymmetric stretching band, similar to the $\text{Au}^-\cdot\text{H}_2\text{O}$ complex. It is instructive at this point to put these findings into context with the well-understood behavior of the halide-water complexes, where it has been established that the red shift of the IHB band increases monotonically with the proton affinities of the respective anions. This is due to the increased stretching of the OH bond involved in the hydrogen bonding interaction, as the proton transfer channel is lowered progressively in energy.¹¹ Interestingly, the red shift of the symmetric stretching band of the anionic silver and copper complexes (situated at 3366 cm^{-1} for $\text{Ag}^-\cdot\text{H}_2\text{O}$ and at 3271 cm^{-1} for $\text{Cu}^-\cdot\text{H}_2\text{O}$, respectively) is much less pronounced than for the gold anion-water complex (displaying a clear, strongly red shifted IHB band). However, the proton affinity of the anions increases from gold to copper, which should lead to the opposite behavior (within the same binding motif, see Figure 3.5). In contrast, the position of the feature identified as antisymmetric stretching mode (3575 cm^{-1} for $\text{Ag}^-\cdot\text{H}_2\text{O}$ and 3520 cm^{-1} for $\text{Cu}^-\cdot\text{H}_2\text{O}$, respectively) is considerably more red shifted and intense than should be the case for a clear-cut SIHB motif, and it was not possible to find any spectral feature above 3600 cm^{-1} , where the F band would be expected to show up in such a case. This demonstrates that the two OH groups cannot be considered to be completely uncoupled in the copper and silver complex. The red shifts of the IHB bands of some known water-anion complexes against the proton affinities of the respective anions are shown in Figure 3.5.^{11,43} It can be seen that the anionic gold water complex is positioned along the line connecting complexes with an SIHB motif, further corroborating its structural assignment.

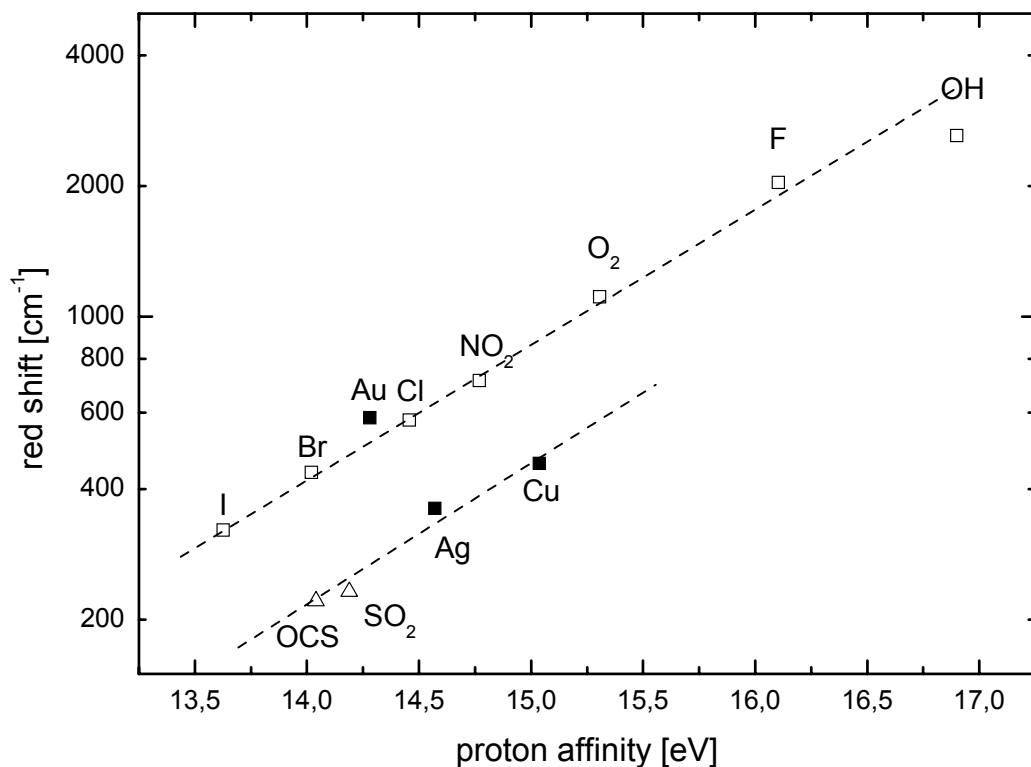


Figure 3.5 IHB band positions for the known anion-water complexes as a function of the proton affinities of the ions (from Ref.^{11,43}); open squares – known SIHB complexes; open triangles – known DIHB complexes; full squares – coinage metal-water complexes; in the case of (suspected) DIHB configurations the lower energy (i.e. symmetric stretch) IHB band is listed

In contrast, Ag^- and Cu^- fall onto a line with anions binding the water ligand in a DIHB motif, pointing towards the earlier theoretical findings which ascribed C_{2v} symmetry at least to the $\text{Cu}^- \cdot \text{H}_2\text{O}$ complex.²⁷ At this point, it is instructive to compare the experimental findings discussed so far to the results of the calculations. They are summarized in Table 3.1 for the different structural motifs and their energetic and geometric properties.

Table 3.1 Theoretical results for some of the energetic and geometric properties of the $M \cdot H_2O$ complexes ($M = Au, Ag, Cu$)

Metal	Symmetry	B3-LYP TZVPP ^a (E_{rel} / meV)	CCSD(T) pVQZ/ MCDF ^a (E_{rel} / meV)	Binding energy ^b (eV)	Angle M-H-O ^b (°)	Angle H-O-H ^b (°)	M-H distance (pm)
Au	C_S	0 (0)	0 (0)	0.539	160	100	245, 346
	C_{2v}	29 (24)	30 (42)	0.509	116	97	285
Ag	C_S	0 (0)	0 (0)	0.448	146	100	268, 342
	C_{2v}	6 (0)	5 (16)	0.443	116	98	298
Cu	C_S	0 (0)	0 (0)	0.489	151	100	241, 329
	C_{2v}	7 (7)	10 (17)	0.479	116	98	274

^aValues in parentheses are zero-point corrected (harmonically for the B3-LYP results and anharmonically (CCSD(T) + B97-1) for the CCSD(T) results)

^bCalculated using CCSD(T)/pVQZ/MCDF

It can be seen that on all levels of theory the C_S symmetry motif is calculated to be the minimum, in line with earlier theoretical results^{26,28} and showing that none of the three complexes under consideration displays a DIHB motif (C_{2v} symmetry). However, the energy barrier between the C_S and the C_{2v} geometries turns out to be low compared to e.g. the $Cl \cdot H_2O$ complex ($\sim 56 \text{ meV}^4$), which displays a clear-cut SIHB motif, especially for the $Ag \cdot H_2O$ (16 meV on a zero-point corrected CCSD(T) level) and the $Cu \cdot H_2O$ complex (17 meV, same level of theory), while it is higher for $Au \cdot H_2O$ (42 meV). The barrier between the two equivalent C_S binding motifs has been determined for the $Cu \cdot H_2O$ complex before to 20 meV, which compares reasonably well with the value presented above.²⁸ The situation is visualized in Figure 3.6, where the potential energy curves of the three $M \cdot H_2O$ complexes are plotted against the M-H-O angle (again employing CCSD(T), but without taking zero-point corrections into account).

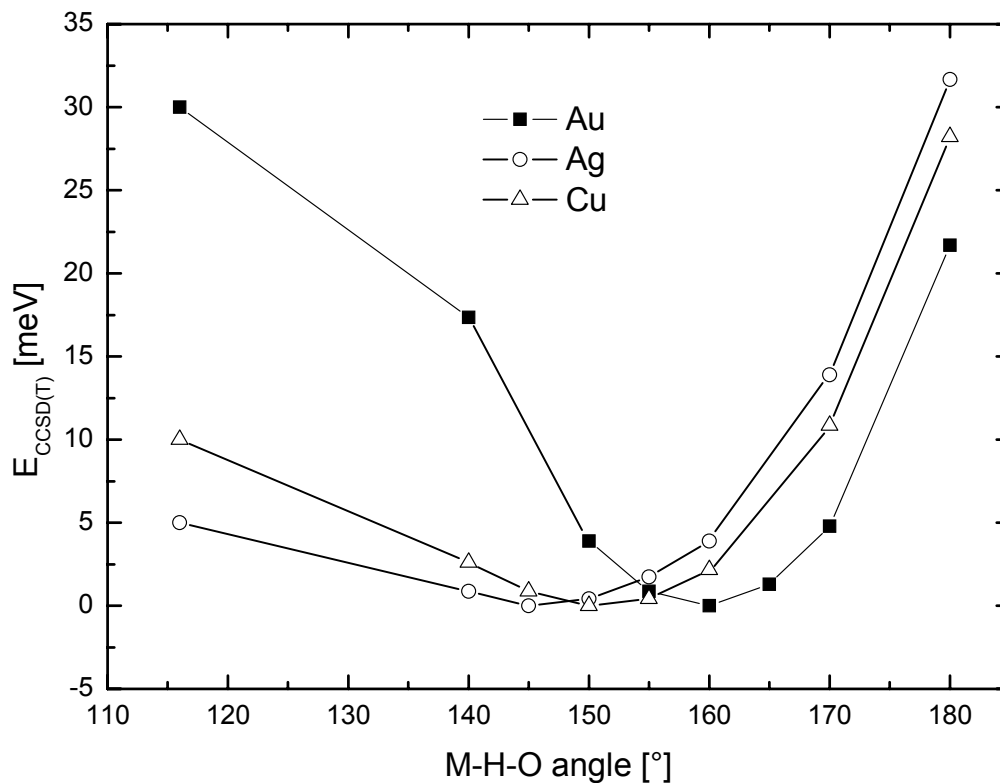


Figure 3.6 Calculated potential energy curves (CCSD(T) without zero-point corrections) from Ref.⁴² for the $M \cdot H_2O$ complexes ($M = Au, Ag, Cu$, see inset) along the M-H-O angle

While all calculated curves show a minimum for the singly hydrogen bonded C_s structure, $Au \cdot H_2O$ is the only case for which the two minima seem to be separated by a substantial barrier, indicating the possibility of a robust SIHB motif. In contrast, the positions of the minima are at smaller angles and the barrier between them is low for $Ag \cdot H_2O$ and $Cu \cdot H_2O$, leading to a very shallow potential. As a consequence, the wave function of the zero-point motion of these species has its maximum value close to the transition state. The frequencies of the OH stretching bands, as calculated for all complexes and symmetry species under consideration, are summarized in Table 3.2, together with the experimentally determined values.

Table 3.2 Experimental and calculated IR band positions of the $M \cdot H_2O$ complexes (M = Au, Ag, Cu)

Metal	Experimental OH stretching bands (cm^{-1}) ^a	Redshift per Ar atom (cm^{-1})	Extrapolated bands for bare complex (cm^{-1})	Symmetry	IHB and F frequencies	
					Harmonic ^b (cm^{-1})	Anharmonic ^c (cm^{-1})
Au	3144, 3671	19, N/A ^d	3182, N/A ^d	C _S	3241, 3659	3199, ^e 3681
				C _{2v}	3561, 3594	3552, ^e 3549
Ag	3366, 3575	33, 7	3432, 3589	C _S	3358, 3624	3253, ^e 3647
				C _{2v}	3560, 3597	3544, ^e 3556
Cu	3271, 3520	22, 12	3315, 3544	C _S	3285, 3616	3146, ^e 3661
				C _{2v}	3517, 3552	3525, ^e 3530

^aCentroids as measured for $M \cdot H_2O \cdot Ar_2$

^bCalculated using DFT (B3-LYP//TZVPP), frequencies have been scaled by 0.9476 (C_S) and 0.9602 (C_{2v}) to account for anharmonicity and match the known IHB frequency in free H₂O molecules, respectively

^cCalculated using CCSD(T)/DFT (CCSD(T)//cc-pVQZ/MCDF and B97-1//aug-pc-2/MWB)

^dF band not measured

^eBand affected by Fermi resonance

Clearly, for $Au \cdot H_2O$ there is a reasonably good agreement between theory and experiment for the anharmonic frequency values based on the SIHB binding motif (C_S symmetry), supporting the earlier assumptions and proving that this species behaves in an analogous way to the halide-water complexes. Unfortunately, the situation is less clear for the other two complexes: For both $Cu \cdot H_2O$ and $Ag \cdot H_2O$ none of the frequency pairs determined for either of the two possible “robust” binding motifs are in satisfactory agreement with the experimental values. Therefore, it seems to be the case that neither of the two motifs (DIHB or SIHB) truly represents the actual structure of these complexes. Their zero-point motion samples different geometries, also exploring structures towards the C_{2v} transition state geometry, in the

vicinity of which the ground state wave function probably has its maximum. The situation may be best described as a dynamic DIHB motif with two different hydrogen bonds. Compared to a clear-cut SIHB motif, the OH stretching modes in the $\text{Cu}^-\cdot\text{H}_2\text{O}$ and $\text{Ag}^-\cdot\text{H}_2\text{O}$ complexes will come closer in energy, as the formerly strong ionic hydrogen bond is weakened by substantial deviation from the linear hydrogen bonding configuration (shifting the lower energy band to the blue), while the formerly free OH group is bound to the ion (shifting its oscillation frequency to the red). This situation is reflected in the recorded mid-infrared spectra⁴² shown in Figure 3.4, as has been outlined before. In a situation characterized by such shallow potential energy surfaces, the influence of the Ar messenger atoms on the binding motif is expected to increase as compared to a clear-cut SIHB or DIHB case. The binding energy of an Ar atom to e.g. Cl^- is $\sim 523 \text{ cm}^{-1}$,⁴⁴ which means it could possibly exceed the barrier height for all three complexes, assuming the dissociation energy of the $\text{M}\cdot\text{Ar}$ ($\text{M} = \text{Au}, \text{Ag}, \text{Cu}$) lies in a similar range. It does not seem unlikely therefore that the attachment of Ar atoms has a profound influence on the structural motifs. This problem has been tackled by recording the spectra of the systems of interest with a varying degree of Ar solvation. The spectra of the bare complexes are inaccessible in the experiment, as the binding energies of Au^- , Ag^- and Cu^- to a water molecule amount to 616 meV, 636 meV and 894 meV,²⁶ above the available mid-infrared excitation energies. Only hot complexes already carrying a significant amount of internal energy prior to excitation could be probed that way, which would not be representative for the ground state minimum structures one is interested in. However, it is possible to record the spectra for different levels of Ar solvation, enabling extrapolation to the properties of the bare systems. All bands are red shifted upon addition of the second Ar atom, with the red shifts being more pronounced for the IHB band and ranging from 19 cm^{-1} ($\text{Au}^-\cdot\text{H}_2\text{O}\cdot\text{Ar}_2$) to 33 cm^{-1} ($\text{Ag}^-\cdot\text{H}_2\text{O}\cdot\text{Ar}_2$). Moreover, while the overall appearance of the spectrum remains the same for the two different degrees of Ar solvation, comparison of the spectra for one and two Ar ligands (as displayed in Figure 3.7) shows subtle changes in the structure of the IHB bands.

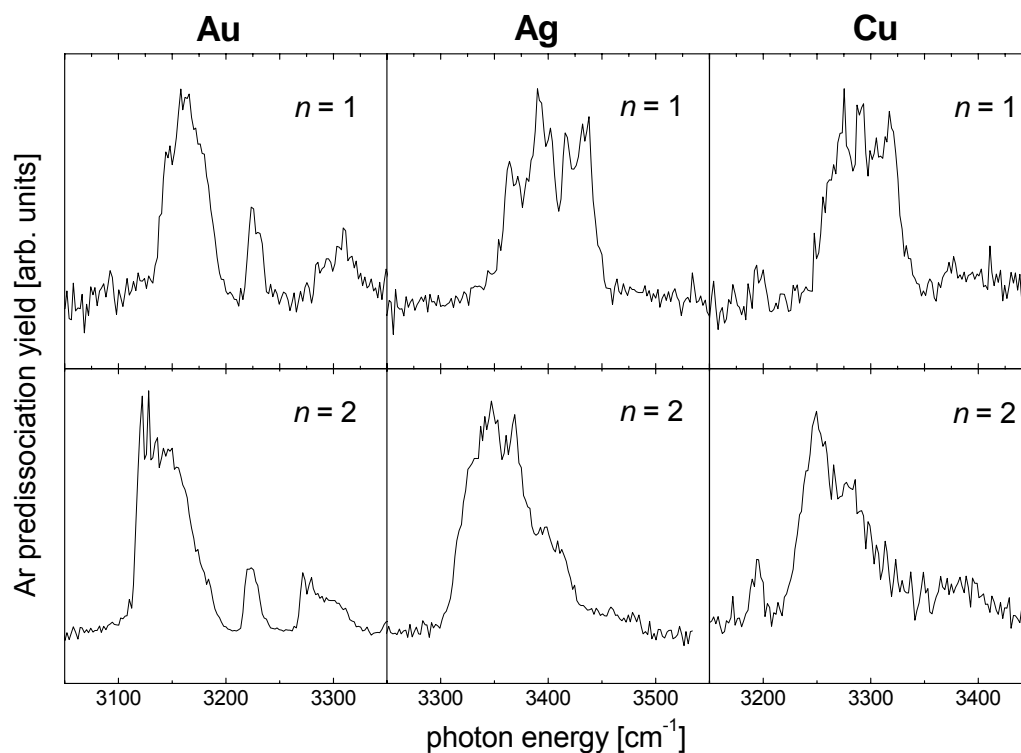


Figure 3.7 IR spectra of the $M \cdot H_2O \cdot Ar_n$ complexes ($M = Au, Ag, Cu$; $n = 1, 2$)

First of all, while the IHB bands for the complexes solvated with one Ar atom are mostly symmetric, addition of a second Ar atom leads to enhancement of the low-energy side of the peak and therefore to a more asymmetric band shape. This means that Ar atom addition favors formation of the asymmetric C_s motif, increasing the barrier between the two identical minimum structures. In addition, the IHB bands of the $Ag^- \cdot H_2O \cdot Ar$ and the $Cu^- \cdot H_2O \cdot Ar$ clusters show an interesting substructure absent in the $Au^- \cdot H_2O \cdot Ar$ system. One explanation could be formation of several Ar isomers in the molecular beam absorbing at slightly different frequencies, as has been observed earlier in the $Cl^- \cdot H_2O \cdot Ar_n$ system.⁴⁵ However, a similar behavior has been described before for the $\Gamma^- \cdot ROH$ ⁴⁶ clusters and also for species where a water ligand is attached to an anion with a negatively charged triatomic domain such as $CH_3CO_2^- \cdot H_2O$ or $CH_3NO_2^- \cdot H_2O$.¹¹ These species have a DIHB geometry in their

ground states, but the potential energy curve along the water rocking motion is shallow. As a consequence, their spectra show unexpected features in the OH stretching region. The substructure of these broad bands has been attributed to simultaneous excitation of the water rocking motion with the OH stretch bands and can be understood on the basis of a Franck-Condon like behavior. The high-frequency OH stretching motion can be thought of being decoupled from the low-frequency water rocking motion. One can therefore first calculate the potential energy curve along the water-rocking motion, constructing a Born-Oppenheimer (BO) surface. Subsequently, the harmonic frequencies for the OH stretch bands at each angle Φ are determined and added to the BO surface, delivering a zero-point corrected BO (ZP-BO) surface and vibrationally adiabatic surfaces according to:^{11,47}

$$U_v^{ad}(\phi) = U_{BO}(\phi) + \left(n_1 + \frac{1}{2}\right) \cdot h \cdot \nu_1(\phi) + \left(n_2 + \frac{1}{2}\right) \cdot h \cdot \nu_2(\phi) \quad (3.1)$$

where ν corresponds to the symmetric and antisymmetric stretching modes at the DIHB configuration and to the OH_{IHB} and free OH stretching modes in the SIHB configuration, respectively, Φ is the angle M-O-H, see Figure 3.8, and n is the number of vibrational quanta in the OH stretching modes ($n_1 = 0$ and $n_2 = 0$ for the zero-point corrected Born-Oppenheimer surface; $n_1 = 1$ and $n_2 = 0$ for the trace labeled “s” and $n_1 = 0$ and $n_2 = 1$ for the trace labeled “as” in Figure 3.8). This has been accomplished for one of the M·H₂O complexes, namely Ag⁻·H₂O as shown in Figure 3.8. All potential energy curves have been calculated according to (3.1). The transitions between the zero-point corrected Born-Oppenheimer surface and the vibrationally adiabatic surfaces are assumed to happen “vertically” in a Franck-Condon-like behavior. The symmetric OH stretch vibration features a large red shift at low and high values for Φ (corresponding to a binding motif of C_s symmetry) as it evolves into the hydrogen bonded IHB band of the SIHB motif.

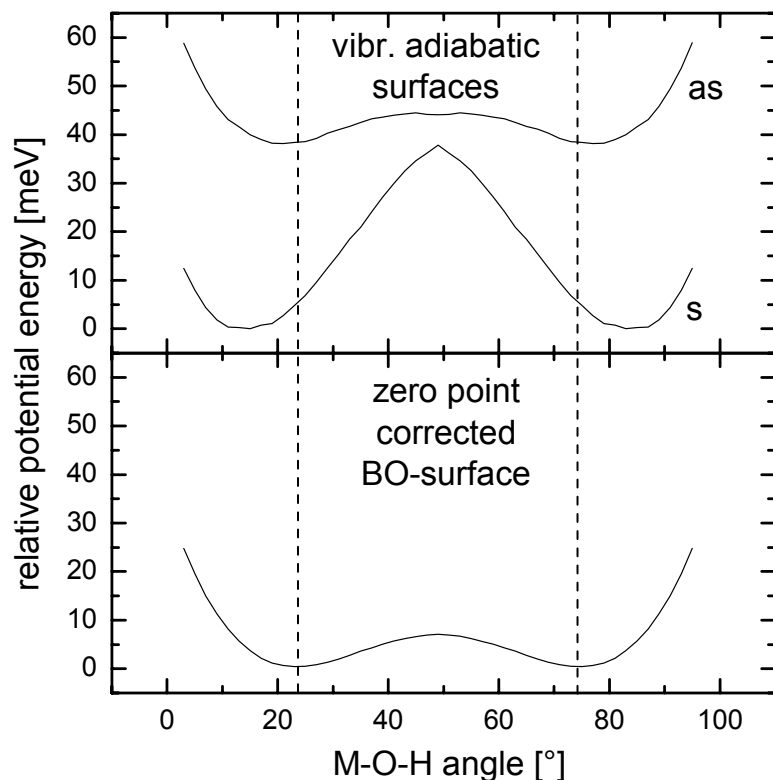


Figure 3.8 Calculated OH Born-Oppenheimer surface and OH stretching fundamentals along the water-rocking motion, measured as angle $\Phi(\text{M-O-H})$ between water and metal (see sketch on top of graph). The symmetric OH stretching mode undergoes a considerable red shift as it develops into the H-bonded IHB band at high and low angles. All values are determined via equation (3.1), with $n_1 = n_2 = 0$ for the lower trace and $n_{1/2} = 1$ for the upper trace. The two dashed lines mark the minimum energy positions of the ground-state BO surface.

Consequently, on the adiabatic surface of the vibrationally excited state, the SIHB motif is preferentially stabilized relative to the DIHB motif as compared to the ground-state BO surface, where it only constitutes a shallow minimum. Hence, an offset in the position of the maximum of the wave function is expected, as the potential energy curve of the vibrationally excited surface resembles more explicitly a clear-cut SIHB motif, meaning its minima lie further away from the C_{2v} structure. This behavior is visualized in Figure 3.8 by the two dashed lines, marking the

positions of the minima on the ground-state BO surface. Excitation of the OH stretch vibration should therefore trigger a structural change of the binding motif along the water-rocking motion, abetting a more asymmetric binding motif. Thus, strong activity of this soft mode is expected in combination with the excitation of the OH stretch modes, following a Franck-Condon-like mechanism. It seems plausible that the pronounced substructure of the IHB bands in the $M\cdot H_2O$ complexes ($M = Ag, Cu$) stems from such a combined excitation of the soft water-rocking and the OH stretching motion.

3.2.4. Summary and conclusions

The binding motifs of the coinage metal anions in complexes with one water molecule have been investigated. In spite of their seeming similarity to the monohydrates of the heavier halide anions (closed-shell anions, comparable proton affinities), $Au\cdot H_2O$ is the only one of the three complexes which displays the clear-cut SIHB motif expected for these systems. In contrast, although the potential energy curves of both the $Ag\cdot H_2O$ and $Cu\cdot H_2O$ complexes still display a minimum for C_s symmetry, their IR spectra prevent an unambiguous assignment to either an SIHB or a DIHB binding motif. Rather, the positions found for the OH stretch bands seem to be situated between the ones expected for the two different distinct structural motifs, indicating that the potential energy surface is flat enough to allow the complexes to explore structures close to the transition state through the zero-point motion in their ground state. This situation is reminiscent of the case of certain molecular anions with negatively charged triatomic domains, which show strong excitation of the water rocking motion upon excitation of an OH stretch band, as the minimum energy structure changes on the ground state and vibrationally excited surface. Even if the asymmetric SIHB motif seems still to be favored for all of the $M\cdot H_2O$ complexes, they therefore do introduce a new binding behavior for atomic anions. However, the reasons for the different binding behavior of a water molecule to the three coinage metal anions have not been understood at this point.

3.3. Anionic hydrated fluorobenzenes

3.3.1. Background

The hydration behavior of small atomic anions such as the halides is well understood, as has been described in detail in the preceding sections. Also, the interaction of anionic molecules with triatomic templates has been investigated in depth and the occurring binding motifs have been unveiled. At the same time, there is a paucity of experimental data on the hydration of extended charge distributions where the negative charge is not localized in a certain area within a molecule but delocalized over all of its constituents. One exception is an infrared study on the dihydrated naphthalene anion.²² We have chosen to investigate the hydration of negatively charged fluorobenzene molecules, as they represent prototypes for anions with spatially large charge distributions. Interestingly, neutral fluorinated benzenes lose the ability to hydrogen bond for fluorination degrees higher than four. This has been demonstrated in a study on complexes of fluorosubstituted benzenes with ammonia.⁴⁸ The binding behavior has been attributed to a continuously decreasing electron density on the fluorine atoms with increasing fluorination. Instead, for hexafluorobenzene it has been shown that a water ligand is bound on top of the molecular plane with the lone pairs of the oxygen pointing towards it.⁴⁹ The binding has been characterized as primarily electrostatic, with a favorable interaction between the dipole moment of the water ligand and the quadrupole moment of the hexafluorobenzene molecule.⁴⁹ Therefore, it will be interesting to see if “charging up” the target molecule will again reverse the binding motifs. In addition, varying the number of fluorine atoms around the ring offers yet another intriguing route for investigation of this class of molecules. There is some disagreement about the exact value of the electron affinity of hexafluorobenzene in the literature. Literature values lie between 0.53 (± 0.05) eV as determined in a flowing afterglow study by Miller *et al.*⁵⁰ and 0.72 eV, resulting from a recent experiment applying photoelectron spectroscopy performed by Eustis *et al.*,⁵¹ but it clearly forms a thermodynamically stable anion. Pentafluorobenzene has an electron affinity smaller than 0.434 eV,⁵² and

the electron affinity of tetrafluorobenzene is unknown. At the other extreme, the bare benzene molecule will certainly not form a stable anion, as its electron affinity has been determined to be $\sim -1.17\text{eV}$.⁵³ However, it is well known that molecules such as benzene or naphthalene are able to accommodate an electron if stabilized by an appropriate number of ligands in clusters or condensed phase environments. Nakajima and coworkers established that about 25 molecules are necessary in order to observe strongly bound excess electron states in $(\text{C}_6\text{H}_6)_n^-$ and $(\text{C}_6\text{H}_5\text{CH}_3)_n^-$ clusters.⁵⁴ In the case of $\text{Nph}_m^-(\text{H}_2\text{O})_n$ clusters, the free naphthalene anion has not been observed in a molecular beam and its electron affinity has been measured to be $-0.20\pm 0.01\text{ eV}$.⁵⁵ However, it can be stabilized already with one water molecule, which was rationalized in light of the stabilization energy inherent to the attachment of a water ligand to the negative transient anion ($\sim 0.3\text{ eV}$ and therefore just enough to pull the system into a thermodynamically stable region). On this basis, it was explained why $\text{Nph}^-\cdot\text{H}_2\text{O}$ showed up only as a very small peak in the mass spectrum, while the cluster with two water ligands was the most abundant by far.^{22,55} Moreover, it was argued that the similarity of the anion-water ($\sim 0.2 - 0.3\text{ eV}$) and the water-water ($\sim 0.25\text{ eV}$)⁵⁶ binding energies should give rise to the maximization of interwater hydrogen bonding, thereby leading to a one-sided hydration motif of the anions, reminiscent of the situation in the heavier halide-water clusters. Indeed, this assumption has been confirmed by an infrared predissociation study of the $\text{Nph}^-(\text{H}_2\text{O})_2$ clusters,²² where the absence of a free OH band signature signaled the involvement of all H atoms in hydrogen bonds. Moreover, a signature assigned to an OH group involved in the formation of an interwater hydrogen bond clearly proved the one-sided binding motif. The fluorobenzenes $\text{C}_6\text{F}_n\text{H}_{6-n}$ constitute ideal prototypes for this kind of diffuse anion, as they offer the opportunity to slowly tune the electron affinity from positive to negative values by stepwise reduction of the number of fluorine atoms around the ring one at a time. It will be of great interest to determine how this will influence the binding motif of a water molecule to the aromatic ring and to what extent the water ligand is actually able to stabilize the negative charge on such a transient anion. In this study, the focus is the $\text{C}_6\text{F}_n\text{H}_{6-n}^-(\text{H}_2\text{O})_n$ cluster system with $n = 4 - 6$. We recorded the IR spectra of these species in the region of the OH

stretch bands of the water molecule, as they should sensitively mirror any change in the binding motif between anion and ligand. We also provide some exploratory calculations on the equilibrium structures of the systems of interest in order to examine possible isomers occurring in our experiment.⁵⁷

3.3.2. Theoretical and mass spectrometric results

In order to elucidate the structural motifs of the anionic complexes under investigation, density-functional theory³⁸ has been employed as implemented in the TURBOMOLE program package,⁴¹ using the B3-LYP functional³⁹ and applying a TZVPP basis set⁴⁰ to all atoms. In this manner, we calculated the minimum energy structures for the three anions under investigation, namely $C_6F_6^-$, $C_6F_5H^-$ and $1,2,3,4-C_6F_4H_2^-$.

3.3.2.1. $C_6F_6^-$

For $C_6F_6^-$ we find the structure to be strongly distorted from the planar D_{6h} geometry of the corresponding neutral C_6F_6 into a geometry of C_{2v} symmetry, with two opposite fluorine atoms strongly angled up ($\sim 23^\circ$ with respect to the carbon ring) while the other four are slightly angled in the opposite direction ($\sim 8^\circ$ with respect to the carbon ring). The result of the calculation is pictured in Figure 3.9 (A); all relevant bond lengths and angles are given in Table 3.3.

Table 3.3 Relevant geometric values for the $C_6F_6^-$ anion as calculated by DFT/B3-LYP/TZVPP (for labeling of atoms compare Figure 3.9)

Atoms	Bond length [pm]
C1-C2 (=C1-C6=C3-C4=C4-C5)	140
C1-C3 (=C5-C6)	137
C1-F7 (=C4-F10)	140
All other C-F	138

Atoms	Angle [°]
C4-C1-F7 (=C1-C4-F10)	157
All other diagonal C-C-F	~ 172

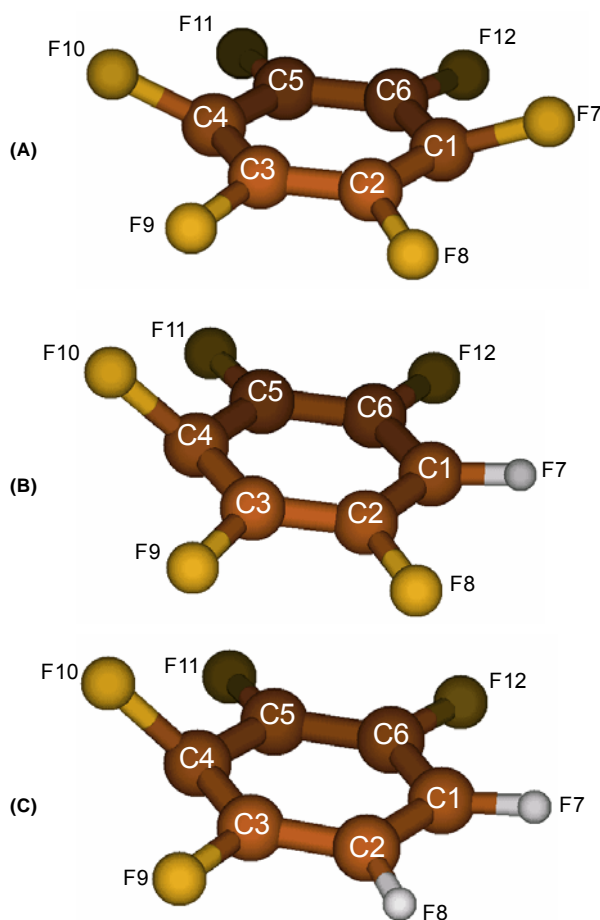


Figure 3.9 Calculated structures (DFT/B3-LYP/TZVPP) of (A) $C_6F_6^-$ (B) $C_6F_5H^-$ (C) 1,2,3,4- $C_6F_4H_2^-$

These findings are in line with earlier calculations,⁵⁸⁻⁶⁰ which come to similar results. In principle, one would expect the distortion found in the hexafluorobenzene anion to be analogous to $C_6H_6^-$, which constitutes a Jahn-Teller case. The additional electron is expected to be located in the $\pi^* E_{1u}$ orbital set, giving rise to two Jahn-Teller geometrical deformations, as is shown in Figure 3.10.⁵⁹

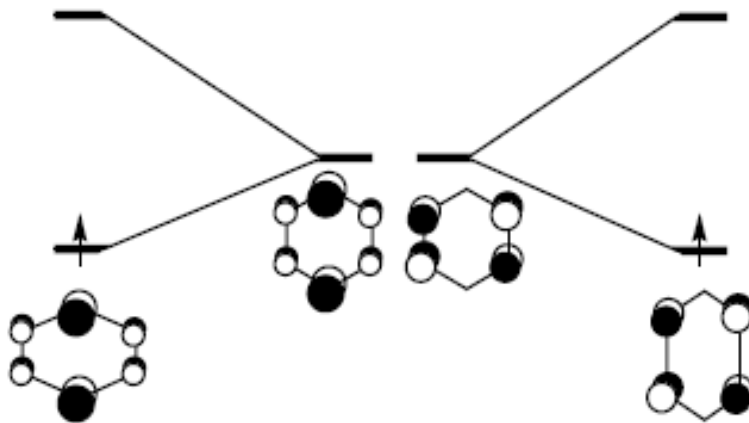


Figure 3.10 Schematic representation of the Jahn-Teller effect and orbital stabilization upon geometric distortion (taken from Ref.⁵⁹)

However, as has been pointed out by Xie *et al.*,⁶⁰ the energy difference between the D_{6h} and C_{2v} geometries amounts to 0.40 eV for the radical anion, a value which considerably exceeds the stabilization energy associated with a Jahn-Teller distortion. Corroborating this point, it turns out that the singly-occupied molecular orbital (SOMO) is totally symmetric. It has been found in calculations by Beregovaya *et al.*⁵⁸ that the loss of planarity in the case of the $C_6F_6^-$ anion is the result of vibronic coupling between the π ground state and the totally symmetric excited σ state, as fluorination decreases the energy gap between the levels of the ${}^2E_{2u}$ and ${}^2A_{1g}$ anion states. This means that the planar structure becomes more unstable toward out-of-plane distortion, leading to the C_{2v} structure found. As expected for a molecule with a positive electron affinity, it is straightforward to produce abundant amounts of the corresponding anion $C_6F_6^-$. Moreover, the recorded mass spectrum shows an intense

progression of $C_6F_6^- \cdot Ar_n$ clusters up to very high degrees of Ar solvation, with $n = 25$ being a magic number in the mass spectrum (Figure 3.11) and the intensity of the mass peaks slowly leveling off.

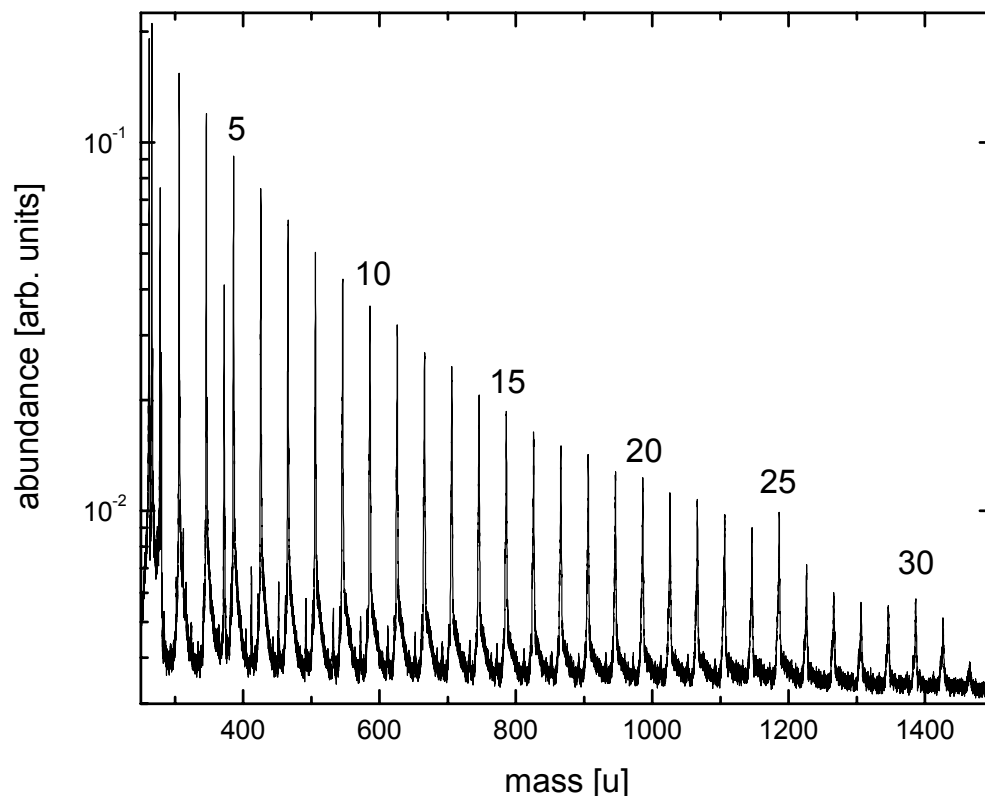


Figure 3.11 Mass spectrum showing the $C_6F_6^- \cdot Ar_n$ anion progression (n is shown in intervals of five, as indicated in the Figure)

It has been found before that the occurrence of magic numbers in the mass spectrum of an ion-ligand progression is indicative of the closure of a solvation shell. For instance, this behavior has been extensively seen and described especially (but not exclusively) in $X^- \cdot RG_n$ clusters ($X = Cl,^{61} I^{62}$ and also O^{63}), where $n = 12$ is a magic number in the mass spectrum with an abrupt decrease in ion intensity for $n = 13$,

mirroring an icosahedral shell closure around the ion. Becker *et al.* showed for the $\Gamma \cdot \text{Xe}_n$ system⁶² that the binding energy for a xenon atom drops by a factor of two upon going from $n = 12$ to $n = 13$, as the second solvation shell starts to fill up, thereby depriving the next xenon atoms from a direct contact to the ion. However, the magic number observed in the mass spectrum of $\text{C}_6\text{F}_6^- \cdot \text{Ar}_n$ is somewhat less pronounced. Also, there is no obvious structural argument for a shell closing to occur upon addition of 25 Ar atoms to the core anion, as this suggests an asymmetric solvation shell. However, it would be conceivable that this is the consequence of the strong distortion of the anion in its ground state towards C_{2v} symmetry.

3.3.2.2. $\text{C}_6\text{F}_5\text{H}^-$

The electron affinity of $\text{C}_6\text{F}_5\text{H}$ is lower than that of hexafluorobenzene and an upper limit of 0.434 eV has been established by Dillow *et al.*⁵² Formation of a thermodynamically stable anion is therefore still expected, and indeed no problems are encountered in the production of this anion in the gas phase. Also, with respect to the nature of the anion produced, the dipole moment of the pentafluorobenzene ($\sim 1.44 \text{ D}^{64}$) is considerably smaller than the critical value determined to form a dipole-bound anion,⁶⁵ and we assume that the ions in the molecular beam are exclusively valence-bound. The mass spectrum of the Ar solvated anionic species $\text{C}_6\text{F}_5\text{H}^- \cdot \text{Ar}_n$ shows again a long progression up to high solvation numbers, displaying two magic numbers in this case for $n = 17$ and $n = 24$. It is interesting to note that the latter is lowered by one in comparison to the $\text{C}_6\text{F}_6^- \cdot \text{Ar}_n$ system upon replacing one of the fluorine atoms by a hydrogen, although we refrain from any structural assignments at this point. Neutral pentafluorobenzene has C_{2v} symmetry and it does not constitute a Jahn-Teller case. However, the distortion the molecule undergoes upon attachment of a negative charge is reminiscent of the hexafluorobenzene case: the fluorine atom opposite to the hydrogen atom is strongly angled up ($\sim 37^\circ$, even considerably more than the corresponding fluorine atoms in the C_6F_6^- case), while all remaining fluorine atoms are angled to a lesser extent in the opposite direction with respect to the carbon ring. The hydrogen atom itself is angled up in line with the

fluorine atom in the opposite position, but only by 8° . This corroborates the assumption that the distortion of the hexafluorobenzene anions from the planar structures of the neutral molecules is not due to a Jahn-Teller effect, in line with the assessment of Xie *et al.*⁶⁰ and Beregovaya *et al.*⁵⁸ The calculated structural parameters of the pentafluorobenzene anion are given in Table 3.4. We recorded the infrared spectrum of this anion employing a vibrational autodetachment route and also via an Ar loss channel as is described in section 3.3.3.3.

Table 3.4 Relevant geometric values for the $C_6F_5H^-$ anion as calculated by DFT/B3-LYP/TZVPP (for labeling of atoms compare Figure 3.9)

Atoms	Bond length [pm]
C1-H7	108
C4-F10	145
C2-F8 (= C6-F12)	137
C3-F9 (= C5-F11)	138
C1-C2 (= C1-C6)	140
C2-C3 (= C5-C6)	137
C3-C4 (= C4-C5)	141
Atoms	Angle [°]
C4-C1-H7	172
C3-C6-F12 (= C5-C2-F8)	175
C2-C5-F11 (= C6-C3-F9)	172
C1-C4-F10	143

3.3.2.3. $C_6F_4H_2^-$

The electron affinities of the various tetrafluorobenzene isomers are unknown, but are expected to be smaller than that of pentafluorobenzene ($EA < 0.434 \text{ eV}^{52}$), as the number of electron-withdrawing fluorine atoms around the ring is decreased. Interestingly, we do not see evidence for the bare anion of tetrafluorobenzene for any geometrical isomer. However, the anion of the 1,2,3,4- $C_6F_4H_2^-$ clustered with two Ar atoms does occur in the mass spectrum, indicating that the electron affinity of this

molecule is slightly negative, but that the weak binding energy of the two Ar atoms to $C_6F_4H_2^-$ is just high enough to stabilize the solvated anion. From $n = 2$ onwards, a long Ar progression is observed, extending to high degrees of Ar solvation. Magic numbers occur for $n = 16$ and $n = 23$, indicating that replacement of another fluorine by a hydrogen atom in the periphery of the arene ring decreases the absolute value of the magic numbers again by one as compared to pentafluorobenzene. The fact that only Ar tagged anionic species are observed in the ion beam also helps to understand the process of ion formation, as one can exclude the possibility that the Ar atoms are attached to a bare anion formed first. Instead, it is likely that neutral $1,2,3,4-C_6F_4H_2 \cdot Ar_n$ clusters initially form in the expansion, which then capture a slow electron and cool down by Ar evaporation, resulting in the Ar progression seen in the mass spectrum. Interestingly, exploratory mass spectra of another tetrafluorobenzene isomer, namely $1,2,4,5-C_6F_4H_2^-$, appear to behave quite differently, in that fifteen Ar atoms were needed to stabilize the anion under the experimental conditions. The structure of the $1,2,3,4-C_6F_4H_2^-$ anion, shown in Figure 3.9, is distorted away from the neutral geometry in a similar fashion as the penta- and hexafluorobenzene: The fluorine opposite to one of the hydrogen atoms is strongly angled up ($\sim 37.8^\circ$) with respect to the molecular plane as defined by the carbon ring, while the respective hydrogen atom is angled up in the same direction, but to a far lesser extent ($\sim 5^\circ$). The other fluorine atoms and the remaining hydrogen are all angled in the opposite direction. Relevant geometrical parameters were calculated in the same way as described above and are summarized in Table 3.5.

3.3.2.4. $C_6F_nH_{6-n}^- \cdot H_2O$

The negative charge in the fluorobenzene anions should be distributed over the whole molecule. However, one would expect it to be primarily localized on the electronegative fluorine atoms, which thereby should potentially serve as anchoring sites in a hydrogen bonding interaction between the anions and the water ligands. The recorded mass spectrum of the $C_6F_6^- \cdot H_2O \cdot Ar_n$ progression is displayed in Figure 3.12 (together with the $C_6F_6^- \cdot Ar_n$ progression which also occurs).

Table 3.5 Relevant geometric values for the 1,2,3,4- $C_6F_4H_2^-$ anion as calculated by DFT/B3-LYP/TZVPP (for labeling of atoms compare Figure 3.9)

Atoms	Bond length [pm]
C6-H12 (= C5-H11)	108
C4-F10	139
C2-F8	138
C3-F9	146
C1-F7	138
C1-C2	137
C2-C3	141
C3-C4	141
C4-C5	137
C5-C6	141
C6-C1	139

Atoms	Angle [°]
C4-C1-F7	176
C3-C6-H12	175
C2-C5-H11	175
C1-C4-F10	176.6
C6-C3-F9	142.2
C5-C2-F8	169.6

Although weaker in signal intensity, the $C_6F_6^- \cdot H_2O \cdot Ar_n$ progression can still be grown out to high Ar solvation numbers. A magic number occurs for $n = 24$, just one below the $n = 25$ observed in the $C_6F_6^- \cdot Ar_n$ progression. This likely means that the water molecule is replacing one of the Ar atoms, a behavior which has been observed before for $Cl^- \cdot H_2O \cdot Ar_n$ clusters,⁴⁵ where the water ligand takes the place of one Ar atom in the icosahedral solvation shell. The mass spectrum of the $C_6F_5H \cdot H_2O \cdot Ar_n$ progression is displayed in Figure 3.13 (together with the $C_6F_5H \cdot Ar_n$ progression, which also occurs). Stable local minimum structures have been determined for the $C_6F_6^- \cdot H_2O$ (see Figure 3.15) and $C_6F_5H \cdot H_2O$ (see Figure 3.17) complexes, and the respective harmonic frequencies have been calculated numerically for the interpretation of the experimental infrared spectra.

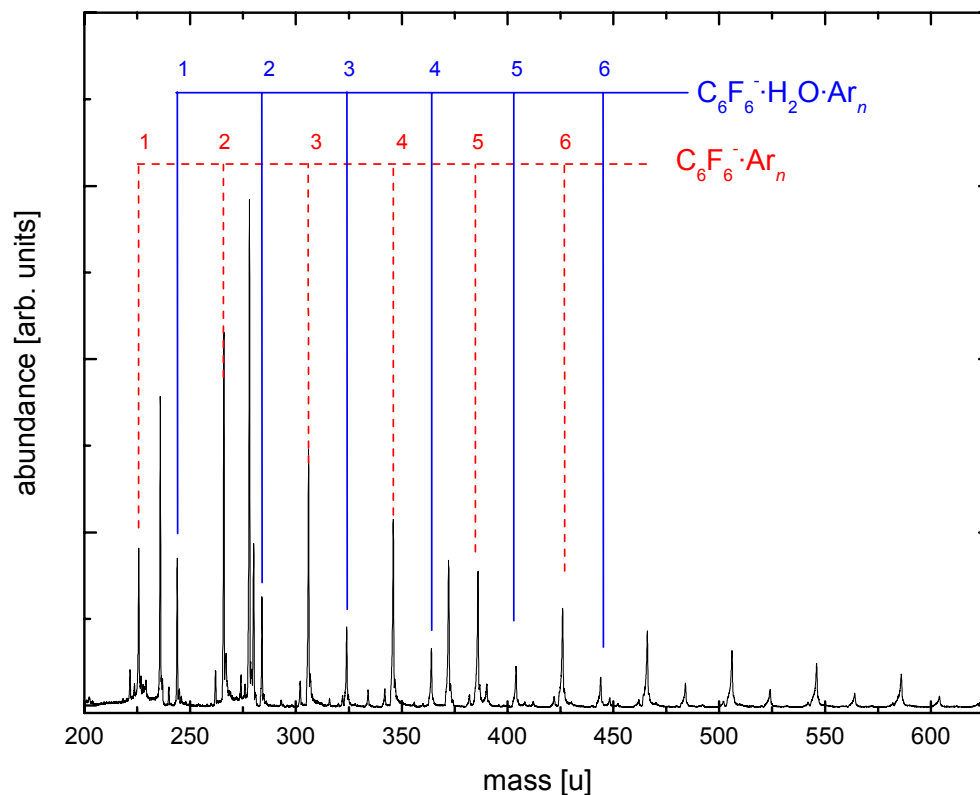


Figure 3.12 Mass spectra of the Ar progressions of $C_6F_6^- \cdot H_2O \cdot Ar_n$ and $C_6F_6^- \cdot Ar_n$, produced by entrainment of small amounts of C_6F_6 and H_2O vapor into an expansion of neat Ar

Anharmonic calculations of the frequency values have been up to now beyond our computational capacities. However, it is possible to account for the intrinsic anharmonic nature of the calculated values in the harmonic approximation by scaling them with an appropriate factor. One way to obtain a reasonable value for the latter factor is to calculate the harmonic frequency values of the respective neutral molecule with the chosen computational method and then determine their ratio to the known experimental values.

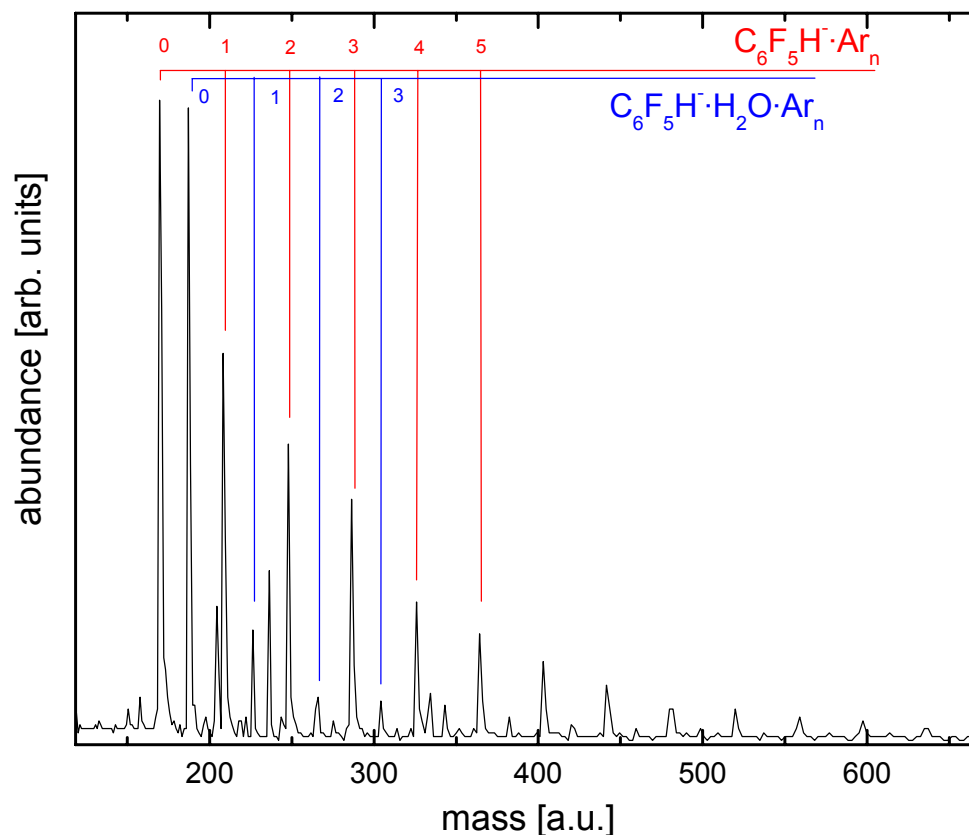


Figure 3.13 Mass Spectrum of $C_6F_5H \cdot H_2O \cdot Ar_n$ and $C_6F_5H^- \cdot Ar_n$ progressions, produced by entrainment of small amounts of C_6F_5H and H_2O vapor into an expansion of neat Ar

However, the quality of this approximation naturally only mirrors the difference in anharmonicity for the vibrational frequency values of the neutral, so that when applied to the respective anion-molecule complex it depends heavily on the extent the ligands are distorted upon interaction with the anion. For this reason, we chose in the present case to refer to a scenario more closely related to the systems we wanted to investigate: The frequency values of the $CS_2^- \cdot H_2O$ complex (which has been found to exhibit a DIHB motif) have been experimentally determined¹¹ and fall relatively close

to the absorptions of the $C_6F_nH_{6-n}^{\cdot-}(H_2O)_n$ complexes in our study, so that they were ideally suited to reference our calculations. In this manner, we extracted a value of $k_s = 0.959$ for the symmetric and $k_{as} = 0.963$ for the antisymmetric OH stretching frequency, respectively.

3.3.3. Results and discussion

3.3.3.1. $C_6F_6^{\cdot-} \cdot H_2O$

The binding energy of the water molecule to the anion has been experimentally determined to be 0.32 eV.⁵¹ It is therefore comparable to the mid-infrared excitation energies, making the loss of Ar atoms the preferential experimental route to record the desired infrared spectra of the cold complexes. All spectra were recorded via loss of all Ar atoms from the parent ion cluster (three in the case of $C_6F_6^{\cdot-} \cdot H_2O$ and two for the other two species, $C_6F_5H \cdot H_2O$ and 1,2,3,4- $C_6F_4H_2 \cdot H_2O$). The spectrum of the $C_6F_6^{\cdot-} \cdot H_2O$ complex is displayed in the range between 3200 and 3800 cm^{-1} for $n = 1$ (Figure 3.14), as the OH oscillators of the water ligand are expected to be active in that region of the infrared spectrum. The two sharp bands in the spectrum at 3620 and 3686 cm^{-1} can be identified as the symmetric and antisymmetric OH stretching vibration of the water molecule bound to the hexafluorobenzene anion in a clear-cut DIHB motif. Varying the number of Ar atoms attached to the anionic chromophore has only negligible influence on the position of the observed vibrational resonances, which change by less than 1 cm^{-1} on using $C_6F_6^{\cdot-} \cdot H_2O \cdot Ar_2$ instead of $C_6F_6^{\cdot-} \cdot H_2O \cdot Ar_3$. There is no signature of a free OH oscillator (which would be a clear indication for an SIHB motif), and the spectral features of the water molecule are conserved but red shifted as should be the case for a DIHB motif according to the discussion in section 3.1.2.1. Also, the splitting between the two bands ($\delta\nu = 66 \text{ cm}^{-1}$) is smaller than for bare water ($\delta\nu = 101 \text{ cm}^{-1}$). One of the features which has been frequently observed before in the infrared spectra of anion-water clusters but is missing in the spectrum shown in Figure 3.14 is the bend overtone of the water molecule.

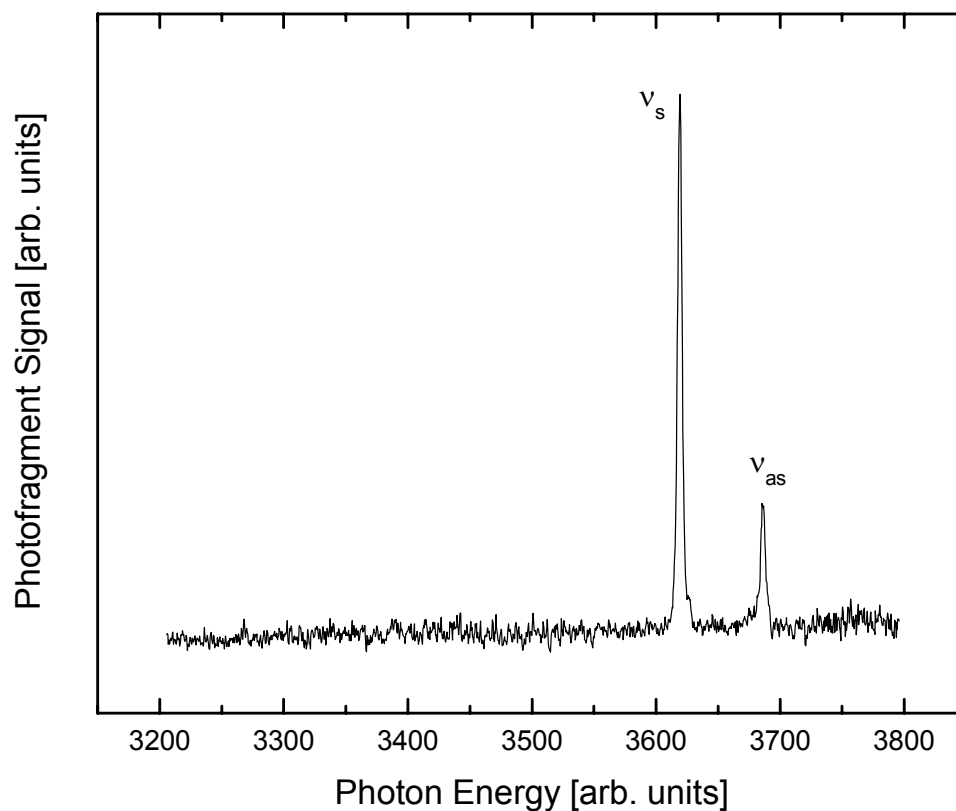


Figure 3.14 Infrared spectrum of $C_6F_6 \cdot H_2O \cdot Ar_3$ (recorded via registering loss of all three Ar atoms); ν_s – symmetric OH stretching mode of the water ligand; ν_{as} – antisymmetric OH stretching mode of the water ligand

This mode, which appears around 3300 cm^{-1} , usually gains intensity through a Fermi interaction with the symmetric OH stretching mode of the water molecule. This could explain its absence in the present case, as the red shifts of the symmetric and asymmetric OH bands are rather small compared to the cases where the bending overtone has been observed. This increases the energetic gap between the latter and the symmetric OH stretch (from which the intensity is usually “stolen”), therefore effectively suppressing the Fermi resonance interaction to an extent where the intensity of the bending overtone is too low to be resolved in this experiment. The

narrow line width of the two bands observed in the experimental spectrum ($\sim 4 \text{ cm}^{-1}$) suggests that only one structural isomer is populated in the molecular beam. In order to shed more light on the specific structure the complex adopts in the gas phase, DFT calculations have been carried out employing the B3-LYP functional and a TZVPP basis set for all atoms, although one can empirically assign a DIHB binding motif to the structures based on the recorded infrared spectrum as discussed above. The symmetry lowering from D_{6h} (C_6F_6) to C_{2v} ($C_6F_6^-$) entails a significant increase in the number of possible different binding sites of the water ligand to the anion. Within the range of 100 meV we find six structural isomers, which are displayed in Figure 3.15 (isomers higher in energy will not be considered since the probability for them to be the dominating fraction of the ensemble of anionic complexes in the molecular beam drops sharply). The two lowest-lying isomers form a DIHB binding motif via hydrogen bonds to two fluorine atoms of the ring, so that the water molecule and the aromatic ring come to lie in the same geometric plane. Isomer 4 (34 meV above the calculated ground state) is the only one constituting an SIHB motif, with the water molecule binding to one of the fluorine atoms while the other OH group points towards the ring, leading approximately to a 90° angle between the planes of the carbon ring and the water ligand. Isomer 3 displays a structure somewhat intermediate between these two motifs. The two high energy isomers 5 and 6 show again a DIHB motif, but with the hydrogen bonds formed to the top of the aromatic ring rather than to the fluorine atoms in the plane of the ring. In order to be able to judge which of these local minimum structures is predominant, the vibrational energy levels for each of the isomers have been calculated numerically. Unfortunately, anharmonic calculations are beyond our computational capabilities, so we confined ourselves to harmonic approximations, which were adjusted with an appropriate scaling factor as described in section 3.3.2.4 in order to roughly account for anharmonicity. The results are shown in Table 3.6 together with the experimental values for direct comparison. It can be seen that with the exception of isomers 3 and 4 all of the considered structures are roughly in agreement with the experiment. However, isomer 1 fits best, which together with the fact that it constitutes the calculated global minimum gives us confidence that this is the dominating structural motif in the ion beam, bearing in

mind that the sharpness of the observed spectral features is a strong hint that only one of the possible isomers is significantly populated.

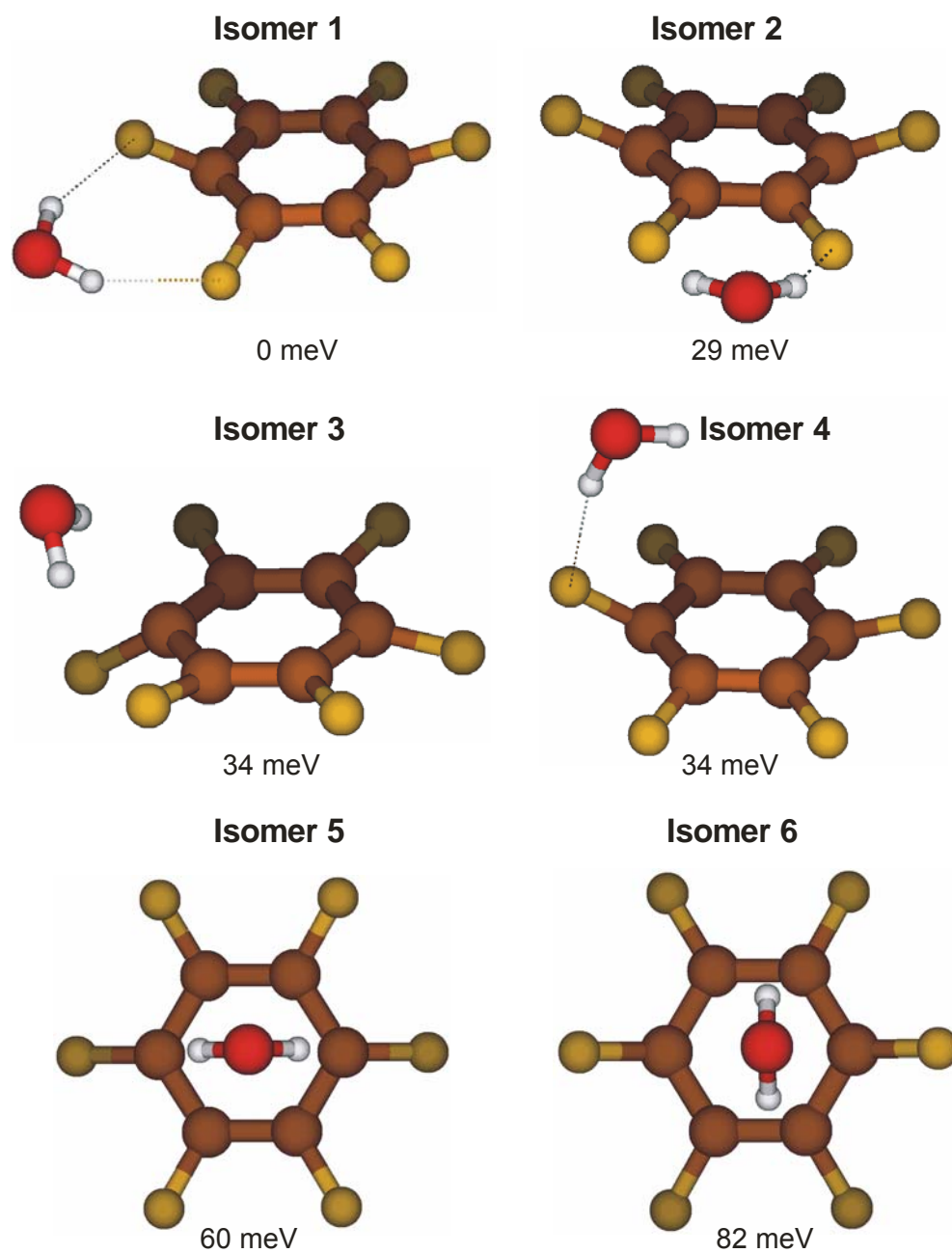


Figure 3.15 Calculated structures (DFT/B3-LYP/TZVPP) of the six isomers within 100 meV above the global energy minimum (isomer 1)

Table 3.6 Experimental and calculated (DFT, B3-LYP, TZVPP, scaled for anharmonicity) positions of the symmetric (ν_s) and antisymmetric (ν_{as}) OH stretching bands of the water molecule in the $C_6F_6^- \cdot H_2O$ complex for the six lowest lying isomers; $\Delta\nu_s / \Delta\nu_{as}$ – corresponding band widths; $\delta\nu$ - splitting between these two bands; the numbers in the first row refer to the respective isomer as labeled in Figure 3.15

	Expt.	1	2	3	4	5	6
ν_s [cm^{-1}]	3617±2	3618	3634	3557	3564	3594	3613
$\Delta\nu_s$ [cm^{-1}]	4.0±0.2						
ν_{as} [cm^{-1}]	3686±2	3691	3715	3690	3718	3667	3693
$\Delta\nu_{as}$ [cm^{-1}]	4.0±0.2						
$\delta\nu$ [cm^{-1}]	69±3	73	82	133	154	73	80

Our structural assessment is in agreement with the findings of Eustis *et al.* with a DFT (MPW1PW91/6-311++G(d,p)) level of theory. They as well assigned a DIHB motif to the $C_6F_6^- \cdot H_2O$ anion, with the water ligand hydrogen bonded to two fluorine atoms of the ring. An interesting aspect arising in that context is the question how easy it is for the different isomers to interconvert into one another. Isomer 1 and 2 are of particular interest in that respect, as first of all they are most relevant to our experiment being the lowest energy structures and secondly interconversion would not require a major rearrangement in terms of the binding motif. However, either one of the hydrogen bonds would have to be broken or the hexafluorobenzene ring would have to rearrange, effectively exchanging a strongly angled CF bond (with respect to the carbon ring) against one that is more weakly angled. A rough estimate for the barrier involved in the second process with the above level of theory (DFT/B3-LYP/TZVPP) amounts to ~ 80 meV, which is too high to be easily overcome, further corroborating our assumption that isomer 1 is the only one present in the experiment.

3.3.3.2. $C_6F_5H \cdot H_2O$ and $1,2,3,4-C_6F_4H_2 \cdot H_2O$

The spectra of the penta- and 1,2,3,4-tetrafluorobenzene anions solvated with one water ligand are shown in Figure 3.16, together with that for the $C_6F_6 \cdot H_2O$ complex for comparison.

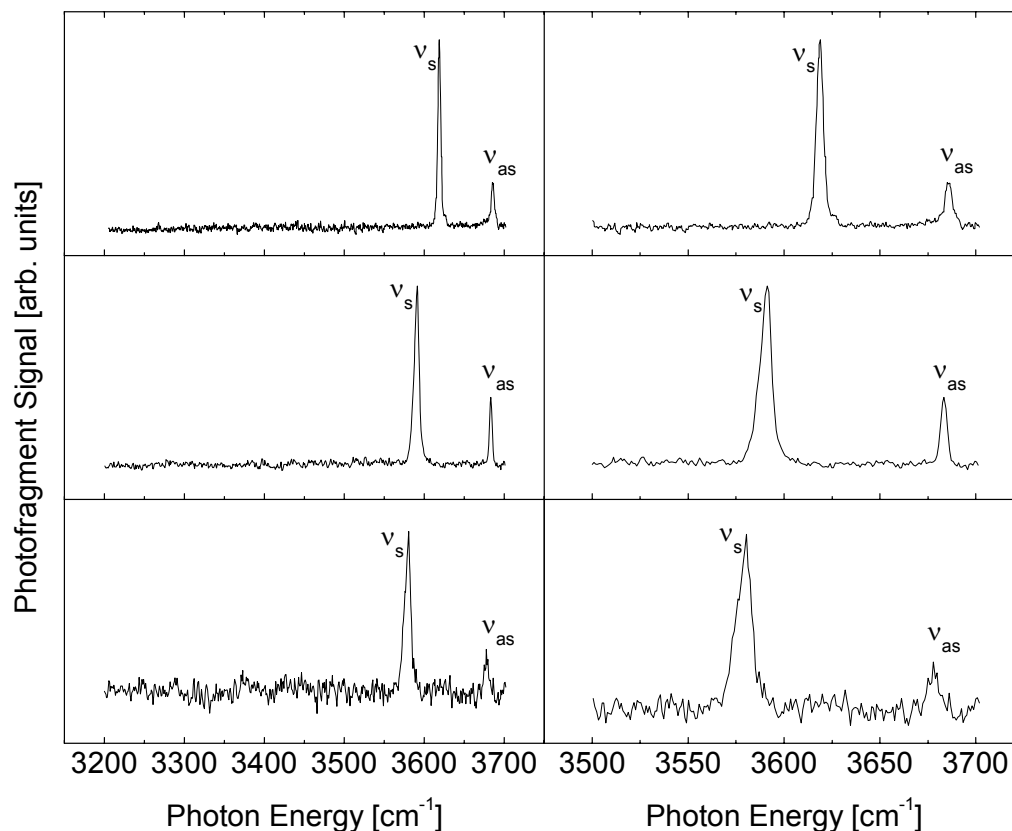


Figure 3.16 Infrared spectra of $C_6F_6 \cdot H_2O \cdot Ar_3$ (top), $C_6F_5H \cdot H_2O \cdot Ar_2$ (center) and $1,2,3,4-C_6F_4H_2 \cdot H_2O \cdot Ar_3$ (bottom) measured via the loss of all Ar atoms both over the entire covered spectral range (left column) and zoomed in around the symmetric (v_s) and antisymmetric (v_{as}) OH stretching vibration (right column)

At first glance, all of them look very similar, as they all display two sharp peaks which have already been assigned for the hydrated hexafluorobenzene to the symmetric and antisymmetric OH stretching vibration of the water molecule, bound

to the anion in a DIHB motif. As expected in this scenario, there is no sign of any vibrational feature at lower energies (spectra recorded down to 3200 cm^{-1} are shown in the left column of Figure 3.16), which could be indicative of some population of an isomer in an SIHB geometry. However, taking a closer look at the symmetric and antisymmetric OH stretching bands (compare right column of Figure 3.16) reveals some subtle differences: First, the red shift of both features increases upon decreasing the number of fluorine atoms around the ring, with the red shift being more pronounced for the symmetric stretch vibration. Hence, the splitting between the two bands increases from 69 cm^{-1} in the case of $\text{C}_6\text{F}_6^- \cdot \text{H}_2\text{O}$ complex to 98 cm^{-1} for 1,2,3,4- $\text{C}_6\text{F}_4\text{H}_2^- \cdot \text{H}_2\text{O}$. The experimental band positions, widths and splittings for all species are listed in Table 3.7.

Table 3.7 Experimental band positions (ν_s for the symmetric, ν_{as} for the antisymmetric OH stretching band), widths ($\Delta\nu_s$ and $\Delta\nu_{as}$ respectively) and splittings ($\delta\nu$) for the $\text{C}_6\text{F}_6^- \cdot \text{H}_2\text{O} \cdot \text{Ar}_3$, $\text{C}_6\text{F}_5\text{H}^- \cdot \text{H}_2\text{O} \cdot \text{Ar}_2$ and 1,2,3,4- $\text{C}_6\text{F}_4\text{H}_2^- \cdot \text{H}_2\text{O} \cdot \text{Ar}_3$ clusters

	Hexafluorobenzene (n = 3)	Pentafluorobenzene (n = 2)	1,2,3,4-Tetrafluorobenzene (n = 3)
ν_s [cm^{-1}]	3617 ± 2	3591 ± 2	3579 ± 2
$\Delta\nu_s$ [cm^{-1}]	4.0 ± 0.2	6 ± 0.1	8 ± 0.4
ν_{as} [cm^{-1}]	3686 ± 2	3683 ± 2	3677 ± 2
$\Delta\nu_{as}$ [cm^{-1}]	4.0 ± 0.2	3 ± 0.4	5 ± 1
$\delta\nu$ [cm^{-1}]	69 ± 3	92 ± 3	98 ± 3

The difference between the anions with respect to their chemical nature delivers a possible explanation for this behavior: As the number of electron withdrawing substituents around the carbon ring is decreased, the negative charge is increasingly

concentrated in a smaller region, therefore leading to stronger interaction between the anion and the water ligand. This would explain the stronger red shift with decreasing degree of fluorination of both the symmetric and asymmetric OH stretching bands. However, the binding energy of the water ligand to the anion decreases in the same direction, contradicting the assertion invoked above somewhat as one would expect the binding energy to increase proportionally to the interaction strength. It is also conceivable that an increasing accumulation of the negative charge leads to a less diffuse distribution over the aromatic ring. This should favor a switching of the binding motif from the observed DIHB towards an SIHB motif, being the preferred structure for the halide anions which constitute an extreme case of a negative charge concentrated on one atom. Consequentially, the symmetric stretching band should gradually turn into a localized IHB band while the nature of the asymmetric stretching vibration should slowly become more like the free OH band. This would explain why the red shift of the former turns out to be more pronounced than for the latter, while the splitting between the two features increases. As the symmetry of the pentafluorobenzene anion is reduced in comparison to the case of the hexafluorobenzene anion, there is an even greater multitude of possible isomers upon attaching a water ligand. An exploratory search for minimum energy structures was performed using the calculated local minimum energy structures found for the $C_6F_6^- \cdot H_2O$ complex (DFT/B3-LYP/TZVPP basis set for all atoms) and permutating the positions of the hydrogen and fluorine atoms through all possible relative positions, leading to a considerable number of isomers relatively close in energy. Due to the large number of calculations necessary following this approach and the otherwise high computational cost, a smaller basis set (TZVP) was chosen for this class of complexes. The experimental spectrum still shows only two sharp features, however, allowing for the conclusion that only one of these isomers is considerably populated (although in the case of the tetrafluorobenzene anion our signal to noise ratio is not good enough to completely exclude some contribution from different isomers). For this reason, isomers lying higher in energy than 100 meV above the (calculated) global energy minimum have not been considered as suitable candidates to be present in the molecular beam. The six most stable isomers are displayed in

Figure 3.17, and some of their calculated relevant energetic properties and vibrational features are summarized in Table 3.8.

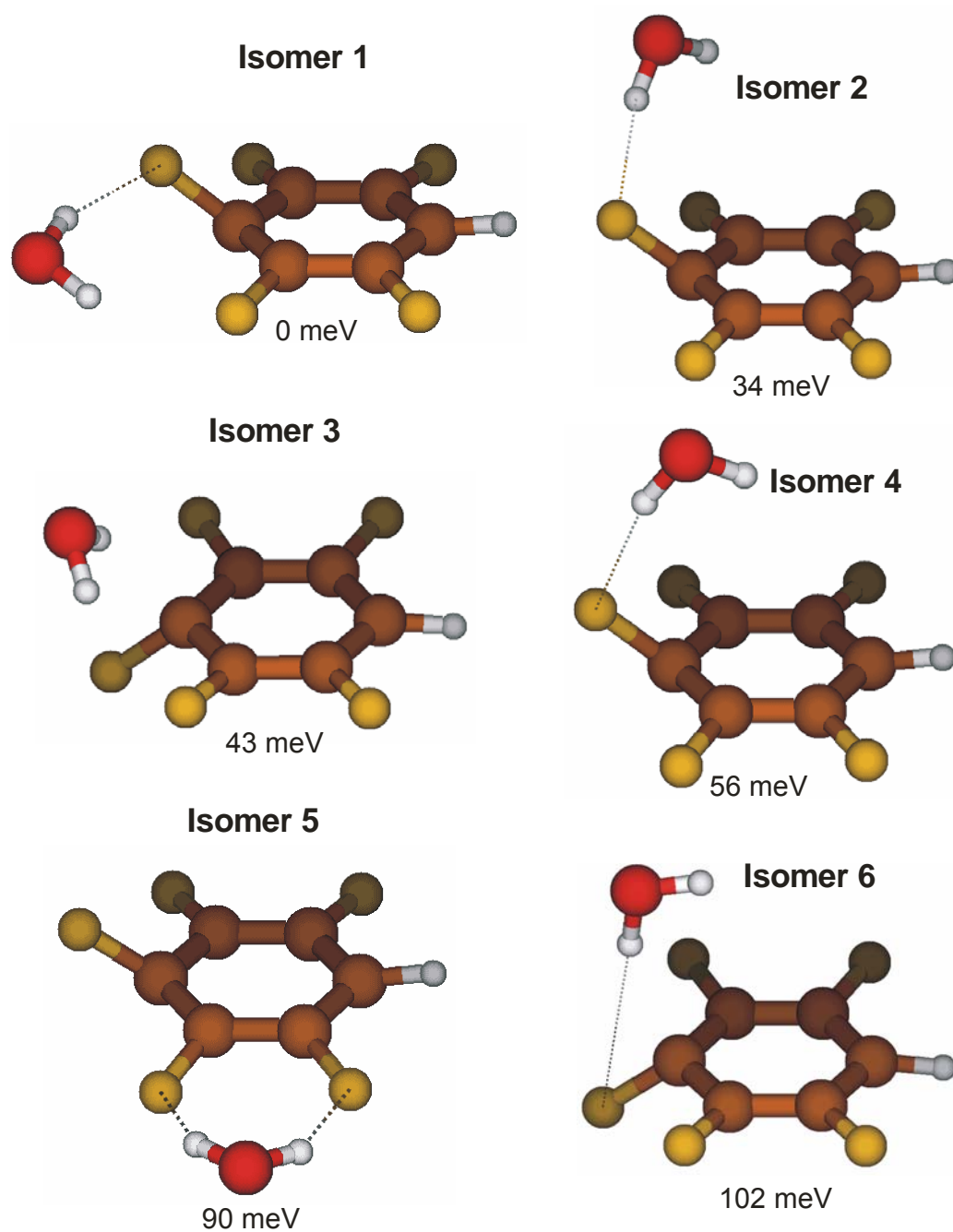


Figure 3.17 Calculated structures (DFT/B3-LYP/TZVPP) of the six isomers within 100 meV above the global energy minimum (isomer 1)

Table 3.8 Experimental and calculated (DFT, B3-LYP, TZVP, scaled for anharmonicity) positions of the symmetric (ν_s) and antisymmetric (ν_{as}) OH stretching bands of the water molecule in the $C_6F_5H^- \cdot H_2O$ complex for the six lowest lying isomers; $\Delta\nu_s / \Delta\nu_{as}$ – corresponding band widths; $\delta\nu$ - splitting between these two bands; the numbers in the first row refer to the respective isomer as labeled in Figure 3.17

	Expt.	1	2	3	4	5	6
ν_s [cm^{-1}]	3591±2	3551	3517	3462	3521	3618	3406
$\Delta\nu_s$ [cm^{-1}]	6.0±0.1						
ν_{as} [cm^{-1}]	3683±2	3689	3696	3670	3704	3704	3705
$\Delta\nu_{as}$ [cm^{-1}]	3.0±0.4						
$\delta\nu$ [cm^{-1}]	92±3	138	179	208	182	85	298

It can be seen that on this theoretical basis a structure with an DIHB motif is predicted to be the global minimum as expected from the experimental results. Moreover, this structure is reminiscent of the global energy minimum geometry found for the $C_6F_6^- \cdot H_2O$ complex and it reproduces the experimentally determined splitting between symmetric and asymmetric OH stretching vibration best (with the exception of isomer 5, which is already 90 meV higher in energy). We tentatively assign therefore isomer 1 to be the dominant isomer found in the experiment. We caution however, that the next three isomers calculated to be close in energy all display more of an SIHB than a DIHB motif. It would therefore be desirable to perform more expensive calculations on this system on a higher level of theory including better anharmonic corrections. The calculated harmonic frequencies were scaled employing the same scaling factor that was chosen for the $C_6F_6^- \cdot H_2O$ complexes ($k_s = 0.959$ for the symmetric and $k_{as} = 0.963$ for the antisymmetric OH stretching frequency, respectively, see section 3.3.2.4). The 1,2,3,4- $C_6F_4H_2^- \cdot H_2O$ turned out to be the last

species in this row we were able to record the infrared spectrum for in the same way. We refrained from performing an extensive search for minimum energy structures for this species based on calculations, as the symmetry is even further lowered, leading to a prohibitively high number of possible isomers. As the signal-to-noise ratio of the spectrum gets worse too, it would become more difficult to assign a specific structure from this perspective as well. Hence, we restrict ourselves to the empirical interpretation given above based on the similarities among all recorded spectra. We were not able to push our investigations of the hydrated fluorobenzene anions further to even lower degrees of fluorination: while 1,2,3-C₆F₃H₃⁻·H₂O complexes could be produced, no charged fragment ions could be registered following exposure of this species to the infrared light. We suggest that from this degree of fluorination onwards the stabilization of the negative charge by the water ligand drops far enough to turn the ejection of an electron via vibrational autodetachment into a faster process than the concurrent Ar loss channel, effectively shutting down the latter. This kind of behavior has been observed before by Weber *et al.* for the CH₃NO₂⁻·Ar_n system,⁶⁶ where as many as three Ar atoms are necessary to make the Ar loss channel prevail over vibrational autodetachment of the electron. Use of this phenomenon as an experimental technique has been first made by Lineberger and coworkers to record very high-resolution spectra of NH₂⁻,⁶⁷ exploiting the fact the vibrational features show up as resonances embedded in the autodetachment continuum. We were able to follow the same route to record the spectrum of the bare pentafluorobenzene both via electron autodetachment and loss of Ar atoms as is discussed in the next section.

3.3.3.3. Bare $C_6F_5H^-$

The spectra of the bare pentafluorobenzene anion recorded both via loss of Ar atoms and vibrational autodetachment of the electron are shown in Figure 3.18.

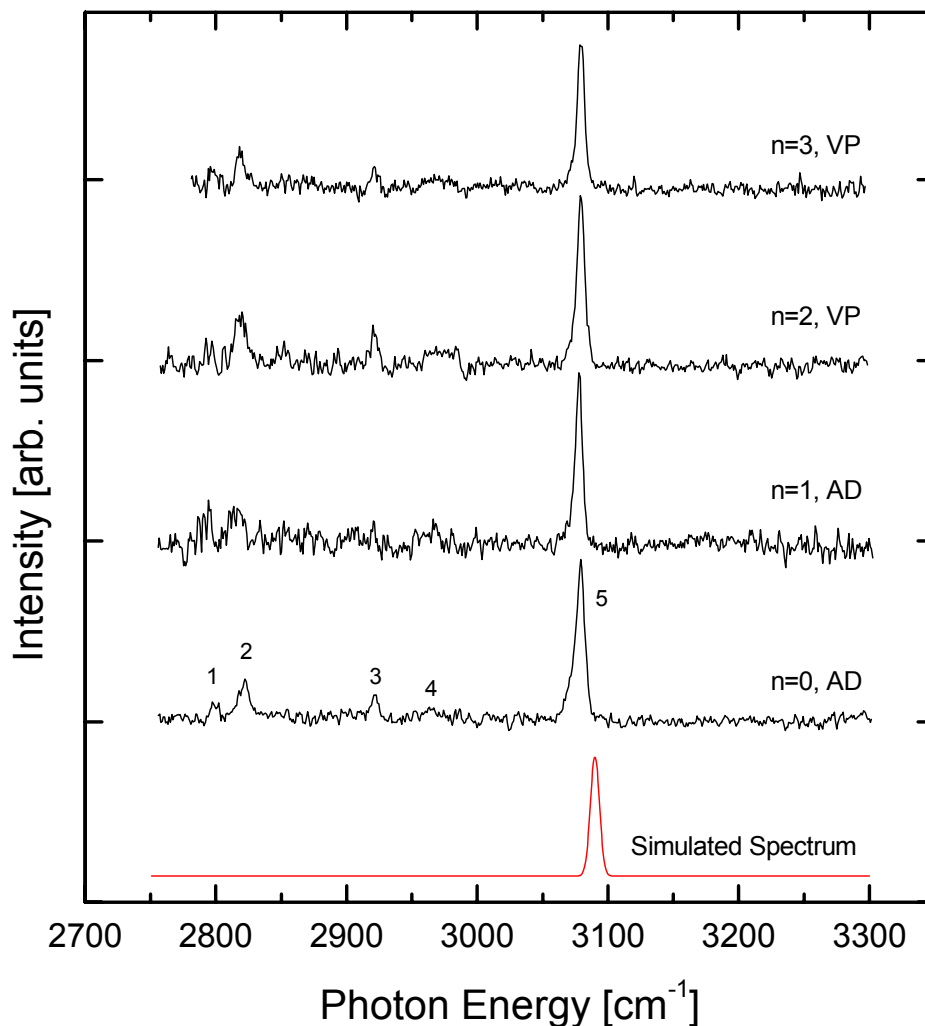


Figure 3.18 Electron autodetachment (AD) and vibrational predissociation (VP) spectra of the $C_6F_5H \cdot Ar_n$ ($n = 0 - 3$) anions. (The VP spectra are recorded via loss of the attached argon atoms). The lowest spectrum is a simulation using the scaled calculated harmonic value for the CH stretching vibration of the bare pentafluorobenzene anion using a Gaussian fit with 6 cm^{-1} half width.

The most recent literature value for the electron affinity (EA) of the neutral molecule⁵² is given as an upper limit of 0.43 eV, while our calculated value amounts to 0.17 eV (DFT, B3-LYP, TZVPP). Thus, the EA could fall into or even below the photon energy range of our spectra. Interestingly, the autodetachment spectra do not show any or only negligible background from direct electron emission following vertical electronic excitations. This may mean that electron emission by autodetachment is much more likely than direct vertical bound-to-free transitions. The structural deviations between the planar neutral molecule (D_{6h} symmetry) and the valence-bound anion, in which some of the fluorine atoms are strongly bent out of the plane of the carbon ring (as described in section 3.3.2.2), are quite large, as can be seen from the optimized anionic structure in Figure 3.9 (DFT, B3-LYP, TZVPP). Based on that, it is plausible that the vertical electron detachment energies lie considerably above the adiabatic EA and therefore out of the range of our OPO, suggesting very small Franck-Condon factors for detachment into low lying vibrational states of the neutral. However, since we observe vibrational autodetachment, we tentatively correct the upper limit of the EA of the pentafluorobenzene molecule to < 0.35 eV ($= 2800$ cm^{-1}), which is the lowest excitation energy of the vibrational feature observed in the experimental spectrum (see Figure 3.18). In light of the fact that our calculated value (0.17 eV) for the EA may not be very accurate (for comparison, a calculation at the same level of theory underestimates the EA of hexafluorobenzene by ~ 85 meV with respect to the experimental value of 0.53 eV), the energy of an infrared photon used may be just higher than the energy necessary to detach an electron. Therefore, one could explain the observation of vibrational autodetachment in the absence of direct detachment by Wigner's threshold law:⁶⁸ near threshold, the cross section will be dominated by $\ell = 0$ (angular momentum of the photoelectron) and the photodetachment cross section σ is proportional to the square root of the energy above the detachment threshold ΔE :

$$\sigma \propto \sqrt{\Delta E}$$

Since the cross section goes to zero for excitation energies close to the threshold energies, direct detachment of a pentafluorobenzene anion may be unfavorable on the interaction timescale between photon and anion. However, resonant excitation of a

vibrational transition deposits the energy in the molecule, considerably extending the timescale available for reaction. Therefore, it might happen on the experimental timescale (\sim tens of μs) despite a low cross section for direct detachment. We caution, however, that our experiment does not allow us to distinguish between any of the suggested mechanisms. It would be desirable therefore to perform either more sophisticated calculations or photoelectron spectroscopy experiments on the $\text{C}_6\text{F}_5\text{H}^-$ anion in order to get a more reliable value for its EA. Attempts to record vibrational predissociation spectra of the pentafluorobenzene anion solvated with one argon atom failed, although there should be no energetic constraint preventing this reaction to occur. This suggests that electron autodetachment is the dominating reaction channel for both the bare and the singly argon-solvated pentafluorobenzene anion following vibrational excitation. Finally, for the anion solvated with two argon atoms the vibrational predissociation channel becomes accessible as the anion becomes more stabilized upon increasing argon solvation. The energy gap between neutral and anionic species therefore grows, slowing down the autodetachment and favoring the competing predissociation channel. This behavior has been observed before for the nitromethane anion, where autodetachment is dominating for the bare and singly argon-solvated anion.⁶⁶ In that case, the doubly argon-solvated species decays with a roughly equal ratio into both channels before predissociation takes over for three or more attached argon atoms. Unfortunately, we are not set up to unambiguously determine how many argon atoms are necessary to close down the autodetachment channel for the pentafluorobenzene anion, as we cannot register the ejected electrons independently but only the neutral products on the linear detector of the time-of-flight mass spectrometer. Argon solvation does not seem to affect the spectra at all, the main feature at $\sim 3079\text{ cm}^{-1}$ remains exactly at the same position in all spectra. The minor bands show the same behavior or at least no noticeable trend correlating the band shifts to the degree of argon solvation. Our harmonic calculations result in only one band in the frequency range of interest, which represents the CH stretch vibration of the pentafluorobenzene anion. After scaling this harmonic value with an appropriate correction factor accounting for anharmonicity (with the scaling factor being the ratio of the known value for the CH stretch vibration of the neutral

molecule⁶⁹ and the calculated value (DFT/B3-LYP/TZVPP basis set for all atoms); see Figure 3.18), it nicely fits to the strongest band in all spectra, even if it overestimates its position by about 10 cm^{-1} . We can therefore clearly assign the strongest spectral feature to the CH stretching vibration of the pentafluorobenzene anion. The less intense bands 1 - 4 are more difficult to interpret, as they cannot stem from excitation of fundamental transitions and are not reflected in our harmonic frequency calculations. We can therefore only tentatively assign them to overtone excitation and combination bands of symmetric and asymmetric CH/CF bending vibrations, the harmonic intensities of which are calculated to be fairly high. For a more rigorous assignment of these bands higher level calculations would be needed, taking the anharmonicity of the vibrations explicitly into account. It is interesting to note that there is no strong feature around the position where the CH stretch vibration would be expected in the spectrum of the $\text{C}_6\text{F}_5\text{H}\cdot\text{H}_2\text{O}$ complex. We do observe a small peak at 3092 cm^{-1} , which could be tentatively assigned to this feature. However, we caution that our signal-to-noise ratio is not good enough to make a specific assignment. Again, the lowest energy isomer with a DIHB motif shows the best agreement with the experimental result, both depicting a slight frequency blue shift of the band as compared to the bare anion and a diminished intensity. However, we refrain from a specific assessment of the problem on the grounds of our theoretical capabilities at this point.

3.3.3.4. Higher degrees of solvation: $\text{C}_6\text{F}_6^-(\text{H}_2\text{O})_2$ and $\text{C}_6\text{F}_5\text{H}^-(\text{H}_2\text{O})_2$

The infrared spectra of the dihydrated hexa- and pentafluorobenzene anions have been recorded as well, in order to gain a better understanding about how the binding motifs will be influenced with increasing numbers of ligand molecules and the potential onset of water network formation. All spectra are displayed in Figure 3.19.

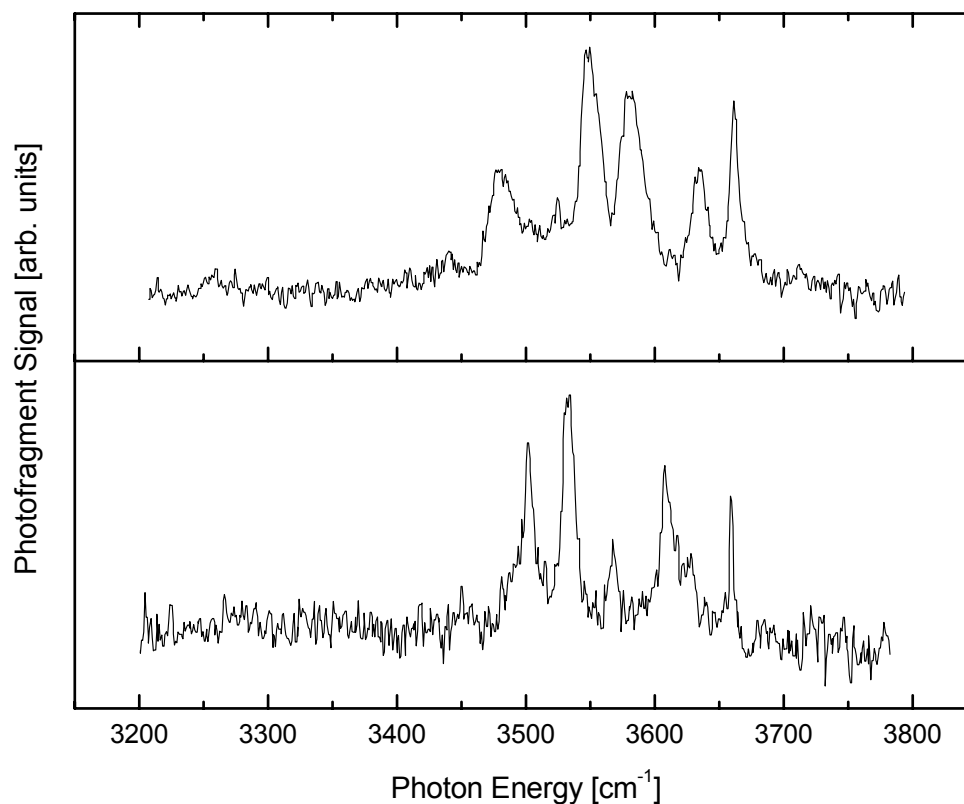


Figure 3.19 Infrared Spectra of $C_6F_6^-(H_2O)_2 \cdot Ar_2$ (top trace) and $C_6F_5H^-(H_2O)_2 \cdot Ar_2$ (bottom trace) measured by monitoring loss of the two Ar atoms upon irradiation

The number of peaks and the overall spectral pattern of the two different cluster species are very similar, even if the exact positioning of the bands and the relative intensities differ, as is to be expected. Also, the bands in the spectrum of the hydrated pentafluorobenzene trimer seem to be somewhat narrower than in the $C_6F_6^-(H_2O)_2$ spectrum, although both parent clusters are tagged with two Ar atoms and should therefore have similar amounts of internal energy, given that they are the same size. In both cases, there are five intense bands, exceeding the number of OH stretching modes (four). Hence, there must be at least two different isomers present in the

molecular beam, which is conceivable with regard to the multitude of isomers already theoretically possible for the monohydrates, and their number should increase upon introducing more water molecules into the solvation shell around the anion. Differences in the relative populations between several isomers might also contribute to the difference in the band widths of the two species. Determining the most stable structure by means of calculations would involve a search for these different structures on a complicated potential energy surface and at the same time require more elaborate theoretical methods, which is why no specific assignments can be made at this point. However, it should be noted that the infrared spectra of both cluster species display intense features at lower wavelengths than was the case for the monohydrates, which seems to be counterintuitive at first glance, as the interaction strength between anion and water ligand is expected to decrease with the number of molecules in the solvation shell increasing. An explanation for this kind of behavior could involve a change in the binding interactions concomitant with the change in the number of ligands. Either the second water molecules binds to the anion in a different motif than the first one, basically adopting an SIHB motif, which seems to be unlikely. Another explanation involves the onset of hydrogen bonding interactions between the two water molecules attached to the anion. In that case, the water molecules are no longer equivalent, but one of them acts as a double hydrogen donor (DD), donating one hydrogen atom to the interwater-hydrogen bond, while the other one plays the role of a hydrogen donor and acceptor (AD), being involved in a hydrogen bonding to the anion and serving at the same time as a docking point for the hydrogen bond from the neighboring water molecule. This kind of behavior has been observed before (see section 3.1.2.2), and the corresponding infrared spectra of the respective anion-water clusters clearly proved that this kind of cooperative hydrogen bonding interactions can lead to significant lowering in the energy of the vibrational signatures of the hydrogen bonds involved.^{19,70} Here, this means that water networks start to form already upon addition of a second water ligand to the respective fluorobenzene anion, although there are still open binding sites available in such an extended charge distribution. It also shows that there is strong competition between ion-water and water-water bonding interactions, which is conceivable in the light of

the fact that the binding energy between anion and ligand drops from 0.32 eV for the first water molecule to 0.22 eV for the second,⁵¹ therefore lowering it into the range of typical interwater hydrogen bonding interactions. As mentioned earlier in section 3.3.1, interwater bonding has been found to take place in the $\text{Nph}^{\cdot-}(\text{H}_2\text{O})_2$ ²² as well, corroborating our interpretation for the hydrated fluorobenzene trimers. We note that Eustis *et al.*⁵¹ postulate based on calculations a structure for the $\text{C}_6\text{F}_6^{\cdot-}(\text{H}_2\text{O})_2$ trimer in which the two water molecules are bound to the anion on opposite ends. Their calculated value for the vertical detachment energy of this species is only in rough agreement with their experimental finding though, while our infrared experiment strongly suggests that both water ligands cannot be bound to the anion in a DIHB motif. We caution however that we likely have several isomers populated in our experiment (one of which could display the structure postulated by Eustis *et al.*) and we cannot assign specific structures based on the level of our calculations.

3.3.4. Summary and conclusions

Infrared predissociation spectra and mass spectra of the hydrated fluorobenzene anions $\text{C}_6\text{F}_x\text{H}_{6-x}^{\cdot-}(\text{H}_2\text{O})_m\cdot\text{Ar}_n$ ($x = 4 - 6$; $m = 1, 2$; $n = 2, 3$) have been monitored in order to elucidate the structural motifs occurring upon solvation of an anion with an extended negative charge distribution. These experimental efforts have been accompanied by calculations on a DFT/B3-LYP/TZVPP level of theory to aid the assignment of specific structures to the experimental spectra, which was unfortunately only possible in the case of $\text{C}_6\text{F}_6^{\cdot-}\cdot\text{H}_2\text{O}$ and $\text{C}_6\text{F}_5\text{H}^{\cdot-}\cdot\text{H}_2\text{O}$: for all other species under study the number of isomers was prohibitively high and the level of theory not sophisticated enough. However, it was possible to unambiguously assign the structures of the bare anions $\text{C}_6\text{F}_6^{\cdot-}$, $\text{C}_6\text{F}_5\text{H}^{\cdot-}$ and $1,2,3,4\text{-C}_6\text{F}_4\text{H}_2^{\cdot-}$. The mass spectrometric results show that the electron affinity of this class of molecules drops from positive in the case of hexafluorobenzene to around zero for tetrafluorobenzene and that it is moreover dependent on the distribution of the fluorine atoms around the aromatic ring. For $\text{C}_6\text{F}_5\text{H}^{\cdot-}$ we were able to record the infrared spectra both of the bare anion via vibrational autodetachment and by recording the loss of attached Ar atoms.

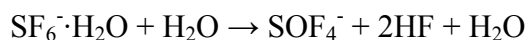
From the infrared spectra it can be clearly concluded that water undergoes rather weak interactions with the fluorobenzene anions. All investigated dimers display a DIHB motif and in the case of the $C_6F_6^- \cdot H_2O$ and $C_6F_5H^- \cdot H_2O$ complexes a specific structure could be tentatively assigned based on calculations. Comparison of the spectra of the three fluorobenzene anions under investigation show that upon reduction of the number of fluorine atoms around the ring either charge localization or a gradual change in the binding motif from a clear-cut DIHB towards a more SIHB-like structure takes place. Moreover, in order to gain insight into the further hydration process, the spectra of $C_6F_6^- \cdot (H_2O)_2 \cdot Ar_2$ and $C_6F_5H^- \cdot (H_2O)_2 \cdot Ar_2$ were recorded and the onset of water network formation was found upon addition of the second water molecule to the respective anion: however, in these cases there have been several different isomers present under the experimental conditions and no specific structural assignments could be made based on the calculations. In order to do so, a more refined theoretical study would be desirable, based on more sophisticated methods and specifically taking into account the anharmonic nature of the normal modes.

3.4. Infrared Spectra of $\text{SF}_6^-(\text{H}_2\text{O})_n$ ($n = 1 - 3$): Incipient reaction and delayed onset of water network formation

3.4.1. Introduction

Similar to the case of the fluorobenzene anions described in section 3.3, the sulfur hexafluoride anion constitutes another example of a highly delocalized excess charge distribution. SF_6^- retains octahedral (O_h) geometry upon electron attachment, with the SF bonds evenly lengthened (from 157.2 pm in the neutral molecule to 171.4 pm in the anion, RI-MP2/TZVPP level of theory) because the negative charge is equally distributed over the respective antibonding σ^* orbitals. Apart from this interest in the $\text{SF}_6^-(\text{H}_2\text{O})_n$ system as a representative for a certain class of anion-molecule complexes, it is desirable to gain more information about the interaction of the SF_6^- anion with surrounding molecules in light of some other aspects. Neutral SF_6 has recently been discovered to represent a potent greenhouse gas with ~ 22200 times the global warming potential of carbon dioxide and it is one of the greenhouse gases listed in the Kyoto protocol.⁷¹ Although its atmospheric concentrations are low, it is of almost exclusively anthropogenic origin and it can accumulate over a long time with a lifetime in the atmosphere of ~ 3200 years⁷² due to its chemical inertness. It is therefore a concern to learn more about the potential reactions of this molecule under atmospheric conditions. In addition, SF_6 is used in several industrial application, e.g. as a plasma etching gas and as a high voltage gaseous dielectric. At the same time, under the conditions in electrical discharges it is found that in the presence of traces of oxygen or water vapor reactions occur, leading to a variety of both neutral products such as SOF_2 , SOF_4 , SO_2F_2 , SO_2 and HF ⁷³ and also ionic species, including $\text{H}_3\text{O}^+(\text{H}_2\text{O})_n$, $\text{SF}_5^+(\text{H}_2\text{O})_n$, $\text{SOF}_3^+(\text{H}_2\text{O})_n$, SOF_x^- , $\text{F}^-(\text{HF})_n$, $\text{OH}^-(\text{H}_2\text{O})_n$, $\text{SF}_6^-(\text{HF})_n$ and $\text{SF}_6^-(\text{H}_2\text{O})_n$. While not much is known about the exact reaction pathways leading to these products, it has been suggested that the SF_6^- anion is involved at least in some of them, either reacting with the trace impurities present or the reaction products of preceding reactions. Moreover, Huey *et al.* studied the reaction yields and rate constants of the sulfur hexafluoride anion with atmospheric trace gases, among them

the acids HCl, HNO₃ and HOCl.⁷⁴ These findings triggered a study by Arnold *et al.* in which they investigated the reaction behaviour of the SF₆⁻ anion with protic solvents such as water and alcohols with short aliphatic chains in an ion flow tube experiment.⁷⁵ Although they were not able to account for all of the above-mentioned reaction products, the following reaction channel



could be established to be dominant, while a second reaction pathway leads to a F⁻·(HF)₂ product ion. Interestingly, they could confirm earlier reports by Knighton *et al.*,⁷⁶ that the reaction of the sulfur hexafluoride anion with small protic ligands is in fact cluster-mediated, meaning that at first an association complex (i.e. SF₆⁻·H₂O) is formed in equilibrium with the reactants, followed by a bimolecular reaction (shown in the reaction equation above) of this intermediate cluster with another solvent molecule leading to the final products of the overall reaction. This proves the importance of cluster formation for the reaction to proceed at least along this pathway. In this context, it is interesting to study the hydration behavior of SF₆⁻ starting with one water molecule and increasing the number of ligands stepwise one at a time from there. Changes in the structures and binding motifs might hint at the onset and mechanism of the reactions described above. We recorded infrared spectra of SF₆⁻·(H₂O)_n (n = 1 - 3) complexes accompanied by calculations and find interesting changes in the SF₆ scaffold upon hydration which indicate possible reaction mechanisms as described in detail in the following sections.⁷⁷

3.4.2. Calculations

The sulfur hexafluoride anion is known to pose significant difficulties to its theoretical treatment by density functional theory. For instance, in a recent study Brinkmann *et al.* managed to arrive at a calculated value of 1.48 eV for its electron affinity employing a KMLYP functional.⁷⁸ This result still overestimates the experimental value (1.07 eV ± 0.01 eV⁷⁹) considerably. In comparison, employing

density functional theory (DFT)³⁸ using the B3-LYP functional³⁹ and applying a TZVPP basis set⁴⁰ (as implemented in the TURBOMOLE program package⁴¹) to all atoms we arrive at a value for the electron affinity of 2.10 eV, which is considerably worse. However, using second order Møller-Plesset perturbation theory including the resolution-of-identity approximation (RI-MP2)⁸⁰ and a TZVPP basis set⁴⁰ for all atoms as included in the TURBOMOLE program package,⁴¹ we calculate a value of 0.70 eV, which in spite of underestimating the experimental result seems to approximate it much better. For this reason, we chose the RI-MP2 method for the treatment of complexes involving the SF_6^- anion. For the bare SF_6^- and its complex with one water molecule we performed two sets of calculations for two different basis sets, one using a TZVPP basis set for all atoms to enable comparison with larger clusters and another one employing a TZVPP basis set only for sulfur but the larger aug-cc-pVTZ basis set for all other atoms. In contrast to the TZVPP basis set, the latter augmented Dunning basis set takes diffuse functions into account and should therefore lead to an improved theoretical description for an anionic system with a rather diffuse electron cloud such as SF_6^- , where this potentially plays a role. For larger cluster systems with an increased number of water ligands we restricted ourselves to the computationally less expensive TZVPP basis set due to the otherwise prohibitively high computational cost. In order to be able to judge the accuracy of our calculations, they can be compared to the results of Gutsev and Bartlett,⁸¹ who performed a high level coupled-cluster calculation for the SF_6^- anion among others. Relevant geometrical parameters, energies and the harmonic vibrational energies of both our calculations and theirs are summarized in Table 3.9.

Table 3.9 Calculated geometric properties, electronic energies and harmonic vibrational frequencies (in cm^{-1}) of SF_6^- from this work and Ref.⁸¹ Note that experimental values for the high frequency t_{1u} mode are 619 cm^{-1} [from Ar matrix isolation studies⁸²] and $683(5) \text{ cm}^{-1}$ [from Ar predissociation spectroscopy⁸³]

Level	SF distance (pm)		
RI-MP2/TZVPP			171.42
RI-MP2/aug-cc-pVTZ			171.43
CCSD(T)/6-311+G(3df) ¹			171.67
Mode	RI-MP2/TZVPP	RI-MP2/aug-cc-pVTZ	CCSD(T)/6-311+G(3df) ¹
$\nu(t_{2u})$	242	239	237
$\nu(t_{1u})$	274	289	306
$\nu(t_{2g})$	344	340	336
$\nu(t_g)$	458	458	447
$\nu(a_{1g})$	651	639	626
$\nu(t_{1u})$	722	712	722

¹ from Ref.⁸¹

It can be seen that the SF bond lengths differ only by ~ 0.25 pm and that the largest deviation in the harmonic vibrational levels amounts to $< 20 \text{ cm}^{-1}$ for the mixed TZVPP/aug-cc-pVTZ and $< 35 \text{ cm}^{-1}$ for the all-TZVPP basis set approach, suggesting that this is an appropriate level of theory for the treatment of this anion. Although the infrared spectra were all monitored by loss of Ar atoms from the parent clusters $\text{SF}_6^-(\text{H}_2\text{O})_n \cdot \text{Ar}$ ($n = 1 - 3$), the Ar atoms were not taken into account in the calculations. The vibrational energy levels were determined for each stationary point identified in the harmonic approximation. All spectra were calculated numerically. In order to account for anharmonic effects and to facilitate comparison with the experimental results we scaled the calculated harmonic frequency values by an appropriate scaling factor as was described for the fluorobenzene-water clusters in section 3.3.2.4. A scaling factor of $k = 0.947$ was applied to all frequencies.

3.4.3. Results and discussion

3.4.3.1. $\text{SF}_6 \cdot \text{H}_2\text{O}$

The spectra of the $\text{SF}_6 \cdot \text{H}_2\text{O} \cdot \text{Ar}_n$ ($n = 1, 2$) clusters, monitored via loss of the attached Ar atom, are shown in Figure 3.20.

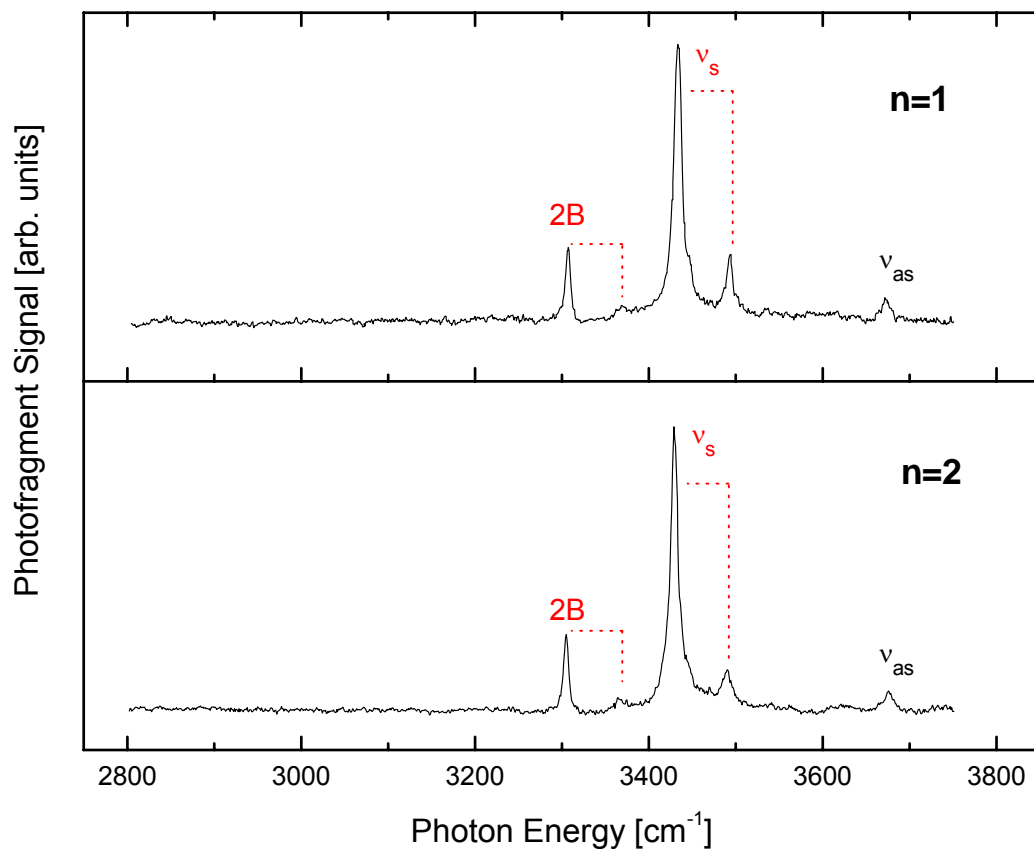


Figure 3.20 Infrared spectra of $\text{SF}_6 \cdot \text{H}_2\text{O} \cdot \text{Ar}_n$ ($n = 1, 2$) monitored by Ar loss; ν_s – symmetric OH stretching mode of the water ligand; ν_{as} – antisymmetric OH stretching mode of the water ligand, 2B – bending overtone of the water ligand; dotted lines mark combinations bands of the bending overtone and the IHB band (ν_s) with the water rocking mode

Just as for the hydrated metal and fluorobenzene anions described in the previous sections, it is useful first of all to compare the experimental spectra to the infrared signatures of the well-known SIHB and DIHB binding motifs. It turns out upon inspection, that the spectrum of the sulfur hexafluoride monohydrate displayed in Figure 3.20 is very similar to that of $\text{I}^- \cdot \text{H}_2\text{O}$. All main features can be explained along the lines of the interpretation given by Ayotte *et al.* and Bailey *et al.*:^{6,18,84} The intense main band at 3430 cm^{-1} (labeled ν_s in Figure 3.20) is the signature of an OH group hydrogen bonded to the anion (IHB band), while the weaker feature at 3676 cm^{-1} (labeled ν_{as} in Figure 3.20) is the signature of the remaining dangling OH group (F band). A band at 3305 cm^{-1} has been attributed to the bend overtone of the water molecule (labeled 2B in Figure 3.20), gaining intensity through a Fermi interaction with the strong IHB band. Two weaker features building upon the bend overtone and the IHB band ($\sim 60 - 70 \text{ cm}^{-1}$ higher in energy, respectively) are assigned to combination levels of these two bands with the water rocking motion (marked with a dotted line in Figure 3.20). The $\text{SF}_6^- \cdot \text{H}_2\text{O}$ complex therefore shows all spectral signatures of an SIHB motif. We note that this is very different from the case of hydrated C_6F_6^- ,⁵⁷ indicating that not all large charge distributions behave similarly upon hydration. Hence, although both molecules represent anionic entities with an extended, delocalized charge distribution and even offer “docking points” for hydrogen bonding of the same chemical nature in form of the fluorine atoms, they display the distinct spectral signatures of two different binding motifs. Moreover, it should be noted that the number of Ar atoms exerts only a negligible influence on the spectra as can be seen in Figure 3.20, where the band positions of the monohydrate basically remain the same both for solvation with one and two Ar messenger atoms. Bearing in mind this unambiguous empirical assessment of the complex geometries with respect to the binding motifs of the water ligand, we performed calculations (at the level of theory described in section 3.4.2) in order to resolve the structures adopted by the complexes under investigation. Surprisingly, in spite of the experimental data pointing towards one clear, dominant structural motif, the calculations turn out to yield several close-lying isomers, the structures of which are shown in Figure 3.21.

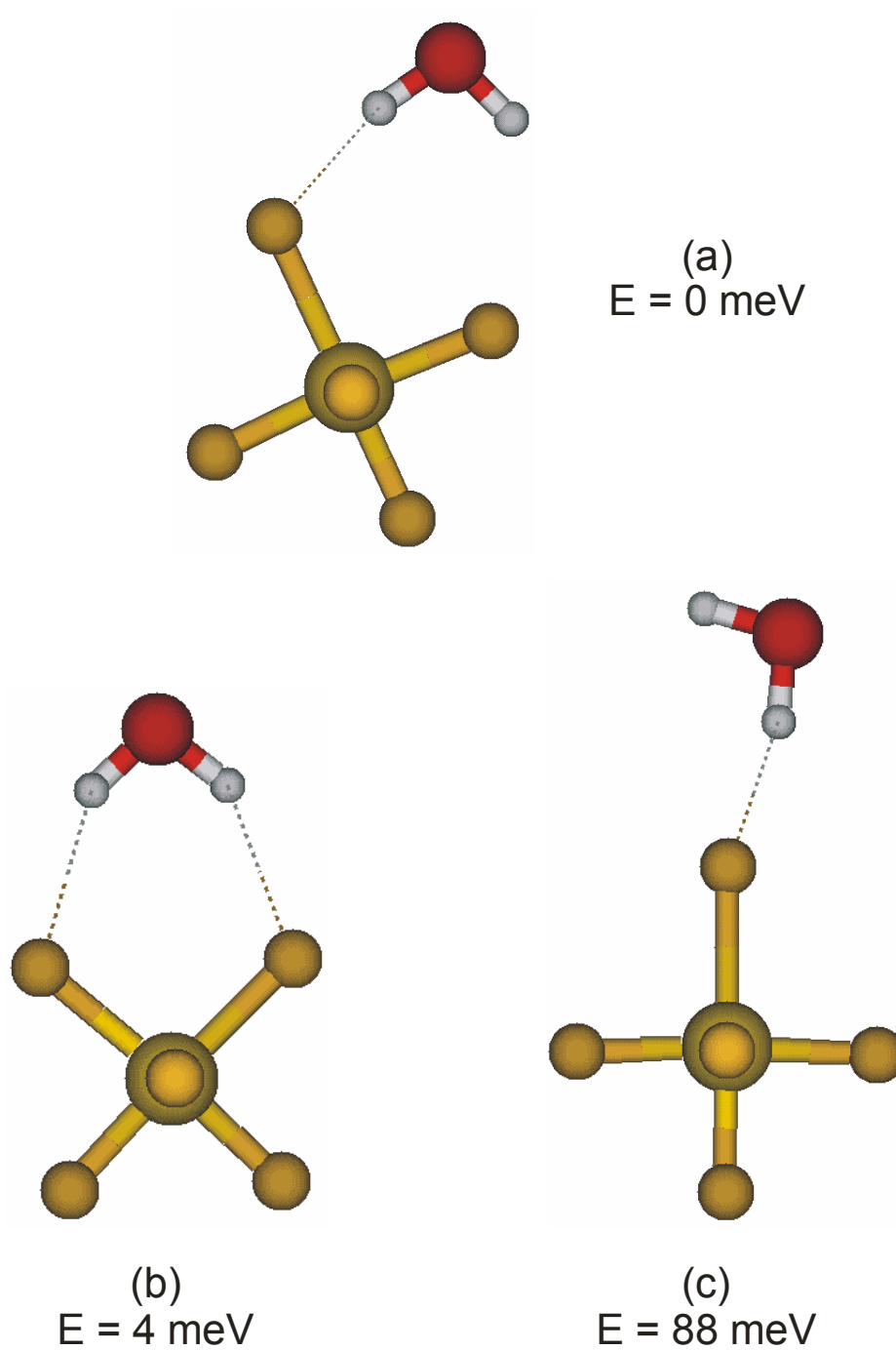


Figure 3.21 Structures of the three isomers lowest in energy of the $\text{SF}_6 \cdot \text{H}_2\text{O}$ complex. Dotted lines indicate hydrogen bonds. Relative energies are based on MP2 calculations (zero-point corrected) with a TZVPP basis set for all atoms.

The isomer lowest in energy (isomer (a), both employing a TZVPP and an aug-cc-pVTZ basis set) indeed displays an SIHB motif with one hydrogen atom involved in a stronger interaction with the anion (FHO angle $\sim 166^\circ$) than the other one, which is only weakly tethered to a neighboring fluorine atom in a more acute FHO angle ($\sim 130^\circ$). The isomer next higher in energy (isomer (b)) lies only 4 meV (TZVPP basis set, zero-point-corrected) above this global energy minimum, which would not allow for a clear identification of one of those two structures as the minimum energy isomer based on the accuracy of our theoretical approach. Moreover, this structure turns out to be a transition state with an imaginary frequency of $\sim i130 \text{ cm}^{-1}$. The structure next higher in energy is found to represent an SIHB motif again with one of the hydrogen atoms involved in an even more linear hydrogen bond than is the case in isomer (a), while the other one is completely free. This structure lies 88 meV above the ground state and constitutes a transition state, which is why it is discarded for further interpretation of the spectra.

Table 3.10 Experimental and calculated (MP2, TZVPP and aug-cc-pVTZ basis set, respectively, scaled for anharmonicity) positions of the symmetric (ν_s) and antisymmetric (ν_{as}) OH stretching bands of the water molecule in the $\text{SF}_6^- \cdot \text{H}_2\text{O}$ complex for the two lowest lying isomers (SIHB ground state and DIHB transition state); the numbering of the isomers in the first row refers to the respective geometry as labeled in Figure 3.21.

Mode	Expt.	Isomer a		Isomer b	
		TZVPP	aug-cc-pVTZ	TZVPP	aug-cc-pVTZ
Bend overtone	3305(2)				
Symmetric OH stretching (ν_s)	3430(2)	3390	3389	3572	3572
Antisymmetric OH stretching (ν_{as})	3676(2)	3704	3689	3624	3630
Water rocking (unscaled)	63(5)	76	78	$i144$	$i126$

In order to enable comparison between theory and experiment we calculated again the vibrational spectra for the two remaining isomers under consideration in the harmonic approximation, scaling our results with a factor of $k = 0.947$ to roughly account for anharmonicity. The results are summarized in Table 3.10 together with the experimental findings. Also, in order to facilitate comparison, the theoretical spectra for both isomer (a) and (b) were simulated (see Figure 3.22), assuming a Gaussian peak shape for the bands with a FWHM (full width at half maximum) of 6 cm^{-1} .

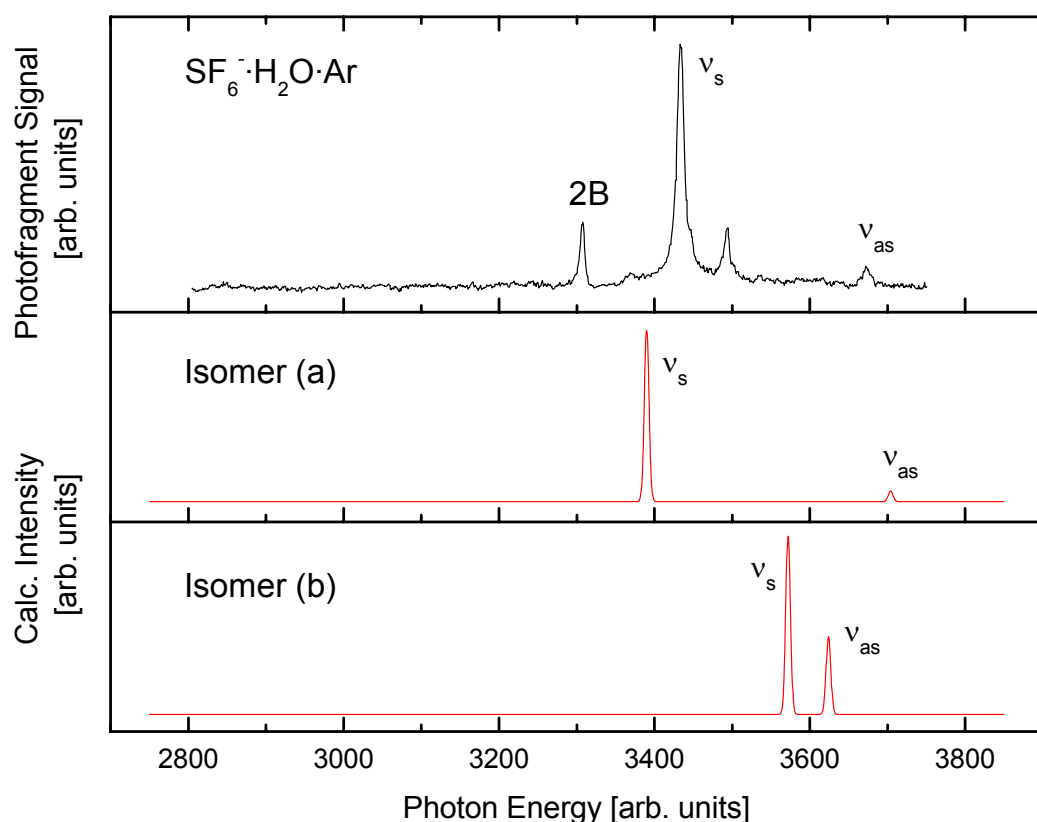


Figure 3.22 Experimental spectrum of the $\text{SF}_6 \cdot \text{H}_2\text{O}$ (monitored by the loss of one Ar atom, see top trace) as compared to the simulated spectra (MP2/TZVPP, scaled for anharmonicity, see text) of isomer (a) and isomer (b), Figure 3.21. Simulations assume a Gaussian peak shape and a FWHM of 6 cm^{-1} .

It can be easily seen that these simulations confirm our earlier empirical assignment of binding motifs to the recorded infrared spectra: while the simulated spectrum of isomer (a) resembles the experimental spectrum reasonably well, this is not at all true for the simulation based on isomer (b). This leads to the conclusion that the relative energy of the symmetric isomer is underestimated in our calculations. The observation of an SIHB binding motif in the $\text{SF}_6^- \cdot \text{H}_2\text{O}$ complex is surprising also in light of an empirical rule established earlier by Robertson *et al.*¹¹ after studying complexes of a water molecule with polyatomic anions in which the negative charge was distributed over a triatomic domain. They found that there exists a connection between the length of this domain and the stability of the DIHB motif. Stable ground state structures with a DIHB motif have been found in a region between ~ 230 pm up to ~ 313 pm. Given that the distance between two neighboring fluorine atoms in the SF_6^- anion amounts to ~ 270 pm, it would fall right into this region of stability for a DIHB binding motif and therefore obviously constitutes an exception to this rule.

3.4.3.2. $\text{SF}_6^- \cdot (\text{H}_2\text{O})_2$

The infrared spectra of both the $\text{SF}_6^- \cdot \text{H}_2\text{O}$ and the $\text{SF}_6^- \cdot (\text{H}_2\text{O})_2$ complexes are shown in Figure 3.23 and comparison shows that both species display the same overall spectral pattern with only some minor differences. Consequently, the general binding motif of the water ligands to the anionic moiety and their local environments cannot change significantly upon addition of a second water molecule. More specifically, the spectrum of the monohydrate has been assigned to a geometry in which the water molecule is bound to the anion via one strong and a second weaker hydrogen bonding interaction to two neighboring fluorine atoms as was explained in the previous paragraph. Hence, the second water ligand is expected to bind to the SF_6^- anion in the same manner, so the only structural issue that remains to be resolved is the relative position to the first ligand. This result is surprising in its own right, because most anions solvated by two water ligands showed the onset of interwater bonding interactions due to the strong propensity of the water molecule to form hydrogen bonded networks.

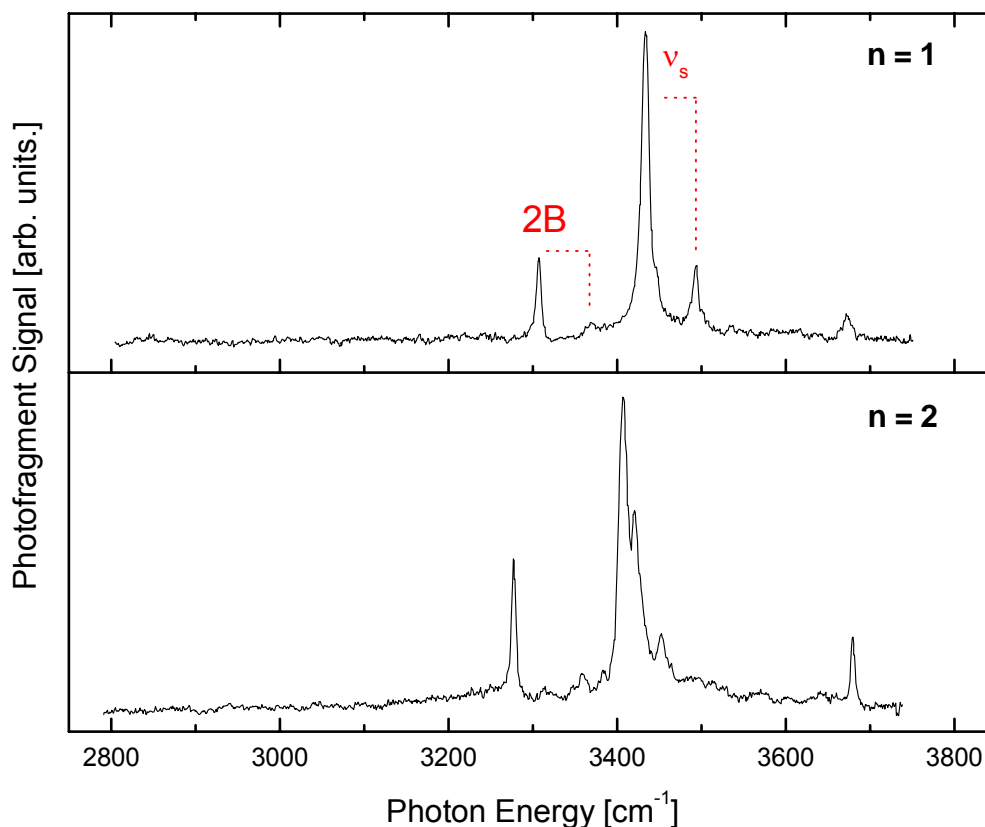


Figure 3.23 Infrared spectra of $\text{SF}_6^-(\text{H}_2\text{O})_n\cdot\text{Ar}$ ($n = 1, 2$) monitored by Ar loss; ν_s – symmetric OH stretching mode of the water ligand; ν_{as} – antisymmetric OH stretching mode of the water ligand; 2B – bending overtone of the water ligand; dotted lines mark combination bands of the bending overtone and the IHB band (ν_s) with the water rocking mode

This is true even for extended charge distributions such as the hexafluorobenzene anion as has been described in chapter 3.3, and this binding behavior usually accompanies drastic changes in the infrared spectral pattern (see e.g. Ref.⁹ and references therein). There are some known exceptions to this bonding behavior, including anions such as F^{-19} and OH^{-21} . However, in these cases the responsible mechanism is the formation of very strong hydrogen bonds, which outweigh the water-water interactions and favor linear binding motifs. This scenario is unlikely to

be at play in the $\text{SF}_6^-(\text{H}_2\text{O})_2$ cluster. It seems to be more favorable for the OH groups of the water ligands to seek interaction with the charge distribution of the core anion than interwater binding. This could be understood in terms of electrostatic interactions dominating in this case over chemical bonding. In order to determine the geometry of the dihydrate, we performed an exploratory computational search for stable isomers. Only a TZVPP basis set was employed in this case due to the otherwise extensively long computation times. The five isomers lowest in energy are shown in Figure 3.24. It can be seen that the first three isomers are very close in energy, lying within an interval of 8 meV, which is certainly too small to make a definitive assignment based on the accuracy of our calculations. Interestingly, in the first two geometries the two water molecules share the one fluorine atom to which both of them undergo strong hydrogen bonding interaction. Only the third isomer, placed 8 meV above the ground state, displays a hydrogen bond between the two water ligands. Anionic structures in which the water molecules do not share any single fluorine atom of the SF_6^- core anion are found to lie considerably higher in energy (> 130 meV). Two representatives of this class are shown in Figure 3.24 but are not considered further for the interpretation of the experimental spectrum due to the large energy difference. Moreover, they constitute saddle points along several normal coordinates. In order to shed more light on the question which of the three lowest-lying isomers contributes significantly to the measured spectrum, we simulated the vibrational spectra of all three candidates, using a harmonic approximation but scaling with an appropriate factor to take anharmonic effects into account in an approximate manner. All simulations are shown in Figure 3.25 together with the experimental infrared spectrum to facilitate comparison. It is obvious that the simulated spectra of the two lowest-lying isomers which do not exhibit any interwater bonding describe the measured spectrum reasonably well, whereas the agreement with the simulation for the third isomer with an interwater hydrogen bond is rather poor. First of all, there is no appreciable intensity in the spectrum where the signature of an interwater interaction would be expected to be. The simulations predict an intense band at 3491 cm^{-1} for isomer (c), in the spectral region where water-water hydrogen bonding signatures usually occur.

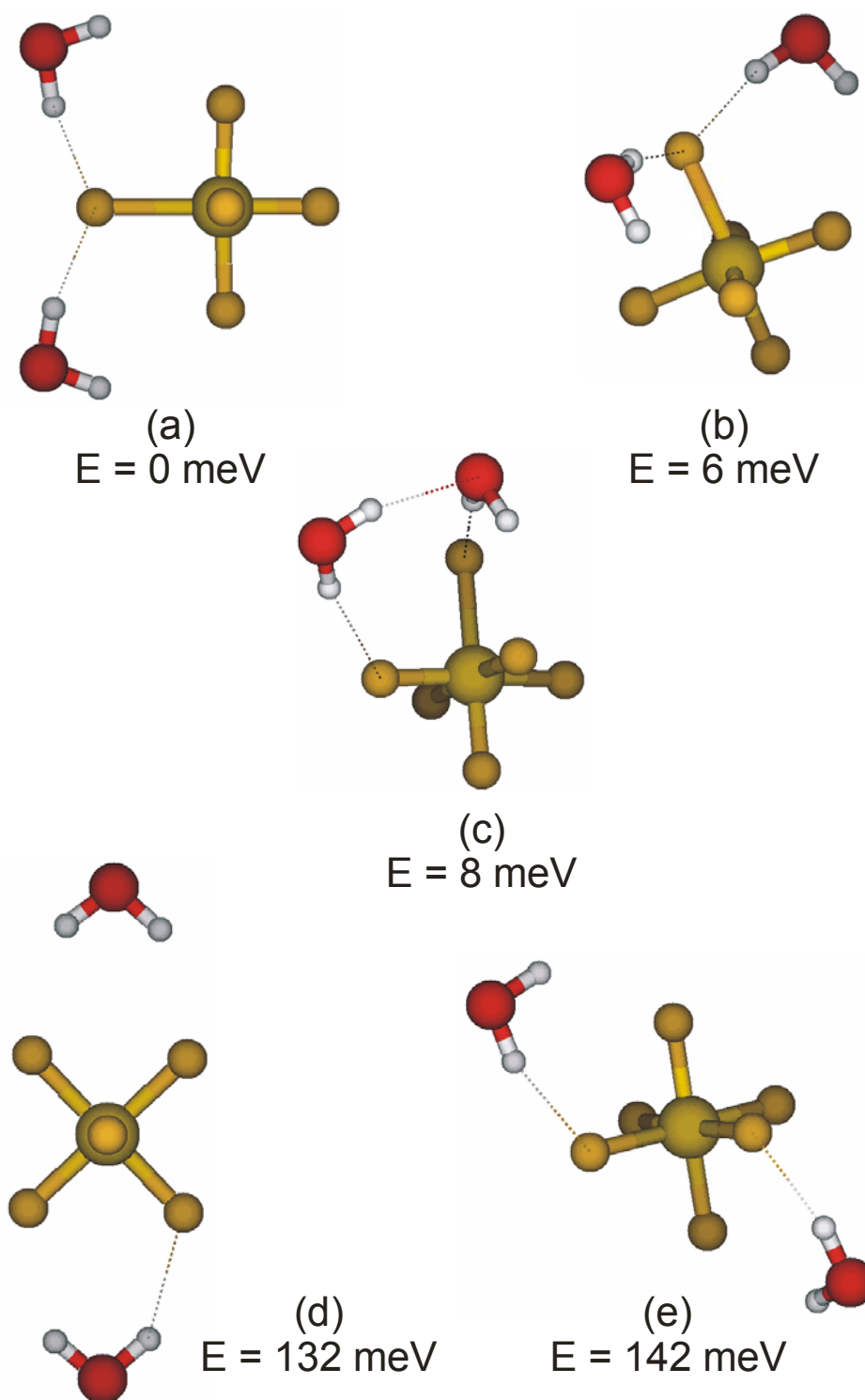


Figure 3.24 Structures of the isomers lowest in energy of the $\text{SF}_6 \cdot (\text{H}_2\text{O})_2$ complex. Dotted lines indicate hydrogen bonds. Relative energies are based on MP2 calculations with a TZVPP basis set for all atoms. Geometries (d) and (e) are saddle points along several coordinates.

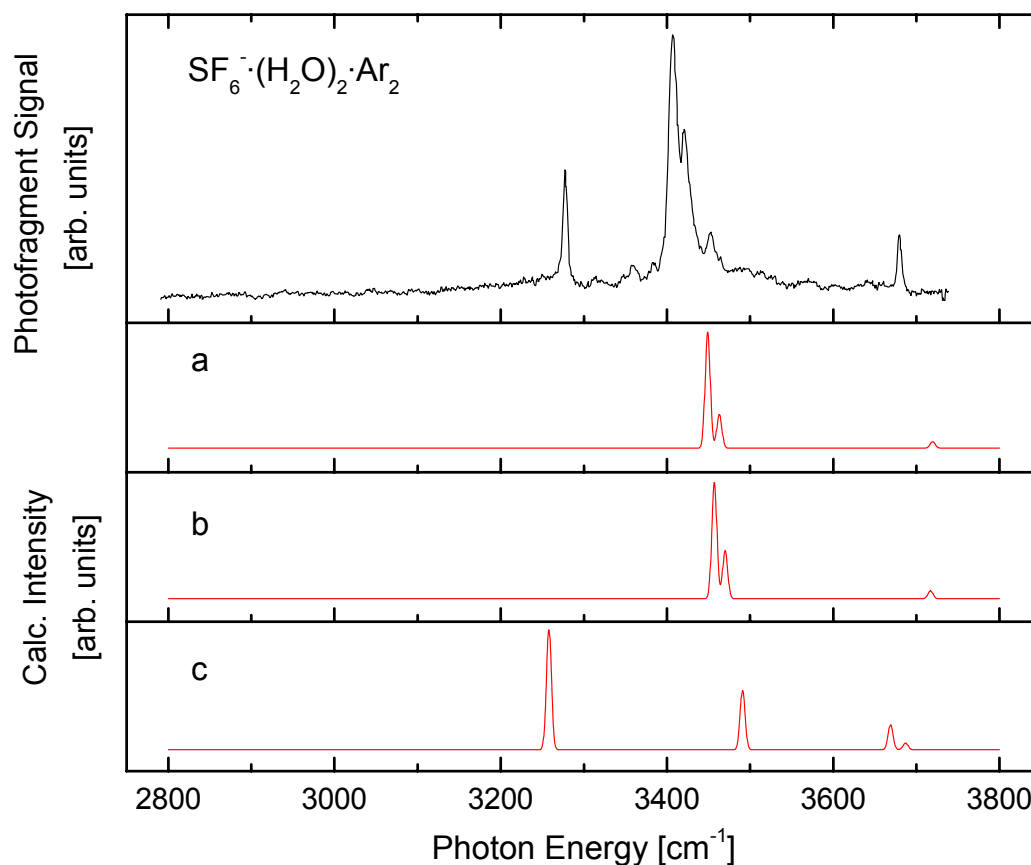


Figure 3.25 Experimental spectrum of the $\text{SF}_6^-(\text{H}_2\text{O})_2$ complex (monitored by the loss of one Ar atom, see top trace) as compared to the simulated spectra (MP2/TZVPP, scaled for anharmonicity, see text) of isomer (a), (b) and (c), Figure 3.24. (Simulations assume a Gaussian peak shape and a FWHM of 6 cm^{-1})

One could argue that there is some small intensity in that frequency region and that also the intense peak at 3290 cm^{-1} could be ascribed to the occurrence of isomer (c) in the ion beam. However, this seems highly unlikely since we observe a similar feature also in the spectrum of the monohydrate at 3305 cm^{-1} , which could be unambiguously assigned to the overtone of the bending mode of the water ligand. This mode is expected to appear in the spectrum of the dihydrate as well, which should either lead

to the occurrence of several bands in this frequency region (which is not observed) or a broadening of the peak in question due to the overlap of the two bands of different origin. Given the sharpness of this feature and the absence of an intense signature of a water-water hydrogen bond, it seems to be justified to exclude isomer (c) from the list of possible candidates. It is more difficult, however, to decide which of the two isomers (a) or (b) is dominant in the molecular beam, as both their simulated spectra match the experimental one fairly well and the calculated energy difference (6 meV) does not allow for exclusion of isomer (b) from our experiment based on the accuracy of the performed calculations. More refined theoretical investigations would be desirable to resolve this issue employing more sophisticated computational methods.

3.4.3.3. $\text{SF}_6^{\cdot-}(\text{H}_2\text{O})_3$

As the onset of water-water bonding interactions could not be observed in the dihydrate, the trihydrate was also studied in order to determine the minimal amount necessary to start water networks. The spectrum of the trihydrate is shown in Figure 3.26. A comparison of the three spectra reveals a drastic change in the vibrational pattern, proving the bonding interactions of the water molecules must change dramatically. Specifically, two broad peaks are observed $\sim 3270 \text{ cm}^{-1}$ and $\sim 3347 \text{ cm}^{-1}$, which are assigned to the overlapping bands of the bend overtones of the water ligands and the IHB bands (ionic H bonds, signatures of the OH groups hydrogen bonded to the anion), respectively, following the interpretation of the similar bands in the mono- and dihydrate. The IHB bands are red shifted upon attaching a water molecule to the $\text{SF}_6^{\cdot-}(\text{H}_2\text{O})_2$ due to cooperative hydrogen bonding effects by about $\sim 77 \text{ cm}^{-1}$. This has been observed in similar cases before, e.g. for the hydration of iodide.^{9,23} The broadness of these bands as compared to the analogous features in the spectra of the mono- and dihydrate may be due to the presence of several isomers in the ion beam. Moreover, the appearance of two sharp bands at $\sim 3529 \text{ cm}^{-1}$ and at $\sim 3574 \text{ cm}^{-1}$ in the frequency region characteristic for the spectral signatures of interwater hydrogen bonds suggests the onset of a hydrogen bonded water network.

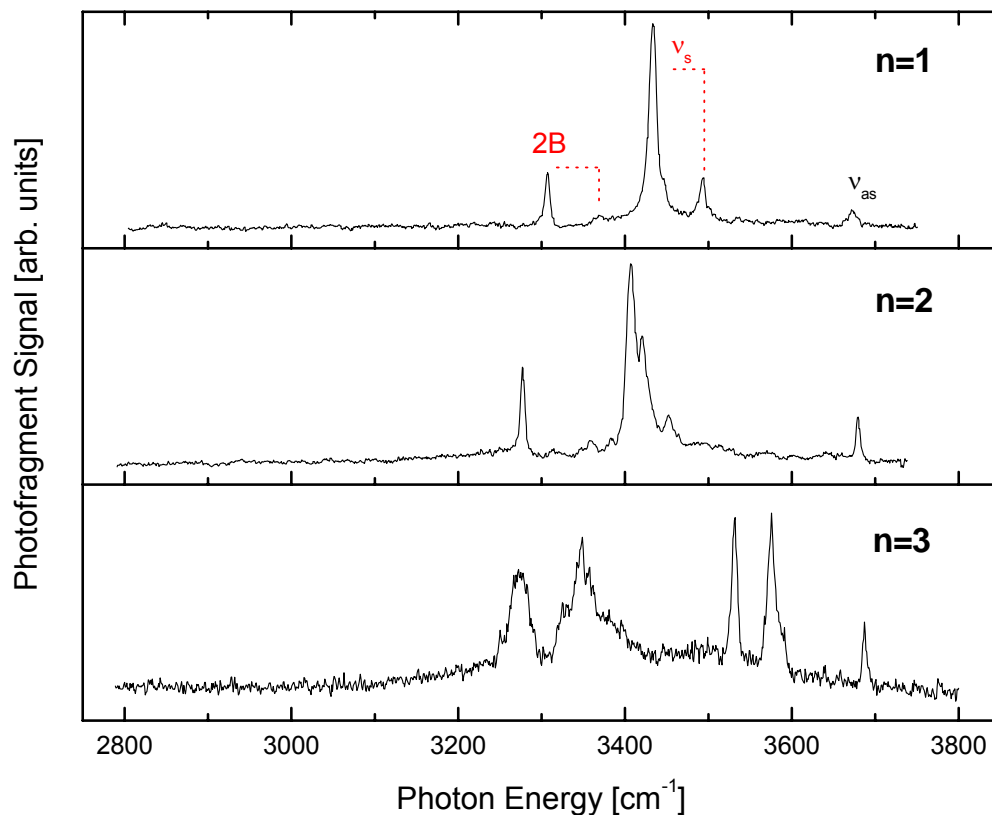


Figure 3.26 Infrared spectra of $\text{SF}_6^-(\text{H}_2\text{O})_n\cdot\text{Ar}$ ($n = 1 - 3$) monitored by Ar loss; ν_s – symmetric OH stretching mode of the water ligand; ν_{as} – antisymmetric OH stretching mode of the water ligand, 2B – bending overtone of the water ligand; dotted lines mark combinations bands of the bending overtone and the IHB band (ν_s) with the water rocking mode

A sharp feature at 3685 cm^{-1} indicates the presence of at least one free OH group. In order to get a more detailed idea about the structure of the cluster anion beyond this empirical assessment, we performed again an exploratory search for minimum energy structures on the potential energy surface. However, due to the flatness of the latter and the large number of possible isomers we restricted ourselves to geometries based on obvious expectations for the ground state structure, for instance the existence of some water-water hydrogen bonds. Specifically, Figure 3.27 shows two isomers.

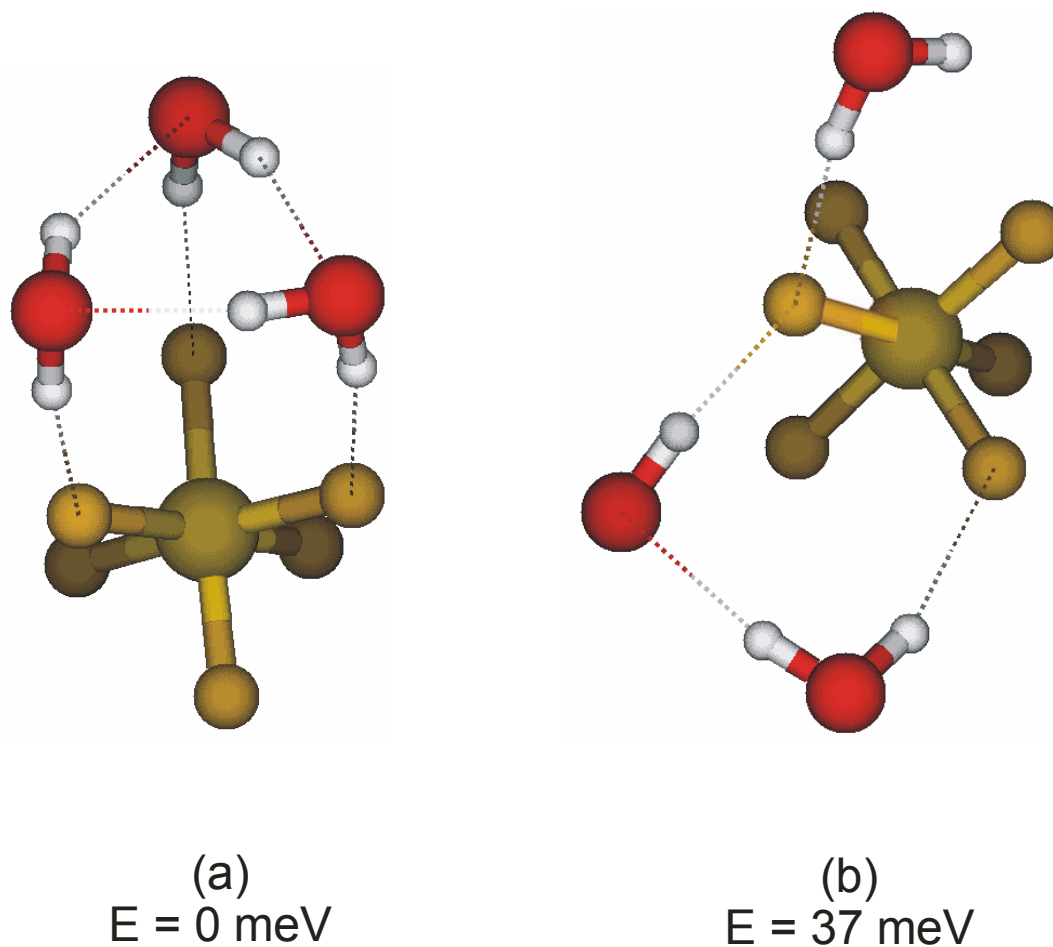


Figure 3.27 Structures of the isomers lowest in energy of the $\text{SF}_6^-(\text{H}_2\text{O})_3$ complex. Dotted lines indicate hydrogen bonds. Relative energies are based on MP2 calculations with a TZVPP basis set for all atoms.

Isomer (a) displays a “ring-like” water sub-cluster, in which all three water molecules are attached to one another and to the anion in hydrogen bonds at the same time. This motif has been found to be the most stable structure in the halide trihydrates, e.g. $\text{I}^-(\text{H}_2\text{O})_3$. It should be noted though, that the water molecules in this case are not all equivalent as two of them are rather weakly tethered to the anion, while only one is involved in a strong hydrogen bond to the SF_6^- . The SF bond involved in this interaction is significantly lengthened to ~ 194 pm as compared to the approximately

undisturbed ~ 173 pm of the other two SF bonds. This kind of distortion of the geometry of the SF_6^- core anion occurs similarly in the mono- and dihydrate (compare preceding paragraphs) and will be rediscussed in terms of the reactivity of the SF_6^- moiety in the next section. The second structure in Figure 3.27 is based on the isomer found to be lowest in energy for the $\text{SF}_6^-(\text{H}_2\text{O})_2$ (isomer (a) in Figure 3.24), meaning that two water molecules are bound to one fluorine atom in a shared attack, while the third one is attached both to the SF_6^- anion and to one of the other water ligands via hydrogen bonds. It is calculated to be higher in energy than the ring-like structure by 37 meV. The spectra of the two species under consideration have been simulated on the same footing as in the case of the dihydrates in the preceding section (harmonic approximation, but scaled with a uniform scaling factor $k = 0.947$ to account for anharmonicity in an approximate way) and the result is shown in Figure 3.28 along with the experimental spectrum of the trihydrate as monitored by loss of one Ar atom to demonstrate the relative accordance. The spectrum of isomer (b) seems to be a better match to the experimental spectrum as it mirrors the free OH, the IHB and the interwater bands rather well (the bend overtone is an anharmonic effect and therefore not recovered by our harmonic simulations). This may mean that isomer (b) is the dominating isomer in the molecular beam, despite the fact that it is placed higher in energy than the ring isomer by the calculations. However, we stress again that the spectrum does not at all exclude the existence of several isomers at the same time under the experimental conditions and that the calculations performed are by no means an exhaustive search for minimum structures but rather educated guesses of the most likely structures.

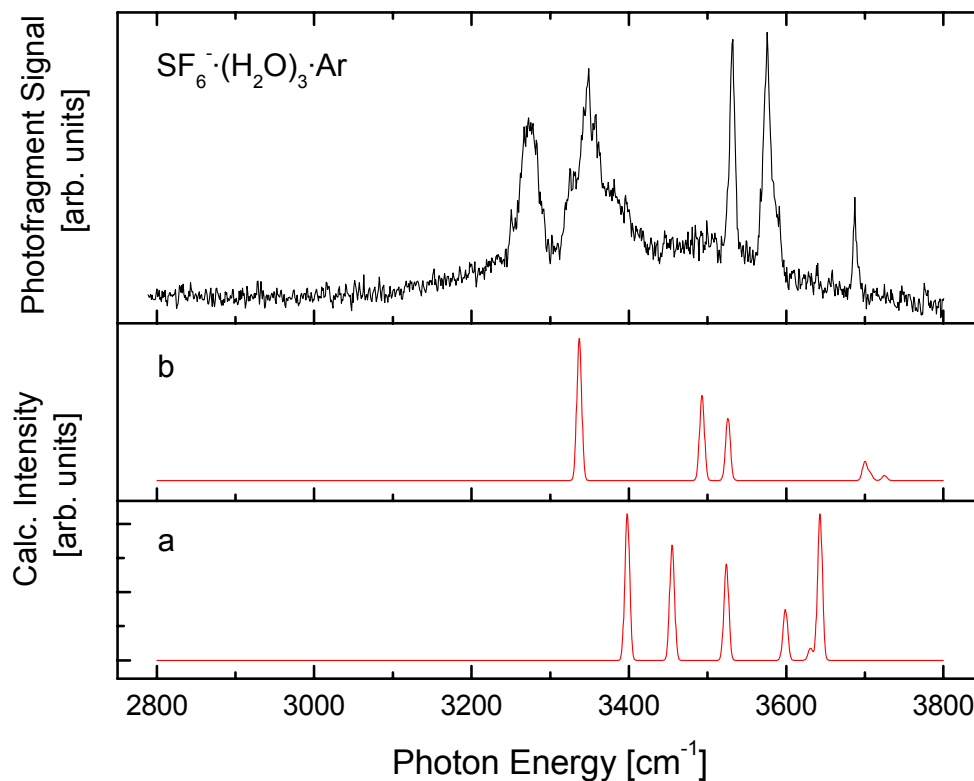


Figure 3.28 Experimental spectrum of the SF₆⁻·(H₂O)₃ (monitored by the loss of one Ar atom, see top trace) as compared to the simulated spectra (MP2/TZVPP, scaled for anharmonicity, see text) of isomer (a) and (b), Figure 3.27. The simulation for isomer (b) fits the experimental spectrum better, although it is higher in energy than isomer (a) (Simulations assume a Gaussian peak shape and a FWHM of 6 cm⁻¹)

3.4.3.4. Structures of the SF₆⁻·(H₂O)_n (n = 1 - 3) clusters and implications for their reactivity

In spite of our intense efforts, we were unsuccessful in triggering any reaction within the SF₆⁻·(H₂O)_n (n = 1 - 3) complexes upon excitation with a mid-IR photon. However, Arnold *et al.* have reported reactions between the SF₆⁻ anion and water in an ion flow tube experiment at room temperature,⁷⁵ with formation of SOF₄⁻ as the

main reaction channel. The structures which have been determined to represent the ground states of the respective clusters in accordance with the experimentally monitored infrared spectra are still useful in order to elucidate the reaction mechanisms involved. The SF bond involved in the strong hydrogen bonding interaction with one or several of the water ligands is significantly stretched from ~ 171 pm in the bare SF_6^- anion to ~ 196 pm in the monohydrate. This implies that attachment of a water molecule leads to localization of electron density in the antibonding σ^* orbital of the respective SF group, diminishing it consequentially in other parts of the molecule. This can be illustrated in a plot of the highest occupied molecular orbital (HOMO) of the $\text{SF}_6^-\cdot(\text{H}_2\text{O})$ complex, shown in Figure 3.29.

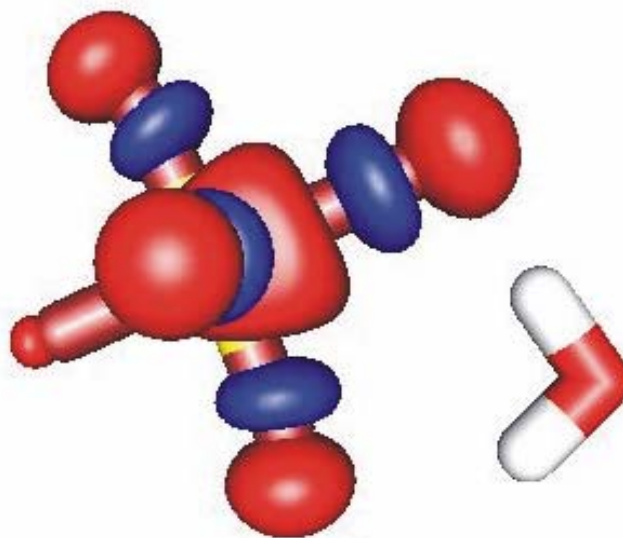
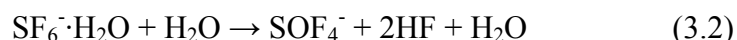


Figure 3.29 Highest occupied molecular orbital (HOMO) of the $\text{SF}_6^-\cdot(\text{H}_2\text{O})$ complex. The localization of negative charge by the presence of the water ligand is clearly visible.

The latter effect manifests itself as a contraction of the SF bond opposite to the “bonding” SF group down to ~ 160 pm from the ~ 171 pm in bare SF_6^- . These findings help to understand the first steps in the reactions of the SF_6^- moiety with protic solvents as described by Arnold *et al.*, attachment of a water molecule seems

to lead to a significant weakening of the SF bond which serves as “anchor” for the ligand, thereby lowering the reaction barrier in collisions of the ion-molecule complex with additional water molecules. It is interesting to note in that context, that the kinetics of these reactions revealed that two solvent molecules were necessary to initiate a reaction leading to products other than the association complex.^{75,76}



The structures at higher hydration levels possess some interesting properties in line with these findings. In the dihydrates, the SF bond involved in the hydrogen bond to the water ligand is stretched even further (~ 206 pm) than in the monohydrate (~ 196 pm), implying that the dissociation threshold is approached upon increasing the number of ligands in the solvation shell. This trend is consistent for both low energy isomers (isomer (a) and (b) in Figure 3.24) determined before to be appropriate candidates for matching the experimental infrared spectrum. Increasing the hydration to the trihydrate, the calculations indicate that the SF bond length is only marginally further increased to ~ 207 pm in isomer (b), while it even shrinks slightly in the case of isomer (a). The special role the attachment of the first two water molecules play in this system is further corroborated by taking a closer look at the binding energies between anion and ligands: for the monohydrate, it is calculated (MP2 level of theory) to amount to ~ 0.45 eV and increases for the second water molecule to ~ 0.48 eV: this is counterintuitive behavior at first glance, as the binding energy of solvent molecules to an anion is usually expected to drop monotonically upon increasing their number. This is compatible with the cooperative behavior in the binding mechanism of the first two water molecules to the SF_6^- anion. Contrary to this behavior, the binding energy drops again for the third water molecule to ~ 0.43 eV, below the value for both the first and the second ligand. Unfortunately, there are no experimental values available for the binding energies to verify these computational results, and it must be cautioned that the level of theory applied in the presented calculations might not be high enough to provide a detailed and reliable background

for further interpretation, particularly in the limit of dissociation and reaction of the systems under consideration. The difference in the values presented above is therefore probably within the error bars of the employed methods. However, they might serve at least as a guideline, in light of the fact that the trend that water molecules promote SF bond breaking seems to be clear. Moreover, they support the assumption that the attachment of the first two water molecules happens in a cooperative fashion, eventually leading to the observation of a cluster-mediated reaction, while the third one does not. However, no reactions could be triggered upon excitation of the $\text{SF}_6^-(\text{H}_2\text{O})_n$ ($n = 1 - 3$) clusters, implying the reaction barrier is not low enough that absorption of one photon in this frequency range would deposit sufficient energy into the cluster to enable the previously observed reaction products. This implies that the reaction barrier must be higher than $\sim 0.40 - 0.45$ eV ($3200 - 3600$ cm^{-1}). In order to understand the energetic requirements we calculated the reaction enthalpies of some candidate reactions. The reaction channel observed experimentally by Arnold *et al.*⁷⁵ is calculated to be exothermic by ~ 1.37 eV:



The reaction partners in those cases in which reactions could be successfully initiated were mostly protic molecules and obviously involvement of an SF group in a strong hydrogen bonding interaction leads to its considerable weakening. This suggests that one of the first crucial steps along the reaction pathway is proton transfer from the respective protic ligand involved to the anionic moiety. The reaction:



is calculated to be endothermic by ~ 1.6 eV. However, it may be overly simplistic to focus on proton transfer as the crucial step alone. In order to arrive at the experimentally observed reaction products more steps need to be involved, and the nature of the potential energy surface along the reaction path is presently unclear. It is interesting in this context to exchange the solvent molecule for one with a higher

acidity in order to shed more light on the reaction channels and the energetic barriers involved. A very suitable candidate is formic acid, as its acidity is noticeably higher than those of water or alcohols. The results of an infrared study on the $\text{SF}_6^- \cdot \text{HCOOH}$ complex as compared to the water clusters described here are presented in the next chapter.

3.4.3.5. Summary and conclusions

The mid-infrared spectra of the $\text{SF}_6^- \cdot (\text{H}_2\text{O})_n$ ($n = 1 - 3$) clusters have been measured. The structures of the ground state geometries could be identified with the aid of accompanying calculations at the MP2 level of theory. The monohydrate was found to display a rather distinct SHB motif, with the water molecule strongly hydrogen bonded to one SF group, the bond length of which is in turn considerably increased, while the remaining OH group is only weakly tethered to one of the neighboring fluorine atoms. Surprisingly, the dihydrate shows the same overall spectral pattern, and indeed the isomers lowest in energy are found to have the two water ligands bound in a shared attack on one SF group in a cooperative manner, even further lengthening its bond. This is unusual in light of the fact that most anions solvated with two water molecules already show the onset of water-water hydrogen bonding interactions, with the exception of some small anions with a strong proton affinity such as F^- . Only for the trihydrate (and presumably for larger clusters) the formation of water networks is found. No reactions could be triggered upon absorption of one infrared photon by the respective cluster chromophores, despite an active search for fragment ion products. However, the cooperative effects in the binding behavior of the first two water molecules are in line with some earlier findings that the reactions between the SF_6^- anion and protic solvent molecules proceed via a cluster-mediated pathway.^{75,76} The fact that protic molecules seem to react readily with the anionic moiety and that attachment of water molecules to the SF_6^- anion leads to a considerable weakening of one of the SF groups points towards a reaction mechanism in which at least one of the initial steps involves proton transfer from one of the ligand molecules.

3.5. References for Chapter III

- ¹ D. H. Powell, G. W. Neilson, and J. E. Enderby, *Journal of Physics-Condensed Matter* **5** (32), 5723 (1993); G. W. Neilson, P. E. Mason, S. Ramos, and D. Sullivan, *Philosophical Transactions of the Royal Society of London Series a-Mathematical Physical and Engineering Sciences* **359** (1785), 1575 (2001).
- ² G. A. Krestov, *Ionic Solvation*. (Prentice Hall, 1994); I. S. Pereygin and N. R. Safiullina, *Zh. Strukt. Khim.* **8**, 205 (1967).
- ³ G. E. Walrafen, *Journal of Chemical Physics* **47** (1), 114 (1967).
- ⁴ S. S. Xantheas, *Journal of Physical Chemistry* **100** (23), 9703 (1996).
- ⁵ C. Bassmann, U. Boesl, D. Yang, G. Drechsler, and E. W. Schlag, *International Journal of Mass Spectrometry and Ion Processes* **159**, 153 (1996).
- ⁶ P. Ayotte, G. H. Weddle, J. Kim, J. Kelley, and M. A. Johnson, *Journal of Physical Chemistry A* **103** (4), 443 (1999).
- ⁷ P. Ayotte, G. H. Weddle, J. Kim, and M. A. Johnson, *Journal of the American Chemical Society* **120** (47), 12361 (1998).
- ⁸ P. Ayotte, J. A. Kelley, S. B. Nielsen, and M. A. Johnson, *Chemical Physics Letters* **316** (5-6), 455 (2000).
- ⁹ W. H. Robertson and M. A. Johnson, *Annual Review of Physical Chemistry* **54**, 173 (2003).
- ¹⁰ S. S. Xantheas and T. H. Dunning, *Journal of Physical Chemistry* **98** (51), 13489 (1994).
- ¹¹ W. H. Robertson, E. A. Price, J. M. Weber, J. W. Shin, G. H. Weddle, and M. A. Johnson, *J. Phys. Chem. A* **107** (34), 6527 (2003).
- ¹² B. F. Yates, H. F. Schaefer, T. J. Lee, and J. E. Rice, *Journal of the American Chemical Society* **110** (19), 6327 (1988).
- ¹³ E. A. Price, W. H. Robertson, E. G. Diken, G. H. Weddle, and M. A. Johnson, *Chemical Physics Letters* **366** (3-4), 412 (2002).
- ¹⁴ W. H. Thompson and J. T. Hynes, *Journal of the American Chemical Society* **122** (26), 6278 (2000).

- 15 K. Hermansson, *Journal of Chemical Physics* **99** (2), 861 (1993).
- 16 E. A. Woronowicz, W. H. Robertson, G. H. Weddle, M. A. Johnson, E. M. Myshakin, and K. D. Jordan, *Journal of Physical Chemistry A* **106** (31), 7086 (2002).
- 17 P. Jungwirth and D. J. Tobias, *Chemical Reviews* **106** (4), 1259 (2006); P. Jungwirth and D. J. Tobias, *Journal of Physical Chemistry A* **106** (2), 379 (2002); P. Jungwirth and D. J. Tobias, *Journal of Physical Chemistry B* **105** (43), 10468 (2001); P. Jungwirth and D. J. Tobias, *Journal of Physical Chemistry B* **106** (25), 6361 (2002).
- 18 P. Ayotte, G. H. Weddle, J. Kim, and M. A. Johnson, *Chemical Physics* **239** (1-3), 485 (1998).
- 19 P. Ayotte, S. B. Nielsen, G. H. Weddle, M. A. Johnson, and S. S. Xantheas, *J. Phys. Chem. A* **103** (50), 10665 (1999).
- 20 F. Huisken, M. Kaloudis, and A. Kulcke, *Journal of Chemical Physics* **104** (1), 17 (1996); G. P. Ayers and A. D. E. Pullin, *Spectrochimica Acta Part a-Molecular and Biomolecular Spectroscopy* **32** (10), 1629 (1976).
- 21 W. H. Robertson, E. G. Diken, E. A. Price, J. W. Shin, and M. A. Johnson, *Science* **299** (5611), 1367 (2003).
- 22 H. Kawamata, T. Maeyama, and N. Mikami, *Chemical Physics Letters* **370** (3-4), 535 (2003).
- 23 P. Ayotte, G. H. Weddle, and M. A. Johnson, *J. Chem. Phys.* **110** (15), 7129 (1999).
- 24 O. M. Cabarcos, C. J. Weinheimer, J. M. Lisy, and S. S. Xantheas, *Journal of Chemical Physics* **110** (1), 5 (1999).
- 25 E. A. Price, N. I. Hammer, and M. A. Johnson, *Journal of Physical Chemistry A* **108** (18), 3910 (2004).
- 26 D. Y. Wu, S. Duani, X. M. Liu, Y. C. Xu, Y. X. Jiang, B. Ren, X. Xu, S. H. Lin, and Z. Q. Tian, *Journal of Physical Chemistry A* **112** (6), 1313 (2008).
- 27 C. G. Zhan and S. Iwata, *Chemical Physics Letters* **232** (1-2), 72 (1995).
- 28 M. S. Taylor, F. Muntean, W. C. Lineberger, and A. B. McCoy, *Journal of Chemical Physics* **121** (12), 5688 (2004).

- ²⁹ F. Misaizu, K. Tsukamoto, M. Sanekata, and K. Fuke, *Laser Chemistry* **15** (2-4), 195 (1995); G. J. Rathbone, T. Sanford, D. Andrews, and W. C. Lineberger, *Chemical Physics Letters* **401** (4-6), 570 (2005).
- ³⁰ D. van Heijnsbergen, G. von Helden, G. Meijer, P. Maitre, and M. A. Duncan, *Journal of the American Chemical Society* **124** (8), 1562 (2002); T. D. Jaeger, D. van Heijnsbergen, S. J. Klippenstein, G. von Helden, G. Meijer, and M. A. Duncan, *Journal of the American Chemical Society* **126** (35), 10981 (2004); M. A. Duncan, *International Reviews in Physical Chemistry* **22** (2), 407 (2003); B. M. Reinhard, A. Lagutschenkov, J. Lemaire, P. Maitre, P. Boissel, and G. Niedner-Schatteburg, *J. Phys. Chem. A* **108** (16), 3350 (2004); J. M. Lisy, *International Reviews in Physical Chemistry* **16** (3), 267 (1997); T. D. Vaden, C. J. Weinheimer, and J. M. Lisy, *Journal of Chemical Physics* **121** (7), 3102 (2004); D. van Heijnsbergen, G. von Helden, M. A. Duncan, A. J. A. van Roij, and G. Meijer, *Physical Review Letters* **83** (24), 4983 (1999); M. A. Duncan, *International Journal of Mass Spectrometry* **200** (1-3), 545 (2000); A. Fielicke, G. Meijer, and G. von Helden, *Journal of the American Chemical Society* **125** (12), 3659 (2003).
- ³¹ M. L. Kimble and A. W. Castleman, *International Journal of Mass Spectrometry* **233** (1-3), 99 (2004); U. Heiz and E. L. Bullock, *Journal of Materials Chemistry* **14** (4), 564 (2004); L. D. Socaciu, J. Hagen, T. M. Bernhardt, L. Woste, U. Heiz, H. Hakkinen, and U. Landman, *Journal of the American Chemical Society* **125** (34), 10437 (2003); H. Häkkinen, W. Abbet, A. Sanchez, U. Heiz, and U. Landman, *Angewandte Chemie-International Edition* **42** (11), 1297 (2003); A. Sanchez, S. Abbet, U. Heiz, W. D. Schneider, H. Häkkinen, R. N. Barnett, and U. Landman, *J. Phys. Chem. A* **103** (48), 9573 (1999).
- ³² B. Yoon, H. Hakkinen, U. Landman, A. S. Worz, J. M. Antonietti, S. Abbet, K. Judai, and U. Heiz, *Science* **307** (5708), 403 (2005).
- ³³ M. L. Kimble, A. W. Castleman, R. Mitric, C. Burgel, and V. Bonacic-Koutecky, *Journal of the American Chemical Society* **126** (8), 2526 (2004); A. S. K. Hashmi and G. J. Hutchings, *Angewandte Chemie-International Edition* **45** (47), 7896 (2006); S. Chretien, S. K. Buratto, and H. Metiu, *Current Opinion in Solid State & Materials Science* **11** (5-6), 62 (2007).
- ³⁴ M. S. Chen and D. W. Goodman, *Chemical Society Reviews* **37** (9), 1860 (2008).
- ³⁵ A. S. Worz, U. Heiz, F. Cinquini, and G. Pacchioni, *Journal of Physical Chemistry B* **109** (39), 18418 (2005).
- ³⁶ E. S. Kryachko, *Journal of Molecular Structure* **880** (1-3), 23 (2008); W. Zheng, X. Li, S. Eustis, A. Grubisic, O. Thomas, H. de Clercq, and K. Bowen,

- Chemical Physics Letters **444** (4-6), 232 (2007); M. S. Taylor, J. Barbera, C. P. Schulz, F. Muntean, A. B. McCoy, and W. C. Lineberger, Journal of Chemical Physics **122** (5) (2005); F. Misaizu, K. Tsukamoto, M. Sanekata, and K. Fuke, Surface Review and Letters **3** (1), 405 (1996).
- 37 F. Muntean, M. S. Taylor, A. B. McCoy, and W. C. Lineberger, Journal of Chemical Physics **121** (12), 5676 (2004).
- 38 R. G. Parr and W. Yang, *Density-Functional Theory of Atoms and Molecules*. (Oxford University Press, New York, 1989).
- 39 A. D. Becke, Physical Review A **38** (6), 3098 (1988); C. T. Lee, W. T. Yang, and R. G. Parr, Physical Review B **37** (2), 785 (1988).
- 40 A. Schäfer, C. Huber, and R. Ahlrichs, J. Chem. Phys. **100** (8), 5829 (1994).
41 R. Ahlrichs, M. Bär, M. Häser, H. Horn, and C. Kölmel, Chemical Physics Letters **162** (3), 165 (1989).
- 42 H. Schneider, A. D. Boese, and J. M. Weber, J. Chem. Phys. **123**, 084307 (2005).
- 43 R. C. Bilodeau, M. Scheer, and H. K. Haugen, Journal of Physics B-Atomic Molecular and Optical Physics **31** (17), 3885 (1998); H. Hotop and W. C. Lineberger, Journal of Physical and Chemical Reference Data **14** (3), 731 (1985); D. G. Leopold, J. Ho, and W. C. Lineberger, Journal of Chemical Physics **86** (4), 1715 (1987).
- 44 T. Lenzer, I. Yourshaw, M. R. Furlanetto, G. Reiser, and D. M. Neumark, Journal of Chemical Physics **110** (19), 9578 (1999).
- 45 S. A. Corcelli, J. A. Kelley, J. C. Tully, and M. A. Johnson, J. Phys. Chem. A **106** (19), 4872 (2002).
- 46 S. B. Nielsen, P. Ayotte, J. A. Kelley, and M. A. Johnson, Journal of Chemical Physics **111** (21), 9593 (1999).
- 47 E. M. Myshakin, K. D. Jordan, E. L. Sibert, and M. A. Johnson, Journal of Chemical Physics **119** (19), 10138 (2003).
- 48 P. C. Singh and G. N. Patwari, Journal of Physical Chemistry A **111** (16), 3178 (2007).
- 49 J. P. Gallivan and D. A. Dougherty, Organic Letters **1** (1), 103 (1999); Y. Danten, T. Tassaing, and M. Besnard, Journal of Physical Chemistry A **103** (18), 3530 (1999).

- 50 T. M. Miller, J. M. Van Doren, and A. A. Viggiano, *International Journal of Mass Spectrometry* **233** (1-3), 67 (2004).
- 51 S. N. Eustis, D. Wang, K. H. Bowen, and G. N. Patwari, *Journal of Chemical Physics* **127** (11) (2007).
- 52 G. W. Dillow and P. Kebarle, *Journal of the American Chemical Society* **111** (15), 5592 (1989).
- 53 R. J. Gulley, S. L. Lunt, J. P. Ziesel, and D. Field, *Journal of Physics B-Atomic Molecular and Optical Physics* **31** (12), 2735 (1998).
- 54 M. Mitsui, A. Nakajima, and K. Kaya, *Journal of Chemical Physics* **117** (21), 9740 (2002); M. Mitsui, A. Nakajima, K. Kaya, and U. Even, *Journal of Chemical Physics* **115** (13), 5707 (2001).
- 55 S. A. Lyapustina, S. K. Xu, J. M. Nilles, and K. H. Bowen, *J. Chem. Phys.* **112** (15), 6643 (2000); J. Schiedt, W. J. Knott, K. Le Barbu, E. W. Schlag, and R. Weinkauff, *J. Chem. Phys.* **113** (21), 9470 (2000).
- 56 J. R. Reimers, R. O. Watts, and M. L. Klein, *Chemical Physics* **64** (1), 95 (1982).
- 57 H. Schneider, K. M. Vogelhuber, and J. M. Weber, *J. Chem. Phys.* **127**, 114311 (2007).
- 58 I. V. Beregovaya and L. N. Shchegoleva, *International Journal of Quantum Chemistry* **88** (4), 481 (2002).
- 59 F. Volatron and C. Roche, *Chemical Physics Letters* **446** (4-6), 243 (2007).
- 60 Y. M. Xie, H. F. Schaefer, and F. A. Cotton, *Chemical Communications* (1), 102 (2003).
- 61 T. Lenzer, I. Yourshaw, M. R. Furlanetto, N. L. Pivonka, and D. M. Neumark, *Journal of Chemical Physics* **115** (8), 3578 (2001).
- 62 I. Becker and O. Cheshnovsky, *Journal of Chemical Physics* **110** (13), 6288 (1999).
- 63 S. T. Arnold, J. H. Hendricks, and K. H. Bowen, *Journal of Chemical Physics* **102** (1), 39 (1995).
- 64 M. Onda, H. Yamada, M. Mori, H. Miyazaki, and I. Yamaguchi, *Journal of Molecular Structure* **319**, 297 (1994).

- 65 W. R. Garrett, *Physical Review A* **3** (3), 961 (1971).
- 66 J. M. Weber, W. H. Robertson, and M. A. Johnson, *Journal of Chemical Physics* **115** (23), 10718 (2001).
- 67 D. M. Neumark, K. R. Lykke, T. Andersen, and W. C. Lineberger, *Journal of Chemical Physics* **83** (9), 4364 (1985).
- 68 E. P. Wigner, *Physical Review* **73** (9), 1002 (1948).
- 69 S. G. Frankiss and D. J. Harrison, *Spectrochimica Acta Part a-Molecular and Biomolecular Spectroscopy* **31** (12), 1839 (1975).
- 70 J. M. Weber, J. A. Kelley, S. B. Nielsen, P. Ayotte, and M. A. Johnson, *Science* **287** (5462), 2461 (2000).
- 71 W. T. Sturges, T. J. Wallington, M. D. Hurley, K. P. Shine, K. Sihra, A. Engel, D. E. Oram, S. A. Penkett, R. Mulvaney, and C. A. M. Brenninkmeijer, *Science* **289** (5479), 611 (2000).
- 72 A. R. Ravishankara, S. Solomon, A. A. Turnipseed, and R. F. Warren, *Science* **259** (5092), 194 (1993).
- 73 R. J. Vanbrunt and J. T. Herron, *Ieee Transactions on Electrical Insulation* **25** (1), 75 (1990).
- 74 L. G. Huey, D. R. Hanson, and C. J. Howard, *Journal of Physical Chemistry* **99** (14), 5001 (1995).
- 75 S. T. Arnold and A. A. Viggiano, *Journal of Physical Chemistry A* **105** (14), 3527 (2001).
- 76 W. B. Knighton, D. R. Zook, and E. P. Grimsrud, *Journal of the American Society for Mass Spectrometry* **1** (5), 372 (1990).
- 77 H. Schneider and J. M. Weber, *J. Chem. Phys.* **127**, 244310 (2007).
- 78 N. R. Brinkmann and H. F. Schaefer, *Chemical Physics Letters* **381** (1-2), 123 (2003).
- 79 E. C. M. Chen, J. R. Wiley, C. F. Batten, and W. E. Wentworth, *Journal of Physical Chemistry* **98** (1), 88 (1994).
- 80 F. Weigend and M. Häser, *Theoretical Chemistry Accounts* **97** (1-4), 331 (1997); F. Weigend, M. Häser, H. Patzelt, and R. Ahlrichs, *Chemical Physics Letters* **294** (1-3), 143 (1998).

- 81 G. L. Gutsev and R. J. Bartlett, *Molecular Physics* **94** (1), 121 (1998).
- 82 C. L. Lugez, M. E. Jacox, R. A. King, and H. F. Schaefer, *Journal of Chemical Physics* **108** (23), 9639 (1998).
- 83 J. C. Bopp, J. R. Roscioli, M. A. Johnson, T. M. Miller, A. A. Viggiano, S. M. Villano, S. W. Wren, and W. C. Lineberger, *Journal of Physical Chemistry A* **111** (7), 1214 (2007).
- 84 C. G. Bailey, J. Kim, C. E. H. Dessent, and M. A. Johnson, *Chemical Physics Letters* **269** (1-2), 122 (1997).

4. Infrared-Triggered Reactions

4.1. *Some general remarks on ion-molecule reactions*

Elucidation of the state-resolved dynamics of chemical reactions is one of the basic problems of chemistry and necessary for a detailed understanding of the mechanisms by which reactions are governed. Reactions involving anions are of particular interest, as they play crucial roles in some of the most common reactions in organic chemistry, e.g. substitutions, eliminations and reactions involving organometallic compounds such as Grignard reactions, aldol condensations and many others.¹ Moreover, anions offer the advantage that they only rarely rearrange, in contrast to cations, for which this is a frequently observed complication. Most of the reactions cited above are extremely important in chemical synthesis and, of course, take place then in some sort of solvent. When it comes to shedding light on ion-molecule reaction mechanisms, it can be advantageous in many cases to study them in the gas phase despite some differences which are inherently involved in removing the solvent molecules from the reactants. However, the interpretation of most experiments conducted in solution suffer from complications such as transport phenomena, cage effects, the presence of counter ions and other solvation effects. Many of these problems can be circumvented by studying the reactions of interest in the gas phase. In addition, experiments in the gas phase have direct implications for photochemical reactions under atmospheric conditions. Examples include dissociation of ground electronic state molecules relevant in the atmosphere by vibrational overtone pumping.² The influence of solvent molecules on ion-molecule reactions may be investigated by attaching them to the ions prior to reaction and stepwise increasing their number one at a time. This can be easily achieved in experiments featuring mass selection, thereby offering another advantage over condensed phase experiments. It is worthwhile to point out some important differences between ion-molecule reactions proceeding in the condensed phase versus gas phase. First, in the gas phase the reactions may take place at substantial collisional energies due to the long range ion-dipole potential between the

reaction partners. This interaction will be effectively absorbed by the solvent molecules in liquid phase, influencing orientation and reactivity of the reacting molecules. Moreover, the reaction can be drastically influenced by differential solvation effects, leading to considerable changes in the relative energy of reactants, products and transition state. This can be illustrated by the example of the S_N2 reaction. It is well-established that in liquid phase, the reaction displays a barrier higher in energy than both reactants and products (the transition state corresponds to a Walden inversion state $[Y\cdots R\cdots X]^-$, compare Figure 4.1).³ In the gas phase, however, a different picture arises^{4,5} and a double-well shape for the potential energy surface along this reaction has been established by Brauman and coworkers.⁶ The explanation for the differences compared to the liquid phase can be found in the relative solvation energies of the species involved: the reactant and product ions which display a relatively localized negative charge are effectively solvated, resulting in considerable stabilization. This is less true for the intermediate entrance and exit channel complexes, and the comparatively diffuse transition state profits least from the solvent stabilization effect, which is why the barrier height is increased in solution relative to reactants and products.⁷ A schematic of the potential energy profile for the reaction is shown in Figure 4.1 (from Ref.⁸). The multitude of fundamental problems inherent even to such a relatively simple chemical reaction is reflected in the long-standing interest, both experimentally and theoretically (compare Ref.^{4,5} and references therein). Important questions related to nucleophilic substitutions range from measurements of the thermal rate constants,⁹ reaction cross-sections and product distributions at different translational energies¹⁰ to studies in variable temperature-selected ion flow drift tube experiments¹¹ and investigations on the complex formation and attack mechanisms⁴ and time-resolved photoelectron spectroscopy experiments,¹² to name a few. Crossed molecular beam imaging experiments reveal new subtle details on the mechanisms involved.^{8,13} Moreover, this reaction has been studied by means of infrared predissociation spectroscopy.¹⁴

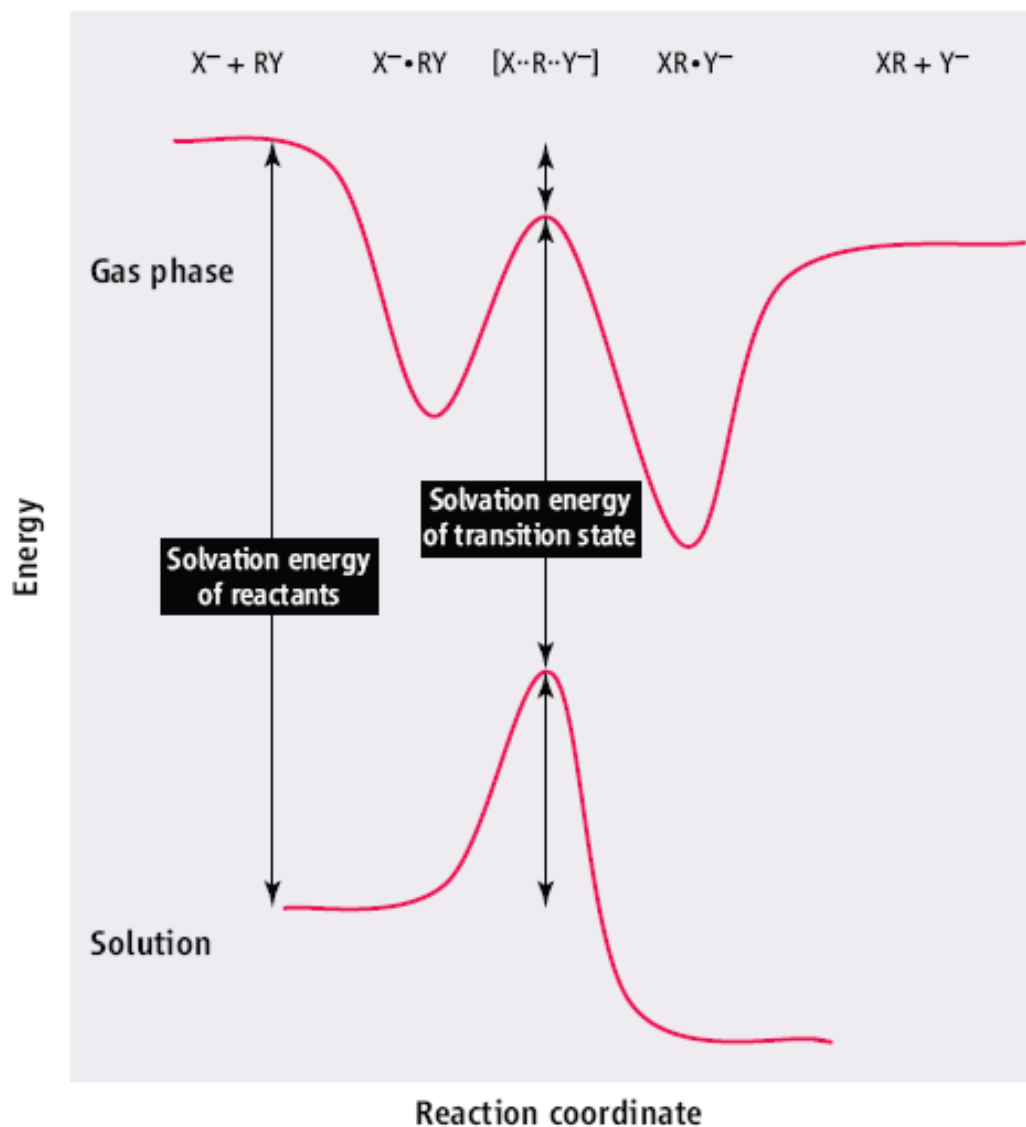
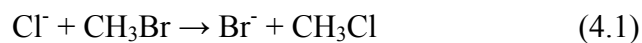


Figure 4.1 One-dimensional potential energy profile for a nucleophilic substitution (S_N2) both in the gas phase and in solution (from Ref.⁸)

This approach offers several interesting features. First, it provides the opportunity to study reactive intermediates “trapped” in their complex structures and thereby to unambiguously identify their geometries. For example, it could be shown that the entrance channel complex for the reaction



adopts C_{3v} symmetry, with the chloride ion attached to the hydrogen atoms of the methyl group in a “pocket-like” conformation, resembling a backside attack of the chloride anion (representing the nucleophile in this case). Another example for elucidation of the structure of a trapped reactive intermediate using infrared predissociation spectroscopy is the characterization of the $\text{OH}\cdot\text{HCH}_2\cdot$ intermediate in the $\text{O}^- + \text{CH}_4$ reaction.¹⁵ In addition, Ar tagging offers the possibility of subtly tuning the internal energy of the complexes under investigation. This was exploited in the study on the reaction between the chloride anion and methylbromide, where Ar tagging of the $\text{Cl}^-\text{CH}_3\text{Br}\cdot\text{Ar}_3$ cluster allowed for the spectroscopic investigation of this cold species, while in the case of the bare complex the reaction could be triggered upon excitation with an infrared photon.

In this work, infrared predissociation spectra of the $\text{SF}_6^-\text{HCOOH}\cdot\text{Ar}_n$ ($n = 0 - 2$) are recorded. The complexes are investigated both with respect to their geometries and their reaction behavior. The obtained results and interpretations are presented in the next section.

4.2. Infrared Spectra of $\text{SF}_6^-\text{HCOOH}\cdot\text{Ar}_n$ ($n = 0 - 2$): Infrared-Triggered Reaction and Ar-Induced Inhibition

4.2.1. Introduction

The importance of the sulfur hexafluoride molecule in industrial applications and in the atmosphere has already been pointed out in section 3.4. It has been described there, too, that in some of the reactions involving SF_6 , its anion is thought to occur as an intermediate, e.g. in electrical discharges. Moreover, it has been shown that the SF_6^- anion does react with atmospheric trace gases¹⁶ and in ion flow tube experiments at room temperature readily undergoes reaction with a number of protic ligands such as water and alcohols with short aliphatic chains.¹⁷ These reactions are cluster-mediated, which means they proceed through a stable anion-ligand complex that is activated in subsequent collisions.^{17,18} The infrared predissociation spectra and the

structures of the $\text{SF}_6^-(\text{H}_2\text{O})_n$ ($n = 1 - 3$) clusters have been described in detail in section 3.4. For these species, no reactions were triggered by infrared absorption in the region of the OH stretching fundamentals, presumably because the barrier associated with this reaction is greater than the photon energy. However, the calculations suggested a cooperative binding mechanism between the SF_6^- anion and the first two water molecules, weakening the SF bond involved in the hydrogen bonding to the water ligands considerably.¹⁹ In anion-molecule reactions, proton transfer often dictates the shape of the potential energy surface governing the behavior of the relevant particles.²⁰ In the case of SF_6^- , dissociative proton transfer could lead to the formation of HF molecules. Consequently, an increase in the acidity of the ligand could lower the barrier to infrared photoactivation. Here, we present infrared studies on complexes of SF_6^- with one formic acid molecule.

4.2.2. Calculations

Calculations on the $\text{SF}_6^- \cdot \text{HCOOH}$ complex have been performed by Skodje and Takahashi.²¹ Briefly, both *ab initio* calculations employing second order Møller-Plesset perturbation theory (MP2) and calculations based on density functional theory (DFT) have been carried out. Two stable geometries were obtained (shown in Figure 4.2). The OH group is strongly hydrogen bonded to the SF_6 moiety in both geometries. The counterpoise corrected difference in energy between the isomers (based on second order Møller-Plesset perturbation theory) is 168 meV, with isomer 1 being more stable. The vibrational frequencies of both isomers have been calculated in the harmonic approximation. Moreover, for six selected modes of the formic acid moiety anharmonicity was taken into account in a one-dimensional model (namely for the C-H stretch, the O-H stretch, the C=O stretch, the O-H bend, the C-H bend, and the C-O stretch).

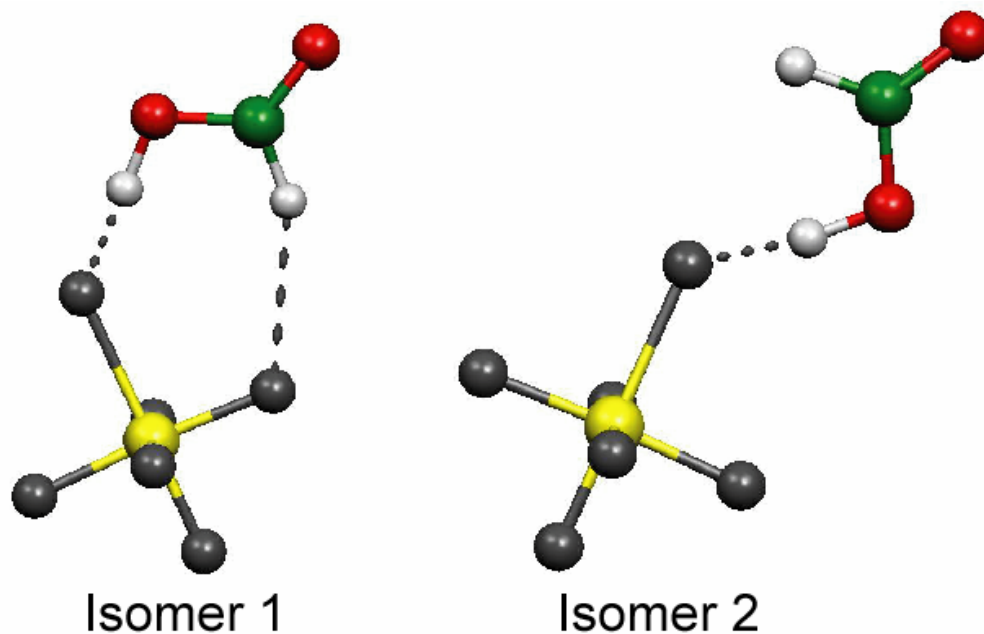


Figure 4.2 Structures of the two lowest lying isomers of $\text{SF}_6 \cdot \text{HCOOH}$, isomer 1 is the global minimum

To obtain an understanding of the effect of mode coupling, four three-dimensional vibrational calculations were performed for isomer 1. Since the O-H and C-H stretching modes have the strongest intensity in the relevant spectral region, the mode coupling of the remaining four coordinates to those two stretching modes was determined in the three-dimensional calculations. The calculation for the transition state only converged at the DFT level of theory. Thus, all the tunneling analysis on the reaction was performed using this method. The details of the theoretical methods applied are to be published in Ref.²²

4.2.3. Results and discussion

4.2.3.1. Structure and vibrational assignments

Figure 4.3 shows the infrared Ar predissociation spectra of the $\text{SF}_6^-\cdot\text{HCOOH}\cdot\text{Ar}_2$, $\text{SF}_6^-\cdot\text{HCOOD}\cdot\text{Ar}_2$, and $\text{SF}_6^-\cdot\text{DCOOH}\cdot\text{Ar}_2$ complexes (no reactions other than Ar evaporation have been found for these parent ions).

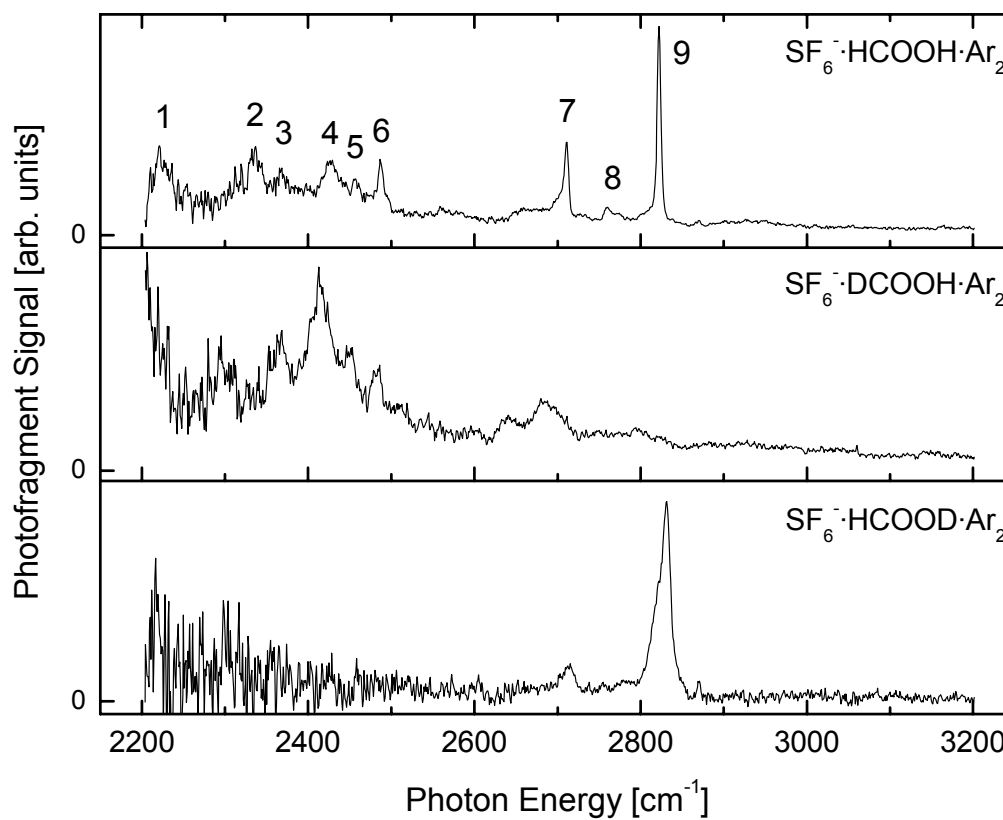


Figure 4.3 Vibrational Ar predissociation spectra of $\text{SF}_6^-\cdot\text{HCOOH}\cdot\text{Ar}_2$, $\text{SF}_6^-\cdot\text{DCOOH}\cdot\text{Ar}_2$ and $\text{SF}_6^-\cdot\text{HCOOD}\cdot\text{Ar}_2$

The spectrum of $\text{SF}_6 \cdot \text{HCOOH} \cdot \text{Ar}_2$ displays two sharp, intense bands at 2710 and 2822 cm^{-1} (bands 7 and 9 in Figure 4.3), respectively, and several overlapping bands between 2200 and 2500 cm^{-1} . In order to guide the interpretation, it is instructive to compare the present spectrum to the case of $\Gamma \cdot \text{HCOOH}$. Robertson *et al.*²³ showed earlier for this complex that the OH stretching vibration is shifted by ca. 800 cm^{-1} to lower energies upon complexation. The CH stretching fundamental on the other hand is red shifted by only ca. 100 cm^{-1} to 2845 cm^{-1} , resulting in a change of the energetic ordering of the two modes. In addition, they observed a strong band at 2740 cm^{-1} which they assigned to the CH bend overtone, gaining intensity through a Fermi resonance with the close-lying OH stretching fundamental. It seems therefore conceivable that the two strong, sharp bands in the spectrum of $\text{SF}_6 \cdot \text{HCOOH} \cdot \text{Ar}_2$ are due to the CH bending overtone and the CH stretching fundamental, while the many bands at lower energies result from Fermi resonances involving the OH stretching fundamental. Assuming that Ar solvation does not significantly affect the vibrational spectra, the experimental results can be compared to the vibrational calculations on the bare $\text{SF}_6 \cdot \text{HCOOH}$ complex. In Table 4.1, the vibrational frequencies and intensities of both the fundamental and the first overtone of six important modes are presented, calculated by the one-dimensional model (see section 4.2.2). It can be clearly seen that the OH stretching fundamental is calculated to be strongly red shifted by $\sim 1100 \text{ cm}^{-1}$ compared to the bare acid in both isomers. As a result of this pronounced red shift, it falls into the spectral region where the broad multiplet of bands is observed in the experimental spectrum. Moreover, the first overtone of the C-O stretching vibration seems to be a suitable candidate for one of the peaks observed in this region, interacting through a Fermi resonance with the OH stretching fundamental. These findings corroborate the empirical assignment made above. Moreover, only two sharp bands are observed in the CH stretching region (bands 7 and 9 in Figure 4.3) but the calculated frequencies for the two isomers found differ by about 40 cm^{-1} for this mode, which means that the existence of several isomers in the ion beam is very unlikely. One could argue that the two bands are the signatures of two CH stretching bands of two different isomers themselves, however this seems to be highly unlikely as well given that the experimental splitting is $\sim 110 \text{ cm}^{-1}$.

Table 4.1 Fundamental and overtone frequencies and intensities calculated by the one-dimensional model (see section 4.2.2) for the two isomers of SF₆⁻HCOOH

Mode	Isomer 1			Isomer 2	
	$\Delta\nu$	ω (cm ⁻¹)	I (km/mol)	ω (cm ⁻¹)	I (km/mol)
C-O str	1	1244	115.2	1251	140.2
	2	2480	0.7	2496	0.8
CH bend	1	1448	7.6	1436	8.2
	2	2902	0.4	2877	1.0
OH bend	1	1519	264.1	1539	181.2
	2	3050	0.9	3085	0.9
C=O str	1	1782	475.3	1781	658.7
	2	3560	3.4	3558	3.7
OH str	1	2443	3082.2	2354	3521.5
CH str	1	2960	77.2	2920	144.3

This assumption is further supported by the fact that the spectrum is very similar for the bare SF₆⁻HCOOH complex. If several isomers were at play, the relative intensities of the bands should change upon Ar solvation due to different thermal populations, which is not the case (see Figure 4.5). For more refined, anharmonic calculations only the energetically more stable isomer 1 was treated. If we assume that one of these two sharp bands is the signature of the CH stretching mode, then the first two overtones of the CH and the OH bend mode are suitable candidates for the second one, based on the calculations. However, the calculated intensities of these two modes are ~ 100 times weaker than that of the CH stretching mode, which directly shows the importance of mode coupling for the understanding of the spectrum. The results of the three-dimensional calculations taking mode coupling into account are shown in Table 4.2.

Table 4.2 Fundamental and overtone frequencies and intensities calculated by the three-dimensional model for isomer 1

Mode	$\Delta\nu$	ω (cm ⁻¹)	I (km/mol)
C-O str	1	1245	121.2
	2	2477	2.0
CH bend	1	1414	5.6
	2	2804	6.9
OH bend	1	1484	268.7
	2	2975	75.2
C=O str	1	1770	595.3
	2	3529	5.0
OH str	1	2465 ^a , 2463 ^b , 2433 ^c , 2447 ^d	3097.6 ^a , 3119.9 ^b , 3009.9 ^c , 3018.5 ^d
CH str	1	2949 ^a , 2951 ^b , 2949 ^c , 2950 ^d	58.7 ^a , 52.5 ^b , 39.7 ^c , 55.2 ^d

a: Calculated using the CH stretch, OH stretch, and C-O stretch modes.

b: Calculated using the CH stretch, OH stretch, and the CH bend modes.

c: Calculated using the CH stretch, OH stretch, and the OH bend modes.

d: Calculated using the CH stretch, OH stretch, and the C=O stretch modes.

It can be seen that taking mode coupling into consideration causes the CH and OH bend overtones to red shift by ~ 100 cm⁻¹ and an increase in their intensities by an order of magnitude, as it effectively enables them to borrow intensity from the strong OH and CH fundamental transitions. Comparing the other modes it can be seen that the mode coupling does not affect their peak positions; thus the simpler one-dimensional model will be used for the deuterated species. As the intensities are very sensitive to small coupling values, fully anharmonic vibrational calculations may be needed to get the theoretical band positions and intensities to better match the experimentally observed spectra. In order to unambiguously assign some of the individual bands and to gain further insight into the interaction between them

especially in the lower frequency region, the Ar loss spectra of selectively deuterated species have been measured as well. The spectra for both the complex deuterated in the formyl position ($\text{SF}_6^- \cdot \text{DCOOH} \cdot \text{Ar}_2$) and for the complex deuterated on the carboxylic group ($\text{SF}_6^- \cdot \text{HCOOD} \cdot \text{Ar}_2$) are shown in Figure 4.3. The results of the one-dimensional vibrational calculations for the deuterated species are given in Table 4.3.

Table 4.3 Fundamental and overtone frequencies and intensities calculated by the one-dimensional model for $\text{SF}_6^- \cdot \text{DCOOH}$ and $\text{SF}_6^- \cdot \text{HCOOD}$

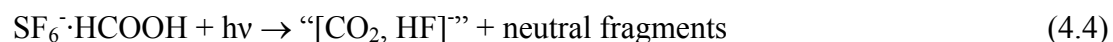
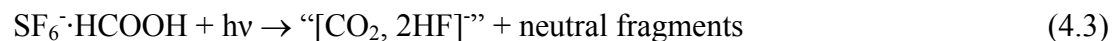
Mode	Δv	$\text{SF}_6^- \cdot \text{DCOOH}$		$\text{SF}_6^- \cdot \text{HCOOD}$	
		ω (cm^{-1})	I (km/mol)	ω (cm^{-1})	I (km/mol)
C-O str	1	1244	94.8	1286	249.2
	2	2483	0.4	2566	2.5
CH(D) bend	1	1048	9.0	1448	10.7
	2	2098	0.2	2901	0.4
OH(D) bend	1	1518	248.6	1077	16.6
	2	3047	0.9	2155	0.1
C=O str	1	1761	492.3	1764	622.1
	2	3519	2.6	3521	4.7
OH(D) str	1	2438	3147.6	1906	1388.3
CH(D) str	1	2219	34.0	2955	34.8

Two intense, sharp bands at 2712 and 2828 cm^{-1} are observed in the high frequency region of the spectrum of $\text{SF}_6^- \cdot \text{HCOOD} \cdot \text{Ar}_2$, while both of these features disappear in the spectrum of the complex deuterated in the formyl position. Based on the calculations, the weaker band at 2712 cm^{-1} (2710 cm^{-1} in the $\text{SF}_6^- \cdot \text{HCOOH} \cdot \text{Ar}_2$ complex, band 7 in Figure 4.3) can therefore be assigned to the overtone of the CH bend vibration, while the more intense band at higher energy (band 9 in Figure 4.3) is

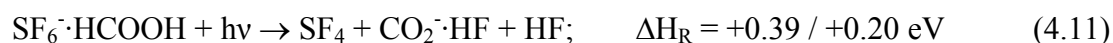
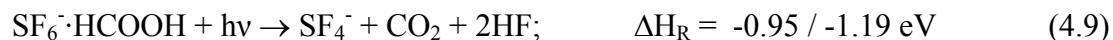
due to the CH stretching fundamental. The spectrum of the complex deuterated in the formyl position retains a feature at 2414 cm^{-1} (corresponding to the band at 2427 cm^{-1} in the $\text{SF}_6^-\cdot\text{HCOOH}\cdot\text{Ar}_2$ complex (band 4 in Figure 4.3) while being absent in the $\text{SF}_6^-\cdot\text{HCOOD}\cdot\text{Ar}_2$ complex) which is affiliated with the OH stretching fundamental. A weaker feature at 2686 cm^{-1} (showing up as an unresolved shoulder on the low frequency side of the CH bending overtone band in the spectrum of the non-deuterated complex) is probably due to a combination band of the OH stretching fundamental with a SF stretch vibration of the hydrogen bonded fluorine which is calculated to occur at $\sim 316\text{ cm}^{-1}$. The band appearing at 2295 cm^{-1} (2336 cm^{-1} in the non-deuterated compound (band 2 in Figure 4.3), while hardly visible in the spectrum of the $\text{SF}_6^-\cdot\text{HCOOD}\cdot\text{Ar}_2$ complex) is assigned to the overtone of the CO stretching vibration, which is calculated to have an excitation frequency in this energy range. The increased intensity of this mode in the spectra of the $\text{SF}_6^-\cdot\text{DCOOH}\cdot\text{Ar}_2$ and the $\text{SF}_6^-\cdot\text{HCOOH}\cdot\text{Ar}_2$ complexes stems from a Fermi resonance with the OH stretching fundamental which cannot be at play in the case of the $\text{SF}_6^-\cdot\text{HCOOD}\cdot\text{Ar}_2$. Finally, a weaker band occurring at 2796 cm^{-1} in the spectrum of $\text{SF}_6^-\cdot\text{DCOOH}\cdot\text{Ar}_2$ (band 8 in Figure 4.3) and at 2761 cm^{-1} for $\text{SF}_6^-\cdot\text{HCOOH}\cdot\text{Ar}_2$ is assigned to the OH bend overtone, based upon the most suitable calculated value. The fact that it is absent in the case of the $\text{SF}_6^-\cdot\text{HCOOD}\cdot\text{Ar}_2$ complex corroborates this interpretation. This is in contradiction with the three-dimensional vibrational calculation, which predicts a rather strong intensity for this transition, however, this might reach the limit of the applicability of the reduced-dimensional treatment. We note that some features remain unexplained (e.g. a band at 2482 cm^{-1} in the spectrum of $\text{SF}_6^-\cdot\text{DCOOH}\cdot\text{Ar}_2$, band 6 in Figure 4.3), an unambiguous interpretation of which would probably require anharmonic calculations for all vibrational degrees of freedom. However, the most important features in the spectra of all three investigated complexes can be assigned in accordance with the presented computational level based on the lowest energy isomer structure as described above.

4.2.3.2. Infrared-triggered reactions

Contrary to the case of the $\text{SF}_6^-(\text{H}_2\text{O})_n$ clusters, we observe infrared triggered reactions in complexes of SF_6^- with formic acid. For $\text{SF}_6^- \cdot \text{HCOOH}$ and $\text{SF}_6^- \cdot \text{HCOOH} \cdot \text{Ar}$ complexes, no loss of neutral ligands from SF_6^- is observed, and the SF_6^- ion is not preserved as an intact molecular species. The absence of the formic acid ligand loss channel is not surprising, as the binding energy of this molecule to the SF_6^- anion is calculated to be 1.22 eV (DFT) and 1.10 eV (MP2), respectively, much greater than the highest accessible photon energy in our experiment. Instead, several new fragment ions were detected upon infrared excitation of the respective anionic complex. Irradiation of the bare $\text{SF}_6^- \cdot \text{HCOOH}$ complex ions results in the following reactions:



The products of reaction channels (4.3) and (4.4) are set into quotation marks, as experimentally the masses of the occurring fragment ions can be observed, but their structures can not be unambiguously assigned at this point. However, educated guesses are possible, supported by calculations on the possible transition state for the reactions, as detailed below. The calculations show that both reactions (4.2) and (4.3) are exothermic, while (4.4) is slightly endothermic:



The values for ΔH_{R} are the DFT / MP2 values, respectively. Consistent with the greater exothermicity for the formation of SF_4^- , this product ion is found to be much more abundant (typically by a factor of about four to five) than the other two

fragment ions, which are observed with approximately equal intensities. Reaction (4.4) is most probably following reaction (4.3), if the original product “[CO₂, 2HF]” possesses enough internal energy to evaporate an HF molecule. Figure 4.4 shows the IR action spectra for the three fragment channels (4.2) - (4.4).

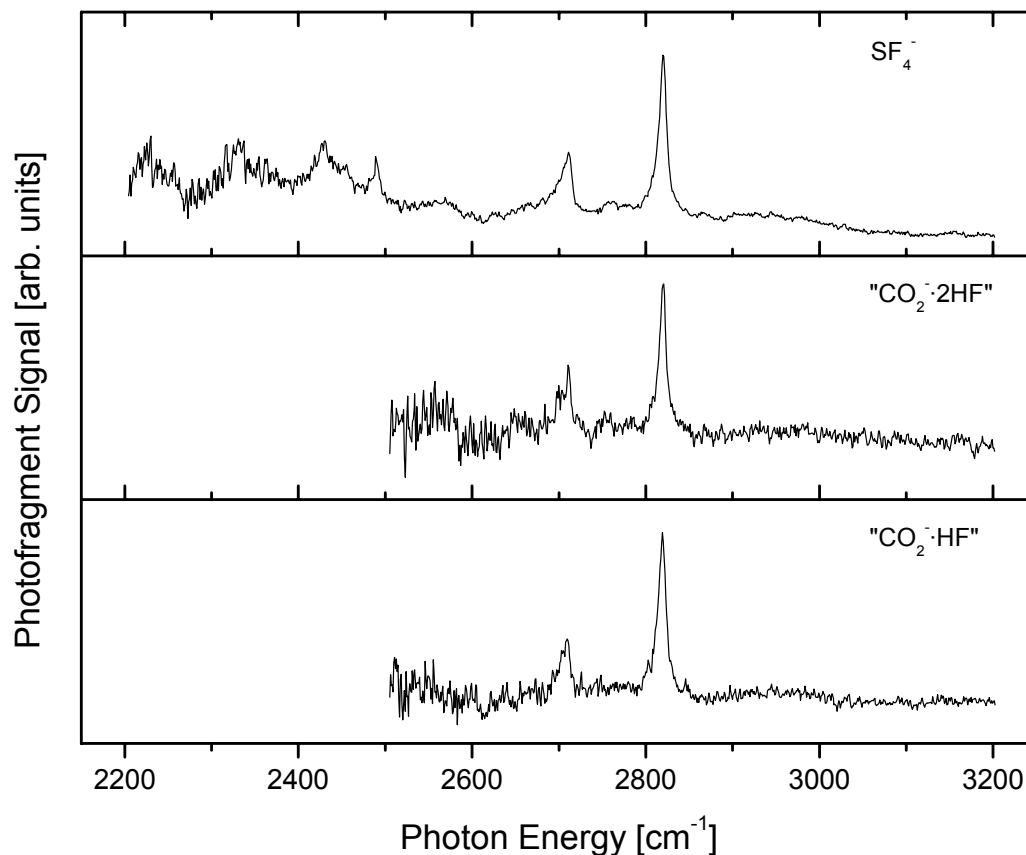


Figure 4.4 Spectrum of SF₆⁻·HCOOH complex recorded via registering the product ions of all possible fragmentation channels: SF₄⁻, “CO₂⁻·2HF” and “CO₂⁻·HF”

These spectra are very similar to those monitored via registering Ar loss from SF₆⁻·HCOOH·Ar₂, with the line widths being narrower for the Ar solvated parent ion. This is likely due to the higher temperature of the bare complexes. As mentioned

above, there is evidence already from the Ar solvated spectrum (shown in Figure 4.3) that only one of the possible isomers is significantly populated in the molecular beam. The similarity of the spectra for bare and Ar solvated $\text{SF}_6^-\cdot\text{HCOOH}$ ions further corroborates this assumption for both species. If several isomers were to coexist in appreciable intensities, then due to the different internal energy contents of the bare and Ar solvated complex one would expect their relative abundances to change drastically for the two species. This in turn should result in different relative intensities of the respective vibrational frequencies, which is not observed experimentally (see Figure 4.5).

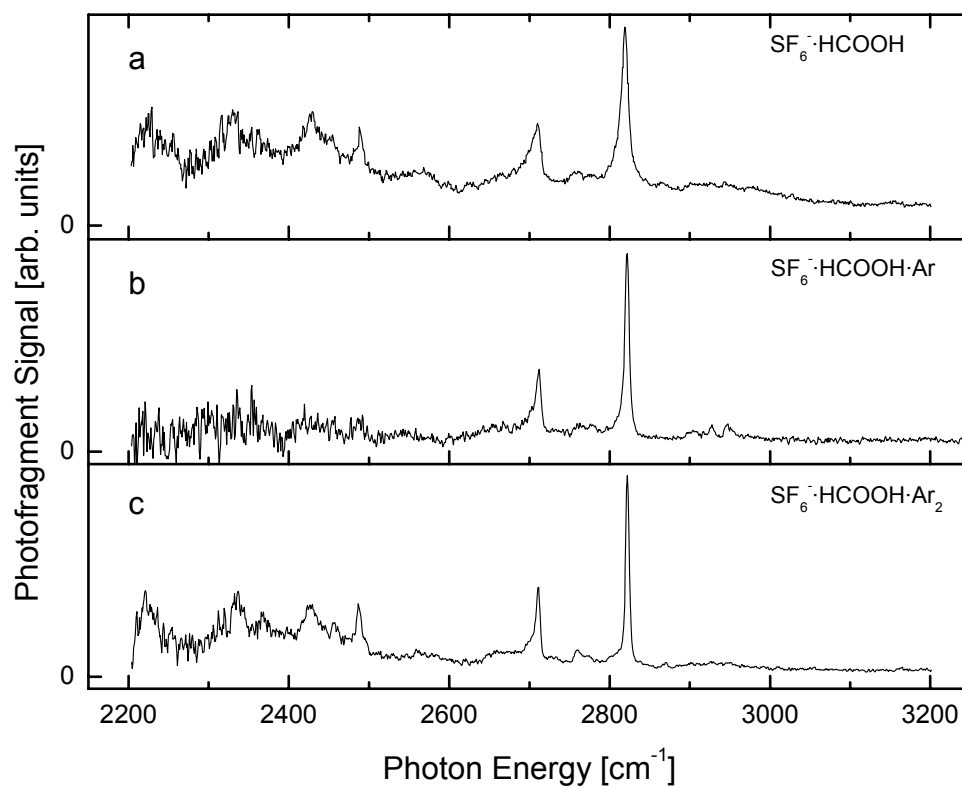


Figure 4.5 Spectra of the $\text{SF}_6^-\cdot\text{HCOOH}$ and the $\text{SF}_6^-\cdot\text{HCOOH}\cdot\text{Ar}$ complexes recorded via registering the product ions of the fragmentation channel leading to the SF_4^- product ion and of the $\text{SF}_6^-\cdot\text{HCOOH}\cdot\text{Ar}_2$ complex via registering the loss of two Ar atoms

The data are therefore consistent with only one isomer being present in the ion beam. For channels (4.3) and (4.4), the signal intensity levels in the OH stretching region are too weak to record spectra with an acceptable signal to noise (S/N) ratio. All three spectra show two bands in the CH stretching region. There is no obvious mode-specificity for the three fragment channels, because the relative intensities for SF_4^- from $\text{SF}_6^- \cdot \text{HCOOH}$ are the same as for Ar evaporation from $\text{SF}_6^- \cdot \text{HCOOH} \cdot \text{Ar}_2$. With $\text{SF}_6^- \cdot \text{HCOOH} \cdot \text{Ar}$ as a parent ion, we find formation of SF_4^- with similar peak positions as for the other species and fragment channels under study (see Figure 4.5). However, the relative intensities of the features at energies below 2600 cm^{-1} and the S/N ratio in this frequency range are greatly reduced in comparison to the spectrum of the bare $\text{SF}_6^- \cdot \text{HCOOH}$ complex monitored by loss of an SF_4^- fragment. In order to shed more light on the reaction mechanisms at play, possible reaction pathways have been calculated based on the experimentally observed fragment ions. One accessible reaction channel could be identified, leading to the $[\text{SF}_4 \cdot \text{CO}_2 \cdot (\text{HF})_2]^-$ product anion. The corresponding adiabatic potential energy curve along the intrinsic reaction coordinate is shown in Figure 4.6. Interestingly, while in the equilibrium configuration of the $\text{SF}_6^- \cdot \text{HCOOH}$ complex the SF2 (labeling as in Figure 4.6) bond is lengthened upon the attack of the formic acid ligand and the formation of a strong hydrogen bond (similar to the case of $\text{SF}_6^- \cdot (\text{H}_2\text{O})_n$ clusters),¹⁹ the F1 fluorine atom undergoes the first reaction, forming HF with the H atom from the CH group of the formic acid moiety. The relevant bond lengths as a function of the reaction coordinate are shown in Figure 4.7. It can be seen that close to the transition state, the transfer of the two hydrogen atoms governs the reaction, with the change in the formyl CH bond length being most significant. The bent structure of the CO_2 moiety in the product complex is consistent with CO_2 being the negative charge carrier after the reaction.²⁴ The negative charge on the thermodynamically unstable CO_2^- (the value for the electron of affinity of CO_2 is: $\text{EA}(\text{CO}_2) \sim -0.6 \text{ eV}^{25}$) is stabilized by solvation with two HF ligands. This also justifies the assignment of the structure of the observed fragment ion in equation (4.10) to a $\text{CO}_2^- \cdot (\text{HF})_2$ cluster. No accessible fragmentation channel was found for isomer 2 as a starting structure.

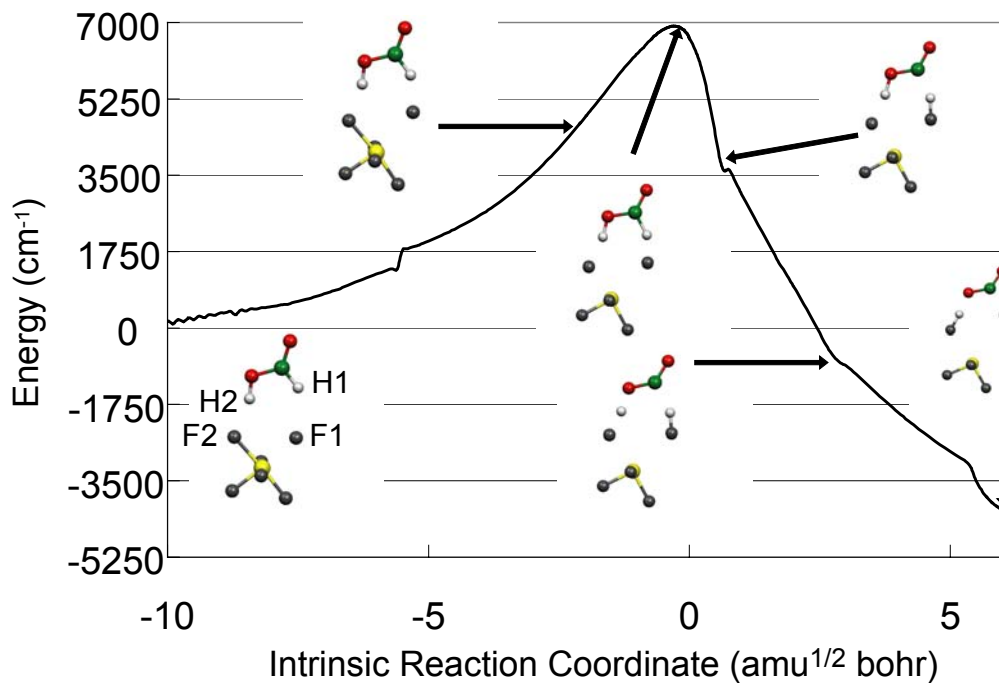


Figure 4.6 Adiabatic potential energy curve along the intrinsic reaction coordinate (calculated at the DFT level of theory)

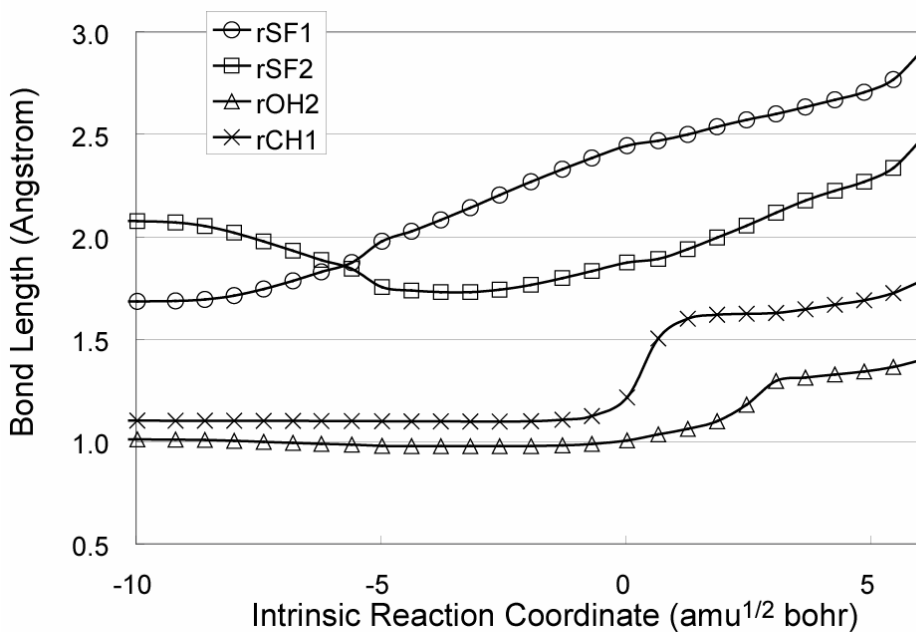


Figure 4.7 Evolution of relevant bond lengths along the reaction coordinate, see Figure 4.6 for the labeling of the atoms

Surprisingly, even the lowest calculated value for the reaction barrier (0.78 eV on the DFT level) is much greater than the energy content of the complex after absorption of an infrared photon (perturbation theory and coupled cluster based calculations using the geometries given by the DFT method gave a much higher barrier of 1.82 and 1.25 eV, respectively). Hence, there is no direct way for the reactants to cross the barrier and the only possibility for the reaction to proceed seems to be via tunneling through the barrier close to the transition state. Since the reaction is a double hydrogen transfer, the tunneling contribution is expected to be large. Based on the experimental detection time of $\tau \sim 20\mu\text{s}$ the dependence of the effective quantum yield on the internal vibrational energy can be calculated.^{21,22} It turns out that even differences of a few hundred wavenumbers lead to drastic changes in the effective quantum yield. This explains the difference in the relative intensities of the SF_4^- yield in the OH stretching and CH stretching regions in the spectra of the $\text{SF}_6^- \cdot \text{HCOOH} \cdot \text{Ar}_n$ complexes for different n . For $n = 0$, there is no specificity of the reaction yield with respect to the photon energy. In other words, the reaction efficiency is uniform over the whole frequency region under study, according to the comparison of the SF_4^- action spectrum for $n = 0$ with the Ar loss action spectrum for $n = 2$ (where the evaporation efficiency is unity). The situation changes dramatically with Ar solvation. The time scale for Ar evaporation (likely on the 10 – 100 ps time scale, see Ref.²⁶ and references therein) is probably much shorter than that for tunneling through the reaction barrier in atomic rearrangement. This implies that the energy usable for SF_6^- activation for $n > 0$ is lower than for $n = 0$ because of Ar evaporation upon IR absorption. Consequently, we observe a photon energy dependence of the reaction efficiency for $n = 1$, leading to inhibition of the reaction at lower photon energies (i.e., in the OH stretching region). For $n = 2$, no SF_4^- formation was detectable, implying a complete suppression of the reaction. The final result according to the PES displayed in Figure 4.6 is formation of the $[\text{SF}_4 \cdots \text{CO}_2 \cdots (\text{HF})_2]^-$ complex. Due to the excess energy available in this product complex, it will dissociate into the experimentally observed $[\text{CO}_2 \cdots (\text{HF})_2]^-$ product and SF_4 . A long-range electron transfer may cause the electron on the CO_2^- to migrate to the SF_4 , resulting predominantly in the SF_4^- production. However, to prove this hypothesis, a high level

multi-reference *ab initio* treatment would be needed, which at present was beyond the available computational resources.

4.2.4. Summary and conclusions

The structures of the $\text{SF}_6^- \cdot \text{HCOOH} \cdot \text{Ar}_n$ ($n = 0 - 2$) complex ions have been investigated using infrared spectroscopy and *ab initio* calculations. It could be shown that the formic acid ligand attaches to the SF_6^- anion via a hydrogen bond involving the acidic proton, while the CH group is weakly tethered to a neighboring fluorine atom. Complexes which are solvated by less than two Ar atoms undergo reactions upon excitation with a mid-infrared photon, leading to three different fragmentation products, namely SF_4^- , $\text{CO}_2^- \cdot (\text{HF})_2$ and $\text{CO}_2^- \cdot \text{HF}$. A possible reaction pathway leading to the $\text{SF}_4^- \cdot \text{CO}_2^- \cdot (\text{HF})_2$ product channel was mapped out computationally and it could be shown that the reaction proceeds predominantly via tunneling through the reaction barrier. This assumption could be corroborated experimentally by studying the effects of differential solvation with Ar atoms on the monitored infrared spectra, thereby effectively varying the internal energy content of the respective anionic complex. No mode specificity is observed for any of the fragmentation channels, meaning that there exists probably no direct coupling between any of the excited modes and the reaction coordinate. This study represents one of the few examples so far, where a reaction in a cluster could be triggered directly upon excitation with one infrared photon exciting fundamental vibrational transitions.

4.3. References for Chapter IV

- ¹ C. H. DePuy, *International Journal of Mass Spectrometry* **200** (1-3), 79 (2000).
- ² D. J. Donaldson, A. F. Tuck, and V. Vaida, *Chemical Reviews* **103** (12), 4717 (2003); V. Vaida, *International Journal of Photoenergy* **7** (2), 61 (2005); V. Vaida, K. J. Feierabend, N. Rontu, and K. Takahashi, *International Journal of Photoenergy* (2008); M. E. Dunn, G. C. Shields, K. Takahashi, R. T. Skodje, and V. Vaida, *Journal of Physical Chemistry A* **112** (41), 10226 (2008); K. Takahashi, K. L. Plath, R. T. Skodje, and V. Vaida, *Journal of Physical Chemistry A* **112** (32), 7321 (2008).
- ³ J. L. Gleave, E. D. Hughes, and C. K. Ingold, *Journal of the Chemical Society*, 236 (1935); C. K. Ingold, *Structure and Reactivity in Organic Chemistry*, 2nd ed. (Cornell University Press, Ithaca, NY, 1969).
- ⁴ B. Bogdanov and T. B. McMahon, *Journal of Physical Chemistry A* **110** (4), 1350 (2006).
- ⁵ J. K. Laerdahl and E. Uggerud, *International Journal of Mass Spectrometry* **214** (3), 277 (2002); S. Schmatz, *Chemphyschem* **5** (5), 600 (2004).
- ⁶ W. N. Olmstead and J. I. Brauman, *Journal of the American Chemical Society* **99** (13), 4219 (1977); J. I. Brauman, *Journal of Mass Spectrometry* **30** (12), 1649 (1995).
- ⁷ J. Chandrasekhar, S. F. Smith, and W. L. Jorgensen, *Journal of the American Chemical Society* **107** (1), 154 (1985).
- ⁸ J. I. Brauman, *Science* **319** (5860), 168 (2008).
- ⁹ S. E. Barlow, J. M. Vandoren, and V. M. Bierbaum, *Journal of the American Chemical Society* **110** (21), 7240 (1988).
- ¹⁰ L. A. Angel and K. M. Ervin, *Journal of the American Chemical Society* **125** (4), 1014 (2003).
- ¹¹ A. A. Viggiano, R. A. Morris, J. S. Paschkewitz, and J. F. Paulson, *Journal of the American Chemical Society* **114** (26), 10477 (1992).
- ¹² R. Wester, A. E. Bragg, A. V. Davis, and D. M. Neumark, *Journal of Chemical Physics* **119** (19), 10032 (2003).

- 13 J. Mikosch, S. Trippel, C. Eichhorn, R. Otto, U. Lourderaj, J. X. Zhang, W. L. Hase, M. Weidemuller, and R. Wester, *Science* **319** (5860), 183 (2008); S. Feil, *Chemie in Unserer Zeit* **42** (2), 67 (2008).
- 14 P. Ayotte, J. Kim, J. A. Kelley, S. B. Nielsen, and M. A. Johnson, *Journal of the American Chemical Society* **121** (29), 6950 (1999).
- 15 E. G. Diken, G. H. Weddle, J. M. Headrick, J. M. Weber, and M. A. Johnson, *J. Phys. Chem. A* **108** (46), 10116 (2004).
- 16 L. G. Huey, D. R. Hanson, and C. J. Howard, *Journal of Physical Chemistry* **99** (14), 5001 (1995).
- 17 S. T. Arnold and A. A. Viggiano, *Journal of Physical Chemistry A* **105** (14), 3527 (2001).
- 18 W. B. Knighton, D. R. Zook, and E. P. Grimsrud, *Journal of the American Society for Mass Spectrometry* **1** (5), 372 (1990).
- 19 H. Schneider and J. M. Weber, *J. Chem. Phys.* **127**, 244310 (2007).
- 20 E. A. Price, W. H. Robertson, E. G. Diken, G. H. Weddle, and M. A. Johnson, *Chemical Physics Letters* **366** (3-4), 412 (2002); J. M. Weber, J. A. Kelley, W. H. Robertson, and M. A. Johnson, *Journal of Chemical Physics* **114** (6), 2698 (2001); P. Ayotte, J. A. Kelley, S. B. Nielsen, and M. A. Johnson, *Chemical Physics Letters* **316** (5-6), 455 (2000); K. Kawaguchi and E. Hirota, *Journal of Chemical Physics* **84** (6), 2953 (1986).
- 21 K. Takahashi, private communication.
- 22 H. Schneider, Takahashi, K., Skodje, R.T., Weber, J.M., in preparation (2009).
- 23 W. H. Robertson, J. A. Kelley, and M. A. Johnson, *Journal of Chemical Physics* **113** (18), 7879 (2000).
- 24 J. Almlof, A. Lund, and K. A. Thuomas, *Chemical Physics Letters* **28** (2), 179 (1974); M. E. Jacox and D. E. Milligan, *Chemical Physics Letters* **28** (2), 163 (1974); D. W. Ovenall and D. H. Whiffen, *Molecular Physics* **4** (2), 135 (1961); J. W. Shin, N. I. Hammer, M. A. Johnson, H. Schneider, A. Glöss, and J. M. Weber, *J. Phys. Chem. A* **109** (14), 3146 (2005).
- 25 M. Knapp, O. Echt, D. Kreisle, T. D. Mark, and E. Recknagel, *Chemical Physics Letters* **126** (3-4), 225 (1986).

- ²⁶ H. Schneider, K. M. Vogelhuber, F. Schinle, J. F. Stanton, and J. M. Weber, *Journal of Physical Chemistry A* **112** (33), 7498 (2008); X. Y. Hong, S. Chen, and D. D. Dlott, *Journal of Physical Chemistry* **99** (22), 9102 (1995); S. Shigeto, Y. Pang, Y. Fang, and D. D. Dlott, *Journal of Physical Chemistry B* **112** (2), 232 (2008); T. Maeyama, I. Yagi, Y. Murota, A. Fujii, and N. Mikami, *Journal of Physical Chemistry A* **110** (51), 13712 (2006); Y. Yamada, J. Okano, N. Mikami, and T. Ebata, *Chemical Physics Letters* **432** (4-6), 421 (2006).

5. Probing anion- π interactions: $\text{Cl}^- \cdot \text{C}_6\text{F}_{6-n}\text{H}_n$ complexes

5.1. Ion coordination and recognition

The selective recognition and binding of ions in solution by specifically designed receptors is an important aspect of supramolecular chemistry. The field of cation coordination dates back into the late 1960s and is based on ground-breaking work of Pedersen, who discovered the coordination chemistry of crown ethers¹ and Dietrich, Lehn, and Sauvage, who reported first results on the coordination chemistry of cryptands.² Since then, there has been intense interest in this particular field of chemistry which therefore has seen a substantial development. In contrast, the field of anion recognition received considerably less attention, although first work on macrobicyclic ammonium cages (katapinands) capable of coordinating to halide anions through electrostatic interactions and hydrogen bonds has been published by Park *et al.*³ only shortly after the above-mentioned results on cation coordination chemistry. This is peculiar in light of the fact that the importance of the chemistry of anions is by no means inferior to that of cations, given that they play a crucial role in many chemical applications such as catalysis and acid-base chemistry. Moreover, they can have a significant impact on the environment, e.g. with respect to the widespread use of fertilizers in agriculture, leading locally to high concentrations of nitrate and phosphate anions, or the production of pertechnetate during the treatment of nuclear fuel. Besides, anions are ubiquitous in biological systems, e.g. 70% of all enzyme substrates are negatively charged and, of course, DNA constitutes a polyanion. These issues directly point towards the importance of the possibility of selectively binding these species. However, the fact that the coordination chemistry of anions only recently started to grow as well may be due to some intrinsic differences between anions and cations.⁴ First, they are larger than the corresponding isoelectronic cations meaning that their charge-to-radius ratio is lower, which in turn leads to comparatively weaker electrostatic interactions. Moreover, many anions can

undergo protonation reactions in protic solvents and are therefore sensitive to the pH value of the solution. This of course impacts any potential receptor, which must function within the appropriate pH window of the anion and also compete with the solvent environment, which might be a difficult task if the latter is capable of forming strong hydrogen bonds to the anion. In addition, anions are usually coordinatively saturated and generally cover a wider size region than cations, ranging from spherical halides to complicated oligophosphate anions. On the one hand, this offers the opportunity for selectivity based on shape but requires on the other hand specifically designed receptors depending on the application in mind. As has been mentioned, the field of anion recognition is important in many areas, with possible applications ranging from supramolecular catalysis (pioneered by Hosseini and Lehn, see book chapter by M.W. Hosseini⁵) to environmental issues, the basic understanding of biological systems, and anion-directed self-assembly as a strategy to develop new synthesis routes for complex molecular architectures. The latter is an important process in nature. For instance, anions have been identified to be crucial as directing agents in protein folding, and self-assembly is at the heart of processes such as formation of DNA from complementary deoxyribonucleic acid, formation of cell membranes and viruses⁶ (see reviews by Beer and Gale^{4,7} and book chapter by Vilar⁸). Further directions can be found in the assembly of coordination nanotubes,⁹ the synthesis of rotaxanes¹⁰ and many others. The synthesis of phase transfer agents, and eventually small molecular sensors and switches are additional areas, which have gained increasing interest.⁶ It is crucial to understand the interactions at play and the conditions which must be met in order to achieve progress. Although the number of synthesized receptors for anion coordination is huge due to their specificity described in the previous section, one can classify them roughly according to the noncovalent interaction forces by which they complex the anionic host.^{4,5} In general, these comprise the following: electrostatic interactions, hydrogen bonds, hydrophobicity, π - π stacking effects, dispersion forces, classical coordination chemistry (e.g. coordination to a metal ion) and, of course, combinations of all these possibilities. The role of aromatic molecules in anion recognition is described in the next section.

5.2. *Aromatic molecules in anion recognition*

The coordination of ions to aromatic molecules offers a new route towards the design of a new versatile class of host molecules. The interactions between cations and aromatic molecules is well understood.¹¹ They constitute relatively strong non-covalent interactions, with the main contributions stemming from electrostatics, such as interaction of partial charges and charge-induced polarization.¹² The supramolecular chemistry of anions in general and their interaction with aromatic units specifically is far less developed. This is partially due to the counterintuitive nature of these interactions, as anions are expected to exhibit repulsive interactions with the negative π electron clouds of aromatic molecules, but also to the experimental challenges involved with the coordination chemistry of anions, as has been outlined in section 5.1.^{5,13,14} Based on the knowledge about cation- π interactions, the question arose if similar binding motifs could be possible for anions, if the electrostatic potential of the aromatic unit was reversed by introduction of appropriate electron-withdrawing substituents. Moreover, it has been well-known that benzene and hexafluorobenzene adopt a “face-to-face” stacking motif in the case of a 1:1 mixture¹⁵ (accompanied by a substantial increase¹⁵ in the melting point as compared to each compound). This behavior can be rationalized in view of the favorable quadrupole-quadrupole interaction between the two molecules, since they both possess a quadrupole moment which is approximately the same with respect to magnitude, but opposite in sign, due to the fact that an sp^2 carbon atom is more electronegative than a hydrogen, but less electronegative than a fluorine atom.¹⁶ The calculated (electrostatic) potential energy surfaces of these two species are shown in Figure 5.1. The sign and magnitude of the quadrupole moments are expected to exert a strong influence on the binding motifs between these aromatic molecules and anions. A schematic representation, including the expected binding motifs between an anion and benzene and hexafluorobenzene, respectively, are displayed in Figure 5.2.

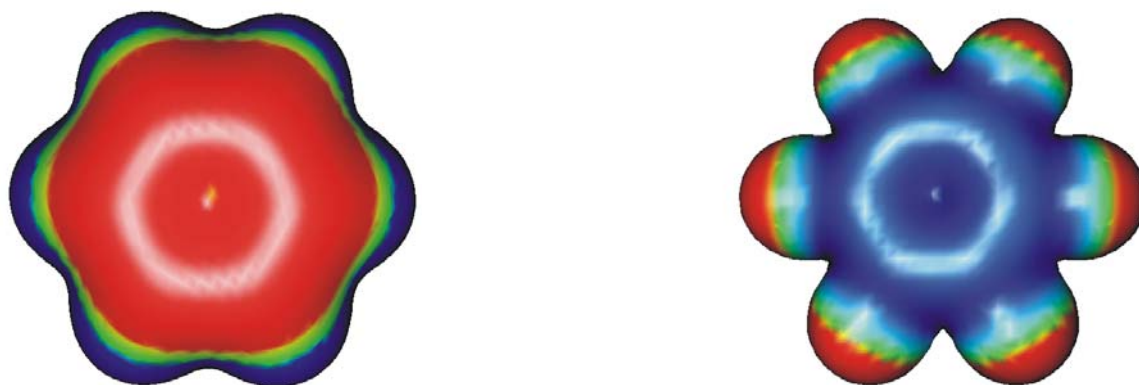


Figure 5.1 Illustration of the electrostatic potential around C_6H_6 (left) and C_6F_6 (right) (calculated with Gaussian03W, HF/3-21G* level¹⁷). The color coding from blue to red represents positive to negative electrostatic potentials.

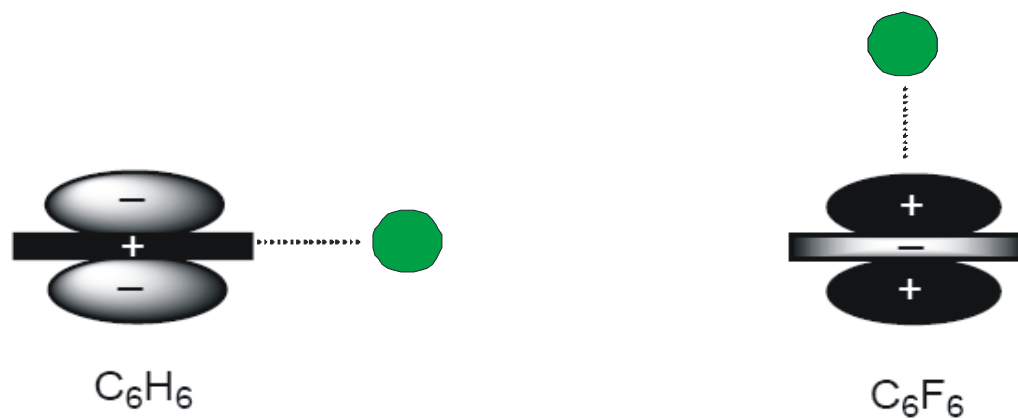


Figure 5.2 Schematic representations of the quadrupole moments of benzene (left) and hexafluorobenzene (right) and their suggested interaction motifs with an anionic moiety

This triggered several theoretical studies,¹⁸⁻²⁴ e.g. an investigation of the interaction between hexafluorobenzene and a number of small anions.²⁴ It was found that in all cases under consideration the interactions are favorable, meaning that stable complexes of this kind should exist. However, the ground state geometries determined differed for the various anions considered, with the expected binding motif where the anion is bound to the top of the aromatic ring in a so called anion- π interaction being the most stable one for the Cl^- and Br^- anions. In contrast, in the case of F^- and CO_3^{2-} anions the minimum energy structures were found to be reminiscent of a nucleophilic attack of the respective anions on one of the carbon atoms of the aromatic ring. It could also be established that the non-covalent interactions (coined “anion- π interactions”²⁴) are dominated by the interaction between the anion and the quadrupole moment of the electron-deficient aromatic unit and polarization contributions, with the latter dominating for systems with only small positive quadrupole moments.^{13,24} Crystallographic data from a search of the Cambridge Structural Database (CSD) provided evidence for the occurrence of such anion- π interactions in crystal structures. Further studies showed similar results for a number of other modified benzene molecules, such as 1,3,5-trinitrobenzene, 1,3,5-trifluorobenzene,²³ hexazine, s-triazine, trifluoro-1,3,5-triazine²¹ and derivatives of those species with differing substituents.¹³ Additionally, larger anions such as $[\text{BF}_4]^-$ and $[\text{PF}_6]^-$, which are commonly used as counterions in organometallic chemistry, show favorable anion- π interactions as well, as has been demonstrated for the case of trifluoro-s-triazine.²⁵ Moreover, it could be shown that even aromatic rings which are not per se electron-deficient can be modified to make the interaction with anions still favorable by complexing them with a metallic cationic atom on the opposite side of the aromatic ring with respect to the anion,²⁶ showing that strong synergistic effects are involved in the interplay between cation- π and anion- π interactions.^{22,27} Also, it has been demonstrated that these anion- π interactions are approximately additive,²⁰ offering potentially the possibility of designing appropriate host molecules to bind anions selectively even in the presence of other, competing interactions (e.g. with the solvent). In spite of these theoretical studies which proved anion- π interactions to be energetically favorable (with their strengths typically

varying between 10 - 50 kJ/mol),²⁸ there is still a paucity of experimental data available. Relatively few crystal structures with this kind of binding motif for complexation of free halides could be clearly identified,^{29,30} although there is an increasing amount of experimental results which support the attractive interaction between anions and electron-deficient arenes, mainly based on crystallographic studies (see Ref.¹⁴ and references therein). However, solution studies providing data on anion- π interactions are even more scarce,^{30,31} and recent experiments on the solution behavior of halide anions with some highly electron-deficient arenes such as tetracyanobenzene, trinitrotoluene, tetracyanopyrazine and others yielded data which were not in accordance with a non-covalent interaction between anions and aromatic molecules.³² This suggests that in many cases several possible binding motifs compete with one another, preventing anion- π interactions to occur abundantly despite their favorable energetics, although they might still contribute to the overall stability and geometric appearance of these complexes. Intense color changes were observed upon adding the tetraalkylammonium salts of Cl⁻, Br⁻ or I⁻ to solutions containing these electron-deficient arenes, indicating that charge-transfer (CT) takes place in the complexes, which would be incompatible with weak anion- π interactions, as by definition they exclude considerable amounts of charge transfer.³² These discoveries prompted further investigations of the nature of the binding of halide anions to electron-deficient arenes, revealing eventually that the halide ions are commonly found in geometries deviating considerably from the structural motif suggested by pure anion- π interactions (for which the anion is expected to be bound to the top of the aromatic ring with a 90° angle between the axis connecting the halide ion to the center of the aromatic ring and the plane defined by the carbon atoms of the latter).^{28,33} In fact, four different binding motifs were identified to dominate the interactions between aromatic molecules and anions, with the anion- π interaction described above being just one of them: strongly covalent σ -complexes (with a short distance between anion and carbon atom, which ultimately adopts an sp³ hybridized geometry), weakly covalent donor π -acceptor complexes (as displayed by structure 2 in Figure 5.3), non-covalent anion- π interaction (structure 1 / Figure 5.3) and finally C-H hydrogen bonding interactions (structure 3 / Figure 5.3).²⁸

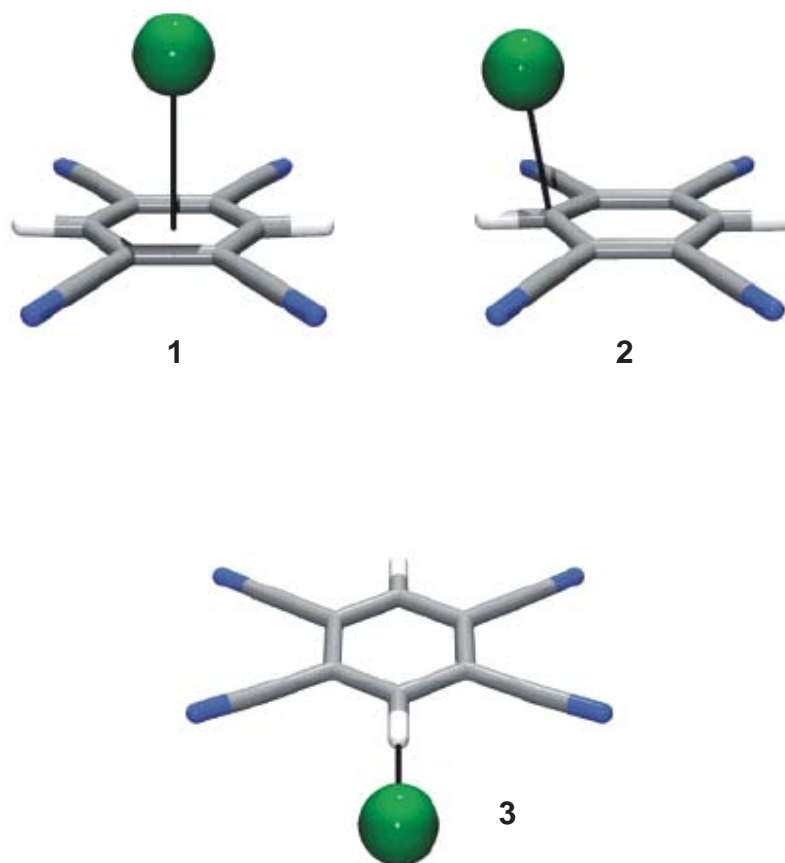


Figure 5.3 Illustration of possible binding motifs for the interaction of anions with electron-deficient arenes on the example of MP2/aug-cc-pVDZ optimized geometries for Cl^- complexes with tetracyanobenzene (from Ref.²⁸)

Strongly covalent σ -complexes correspond to a nucleophilic attack of the respective anion on one of the carbon atoms of the aromatic ring. The result is a strong, covalent σ bond between the two reaction partners, with the attacked carbon atom taking on a sp^3 hybridized, tetrahedral local geometry and the aromaticity of the arene ring being lost. This binding motif is the only stable structural motif for the fluorine anion placed on top of electron-deficient aromatic rings, as has been mentioned already above.²⁴ In fact, this is the structure of the so-called “Meisenheimer-complex” or “ σ -complex”,³⁴ long known to be a reactive intermediate in the aromatic nucleophilic

substitution reaction, which is the analogue to the electrophilic substitution reaction for electron-deficient aromatic systems. Examples in which strongly bound σ -complexes have been determined computationally to represent the most stable structures include complexes of CN^- and CO_3^{2-} with hexafluorobenzene²⁴ and of CN^- , NC^- and CO_3^{2-} with triazine.¹⁸ Weakly covalent donor π -acceptor complexes display less charge-transfer from the anion to the ring and consequently the covalent bonding interaction is weaker, the anion-carbon distance larger and the aromatic ring still close to planar. However, the charge transfer is still finite, explaining the behavior found for mixtures of halide anions with some electron-deficient aromatic systems in solution.³² The structural motif characterizing these complexes places the anion not on top of the center of the aromatic ring but rather outside the ring perimeter and is widely found both in solid and in solution phase,³² indicating that this is one of the preferred binding motifs for (less nucleophilic) halide anions to electron-deficient arenes. Finally, also non-covalent anion- π interactions are possible for less nucleophilic halide anions. They are characterized by negligible charge-transfer of less than 0.01 e and a comparatively highly symmetric geometry in which the halide is ideally placed on top of the aromatic ring along the axis perpendicular to the center of the plane defined by the carbon atoms. As mentioned above, although this motif has been established in numerous computational studies to be energetically quite favorable, there is only a limited data set for which this binding motif is actually found experimentally. Summarizing, it can be stated that strongly bound σ -complexes are likely to display the ground state structure for nucleophilic anions such as RO^- , CN^- and F^- , while more weakly bound anion- π complexes are more likely for more diffuse, less nucleophilic anions such as ClO_4^- , BF_4^- and PF_6^- and aromatic units of moderate electron affinity. For anions of intermediate nucleophilicity (e.g. Cl^- , Br^- or NO_3^-) anion- π complexes are still possible in complexes with arenes with intermediate electron affinity, while as the latter one increases eventually weakly bound σ -complexes start to prevail.³³ However, whenever aryl C-H groups are present, there is the possibility of hydrogen bond formation to the anion in concurrence to π -system binding.³³ Generally, one can classify hydrogen bonds quantitatively by the magnitude of their gas phase binding energies, ΔE (provided by

electronic structure calculations). Hydrogen bonds with ΔE values < 17 kJ/mol are considered to be weak, those between 17 - 63 kJ/mol moderate, and eventually values > 63 kJ/mol are considered strong^{35,36} (in aqueous solution these strong interactions can be considerably attenuated). An important feature of hydrogen bonding interactions is their high degree of directionality, with the “ideal” hydrogen bond displaying an angle $\angle(XHY)$ close to 180° . While at first glance it can be argued that the interaction strength between an anion and aryl C-H groups should be weak, studies on the enthalpies of formation for the chloride-benzene complex resulted in a value of ~ -40 kJ/mol,^{37,38} while theoretical investigations of benzene complexes with the Cl^- , NO_3^- and ClO_4^- anions yielded values in the range of -32 kJ/mol to -39 kJ/mol,³⁵ providing further evidence that in fact hydrogen bonding interactions in these species are of moderate strength. Moreover, it is possible to subtly tune the acidity of the aryl C-H group over a considerably broad range by introduction of electron-withdrawing substituents into the aromatic ring system. This trend could be established already in early mass-spectrometric studies³⁹ and more recently, the gas phase binding energies of the highly electron-deficient 1,2,4,5-tetracyanobenzene for complex formation with a chloride anion through hydrogen bonding has been determined to be -113 kJ/mol, establishing that these complexes do display strong hydrogen bonds.²⁸ In fact, searching the Cambridge Structural Data Base yields far more examples for interactions between anions and arenes via hydrogen bonding as compared to anion- π interactions.³³ The aforementioned examples highlight that the binding motifs between anions and electron-deficient arenes are dominated by several interaction forces of comparable strength competing with one another. The final structural motif will depend on the properties of the respective system and can possibly be influenced e.g. by changing the substituents and therefore the electron density and affinity of the aromatic unit. As most studies so far are theoretical and experimental data are still lacking, it is clear that much more experimental work is necessary in order to improve the understanding of the subtle interplay of these binding forces. In the following paragraph, an infrared predissociation study on $\text{Cl}^- \cdot \text{C}_6\text{F}_n\text{H}_{6-n}$ complexes in the gas phase is presented, aimed to contribute to the clarification of this problem.

5.3. $\text{Cl}^- \cdot \text{C}_6\text{F}_n\text{H}_{6-n}$ complexes as prototypes for the investigation of the binding behavior between anions and aromatic molecules

5.3.1. Introduction

In the previous section, it has been pointed out that experimental data on the interactions and geometries of complexes between anions and electron-deficient aromatic molecules are still rather scarce. Infrared predissociation spectroscopy applied in combination with electronic structure calculations has been very successful in the past in elucidating the structural motifs of ion-molecule complexes in the gas phase. $\text{Cl}^- \cdot \text{C}_6\text{F}_n\text{H}_{6-n}$ complexes have been chosen as prototypes for the investigation of the binding behavior between an anion and aromatic molecules⁴⁰ for several reasons. First, fluorinated organic compounds are an interesting class of molecules, as they play an important role in pharmaceutical and crop production products.⁴¹ They offer the opportunity to subtly tune their properties depending on the number of fluorine atoms chosen to be introduced in the respective parent molecular structure. This behavior can be exploited in the case of the fluorinated benzenes to modify their electronic properties and the two limiting cases benzene and hexafluorobenzene possess quadrupole moments of similar magnitude but opposite sign, leading to their unique interaction and binding behavior upon mixing, as has been detailed in the previous paragraphs. At the same time, fluorinated benzene molecules possess aryl C-H groups up to pentafluorobenzene. In complexes with anions they offer therefore, at least for the higher fluorinated (electron-deficient) representatives, in principle all of the binding motifs mentioned above. The structural motifs adopted for the two limiting cases are already known: complexes of hexafluorobenzene with various anions have been described and specifically the chlorine atom is thought to bind in an anion- π interaction to the top of the fully fluorinated ring.²⁴ The geometries of the halide-benzene complexes on the other hand have been established in pioneering experiments by Bieske and co-workers in a study combining infrared experiments and calculations.^{42,43} Interestingly, they find that the ground state structures of these

complexes are all characterized by bifurcated hydrogen bonds of the respective halide anion to two neighboring CH groups in the plane of the aromatic ring. However, the binding behavior of anions to the arenes of intermediate fluorination degree is unknown. The questions to be addressed in this study were specifically (i) how many fluorine atoms are necessary to make the binding motif switch from coordination in the plane of the ring to the top of the ring and (ii) how the distribution of the fluorine atoms around the ring (i.e. the structural isomers resulting from the permutation of the respective ligand positions around the ring) will influence the binding motif. Infrared predissociation spectroscopy is applied to Ar solvated clusters $A^- \cdot C_6F_nH_{6-n} \cdot Ar_m$ ($n = 0 - 5$, $A^- = Cl^-, I^-, SF_6^-$). This enables the simultaneous study of both the influence of the electronic nature of the aromatic ring (varied by changing the number of fluorine atoms attached to it) and the Lewis acidity of the respective anion by going from the small atomic chloride anion to the more diffuse negative charge distribution in the sulfur hexafluoride anion. Results are presented for the fluorobenzene molecules up to pentafluorobenzene, as hexafluorobenzene has no infrared signature active in the mid-infrared range available in the experiment (represented by the aryl CH groups in the cases of the benzene and the fluorobenzene molecules). The use of Ar solvation ensures that the infrared spectra result from irradiation of cold clusters, as fragment ions are monitored following the evaporation of the weakly bound Ar atom (bond energy of the $Cl^- \cdots Ar$ bond: $D_0 = 523 \text{ cm}^{-1}$).⁴⁴

5.3.2. Calculations

As in the studies described in the previous chapters, the minimum energy structures of the complexes under consideration and their harmonically approximated vibrational frequencies have been calculated in order to aid the interpretation of the experimentally obtained data and to be able to assign the appropriate geometrical motifs to the systems under study. Both DFT (density functional theory,⁴⁵ employing the B3-LYP functional⁴⁶ in all cases considered here) and *ab initio* RI-MP2⁴⁷ (second-order Møller-Plesset perturbation theory applying the resolution-of-identity approximation for the evaluation of two-electron integrals) calculations have been

performed as implemented in the TURBOMOLE program package.⁴⁸ Due to the relatively large size of the systems investigated and the large number of complexes considered, only a TZVP basis set⁴⁹ has been applied in all cases. The vibrational frequencies (in the harmonic approximation) have been calculated on the DFT level of theory. In order to ease the comparison with the experimentally measured values and to obtain a physically more realistic picture, all calculated values have been scaled with an anharmonic correction factor of $k = 0.960$, as determined by the ratio of the calculated value for the frequency of the normal mode mostly due to the CH group of pentafluorobenzene and its well-known experimentally measured value.⁵⁰ All calculations have been performed without taking the Ar atoms attached to the ion-molecule complex into account. However, the interaction strength between an Ar atom and a benzene molecule ($D_0 = 314 \pm 7 \text{ cm}^{-1}$)⁵¹ is comparable to the $\text{Cl}^- \cdots \text{Ar}$ interaction energy (see above), and it has been shown in a theoretical study on the $\text{Cl}^- \cdot \text{C}_6\text{H}_6 \cdot \text{Ar}$ cluster that the Ar atom is bound half way between the chloride anion and the benzene ring in order to maximize the interaction energy with both entities.⁵²

5.3.3. The $\text{Cl}^- \cdot \text{C}_6\text{H}_6$ complex dimer

It is instructive to take at first a close look at the infrared spectrum of the $\text{Cl}^- \cdot \text{C}_6\text{H}_6$ complex dimer (shown in Figure 5.4), as it constitutes the first representative of the $\text{Cl}^- \cdot \text{C}_6\text{F}_n\text{H}_{6-n}$ complexes under investigation and also the one of highest symmetry. The interpretation of its spectrum and the conclusions which can be drawn from it concerning its minimum energy structure should therefore be valuable for the evaluation of the experimentally obtained data of the other species. Bieske and co-workers were able to derive in pioneering experiments^{42,43} the structures of the halide-benzene complexes from their infrared spectra (with the exception of the fluoride-benzene complex due to its high binding energy).

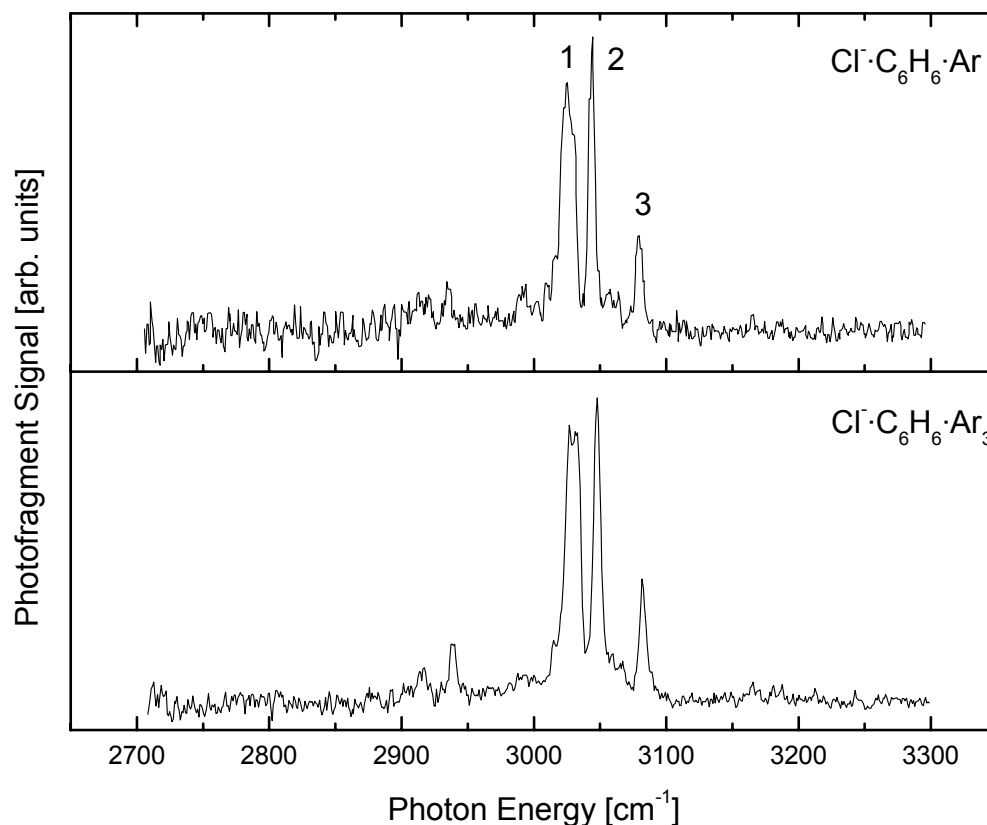


Figure 5.4 Ar predissociation spectra for $\text{Cl}\cdot\text{C}_6\text{H}_6\cdot\text{Ar}$ (top trace) and $\text{Cl}\cdot\text{C}_6\text{H}_6\cdot\text{Ar}_3$ (bottom trace)

However, before following their arguments, it is worth discussing the infrared spectrum of the free benzene molecule. Although it has only one infrared active mode ν_{20} (e_{1u}) (following the Wilson numbering⁵³ of the modes of benzene) in the CH stretching region between 3040 cm^{-1} to 3100 cm^{-1} , it shows a characteristic “triad” of absorption bands (namely at 3048 cm^{-1} , 3079 cm^{-1} and 3101 cm^{-1}) which actually is an unresolved tetrad due to Fermi resonances of the infrared active ν_{20} mode with the energetically near degenerate modes $[\nu_1 + \nu_6 + \nu_{19}]$, $[\nu_8 + \nu_{19}]$ and $[\nu_3 + \nu_6 + \nu_{15}]$.⁵⁴⁻⁵⁶ The exact interaction scheme resulting in the Fermi tetrad is shown in Figure 5.5 (from Ref.⁵⁴).

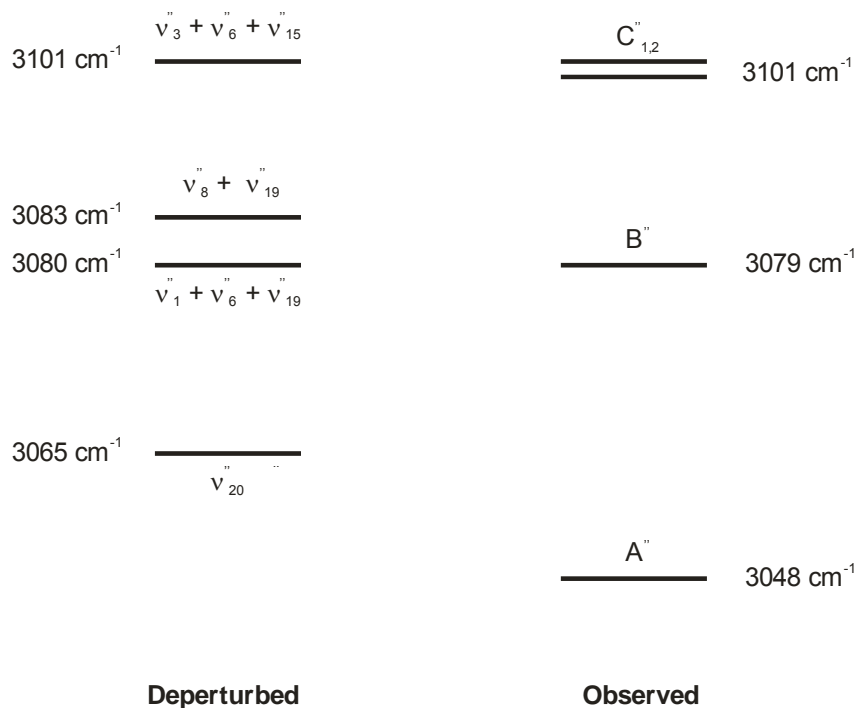


Figure 5.5 Benzene CH stretching tetrad (according to Ref.^{54,56})

Comparison to the spectrum of the chloride-benzene complex in Figure 5.4 immediately shows that the spectrum changes appreciably, with two intense bands at 3028 cm⁻¹ and 3046 cm⁻¹ being red-shifted with regard to the band positions of the Fermi tetrad of the free benzene molecule. This leads directly to the conclusion that the chloride anion is not bonded to the top of the aromatic ring, as in this case (in spite of the symmetry lowering from D_{6h} to C_{6v}) almost no alteration of the frequencies of benzene was to be expected,⁴² while ionic hydrogen bonds result in the observed red shift of the CH stretching bands. This is in line with the structural expectations from an electrostatic point of view, as the negative charge of the chloride anion and the π electron cloud of the benzene molecule should result in a repulsive mutual interaction. The calculations performed by Bieske and co-workers^{42,43} converged to two stable minimum structures, namely one displaying a bifurcated double hydrogen bond between the chloride anion and the benzene molecule

(geometry 1 in Figure 5.6) and a second one in which the chloride anion is bound to the benzene ligand by one linear hydrogen bond to one of the CH groups (geometry 2 in Figure 5.6).

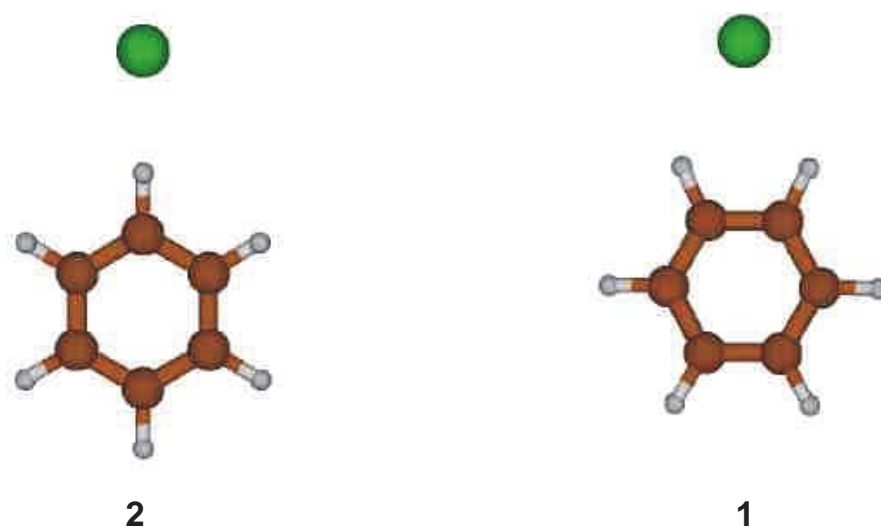


Figure 5.6 Calculated minimum energy structures for the chloride-benzene complex

Structure 1 is calculated to be slightly more stable. Based on the simulation of the vibrational spectra for both species (in the harmonic approximation, scaled with an appropriate factor to account for anharmonicity) they were able to exclude the linear structure in line with the calculated trend for the relative stabilities of the two binding motifs. The most important argument is the absence of a strongly red-shifted band which would be expected from the hydrogen bonded CH group in the linear motif. These findings were in contradiction to an earlier study of these clusters, which predicted the bifurcated motif to be the most stable one only for the iodide-benzene complex, while all other halide-benzene complexes were expected to display the linear motif.³⁷ However, this difference could be attributed to the different level of theory applied, with the higher level calculations of Bieske and co-workers being in

line with the experimental findings. The exact assignment of the experimentally obtained bands to the appropriate modes of the complex is difficult due to the expected occurrence of Fermi resonances already at play in the free benzene molecule. For the chloride-benzene complex, due to the symmetry lowering from D_{6h} to C_{2v} , even more modes should be theoretically allowed to interact at least arguing from a symmetry based point of view. Most of the observed bands could be tentatively assigned based on spectra of cold $Cl^- \cdot C_6H_6 \cdot Ar_n$ ($n = 1,2$)⁴³ and an equally well resolved spectrum of the bare $Cl^- \cdot C_6H_6$ complex.⁵⁷ The three main bands could be assigned in the following way (labeling of the peaks is given in Figure 5.4): band 1 is an overlap of the ν_{20} mode (the only one also active in the free benzene) and the ν_7 band, band 2 is the only pure one as only the ν_2 mode contributes (which explains the sharpness of this feature), and finally band 3 is the result of Fermi interactions of the ν_{20} mode with several combination bands of lower frequency. The remaining smaller bands can be assigned to combination bands and features of the benzene ligand becoming infrared active due to the symmetry lowering as compared to the free molecule. It is important to keep the following points in mind from this discussion for the interpretation of the spectra of the chloride-fluorobenzene complexes which is to follow: the most intense features in the infrared spectrum of a hydrogen bonded complex usually stem from ionic hydrogen bonds (which means for the systems under consideration between the aryl CH groups and the anion). As mentioned above and as is obviously the case for the free benzene molecule, other modes may possibly borrow intensity from these intense features through Fermi resonances, e.g. through mixing of the intense CH bands with overtones and combination bands of CC/CF stretching modes, thereby greatly complicating the observed spectra. However, the centroid frequencies will encode the structural properties of the complexes as detailed above, and their elucidation is at the heart of the study presented.

5.3.4. Spectra and structures of the $\text{Cl}^- \cdot \text{C}_6\text{F}_n\text{H}_{6-n}$ complexes

The spectra of all $\text{Cl}^- \cdot \text{C}_6\text{F}_n\text{H}_{6-n}$ complexes (monitored via the loss of weakly bound Ar messenger atoms) are displayed in Figure 5.7 and Figure 5.8.

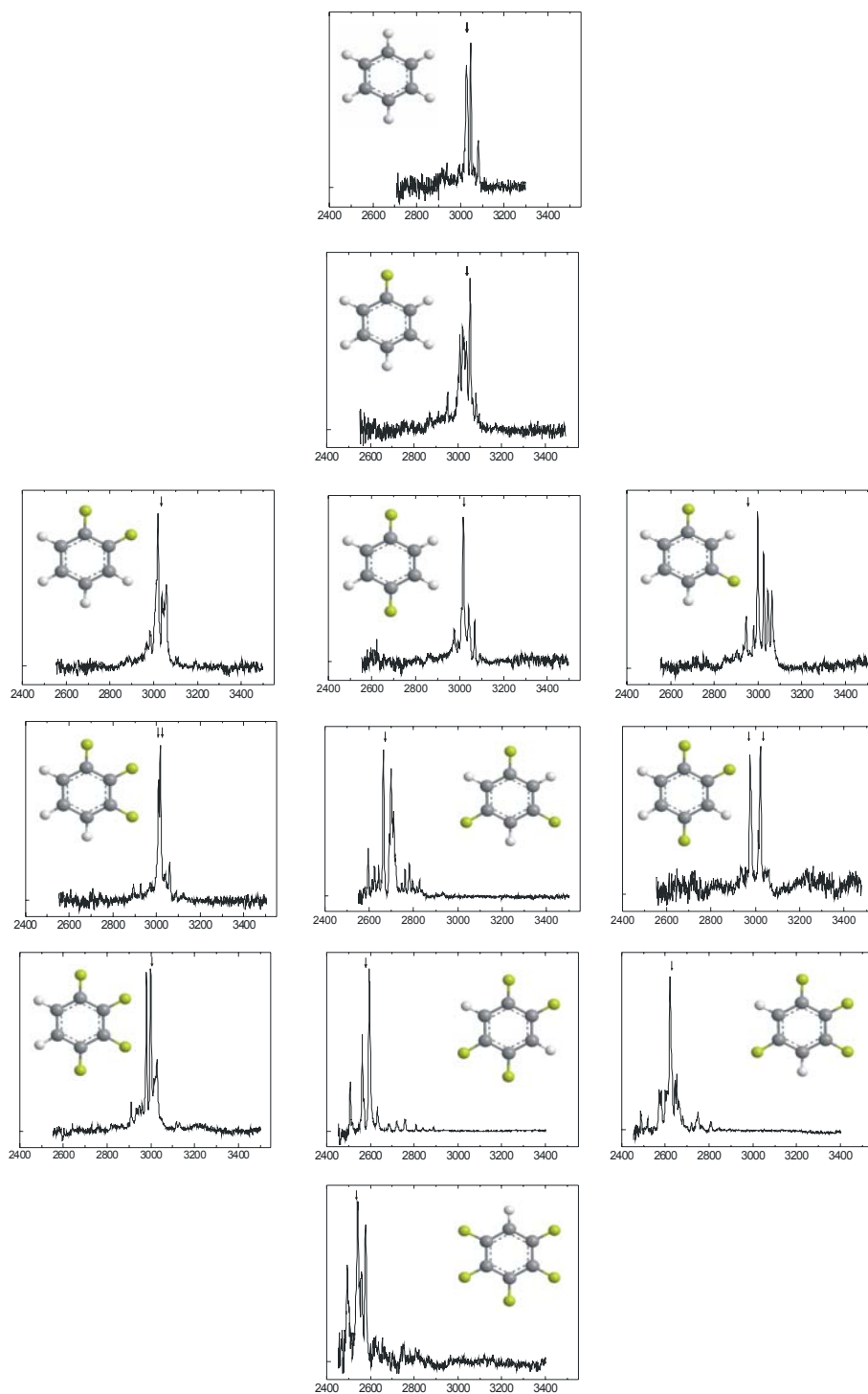


Figure 5.7 Ar predissociation spectra for all isomers at all fluorination levels (each row corresponds to a certain number of fluorine atoms - marked as green in the sketches of the ligand structures - in the ligand, starting with benzene on top) of $\text{Cl}^{\cdot}\text{C}_6\text{F}_n\text{H}_{6-n}\cdot\text{Ar}_m$ clusters. Horizontal axis: photon energy in cm^{-1} ; Vertical axis: photofragment yield in arbitrary units. The arrows indicate the calculated scaled harmonic frequencies of the most intense CH stretching bands

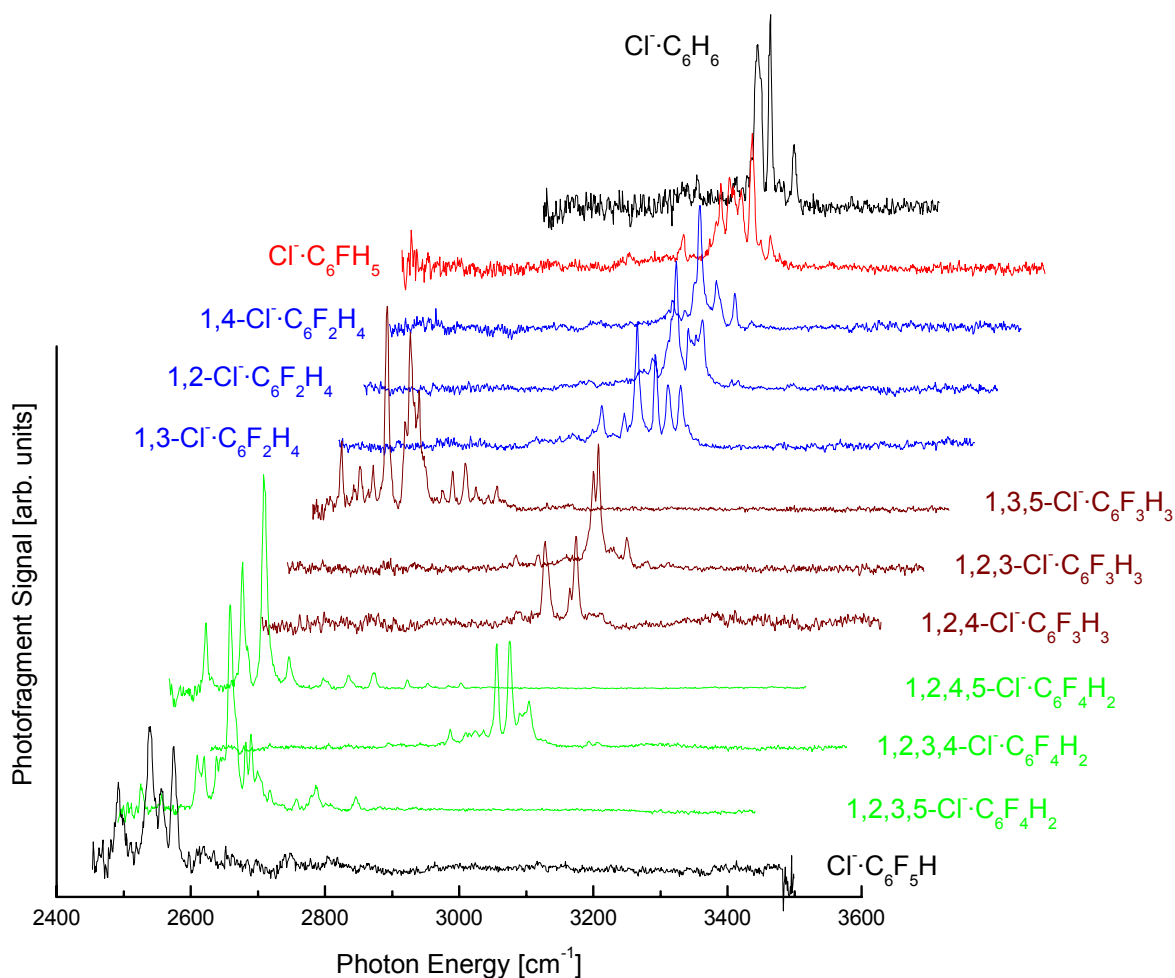


Figure 5.8 Ar predissociation spectra for all isomers at all fluorination levels (complexes with equal number of fluorine atoms in the ligand are marked by the same color) of $\text{Cl}^{\cdot}\text{C}_6\text{F}_n\text{H}_{6-n}\cdot\text{Ar}_m$ clusters (monitored by the loss of the Ar messenger atoms)

The spectra are complicated, each consisting of a multitude of bands. The identification of every single one of these would clearly require a major effort using high level anharmonic calculations. However, as has been pointed out above, the main structural information, the clarification of which is the aim of this study, is encoded in the centroid of the bands for each spectrum. As can be clearly seen, these bands fall into different classes, allowing for differentiation between two distinct spectral motifs: (i) a high-energy motif, characterized by absorption bands with a centroid around 3000 cm^{-1} and (ii) a low-energy motif, with the centroid of the absorption bands shifted to frequencies around $2400 - 2600\text{ cm}^{-1}$. The signature in the spectrum of the chloride-benzene complex (centroid of the absorption bands $\sim 3030\text{ cm}^{-1}$; shown in the top trace of both Figure 5.7 and Figure 5.8) is only weakly shifted in comparison to the free benzene molecule and fully consistent with the spectrum of this complex reported previously by Bieske and co-workers,^{42,43} who were able to assign the spectral features to a bifurcated hydrogen bonding motif, as has been detailed in the previous section. Figure 5.8 illustrates that the spectral motif observed does not purely depend on the number of fluorine atoms in the arene ligand, but also on their specific distribution around the ring. Out of the twelve complexes investigated, only four display the low-energy vibrational signature, namely 1,3,5-trifluorobenzene, 1,2,4,5- and 1,2,3,5-tetrafluorobenzene and pentafluorobenzene. These four molecules are the only ones which are restricted to bind the chloride anion by one CH aryl group, thereby enforcing on the complex a linear hydrogen bonding motif. As has been discussed before, the characteristic spectral feature of a singly hydrogen bonded CH group is a strongly red-shifted band as compared to the free molecule, which is exactly what is found for the complexes of the chloride anion with these four fluorobenzene molecules. All other molecules under consideration have at least two neighboring CH groups, thereby always offering the possibility to coordinate to the anion via the bifurcated motif, which has been proved to be dominant in the chloride-benzene complex. Although the appearance of the spectra differs considerably between the individual complexes (as is to be expected due to the differences in the overall symmetry and exact chemical nature of the ligands), the centroids of the absorption bands of all complexes offering the bifurcated binding

motif are placed around $\sim 3000 \text{ cm}^{-1}$ in the spectra, only slightly red shifted from the values of the free benzene molecule. Therefore, one can empirically assign the high-energy spectral features to the bifurcated structural motifs. This interpretation is corroborated by our DFT calculations, which converge into the geometries displaying the bifurcated binding motif whenever possible and yield the linearly bound complex as the ground state structure only for the four ligands that have only isolated CH aryl groups. Even if the frequency calculations performed in the harmonic approximation are incapable of recovering the exact spectra (as features such as Fermi resonances are anharmonic in nature), the most intense calculated features are roughly consistent with the centroids of the absorption bands found experimentally. One can therefore generally conclude that the chloride anion prefers bifurcated bonding to two neighboring CH groups over linear bonding. 1,2,4-trifluorobenzene constitutes an interesting case in that respect, as within one ligand, it offers simultaneously the opportunity for linear and bifurcated docking of the chloride anion. As can be seen from the spectrum though, only the high energy motif is observed, consistent with the DFT calculations, which place the linear structure $\sim 160 \text{ meV}$ higher in energy than the bifurcated motif, corroborating the statements made above.

5.3.5. Vibrational spectrum and binding motif for the $\text{Cl}^- \cdot \text{C}_6\text{F}_5\text{H}$ complex

It is interesting at this point to take a closer look at the spectrum of the chloride-pentafluorobenzene complex as compared to the case of the chloride-benzene complex (see Figure 5.9), as these two species constitute the two “extreme ends” with respect to the fluorination degree of the ligand of the complex series under investigation in this study. The infrared signatures of the chloride-pentafluorobenzene complex are centered around $\sim 2540 \text{ cm}^{-1}$, strongly red-shifted in comparison to the typical CH stretching region and also to the signatures of the bifurcated motif as displayed by the spectrum of the chloride-benzene complex. This implies a linearly hydrogen bonded structure.

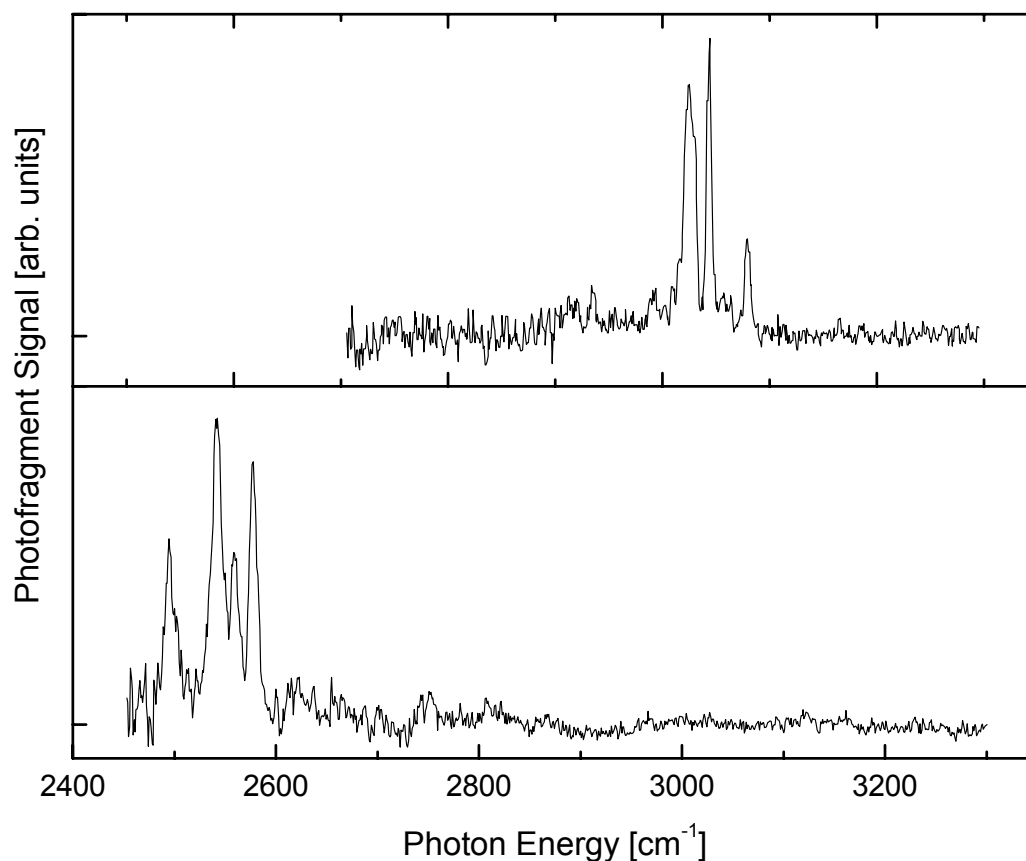


Figure 5.9 Ar predissociation spectra for $\text{Cl}\cdot\text{C}_6\text{H}_6\cdot\text{Ar}$ (top trace) and $\text{Cl}\cdot\text{C}_6\text{F}_5\text{H}\cdot\text{Ar}$ (bottom trace)

In addition, no vibrational bands are found around 3103 cm^{-1} (the CH stretching band of the free pentafluorobenzene molecule),⁵⁰ where the spectroscopic signature of a ring-bound geometry is expected (scaled harmonic calculation: 3095 cm^{-1}), as in this case the structure and therefore also the spectral features of the ligand should be only weakly perturbed. The DFT calculations predict the frequency of the CH stretching vibration corresponding to a linear hydrogen bond between the remaining aryl CH group and the chloride anion to be at 2548 cm^{-1} , in reasonable agreement with the experimentally determined centroid of the absorption bands. However, the spectrum

is quite complicated given that in a harmonic picture one would expect only one normal mode in this frequency range, namely the vibrational signature of the CH group. This can be rationalized though by bearing in mind that already the spectrum of the free benzene molecule shows an unresolved tetrad in the frequency region of the CH stretching modes due to Fermi resonances with energetically closely spaced combination bands. Given that the symmetry of the complex is even lower, it seems reasonable that Fermi interactions with energetically almost degenerate CC/CF combination bands and/or overtones, “borrowing” intensity from the very intense CH stretching modes, lead to the observed cluster of bands around 2540 cm^{-1} . Clearly, these Fermi interactions are not the same as in benzene due to the different mode structure. An exact assignment of the individual bands is not possible on the basis of the harmonic approximation frequency calculations. However, several modes based on CC stretching and CF stretching modes that are likely candidates for causing the observed bands through combination bands and overtones can be identified (see Table 5.1).

Table 5.1 Candidates for Fermi interaction responsible for the group of bands around 2540 cm^{-1} in the spectrum of the $\text{Cl}^- \cdot \text{C}_6\text{F}_5\text{H}$ complex

Fundamental of mode 36	2643 cm^{-1}	CH stretch
Combination band modes 34 + 26	2706 cm^{-1}	ring deformation, CC/CF stretching
Combination band modes 32 + 26	2570 cm^{-1}	ring deformation, CC/CF stretching
Combination band modes 31 + 26	2461 cm^{-1}	CH wagging, ring deformation, CC/CF stretching
Overtone of mode 34	2801 cm^{-1}	ring deformation, CC/CF stretching

The observation of this strongly red shifted signature of the aryl CH group in the infrared spectrum indicates that the chloride anion is bound to its fluorobenzene ligand via a hydrogen bond in the plane of the ring even in the case of a highly fluorinated arene such as the pentafluorobenzene, which is electron-deficient and should offer favorable binding interactions to the top of the ring. Indeed, the DFT calculations find a local minimum energy structure in this geometry, which is placed ~ 300 meV higher in energy than the hydrogen bonded ground state (see Figure 5.10).

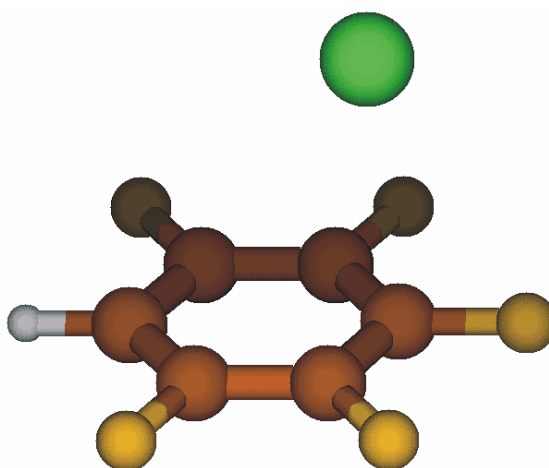


Figure 5.10 Calculated structure for the $\text{Cl}^- \cdot \text{C}_6\text{F}_5\text{H}$ complex (DFT/B3-LYP/TZVP) via ring bonding

More precisely, local minima are calculated to exist above every carbon atom except that belonging to the CH group, with the minimum above the carbon para to the CH group being lowest in energy, followed by the meta and ortho positions. The calculated energies of these ring-bound isomers all fall within 10 meV. The fact that hydrogen bonds constitute a binding motif in anion complexes with highly electron-deficient aromatics competitive to the binding to the top of the ring has been discussed in the previous sections and has been described in more detail by Berryman *et al.*²⁸ (although they did not study anion-arene complexes with only one aryl CH

group in the aromatic unit). This behavior is not too surprising in light of the fact that introducing strongly electron-withdrawing groups into the aromatic ring is expected to significantly raise the acidity of the remaining CH groups, thereby strengthening the interaction even with a proton acceptor of rather moderate strength such as the chloride anion.⁵⁸ As has been detailed in the first chapter on anion hydration, the energy position of the OH infrared absorption band decreases with increasing proton affinity of the anion.⁵⁹ This implies at the same time that the infrared absorption band in an ionic hydrogen bond will decrease in frequency with increasing acidity of the proton in complexes involving the same anion and consequently low CH stretching frequencies should suggest hydrogen bonds involving a rather acidic proton. In order to verify this kind of behavior on a more quantitative basis, MP2 calculations have been performed in order to characterize the CH stretching potential energy surface for the acidic proton in the $\text{Cl}^- \cdot \text{C}_6\text{F}_5\text{H}$ complex. A low-lying proton transfer channel can be identified, resulting in a $\text{C}_6\text{F}_5^- \cdots \text{HCl}$ state (which shows up as a shelf in the potential energy surface, see Figure 5.11) ~ 1.5 eV above the $\text{C}_6\text{F}_5\text{H} \cdots \text{Cl}^-$ ground state. This explains in turn the strong anharmonicity of the potential around the minimum energy structure, resulting in the huge observed red shift of the vibrational signature of the CH group. There is yet another issue which deserves further consideration in view of the relative acidities of the hydrogen atoms in the aryl CH groups: As the lower-energy absorption band exclusively occurs in the case of the complexes in which the chloride anion is forced to bind to isolated CH groups, one could arrive at the conclusion that the hydrogen atom in a CH group surrounded by two CF groups is more acidic than a hydrogen atom belonging to one of two neighboring CH groups. Investigations of the thermochemistry of the species involved, however,⁶⁰ revealed that the acidity of fluorobenzenes always increases with increasing fluorination level, with one of the largest changes occurring from $n = 0$ to $n = 1$. As the complexes with bifurcated bonding show only a weak dependence of the CH stretching frequencies on the fluorination level, it can be assumed that the bifurcated binding motif effectively shuts down the proton-transfer channel. Qualitatively this can be rationalized through the fact that the anion interacts with two hydrogen atoms instead of one, thereby weakening the exerted force on

every single one. In the linear motif, however, the increasing acidity is clearly observed, as the much stronger dependence of the CH stretching position on the number of fluorine atoms shows (see Figure 5.12).

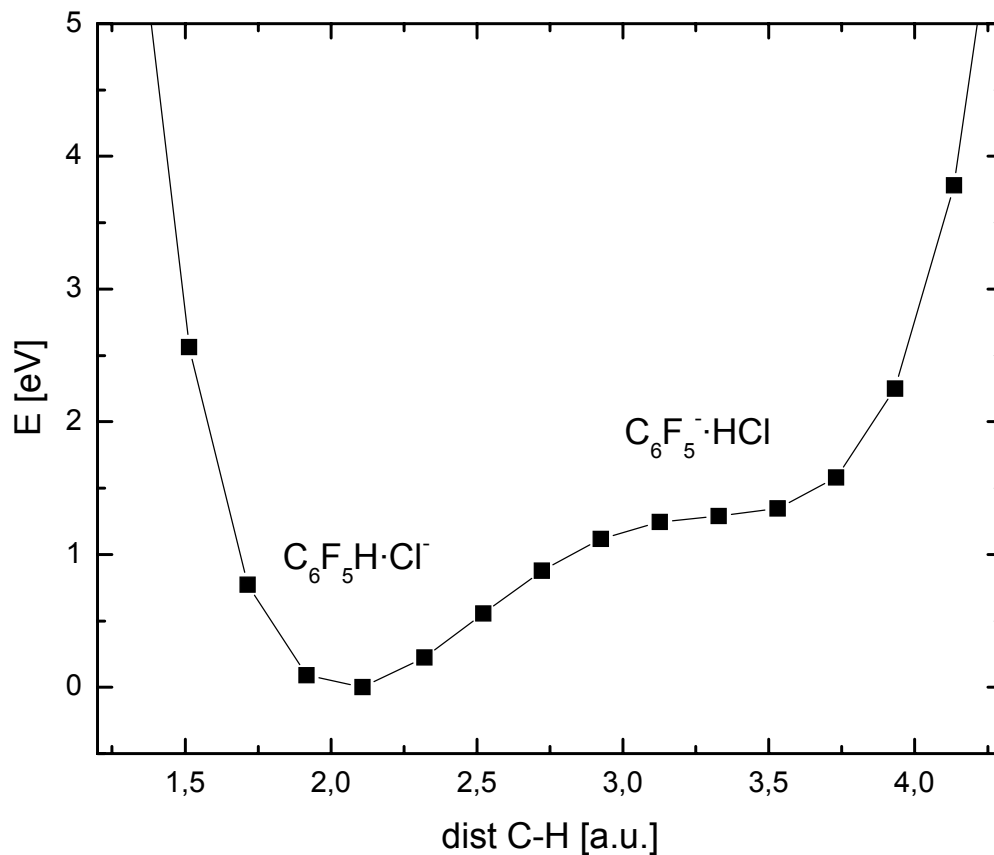


Figure 5.11 Calculated potential energy surface along the CH stretching coordinate in [C₆F₅...H...Cl]⁻ (MP2/TZVP). The squares are single-point energies at various C-H distances, with fixed C-Cl distance, whereas the rest of the coordinates were relaxed but constrained to C_{2v} symmetry.

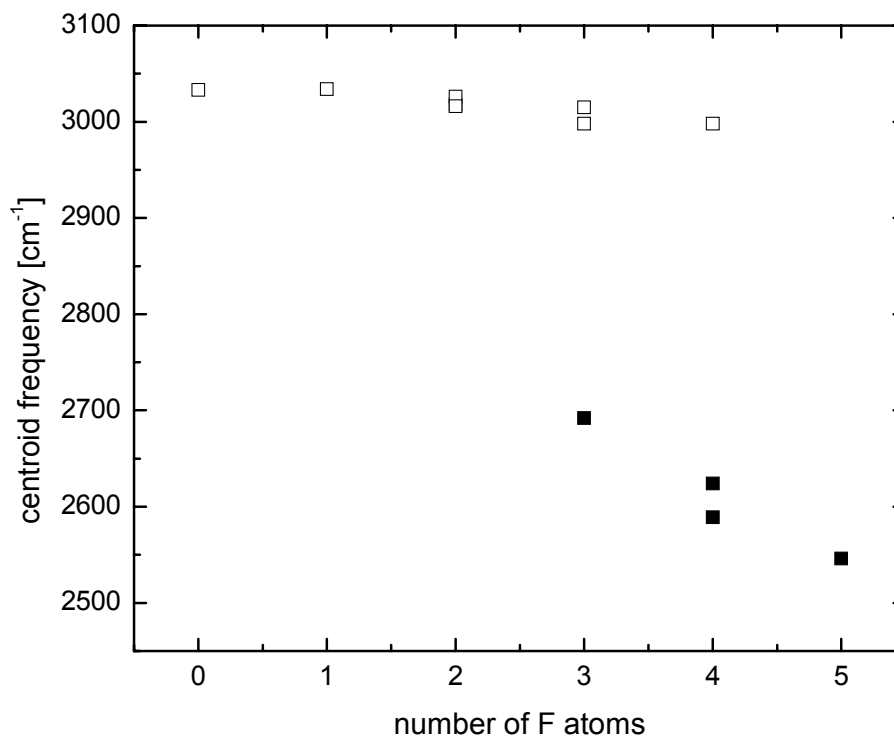


Figure 5.12 Centroid frequency as a function of the number of fluorine atoms. Open squares denote complexes with bifurcated hydrogen bonds, while data corresponding to hydrogen bonds involving isolated CH groups are shown as full squares.

5.3.6. Role of the anion

The conclusions drawn in the previous section have all been based on the variations in the chemical nature of the ligand (tuned by the degree of fluorination) bound to the chloride anion. However, the binding interaction between the two entities must be influenced by the anion, too, and it has been pointed out before, that diffuse, less nucleophilic anions (such as e.g. BF_4^-) can lead to a preference in the binding motif towards the anion- π complexes.³³ Therefore, anions other than chloride might differ from the observed preference of binding to the last remaining hydrogen atom in the pentafluorobenzene ligand in the presence of a competing positive electrostatic

potential above the carbon ring. In order to choose an anion to bias binding to the top of the aromatic ring, it helps to consider the nature of the two interacting charge distributions in view of Pearson's HSAB (hard and soft acid and base) principle.⁶¹ The positive charge in the ring certainly constitutes a softer Lewis acid than the hydrogen atom in the ring, implying that the right strategy should be switching to anions representing softer bases than chloride. Just moving down in the periodic table, this condition is necessarily fulfilled by one of the heavier halides, e.g. the iodide anion, and the sulfur hexafluoride anion should be even softer, given its large size and its highly symmetric charge distribution. In order to test these ideas and the influence of the anion, infrared spectroscopy has been performed on the $\text{I}^- \cdot \text{C}_6\text{F}_5\text{H}$ and the $\text{SF}_6^- \cdot \text{C}_6\text{F}_5\text{H}$ complexes. However, neither of the two spectra shows evidence of a ring-bound complex, as can be seen in Figure 5.13.

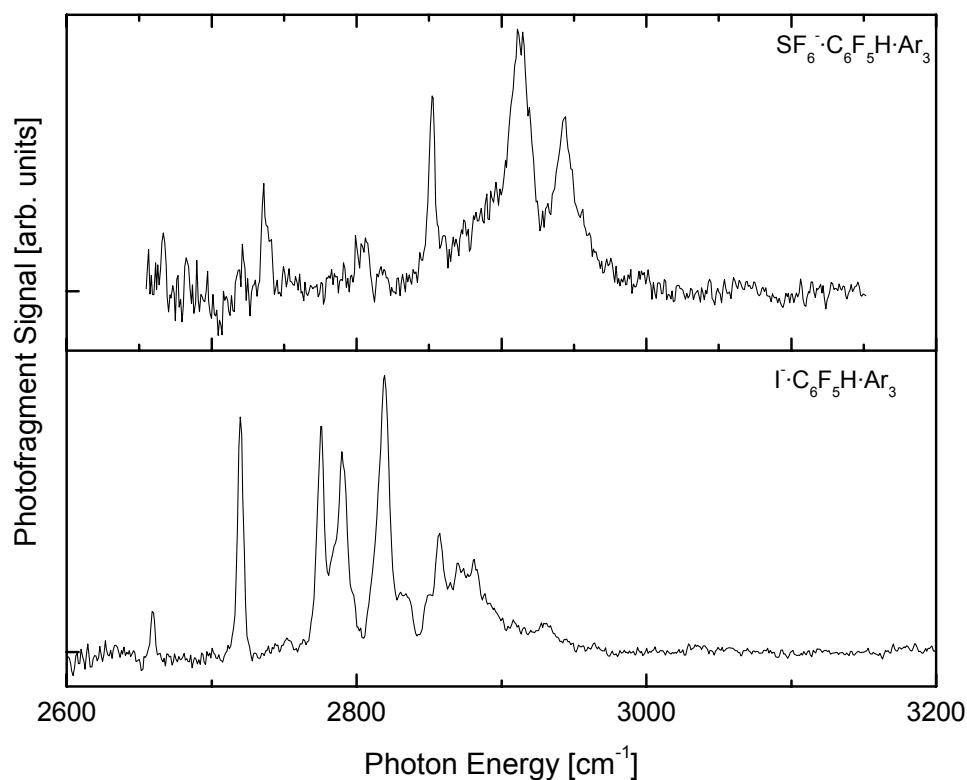


Figure 5.13 Infrared predissociation spectra of $\text{X}^- \cdot \text{C}_6\text{F}_5\text{H} \cdot \text{Ar}_3$ with $\text{X} = \text{SF}_6$ (top trace) and I (bottom trace)

Rather, they both display a complex series of intense bands, the centroid of which is red shifted as compared to the CH stretching positions of the aryl CH groups in the free benzene molecule. This indicates that the complexes are both still hydrogen bonded, with the centroid frequency shifting with the increasing ion radius (and essentially inversely with the decreasing proton affinity) from Cl^- (2546 cm^{-1}) to I^- (2818 cm^{-1}) and SF_6^- (2912 cm^{-1}).

5.3.7. Summary and conclusions

Mass selected complexes $\text{A}^-\text{C}_6\text{F}_n\text{H}_{6-n}\cdot\text{Ar}_m$ ($n = 0 - 5$, $\text{A}^- = \text{Cl}^-$, I^- , SF_6^-) have been studied by infrared predissociation spectroscopy, accompanied by (DFT and MP2) calculations to shed light on the interaction between negative ions and aromatic molecules. Fluorobenzene molecules have been chosen as model systems, as their charge distributions can be tuned by varying the degree of fluorination. It could be demonstrated that full fluorination around the ring is needed to force the anions to bind to the aromatic ring. At all lower levels of fluorination, anion-fluorobenzene complexes are bound via ionic hydrogen bonds. Investigating the influence of the size of the anion revealed that it does play a role with respect to the distortion of the hydrogen bonded CH groups. However, the preferred binding motif always remains hydrogen- rather than ring-bonded. The analysis of the $\text{Cl}^-\text{C}_6\text{F}_n\text{H}_{6-n}$ complexes revealed that bifurcated hydrogen bonds with two neighboring CH groups are preferred over binding to a single CH group in a linear hydrogen bond, a finding which had been established before by Bieske and co-workers in the case of the $\text{Cl}^-\text{C}_6\text{H}_6$ complex.^{42,43} Overall, it has been shown that infrared predissociation spectroscopy on anionic complexes in the gas phase is a powerful tool to investigate the interaction between anions and electron-deficient arenes and can yield valuable results at least partially filling the experimental gap in this field. In the study presented here no complexes displaying an anion- π binding motif could be found, but other experimental data clearly prove that these interactions do exist. One could envision the investigation of other molecular systems which would be designed in a way to favor the respective geometries. For instance, other electron-deficient aromatic

units which have been theoretically suggested to display very favorable interactions with anions such as cyanuric acids could be studied. Even more promising, species could be chosen which would still allow for the obviously preferred hydrogen bonding, but in which the anion- π interaction would be used to influence the conformation. One possibility would be to replace the hydrogen atom in the pentafluorobenzene molecule by an aliphatic chain with an appropriate anion binding site at the end (e.g. a CH_2OH group), thereby introducing a flexible lariat which would enable the anion to be hydrogen bonded and attached to the aromatic unit at the same time. Comparison to electron rich aromats such as benzene would then reveal the influence of the electron density in the arene ring on the overall binding motif of the system under investigation.

5.4. References for Chapter V

- ¹ C. J. Pedersen, *Journal of the American Chemical Society* **89** (26), 7017 (1967).
- ² B. Dietrich, J. M. Lehn, and J. P. Sauvage, *Tetrahedron Letters* (34), 2885 (1969); B. Dietrich, J. M. Lehn, and J. P. Sauvage, *Tetrahedron Letters* (34), 2889 (1969).
- ³ C. H. Park and H. E. Simmons, *Journal of the American Chemical Society* **90** (9), 2431 (1968).
- ⁴ P. D. Beer and P. A. Gale, *Angewandte Chemie-International Edition* **40** (3), 486 (2001).
- ⁵ A. Bianchi, Bowman-James, E., Garcia-Espana, E., *Supramolecular Chemistry of Anions*. (WILEY-VCH, New York, 1997).
- ⁶ P. D. Beer, Gale, P.A., Smith, D.K., *Supramolecular Chemistry*. (New York, 1999).
- ⁷ P. A. Gale, *Coordination Chemistry Reviews* **213**, 79 (2001); P. A. Gale, *Coordination Chemistry Reviews* **199**, 181 (2000).
- ⁸ J. L. Atwood, Steed, J.W., *Encyclopedia of Supramolecular Chemistry*. (CRC Press, Boca Raton, FL, 2004).
- ⁹ M. Aoyagi, K. Biradha, and M. Fujita, *Journal of the American Chemical Society* **121** (32), 7457 (1999).
- ¹⁰ C. Reuter, W. Wienand, G. M. Hubner, C. Seel, and F. Vogtle, *Chemistry-a European Journal* **5** (9), 2692 (1999); G. M. Hubner, J. Glaser, C. Seel, and F. Vogtle, *Angewandte Chemie-International Edition* **38** (3), 383 (1999).
- ¹¹ J. C. Ma and D. A. Dougherty, *Chemical Reviews* **97** (5), 1303 (1997); D. A. Dougherty, *Science* **271** (5246), 163 (1996).
- ¹² E. Cubero, F. J. Luque, and M. Orozco, *Proceedings of the National Academy of Sciences of the United States of America* **95** (11), 5976 (1998).
- ¹³ C. Garau, A. Frontera, D. Quinonero, P. Ballester, A. Costa, and P. M. Deya, *Chemphyschem* **4** (12), 1344 (2003).
- ¹⁴ B. L. Schottel, H. T. Chifotides, and K. R. Dunbar, *Chemical Society Reviews* **37** (1), 68 (2008).

- ¹⁵ J. H. Williams, J. K. Cockcroft, and A. N. Fitch, *Angewandte Chemie-International Edition in English* **31** (12), 1655 (1992).
- ¹⁶ E. V. Anslyn, Dougherty, D.A., *Modern Physical Organic Chemistry*. (University Science Books, Sausalito, CA, 2006).
- ¹⁷ M. J. Frisch, G. W. Trucks, H. B. Schlegel, G. E. Scuseria, M. A. Robb, J. R. Cheeseman, J. A. Montgomery, J. Vreven, T. , K. N. Kudin, J. C. Burant, J. M. Millam, S. S. Iyengar, J. Tomasi, V. Barone, B. Mennucci, M. Cossi, G. Scalmani, N. Rega, G. A. Petersson, H. Nakatsuji, M. Hada, M. Ehara, K. Toyota, R. Fukuda, J. Hasegawa, M. Ishida, T. Nakajima, Y. Honda, O. Kitao, H. Nakai, M. Klene, X. Li, J. E. Knox, H. P. Hratchian, J. B. Cross, V. Bakken, C. Adamo, J. Jaramillo, R. Gomperts, R. E. Stratmann, O. Yazyev, A. J. Austin, R. Cammi, C. Pomelli, J. W. Ochterski, P. Y. Ayala, K. Morokuma, G. A. Voth, P. Salvador, J. J. Dannenberg, V. G. Zakrzewski, S. Dapprich, A. D. Daniels, M. C. Strain, O. Farkas, D. K. Malick, A. D. Rabuck, K. Raghavachari, J. B. Foresman, J. V. Ortiz, Q. Cui, A. G. Baboul, S. Clifford, J. Cioslowski, B. B. Stefanov, G. Liu, A. Liashenko, P. Piskorz, I. Komaromi, R. L. Martin, D. J. Fox, T. Keith, M. A. Al-Laham, C. Y. Peng, A. Nanayakkara, M. Challacombe, P. M. W. Gill, B. Johnson, W. Chen, M. W. Wong, C. Gonzalez, and J. A. Pople, *Gaussian 03* (Gaussian, Inc, Wallingford CT, 2004).
- ¹⁸ I. Alkorta, I. Rozas, and J. Elguero, *Journal of the American Chemical Society* **124** (29), 8593 (2002); D. Kim, P. Tarakeshwar, and K. S. Kim, *Journal of Physical Chemistry A* **108** (7), 1250 (2004).
- ¹⁹ A. Frontera, F. Saczewski, M. Gdaniec, E. Dziemidowicz-Borys, A. Kurland, P. M. Deya, D. Quinero, and C. Garau, *Chemistry-a European Journal* **11** (22), 6560 (2005); C. Garau, A. Frontera, D. Quinero, P. Ballester, A. Costa, and P. M. Deya, *Journal of Physical Chemistry A* **108** (43), 9423 (2004); C. Garau, A. Frontera, D. Quinero, P. Ballester, A. Costa, and P. M. Deya, *Chemical Physics Letters* **392** (1-3), 85 (2004).
- ²⁰ C. Garau, D. Quinero, A. Frontera, P. Ballester, A. Costa, and P. M. Deya, *Journal of Physical Chemistry A* **109** (41), 9341 (2005).
- ²¹ M. Mascal, A. Armstrong, and M. D. Bartberger, *Journal of the American Chemical Society* **124** (22), 6274 (2002).
- ²² D. Quinero, A. Frontera, C. Garau, P. Ballester, A. Costa, and P. M. Deya, *Chemphyschem* **7** (12), 2487 (2006).
- ²³ D. Quinero, C. Garau, A. Frontera, P. Ballester, A. Costa, and P. M. Deya, *Chemical Physics Letters* **359** (5-6), 486 (2002).

- 24 D. Quinonero, C. Garau, C. Rotger, A. Frontera, P. Ballester, A. Costa, and P. M. Deya, *Angewandte Chemie-International Edition* **41** (18), 3389 (2002).
- 25 C. Garau, D. Quinonero, A. Frontera, D. Escudero, P. Ballester, A. Costa, and P. M. Deya, *Chemical Physics Letters* **438**, 104 (2007).
- 26 C. Garau, D. Quinonero, A. Frontera, P. Ballester, A. Costa, and P. M. Deya, *New Journal of Chemistry* **27** (2), 211 (2003).
- 27 I. Alkorta, D. Quinonero, C. Garau, A. Frontera, J. Elguero, and P. M. Deya, *Journal of Physical Chemistry A* **111** (16), 3137 (2007).
- 28 O. B. Berryman, V. S. Bryantsev, D. P. Stay, D. W. Johnson, and B. P. Hay, *Journal of the American Chemical Society* **129** (1), 48 (2007).
- 29 S. Demeshko, S. Dechert, and F. Meyer, *Journal of the American Chemical Society* **126** (14), 4508 (2004).
- 30 P. de Hoog, P. Gamez, H. Mutikainen, U. Turpeinen, and J. Reedijk, *Angewandte Chemie-International Edition* **43** (43), 5815 (2004).
- 31 H. Maeda and H. Furuta, *Journal of Porphyrins and Phthalocyanines* **8** (1-3), 67 (2004); H. Maeda, A. Osuka, and H. Furuta, *Journal of Inclusion Phenomena and Macrocyclic Chemistry* **49** (1-2), 33 (2004).
- 32 Y. S. Rosokha, S. V. Lindeman, S. V. Rosokha, and J. K. Kochi, *Angewandte Chemie-International Edition* **43** (35), 4650 (2004).
- 33 B. P. Hay and V. S. Bryantsev, *Chemical Communications* (21), 2417 (2008).
- 34 C. J. Jackson, Gazzolo, F.H., *Journal of the American Chemical Society* **23**, 376 (1900); J. Meisenheimer, *Justus Liebigs Annalen Der Chemie* **323** (1/3), 205 (1902); M. J. Strauss, *Chemical Reviews* **70** (6), 667 (1970); M. J. Strauss, *Accounts of Chemical Research* **7** (6), 181 (1974); C. F. Bernasconi, *Accounts of Chemical Research* **11** (4), 147 (1978).
- 35 V. S. Bryantsev and B. P. Hay, *Journal of the American Chemical Society* **127** (23), 8282 (2005).
- 36 G. A. Jeffrey, *An Introduction to Hydrogen Bonding*. (Oxford University Press, New York, 1997).
- 37 K. Hiraoka, S. Mizuse, and S. Yamabe, *Chemical Physics Letters* **147** (2-3), 174 (1988).

- 38 J. W. Larson and T. B. McMahon, *Journal of the American Chemical Society* **106** (3), 517 (1984).
- 39 P. Kebarle and S. Chowdhury, *Chemical Reviews* **87** (3), 513 (1987); G. J. C. Paul and P. Kebarle, *Journal of the American Chemical Society* **113** (4), 1148 (1991); M. A. French, S. Ikuta, and P. Kebarle, *Canadian Journal of Chemistry-Revue Canadienne De Chimie* **60** (15), 1907 (1982).
- 40 H. Schneider, K. M. Vogelhuber, F. Schinle, and J. M. Weber, *J. Am. Chem. Soc.* **129**, 13022 (2007).
- 41 P. Maienfisch and R. G. Hall, *Chimia* **58** (3), 93 (2004).
- 42 Z. M. Loh, R. L. Wilson, D. A. Wild, E. J. Bieske, and A. Zehnacker, *J. Chem. Phys.* **119** (18), 9559 (2003).
- 43 C. D. Thompson, B. L. J. Poad, C. Emmeluth, and E. Bieske, *Chemical Physics Letters* **428** (1-3), 18 (2006).
- 44 T. Lenzer, I. Yourshaw, M. R. Furlanetto, G. Reiser, and D. M. Neumark, *Journal of Chemical Physics* **110** (19), 9578 (1999).
- 45 R. G. Parr and W. Yang, *Density-Functional Theory of Atoms and Molecules*. (Oxford University Press, New York, 1989).
- 46 A. D. Becke, *Physical Review A* **38** (6), 3098 (1988); C. T. Lee, W. T. Yang, and R. G. Parr, *Physical Review B* **37** (2), 785 (1988).
- 47 F. Weigend and M. Häser, *Theoretical Chemistry Accounts* **97** (1-4), 331 (1997); F. Weigend, M. Häser, H. Patzelt, and R. Ahlrichs, *Chemical Physics Letters* **294** (1-3), 143 (1998).
- 48 R. Ahlrichs, M. Bär, M. Häser, H. Horn, and C. Kölmel, *Chemical Physics Letters* **162** (3), 165 (1989).
- 49 A. Schäfer, C. Huber, and R. Ahlrichs, *J. Chem. Phys.* **100** (8), 5829 (1994).
- 50 S. G. Frankiss and D. J. Harrison, *Spectrochimica Acta Part a-Molecular and Biomolecular Spectroscopy* **31** (12), 1839 (1975).
- 51 R. K. Sampson and W. D. Lawrance, *Australian Journal of Chemistry* **56** (4), 275 (2003).
- 52 M. Alberti, A. Castro, A. Lagana, M. Moix, F. Pirani, and D. Cappelletti, *European Physical Journal D* **38** (1), 185 (2006).

- 53 E. B. Wilson, *Physical Review* **45** (10), 0706 (1934).
- 54 R. H. Page, Y. R. Shen, and Y. T. Lee, *Journal of Chemical Physics* **88** (9), 5362 (1988).
- 55 R. H. Page, Y. R. Shen, and Y. T. Lee, *Journal of Chemical Physics* **88** (8), 4621 (1988).
- 56 J. Pliva and A. S. Pine, *Journal of Molecular Spectroscopy* **126** (1), 82 (1987).
- 57 M. Tschurl, C. Ueberfluss, and U. Boesl, *Chemical Physics Letters* **439** (1-3), 23 (2007).
- 58 I. Alkorta, I. Rozas, and J. Elguero, *Journal of Fluorine Chemistry* **101** (2), 233 (2000).
- 59 W. H. Robertson, E. A. Price, J. M. Weber, J. W. Shin, G. H. Weddle, and M. A. Johnson, *J. Phys. Chem. A* **107** (34), 6527 (2003); H. Schneider, A. D. Boese, and J. M. Weber, *J. Chem. Phys.* **123**, 084307 (2005).
- 60 H. H. Buker, N. M. M. Nibbering, D. Espinosa, F. Mongin, and M. Schlosser, *Tetrahedron Letters* **38** (49), 8519 (1997).
- 61 R. G. Pearson, *Journal of the American Chemical Society* **85** (22), 3533 (1963).

Bibliography

- Ahlrichs, R., M. Bär, et al. (1989). *Chemical Physics Letters* **162**(3): 165-169.
- Alberti, M., A. Castro, et al. (2006). *European Physical Journal D* **38**(1): 185-191.
- Alkorta, I., D. Quinonero, et al. (2007). *Journal of Physical Chemistry A* **111**(16): 3137-3142.
- Alkorta, I., I. Rozas, et al. (2000). *Journal of Fluorine Chemistry* **101**(2): 233-238.
- Alkorta, I., I. Rozas, et al. (2002). *Journal of the American Chemical Society* **124**(29): 8593-8598.
- Almlof, J., A. Lund, et al. (1974). *Chemical Physics Letters* **28**(2): 179-181.
- Angel, L. A. and K. M. Ervin (2003). *Journal of the American Chemical Society* **125**(4): 1014-1027.
- Anslyn, E. V., Dougherty, D.A. (2006). *Modern Physical Organic Chemistry*. Sausalito, CA, University Science Books.
- Aoyagi, M., K. Biradha, et al. (1999). *Journal of the American Chemical Society* **121**(32): 7457-7458.
- Armentrout, P. B. (2000). *International Journal of Mass Spectrometry* **200**(1-3): 219-241.
- Armentrout, P. B. (2001). *Annual Review of Physical Chemistry* **52**: 423-461.

- Armentrout, P. B. (2003). *International Journal of Mass Spectrometry* **227**(3): 289-302.
- Armentrout, P. B. and T. Baer (1996). *Journal of Physical Chemistry* **100**(31): 12866-12877.
- Arnold, S. T., J. H. Hendricks, et al. (1995). *Journal of Chemical Physics* **102**(1): 39-47.
- Arnold, S. T. and A. A. Viggiano (2001). *Journal of Physical Chemistry A* **105**(14): 3527-3531.
- Atwood, J. L., Steed, J.W. (2004). *Encyclopedia of Supramolecular Chemistry*. Boca Raton, FL, CRC Press.
- Ayers, G. P. and A. D. E. Pullin (1976). *Spectrochimica Acta Part a-Molecular and Biomolecular Spectroscopy* **32**(10): 1629-1639.
- Ayotte, P., J. A. Kelley, et al. (2000). *Chemical Physics Letters* **316**(5-6): 455-459.
- Ayotte, P., J. Kim, et al. (1999). *Journal of the American Chemical Society* **121**(29): 6950-6951.
- Ayotte, P., S. B. Nielsen, et al. (1999). *Journal of Physical Chemistry* **103**(50): 10665-10669.
- Ayotte, P., G. H. Weddle, et al. (1999). *Journal of Physical Chemistry* **110**(15): 7129-7132.
- Ayotte, P., G. H. Weddle, et al. (1998). *Chemical Physics* **239**(1-3): 485-491.
- Ayotte, P., G. H. Weddle, et al. (1998). *Journal of the American Chemical Society* **120**(47): 12361-12362.

- Ayotte, P., G. H. Weddle, et al. (1999). *Journal of Physical Chemistry A* **103**(4): 443-447.
- Bailey, C. G., J. Kim, et al. (1997). *Chemical Physics Letters* **269**(1-2): 122-127.
- Barlow, S. E., J. M. Vandoren, et al. (1988). *Journal of the American Chemical Society* **110**(21): 7240-7242.
- Bassmann, C., U. Boesl, et al. (1996). *International Journal of Mass Spectrometry and Ion Processes* **159**: 153-167.
- Becke, A. D. (1988). *Physical Review A* **38**(6): 3098-3100.
- Becker, I. and O. Cheshnovsky (1999). *Journal of Chemical Physics* **110**(13): 6288-6297.
- Beer, P. D. and P. A. Gale (2001). *Angewandte Chemie-International Edition* **40**(3): 486-516.
- Beer, P. D., Gale, P.A., Smith, D.K. (1999). *Supramolecular Chemistry*. New York.
- Beregovaya, I. V. and L. N. Shchegoleva (2002). *International Journal of Quantum Chemistry* **88**(4): 481-488.
- Bernasconi, C. F. (1978). *Accounts of Chemical Research* **11**(4): 147-152.
- Berryman, O. B., V. S. Bryantsev, et al. (2007). *Journal of the American Chemical Society* **129**(1): 48-58.
- Beyer, M. K. (2007). *Mass Spectrometry Reviews* **26**(4): 517-541.
- Bianchi, A., Bowman-James, E., Garcia-Espana, E. (1997). *Supramolecular Chemistry of Anions*. New York, WILEY-VCH.

Bieske, E. J. (2003). *Chemical Society Reviews* **32**(4): 231-237.

Bieske, E. J. and O. Dopfer (2000). *Chemical Reviews* **100**(11): 3963-3998.

Bieske, E. J. and J. P. Maier (1993). *Chemical Reviews* **93**(8): 2603-2621.

Bilodeau, R. C., M. Scheer, et al. (1998). *Journal of Physics B-Atomic Molecular and Optical Physics* **31**(17): 3885-3891.

Boesl, U. and W. J. Knott (1998). *Mass Spectrometry Reviews* **17**(4): 275-305.

Boesl, U., R. Weinkauff, et al. (1992). *International Journal of Mass Spectrometry and Ion Processes* **112**(2-3): 121-166.

Bogdanov, B. and T. B. McMahon (2006). *Journal of Physical Chemistry A* **110**(4): 1350-1363.

Böhme, D. K. and H. Schwarz (2005). *Angewandte Chemie-International Edition* **44**(16): 2336-2354.

Bondybey, V. E. and M. K. Beyer (2002). *International Reviews in Physical Chemistry* **21**(2): 277-306.

Bopp, J. C., J. R. Roscioli, et al. (2007). *Journal of Physical Chemistry A* **111**(7): 1214-1221.

Bowers, M. T., Ed. (1979). *Gas Phase Ion Chemistry*. New York, Academic Press.

Bowers, M. T., A. G. Marshall, et al. (1996). *J. Phys. Chem.* **100**(31): 12897-12910.

Brauman, J. I. (1995). *Journal of Mass Spectrometry* **30**(12): 1649-1651.

- Brauman, J. I. (2008). *Science* **319**(5860): 168-168.
- Braun, J. E., T. Mehnert, et al. (2000). *International Journal of Mass Spectrometry* **203**(1-3): 1-18.
- Brinkmann, N. R. and H. F. Schaefer (2003) *Chemical Physics Letters* **381**(1-2): 123-128.
- Brutschy, B. (1992). *Chemical Reviews* **92**(7): 1567-1587.
- Bryantsev, V. S. and B. P. Hay (2005). *Journal of the American Chemical Society* **127**(23): 8282-8283.
- Buker, H. H., N. M. M. Nibbering, et al. (1997). *Tetrahedron Letters* **38**(49): 8519-8522.
- Cabarcos, O. M., C. J. Weinheimer, et al. (1999). *Journal of Chemical Physics* **110**(1): 5-8.
- Campargue, R. (1970). *Journal of Chemical Physics* **52**(4): 1795.
- Castleman, A. W. and K. H. Bowen (1996). *Journal of Physical Chemistry* **100**(31): 12911-12944.
- Chandrasekhar, J., S. F. Smith, et al. (1985). *Journal of the American Chemical Society* **107**(1): 154-163.
- Chen, E. C. M., J. R. Wiley, et al. (1994). *Journal of Physical Chemistry* **98**(1): 88-94.
- Chen, M. S. and D. W. Goodman (2008). *Chemical Society Reviews* **37**(9): 1860-1870.
- Cheshnovsky, O., S. H. Yang, et al. (1987). *Review of Scientific Instruments* **58**(11): 2131-2137.

- Chretien, S., S. K. Buratto, et al. (2007). *Current Opinion in Solid State & Materials Science* **11**(5-6): 62-75.
- Clemmer, D. E. and M. F. Jarrold (1997). *Journal of Mass Spectrometry* **32**(6): 577-592.
- Collings, B. A., K. Athanassenas, et al. (1994). *Journal of Chemical Physics* **101**(5): 3506-3513.
- Continetti, R. E. (1998). *International Reviews in Physical Chemistry* **17**(2): 227-260.
- Corcelli, S. A., J. A. Kelley, et al. (2002). *J. Phys. Chem. A* **106**(19): 4872-4879.
- Crim, F. F. (1993). *Annual Review of Physical Chemistry* **44**: 397-428.
- Cubero, E., F. J. Luque, et al. (1998). *Proceedings of the National Academy of Sciences of the United States of America* **95**(11): 5976-5980.
- Danten, Y., T. Tassaing, et al. (1999). *Journal of Physical Chemistry A* **103**(18): 3530-3534.
- de Hoog, P., P. Gamez, et al. (2004). *Angewandte Chemie-International Edition* **43**(43): 5815-5817.
- Demeshko, S., S. Dechert, et al. (2004). *Journal of the American Chemical Society* **126**(14): 4508-4509.
- DePuy, C. H. (2000). *International Journal of Mass Spectrometry* **200**(1-3): 79-96.
- Dessent, C. E. H., M. A. Johnson, et al. (1999). Electron transfer and charge separation in clusters. *Electron Transfer-from Isolated Molecules to Biomolecules, Pt 1.* **106**: 265-302.

- Dessent, C. E. H., J. Kim, et al. (1998). *Accounts of Chemical Research* **31**(9): 527-534.
- Diederich, T., J. Tiggesbäumker, et al. (2002). *Journal of Chemical Physics* **116**(8): 3263-3269.
- Dietrich, B., J. M. Lehn, et al. (1969). *Tetrahedron Letters*(34): 2889-&.
- Dietrich, B., J. M. Lehn, et al. (1969). *Tetrahedron Letters*(34): 2885-&.
- Diken, E. G., G. H. Weddle, et al. (2004). *J. Phys. Chem. A* **108**(46): 10116-10121.
- Dillow, G. W. and P. Kebarle (1989). *Journal of the American Chemical Society* **111**(15): 5592-5596.
- Djafari, S., G. Lembach, et al. (1996). *Zeitschrift Fur Physikalische Chemie-International Journal of Research in Physical Chemistry & Chemical Physics* **195**: 253-272.
- Donaldson, D. J., A. F. Tuck, et al. (2003). *Chemical Reviews* **103**(12): 4717-4729.
- Dopfer, O. (2003). *International Reviews in Physical Chemistry* **22**(3): 437-495.
- Dopfer, O. (2005). *Zeitschrift Fur Physikalische Chemie-International Journal of Research in Physical Chemistry & Chemical Physics* **219**(2): 125-168.
- Dougherty, D. A. (1996). *Science* **271**(5246): 163-168.
- Dunbar, R. C. (2000). *International Journal of Mass Spectrometry* **200**(1-3): 571-589.
- Duncan, M. A. (1997). *Annual Review of Physical Chemistry* **48**: 69-93.

- Duncan, M. A. (2000). *International Journal of Mass Spectrometry* **200**(1-3): 545-569.
- Duncan, M. A. (2003). *International Reviews in Physical Chemistry* **22**(2): 407-435.
- Dunn, M. E., G. C. Shields, et al. (2008). *Journal of Physical Chemistry A* **112**(41): 10226-10235.
- Ebata, T., A. Fujii, et al. (1998). *International Reviews in Physical Chemistry* **17**(3): 331-361.
- Elles, C. G. and F. F. Crim (2006). *Annual Review of Physical Chemistry* **57**: 273-302.
- Eustis, S. N., D. Wang, et al. (2007). *Journal of Chemical Physics* **127**(11).
- Farrar, J. M. (2003). *International Reviews in Physical Chemistry* **22**(4): 593-640.
- Federmann, F., K. Hoffmann, et al. (1999). *European Physical Journal D* **9**(1-4): 11-14.
- Feil, S. (2008). *Chemie in Unserer Zeit* **42**(2): 67-67.
- Fielicke, A., G. Meijer, et al. (2003). *Journal of the American Chemical Society* **125**(12): 3659-3667.
- Frankiss, S. G. and D. J. Harrison (1975). *Spectrochimica Acta Part a-Molecular and Biomolecular Spectroscopy* **31**(12): 1839-1864.
- Freiser, B. S. (1996). *Journal of Mass Spectrometry* **31**(7): 703-715.
- French, M. A., S. Ikuta, et al. (1982). *Canadian Journal of Chemistry-Revue Canadienne De Chimie* **60**(15): 1907-1918.

- Frisch, M. J., G. W. Trucks, et al. (2004). Gaussian 03. Wallingford CT, Gaussian, Inc.
- Frontera, A., F. Saczewski, et al. (2005). Chemistry-a European Journal **11**(22): 6560-6567.
- Fujii, A., T. Sawamura, et al. (1994). Chemical Physics Letters **225**(1-3): 104-107.
- Gale, P. A. (2000). Coordination Chemistry Reviews **199**: 181-233.
- Gale, P. A. (2001). Coordination Chemistry Reviews **213**: 79-128.
- Gallivan, J. P. and D. A. Dougherty (1999). Organic Letters **1**(1): 103-105.
- Gantefor, G., G. S. IckingKonert, et al. (1996). International Journal of Mass Spectrometry and Ion Processes **159**: 81-109.
- Garau, C., A. Frontera, et al. (2003). Chemphyschem **4**(12): 1344-1348.
- Garau, C., A. Frontera, et al. (2004). Chemical Physics Letters **392**(1-3): 85-89.
- Garau, C., A. Frontera, et al. (2004). Journal of Physical Chemistry A **108**(43): 9423-9427.
- Garau, C., D. Quinonero, et al. (2003). New Journal of Chemistry **27**(2): 211-214.
- Garau, C., D. Quinonero, et al. (2005). Journal of Physical Chemistry A **109**(41): 9341-9345.
- Garau, C., D. Quinonero, et al. (2007). Chemical Physics Letters **438**: 104-108.
- Garrett, W. R. (1971). Physical Review A **3**(3): 961-&.

- Gleave, J. L., E. D. Hughes, et al. (1935). *Journal of the Chemical Society*: 236-244.
- Grebenev, S., E. Lugovoi, et al. (2001). *Faraday Discussions* **118**: 19-32.
- Gulley, R. J., S. L. Lunt, et al. (1998). *Journal of Physics B-Atomic Molecular and Optical Physics* **31**(12): 2735-2751.
- Gutsev, G. L. and R. J. Bartlett (1998). *Molecular Physics* **94**(1): 121-125.
- Häkkinen, H., W. Abbet, et al. (2003). *Angewandte Chemie-International Edition* **42**(11): 1297-1300.
- Hashmi, A. S. K. and G. J. Hutchings (2006). *Angewandte Chemie-International Edition* **45**(47): 7896-7936.
- Hay, B. P. and V. S. Bryantsev (2008). *Chemical Communications*(21): 2417-2428.
- Heiz, U. and E. L. Bullock (2004). *Journal of Materials Chemistry* **14**(4): 564-577.
- Hendricks, J. H., H. L. de Clercq, et al. (2002). *Journal of Chemical Physics* **116**(18): 7926-7938.
- Hermansson, K. (1993). *Journal of Chemical Physics* **99**(2): 861-868.
- Hiraoka, K., S. Mizuse, et al. (1988). *Chemical Physics Letters* **147**(2-3): 174-178.
- Hong, X. Y., S. Chen, et al. (1995). *Journal of Physical Chemistry* **99**(22): 9102-9109.
- Hotop, H. and W. C. Lineberger (1985). *Journal of Physical and Chemical Reference Data* **14**(3): 731-750.

- Hubner, G. M., J. Glaser, et al. (1999). *Angewandte Chemie-International Edition* **38**(3): 383-386.
- Huey, L. G., D. R. Hanson, et al. (1995). *Journal of Physical Chemistry* **99**(14): 5001-5008.
- Huisken, F., M. Kaloudis, et al. (1996). *Journal of Chemical Physics* **104**(1): 17-25.
- Ingold, C. K. (1969). *Structure and Reactivity in Organic Chemistry*. Ithaca, NY, Cornell University Press.
- Irion, M. P. (1992). *International Journal of Mass Spectrometry and Ion Processes* **121**(1-2): 1-47.
- Jackson, C. J., Gazzolo, F.H. (1900). *Journal of the American Chemical Society* **23**: 376.
- Jacox, M. E. and D. E. Milligan (1974). *Chemical Physics Letters* **28**(2): 163-168.
- Jaeger, T. D., D. van Heijnsbergen, et al. (2004). *Journal of the American Chemical Society* **126**(35): 10981-10991.
- Jeffrey, G. A. (1997). *An Introduction to Hydrogen Bonding*. New York, Oxford University Press.
- Johnson, M. A. and W. C. Lineberger (1988). *Techniques for the Study of Gas-Phase Ion Molecule Reactions*. J. M. Farrar and W. Saunders. New York, Wiley: 591.
- Jungwirth, P. and D. J. Tobias (2001). *Journal of Physical Chemistry B* **105**(43): 10468-10472.
- Jungwirth, P. and D. J. Tobias (2002). *Journal of Physical Chemistry A* **106**(2): 379-383.

- Jungwirth, P. and D. J. Tobias (2002). *Journal of Physical Chemistry B* **106**(25): 6361-6373.
- Jungwirth, P. and D. J. Tobias (2006). *Chemical Reviews* **106**(4): 1259-1281.
- Kawaguchi, K. and E. Hirota (1986). *Journal of Chemical Physics* **84**(6): 2953-2960.
- Kawamata, H., T. Maeyama, et al. (2003). *Chemical Physics Letters* **370**(3-4): 535-541.
- Kebarle, P. and S. Chowdhury (1987). *Chemical Reviews* **87**(3): 513-534.
- Kim, D., P. Tarakeshwar, et al. (2004). *Journal of Physical Chemistry A* **108**(7): 1250-1258.
- Kimble, M. L. and A. W. Castleman (2004). *International Journal of Mass Spectrometry* **233**(1-3): 99-101.
- Kimble, M. L., A. W. Castleman, et al. (2004). *Journal of the American Chemical Society* **126**(8): 2526-2535.
- Klots, C. E. (1985). *Journal of Chemical Physics* **83**(11): 5854-5860.
- Knapp, M., O. Echt, et al. (1986). *Chemical Physics Letters* **126**(3-4): 225-231.
- Knickelbein, M. B. (1999). *Philosophical Magazine B-Physics of Condensed Matter Statistical Mechanics Electronic Optical and Magnetic Properties* **79**(9): 1379-1400.
- Knighton, W. B., D. R. Zook, et al. (1990). *Journal of the American Society for Mass Spectrometry* **1**(5): 372-381.
- Krestov, G. A. (1994). *Ionic Solvation*, Prentice Hall.

- Kryachko, E. S. (2008). *Journal of Molecular Structure* **880**(1-3): 23-30.
- Laerdahl, J. K. and E. Uggerud (2002). *International Journal of Mass Spectrometry* **214**(3): 277-314.
- Larson, J. W. and T. B. McMahon (1984). *Journal of the American Chemical Society* **106**(3): 517-521.
- Lee, C. T., W. T. Yang, et al. (1988). *Physical Review B* **37**(2): 785-789.
- Lenzer, T., I. Yourshaw, et al. (2001). *Journal of Chemical Physics* **115**(8): 3578-3589.
- Lenzer, T., I. Yourshaw, et al. (1999). *Journal of Chemical Physics* **110**(19): 9578-9586.
- Leopold, D. G., J. Ho, et al. (1987). *Journal of Chemical Physics* **86**(4): 1715-1726.
- Lisy, J. M. (1997). *International Reviews in Physical Chemistry* **16**(3): 267-289.
- Lisy, J. M. (2006). *Journal of Chemical Physics* **125**(13).
- Loh, Z. M., R. L. Wilson, et al. (2003). *J. Chem. Phys.* **119**(18): 9559-9567.
- Lugez, C. L., M. E. Jacox, et al. (1998). *Journal of Chemical Physics* **108**(23): 9639-9650.
- Lyapustina, S. A., S. K. Xu, et al. (2000). *J. Chem. Phys.* **112**(15): 6643-6648.
- Ma, J. C. and D. A. Dougherty (1997). *Chemical Reviews* **97**(5): 1303-1324.
- Maeda, H. and H. Furuta (2004). *Journal of Porphyrins and Phthalocyanines* **8**(1-3): 67-75.

- Maeda, H., A. Osuka, et al. (2004). *Journal of Inclusion Phenomena and Macrocyclic Chemistry* **49**(1-2): 33-36.
- Maeyama, T., I. Yagi, et al. (2006). *Journal of Physical Chemistry A* **110**(51): 13712-13716.
- Maienfisch, P. and R. G. Hall (2004). *Chimia* **58**(3): 93-99.
- Marshall, A. G. and L. Schweikhard (1992). *International Journal of Mass Spectrometry and Ion Processes* **118**: 37-70.
- Mascal, M., A. Armstrong, et al. (2002). *Journal of the American Chemical Society* **124**(22): 6274-6276.
- Meisenheimer, J. (1902). *Justus Liebigs Annalen Der Chemie* **323**(1/3): 205-246.
- Metz, R. B. (2004). *International Reviews in Physical Chemistry* **23**(1): 79-108.
- Mikosch, J., S. Trippel, et al. (2008). *Science* **319**(5860): 183-186.
- Miller, T. M., J. M. Van Doren, et al. (2004). *International Journal of Mass Spectrometry* **233**(1-3): 67-73.
- Misaizu, F., K. Tsukamoto, et al. (1995). *Laser Chemistry* **15**(2-4): 195-207.
- Misaizu, F., K. Tsukamoto, et al. (1996). *Surface Review and Letters* **3**(1): 405-410.
- Mitsui, M., A. Nakajima, et al. (2002). *Journal of Chemical Physics* **117**(21): 9740-9749.
- Mitsui, M., A. Nakajima, et al. (2001). *Journal of Chemical Physics* **115**(13): 5707-5710.

- Müller-Dethlefs, K., O. Dopfer, et al. (1994). *Chemical Reviews* **94**(7): 1845-1871.
- Müller-Dethlefs, K. and E. W. Schlag (1998). *Angewandte Chemie-International Edition* **37**(10): 1346-1374.
- Muntean, F., M. S. Taylor, et al. (2004). *Journal of Chemical Physics* **121**(12): 5676-5687.
- Myshakin, E. M., K. D. Jordan, et al. (2003). *Journal of Chemical Physics* **119**(19): 10138-10145.
- Neilson, G. W., P. E. Mason, et al. (2001). *Philosophical Transactions of the Royal Society of London Series a-Mathematical Physical and Engineering Sciences* **359**(1785): 1575-1591.
- Nesbitt, D. J. and R. W. Field (1996). *Journal of Physical Chemistry* **100**(31): 12735-12756.
- Neumark, D. M. (2001). *Annual Review of Physical Chemistry* **52**: 255-277.
- Neumark, D. M. (2005). *Physical Chemistry Chemical Physics* **7**(3): 433-442.
- Neumark, D. M., K. R. Lykke, et al. (1985). *Journal of Chemical Physics* **83**(9): 4364-4373.
- Niedner-Schatteburg, G. and V. E. Bondybey (2000). "FT-ICR studies of solvation effects in ionic water cluster reactions." *Chemical Reviews* **100**(11): 4059-4086.
- Nielsen, S. B., P. Ayotte, et al. (1999). *Journal of Chemical Physics* **111**(21): 9593-9599.
- Oepts, D., A. F. G. Vandermeer, et al. (1995). *Infrared Physics & Technology* **36**(1): 297-308.

- Olkhov, R. V., S. A. Nizkorodov, et al. (1998). *Journal of Chemical Physics* **108**(24): 10046-10060.
- Olmstead, W. N. and J. I. Brauman (1977). *Journal of the American Chemical Society* **99**(13): 4219-4228.
- Onda, M., H. Yamada, et al. (1994). *Journal of Molecular Structure* **319**: 297-299.
- Oomens, J., D. T. Moore, et al. (2004). *Physical Chemistry Chemical Physics* **6**(4): 710-718.
- Oomens, J., B. G. Sartakov, et al. (2006). *International Journal of Mass Spectrometry* **254**(1-2): 1-19.
- Ovenall, D. W. and D. H. Whiffen (1961). *Molecular Physics* **4**(2): 135-144.
- Page, R. H., Y. R. Shen, et al. (1988). *Journal of Chemical Physics* **88**(9): 5362-5376.
- Page, R. H., Y. R. Shen, et al. (1988). *Journal of Chemical Physics* **88**(8): 4621-4636.
- Parent, D. C. and S. L. Anderson (1992). *Chemical Reviews* **92**(7): 1541-1565.
- Park, C. H. and H. E. Simmons (1968). *Journal of the American Chemical Society* **90**(9): 2431-&.
- Parr, R. G. and W. Yang (1989). *Density-Functional Theory of Atoms and Molecules*. New York, Oxford University Press.
- Paul, G. J. C. and P. Kebarle (1991). *Journal of the American Chemical Society* **113**(4): 1148-1154.
- Pearson, R. G. (1963). *Journal of the American Chemical Society* **85**(22): 3533 - 3539.

- Pedersen, C. J. (1967). *Journal of the American Chemical Society* **89**(26): 7017-&.
- Perelygin, I. S. and N. R. Safiullina (1967). *Zh. Strukt. Khim.* **8**: 205.
- Pliva, J. and A. S. Pine (1987). *Journal of Molecular Spectroscopy* **126**(1): 82-98.
- Powell, D. H., G. W. Neilson, et al. (1993). *Journal of Physics-Condensed Matter* **5**(32): 5723-5730.
- Price, E. A., N. I. Hammer, et al. (2004). *Journal of Physical Chemistry A* **108**(18): 3910-3915.
- Price, E. A., W. H. Robertson, et al. (2002). *Chemical Physics Letters* **366**(3-4): 412-416.
- Quinonero, D., A. Frontera, et al. (2006). *Chemphyschem* **7**(12): 2487-2491.
- Quinonero, D., C. Garau, et al. (2002). *Chemical Physics Letters* **359**(5-6): 486-492.
- Quinonero, D., C. Garau, et al. (2002). *Angewandte Chemie-International Edition* **41**(18): 3389-3392.
- Rathbone, G. J., T. Sanford, et al. (2005). *Chemical Physics Letters* **401**(4-6): 570-574.
- Ravishankara, A. R., S. Solomon, et al. (1993). *Science* **259**(5092): 194-199.
- Reimers, J. R., R. O. Watts, et al. (1982). *Chemical Physics* **64**(1): 95-114.
- Reinhard, B. M., A. Lagutschenkov, et al. (2004). *J. Phys. Chem. A* **108**(16): 3350-3355.

- Reuter, C., W. Wienand, et al. (1999). *Chemistry-a European Journal* **5**(9): 2692-2697.
- Riehn, C., K. Buchhold, et al. (2000). *Journal of Chemical Physics* **112**(3): 1170-1177.
- Robertson, W. H., E. G. Diken, et al. (2003). *Science* **299**(5611): 1367-1372.
- Robertson, W. H. and M. A. Johnson (2003). *Annual Review of Physical Chemistry* **54**: 173-213.
- Robertson, W. H., J. A. Kelley, et al. (2000). *Journal of Chemical Physics* **113**(18): 7879-7884.
- Robertson, W. H., J. A. Kelley, et al. (2000). *Review of Scientific Instruments* **71**(12): 4431-4434.
- Robertson, W. H., E. A. Price, et al. (2003). *J. Phys. Chem. A* **107**(34): 6527-6532.
- Rodgers, M. T. and P. B. Armentrout (2000). *Mass Spectrometry Reviews* **19**(4): 215-247.
- Rosokha, Y. S., S. V. Lindeman, et al. (2004). *Angewandte Chemie-International Edition* **43**(35): 4650-4652.
- Sampson, R. K. and W. D. Lawrance (2003). *Australian Journal of Chemistry* **56**(4): 275-277.
- Sanchez, A., S. Abbet, et al. (1999). *J. Phys. Chem. A* **103**(48): 9573-9578.
- Sanov, A. and W. C. Lineberger (2004). *Physical Chemistry Chemical Physics* **6**(9): 2018-2032.
- Schäfer, A., C. Huber, et al. (1994). *Journal of Chemical Physics* **100**(8): 5829-5835.

- Schiedt, J., W. J. Knott, et al. (2000). *Journal of Chemical Physics* **113**(21): 9470-9478.
- Schmatz, S. (2004). *Chemphyschem* **5**(5): 600-617.
- Schneider, H., A. D. Boese, et al. (2005). *Journal of Chemical Physics* **123**: 084307.
- Schneider, H., Takahashi, K., Skodje, R.T., Weber, J.M. (2009). in preparation.
- Schneider, H., K. M. Vogelhuber, et al. (2008). *Journal of Physical Chemistry A* **112**(33): 7498-7506.
- Schneider, H., K. M. Vogelhuber, et al. (2007). *Journal of the American Chemical Society* **129**: 13022.
- Schneider, H., K. M. Vogelhuber, et al. (2007). *Journal of Chemical Physics* **127**: 114311.
- Schneider, H. and J. M. Weber (2007). *Journal of Chemical Physics* **127**: 244310.
- Schooss, D. (1999). Dissertation, Universität Karlsruhe (TH).
- Schooss, D., S. Gilb, et al. (2000). *Journal of Chemical Physics* **113**(13): 5361-5371.
- Schottel, B. L., H. T. Chifotides, et al. (2008). *Chemical Society Reviews* **37**(1): 68-83.
- Schröder, D. and H. Schwarz (2003). *Modern Mass Spectrometry*. **225**: 133-152.
- Schwarz, H. (2003). *Angewandte Chemie-International Edition* **42**(37): 4442-4454.
- Schwarz, H. (2004). *International Journal of Mass Spectrometry* **237**(1): 75-105.

- Shigeto, S., Y. Pang, et al. (2008). *Journal of Physical Chemistry B* **112**(2): 232-241.
- Shin, J. W., N. I. Hammer, et al. (2005). *J. Phys. Chem. A* **109**(14): 3146-3152.
- Shvartsburg, A. A., R. R. Hudgins, et al. (2001). *Chemical Society Reviews* **30**(1): 26-35.
- Simard, B., S. Denommee, et al. (2002). *Chemical Physics Letters* **357**(3-4): 195-203.
- Singh, P. C. and G. N. Patwari (2007). *Journal of Physical Chemistry A* **111**(16): 3178-3183.
- Socaciu, L. D., J. Hagen, et al. (2003). *Journal of the American Chemical Society* **125**(34): 10437-10445.
- Solca, N. and O. Dopfer (2000). *Chemical Physics Letters* **325**(4): 354-359.
- Stoermer, C. W., S. Gilb, et al. (1998). *Review of Scientific Instruments* **69**(4): 1661-1664.
- Stolow, A., A. E. Bragg, et al. (2004). *Chemical Reviews* **104**(4): 1719-1757.
- Strauss, M. J. (1970). *Chemical Reviews* **70**(6): 667-&.
- Strauss, M. J. (1974). *Accounts of Chemical Research* **7**(6): 181-188.
- Sturges, W. T., T. J. Wallington, et al. (2000). *Science* **289**(5479): 611-613.
- Takahashi, K., Skodje R.T., private communication.
- Takahashi, K., K. L. Plath, et al. (2008). *Journal of Physical Chemistry A* **112**(32): 7321-7331.

- Taylor, M. S., J. Barbera, et al. (2005). *Journal of Chemical Physics* **122**(5).
- Taylor, M. S., F. Muntean, et al. (2004). *Journal of Chemical Physics* **121**(12): 5688-5699.
- Terasaki, A., S. Minemoto, et al. (1999). *European Physical Journal D* **9**(1-4): 163-168.
- Thompson, C. D., B. L. J. Poad, et al. (2006). *Chemical Physics Letters* **428**(1-3): 18-22.
- Thompson, W. H. and J. T. Hynes (2000). *Journal of the American Chemical Society* **122**(26): 6278-6286.
- Tschurl, M., C. Ueberfluss, et al. (2007). *Chemical Physics Letters* **439**(1-3): 23-28.
- Vaden, T. D., C. J. Weinheimer, et al. (2004). *Journal of Chemical Physics* **121**(7): 3102-3107.
- Vaida, V. (2005). *International Journal of Photoenergy* **7**(2): 61-70.
- Vaida, V., K. J. Feierabend, et al. (2008). *International Journal of Photoenergy*.
- van Heijnsbergen, D., G. von Helden, et al. (1999). *Physical Review Letters* **83**(24): 4983-4986.
- van Heijnsbergen, D., G. von Helden, et al. (2002). *Journal of the American Chemical Society* **124**(8): 1562-1563.
- Vanbrunt, R. J. and J. T. Herron (1990). *Ieee Transactions on Electrical Insulation* **25**(1): 75-94.
- Viggiano, A. A., S. T. Arnold, et al. (1998). *International Reviews in Physical Chemistry* **17**(2): 147-184.

Viggiano, A. A., R. A. Morris, et al. (1992). *Journal of the American Chemical Society* **114**(26): 10477-10482.

Volatron, F. and C. Roche (2007). *Chemical Physics Letters* **446**(4-6): 243-249.

Walrafen, G. E. (1967). *Journal of Chemical Physics* **47**(1): 114-&.

Wang, X. B., X. Yang, et al. (2002). *International Reviews in Physical Chemistry* **21**(3): 473-498.

Weber, J. M. (2005). *Review of Scientific Instruments* **76**: 043301.

Weber, J. M., J. A. Kelley, et al. (2000). *Science* **287**(5462): 2461-2463.

Weber, J. M., J. A. Kelley, et al. (2001). *Journal of Chemical Physics* **114**(6): 2698-2706.

Weber, J. M., W. H. Robertson, et al. (2001). *Journal of Chemical Physics* **115**(23): 10718-10723.

Weigend, F. and M. Häser (1997). *Theoretical Chemistry Accounts* **97**(1-4): 331-340.

Weigend, F., M. Häser, et al. (1998). *Chemical Physics Letters* **294**(1-3): 143-152.

Weinkauff, R., K. Walter, et al. (1989). *Zeitschrift Fur Naturforschung Section a-a Journal of Physical Sciences* **44**(12): 1219-1225.

Weis, P., S. Gilb, et al. (2002). *International Journal of Mass Spectrometry* **216**(1): 59-73.

Wester, R., A. E. Bragg, et al. (2003). *Journal of Chemical Physics* **119**(19): 10032-10039.

- Wigner, E. P. (1948). *Physical Review* **73**(9): 1002-1009.
- Wiley, W. C. and I. H. McLaren (1955). *Review of Scientific Instruments* **26**(12): 1150-1157.
- Williams, J. H., J. K. Cockcroft, et al. (1992). *Angewandte Chemie-International Edition in English* **31**(12): 1655-1657.
- Wilson, E. B. (1934). *Physical Review* **45**(10): 0706-0714.
- Woronowicz, E. A., W. H. Robertson, et al. (2002). *Journal of Physical Chemistry A* **106**(31): 7086-7089.
- Worz, A. S., U. Heiz, et al. (2005). *Journal of Physical Chemistry B* **109**(39): 18418-18426.
- Wu, D. Y., S. Duani, et al. (2008). *Journal of Physical Chemistry A* **112**(6): 1313-1321.
- Wytttenbach, T. and M. T. Bowers (2003). *Modern Mass Spectrometry*. **225**: 207-232.
- Xantheas, S. S. (1996). *Journal of Physical Chemistry* **100**(23): 9703-9713.
- Xantheas, S. S. and T. H. Dunning (1994). *Journal of Physical Chemistry* **98**(51): 13489-13497.
- Xie, Y. M., H. F. Schaefer, et al. (2003). *Chemical Communications*(1): 102-103.
- Yamada, Y., J. Okano, et al. (2006). *Chemical Physics Letters* **432**(4-6): 421-425.
- Yates, B. F., H. F. Schaefer, et al. (1988). *Journal of the American Chemical Society* **110**(19): 6327-6332.

Yoon, B., H. Hakkinen, et al. (2005). *Science* **307**(5708): 403-407.

Zhan, C. G. and S. Iwata (1995). *Chemical Physics Letters* **232**(1-2): 72-78.

Zheng, W., X. Li, et al. (2007). *Chemical Physics Letters* **444**(4-6): 232-236.